EMERGING INFECTIOUS DISEASES®

U.S. CENTERS FOR DISEASE CONTROL AND PREVENTION

Vaccine-Preventable Diseases

February 2026

Juan Manuel Blanes, *An Episode of Yellow Fever in Buenos Aires*, 1871. Oil on canvas. 230 cm × 180 cm. Museo Nacional de Artes Visuales, Montevideo, Uruguay. Source: Wikimedia Commons.

Pages 169–314

EMERGING INFECTIOUS DISEASES
A Peer-Reviewed Journal Tracking and Analyzing Disease Trends

Emerging Infectious Diseases is published monthly by the Centers for Disease Control and Prevention, 1600 Clifton Rd NE, Mailstop H16-2, Atlanta, GA 30329-4018, USA. Telephone 404-639-1960; email eideditor@cdc.gov

EMERGING INFECTIOUS DISEASES®

Vaccine-Preventable Diseases **February 2026**

On the Cover

Juan Manuel Blanes, *An Episode of Yellow Fever in Buenos Aires*, 1871. Oil on canvas. 230 cm × 180 cm. Museo Nacional de Artes Visuales, Montevideo, Uruguay. Source: Wikimedia Commons.

About the Cover p. 312

Synopses

Life-Threatening SARS-CoV-2–Associated Encephalopathy and Multiorgan Failure in Children, Asia and Oceania, 2022–2024
M. Kasai et al. **169**

Research

Predictors of Fatal Outcomes among Pediatric Patients Hospitalized Rocky Mountain Spotted Fever, Sonora, Mexico, 2004–2024
S. Bellman et al. **180**

***Leptotrombidium imphalum* Chiggers as Vector for Scrub Typhus in Human Settlements, India, 2022–2023**
C.S. Devamani et al. **191**

Using Routine Surveillance Data to Assess Dengue Virus Transmission Risk in Travelers Returning to the United States
K. Rysava et al. **202**

Pulmonary Complications in Fatal Yellow Fever, Brazil, 2017–2019
A.N. Duarte-Neto et al. **211**

Dispatches

Characteristics and Transmission Dynamics of Global Travel-Related Mpox Cases Caused by Clade Ib Monkeypox Virus
H. Laurenson-Schafer et al. **225**

Rabies Reemergence, Central Europe, 2022–2024
E. Robardet et al. **229**

***Desulfovibrio* Bacteremia in Patients with Abdominal Infections, Japan, 2020–2025**
N. Watanabe et al. **233**

Retail Milk Monitoring of Influenza A(H5N1) in Dairy Cattle, United States, 2024–2025
N.N. Tarbuck et al. **238**

Genomic Analysis of Doxycycline Resistance–Associated 16S rRNA Mutations in *Treponema pallidum* Subspecies *Pallidum*
G.S. Long et al. **242**

Effectiveness of RSV Vaccines against RSV-Associated Thromboembolic Events
R.E. Wiegand et al. **246**

Multiplex PCR to Differentiate Monkeypox Virus Clades
C.T. Williams et al. **250**

Measles Outbreak Driven by Nosocomial Transmission, Armenia, February–July 2023
K. Palayan et al. **255**

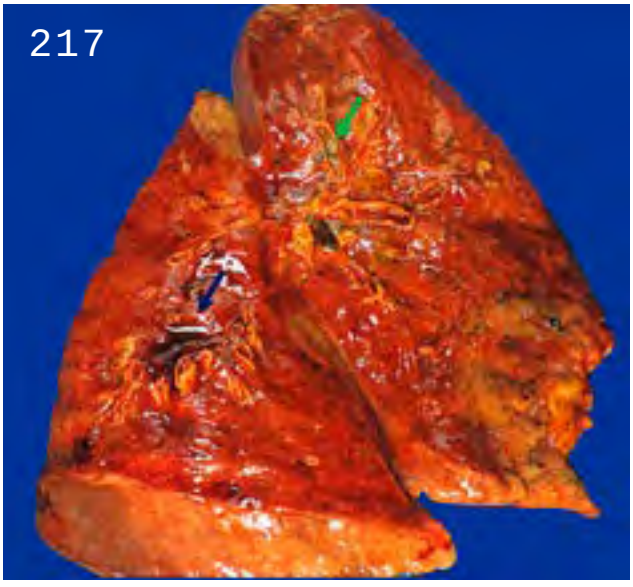

EMERGING INFECTIOUS DISEASES®

February 2026

Avian Influenza A(H9N2) Virus Transmission across Chicken Production and Distribution Networks, Vietnam
M. Hennessey et al. **259**

Autochthonous Rat Lungworm *Angiostrongylus cantonensis* Infections in Accidental and Definitive Hosts, San Diego, California, USA
S. Nakagun et al. **265**

Temporal Clustering of *Mycoplasma pneumoniae*–Associated Encephalitis and Stroke, South Korea, 2024
S.H. Song et al. **270**

Case of *Legionella pneumophila* Serogroup 1 Infection Linked to a Water Flosser, France
C. Slekovec et al. **274**

***Neospora caninum* Infection in Marine Mammals Stranding in Northeastern Pacific Ocean Region**
S.A. Raverty et al. **277**

Donor-Derived West Nile Virus Infection in Kidney Transplant Recipients, France
A. Truffot et al. **281**

Research Letters

Severe Respiratory Diphtheria-Like Illness Caused by Toxigenic *Corynebacterium ulcerans*
R. Helleren et al. **285**

Acute Severe Hepatitis B Virus Infection in Previously Vaccinated Patient during Acalabrutinib Treatment
L. Rojek et al. **287**

Invasive Pneumococcal Disease among Childbearing-Age Women, United States, 2007–2023
N. Prasad et al. **290**

Multicenter Serologic Investigation of Influenza D Virus in Cats and Dogs, Europe, 2015–2024
C.M. Trombetta et al. **293**

Vesicular Disease Caused by Seneca Valley Virus in Pigs, England, 2022
B. Armson et al. **295**

Vaccine-Like African Swine Fever Virus Strain in Domestic Pigs, Thailand, 2024
T.T. Nguyen et al. **299**

Monkeypox Virus Antibodies in Healthy Persons after Vaccination, United Kingdom
V.H. Sheridan et al. **302**

Airport Malaria Cluster in Certified Malaria-Free Country, Libya, 2024
A.M. Alarbi et al. **305**

EIN Letter

***Candida auris* Testing by the Antimicrobial Resistance Laboratory Network, United States, 2022–2023**
J.E. Laury et al. **308**

About the Cover

Yellow Fever in Buenos Aires
T. Chorba **311**

Etymologia

Mumps
S. Mohan, A. Khan **258**

Correction
Vol. 32, No. 1 **310**
Essential taxonomic information was inadvertently omitted from Detection of Novel Thermotolerant *Tepidimonas* sp. Bacteria in Human Respiratory Specimens, Hong Kong, China, 2024

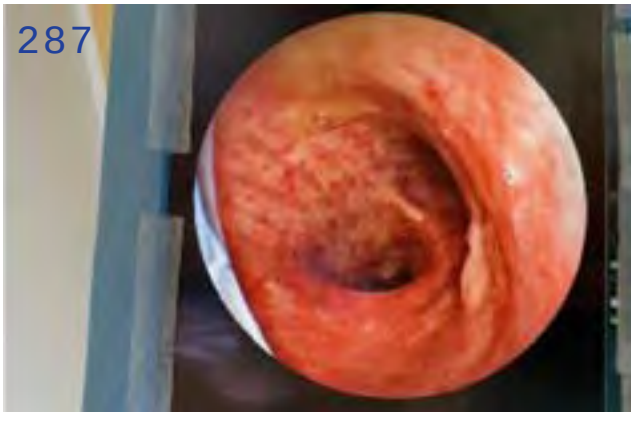

Life-Threatening SARS-CoV-2–Associated Encephalopathy and Multiorgan Failure in Children, Asia and Oceania, 2022–2024

Mariko Kasai,[1] Hiroshi Sakuma, Motomasa Suzuki,[1] Masahiro Nishiyama,[1] Nanako Kawata,[1] Jainn-Jim Lin,[1] Kuang-Lin Lin, Velda Han, Shekeeb S. Mohammad, Russell C. Dale, Terrence Thomas, Kazuhiro Muramatsu, Osamu Mitani, Yoshiyuki Kobayashi, Kouhei Ishida, Yuichi Abe, Ichiro Kuki, Jun-ichi Takanashi

SARS-CoV-2 infections in children occasionally manifest with severe neurologic signs. We report a case series of life-threatening encephalopathy associated with SARS-CoV-2 in 25 children in Australia, Japan, Singapore, and Taiwan during February 2022–January 2024. All children had severe encephalopathy develop, characterized by rapidly progressive cerebral edema, conditions known as acute shock with encephalopathy and multiorgan failure or acute fulminant cerebral edema. Among the 25 patients, 22 (88%) eventually died; 11 (44%) children died within 24 hours of hospitalization. In addition, 18 (72%) had illness manifest with shock, and 14 (56%) had multiorgan failure develop within 6 hours of neurologic onset. Serum concentrations of cytokines/chemokines including interleukin 6 and tumor necrosis factor-α were significantly higher within 24 hours of onset than for controls. SARS-CoV-2–associated encephalopathy cases such as those described here represent an emerging neurologic crisis with high mortality rate resulting from rapidly progressive brain edema and multiorgan failure.

SARS-CoV-2, which primarily causes respiratory illness, is associated with diverse central and peripheral nervous system complications. Multisystem inflammatory syndrome in children is often associated with neurologic syndromes, and SARS-CoV-2–triggered encephalopathy syndromes, such as life-threatening acute fulminant cerebral edema (AFCE), have been reported (*1*,*2*). Previously, we reported that SARS-CoV-2–associated encephalopathy had a poor prognosis because of a higher incidence of AFCE and acute shock with encephalopathy and multiorgan failure (ASEM) than for non–SARS-CoV-2–associated encephalopathy (*1*,*2*). Both AFCE and ASEM are devastating, infection-triggered encephalopathy syndromes that result in high mortality rates in children (*3*) and typically occur in healthy children triggered by viral infections. Illness in such cases manifests with acute encephalopathy symptoms, shock, multiorgan

Author affiliations: Tokyo Metropolitan Institute of Medical Science, Tokyo, Japan (M. Kasai, H. Sakuma); Aichi Children's Health and Medical Center, Aichi, Japan (M. Suzuki); Hyogo Prefectural Kobe Children's Hospital, Kobe, Japan (M. Nishiyama); Tokyo Metropolitan Children's Medical Center, Tokyo (N. Kawata); Chang Gung Children's Hospital and Chang Gung Memorial Hospital, School of Medicine, College of Medicine, Chang Gung University, Taoyuan, Taiwan (J.-J. Lin, K.-L. Lin); Khoo Teck Puat-National University Children's Medical Institute, Singapore (V. Han); Yong Loo Lin School of Medicine, National University of Singapore, Singapore (V. Han); Kids Neuroscience Centre, The Children's Hospital at Westmead, Faculty of Medicine and Health, University of Sydney, Westmead, New South Wales, Australia (V. Han, S.S. Mohammad, R.C. Dale); KK Women's and Children's Hospital, Singapore (T. Thomas); Jichi Medical University, Tochigi, Japan (K. Muramatsu); Fukuyama City Hospital, Hiroshima, Japan (O. Mitani); Hiroshima University Hospital, Hiroshima (Y. Kobayashi); Sapporo Medical University School of Medicine, Sapporo, Japan (K. Ishida); National Center for Child Health and Development, Tokyo (Y. Abe); Osaka City General Hospital, Osaka, Japan (I. Kuki); Tokyo Women's Medical University Yachiyo Medical Center, Chiba, Japan (J. Takanashi)

DOI: https://doi.org/10.3201/eid3202.250549

[1]These authors contributed equally to this article.

failure, and rapidly progressive diffuse cerebral edema (*4*,*5*). A hypercytokine state has been suggested as the underlying mechanism for the pathogenesis of ASEM/AFCE, although reports are rare, and development of effective treatment strategies remains challenging. Several reports have addressed the emergence of severe cases of SARS-CoV-2 ASEM/AFCE in children (*6*–*8*); however, we know of no review of the literature for SARS-CoV-2 ASEM/AFCE cases, and only a few case series exist, none of which include diverse international populations.

Here, we report an international case series and a scoping review designed to outline the common clinical manifestations of SARS-CoV-2 ASEM/AFCE in diverse populations. Furthermore, we aim to describe proinflammatory cytokine and chemokine profiles in serum from patients with SARS-CoV-2 ASEM/AFCE to underscore the predominant immune pathology in the early stages of disease onset.

Methods

Study Population

We conducted an international multicenter collaborative study in pediatric patients <18 years of age who had ASEM/AFCE develop during or after SARS-CoV-2 infection. The study enrolled children who fulfilled the ASEM/AFCE criteria in collaborating hospitals in 4 countries—Australia, Japan, Singapore, and Taiwan—during February 2022–January 2024. We sent web-based questionnaires to child neurologists in collaborative research institutes and obtained clinical information. We collected information on major clinical symptoms, along with the timing of the symptom onset. In addition, we collected serum samples from facilities in Japan that provided consent to obtain specimens.

We used international consensus criteria (*3*,*9*) to define ASEM/AFCE as a febrile illness preceding or concurrent with the onset of neurologic manifestations, rapid reduction of consciousness, or seizures with progressive diffuse cerebral edema. Shock and multiorgan failure (≥3 of the following: anemia, thrombocytopenia, disseminated intravascular coagulation, acidosis, elevated hepatocellular enzymes, and renal dysfunction) are essential for ASEM. We excluded patients who had traumatic brain injury, metabolic disorders, or marked hyponatremia. All patients tested positive for SARS-CoV-2 by reverse transcription PCR or antigen testing.

We evaluated outcomes by using a pediatric cerebral performance category (PCPC) score (*10*). In brief, we graded outcomes into 6 categories: presymptomatic state (PCPC = 1), mild disability (PCPC = 2; age-appropriate interaction, minor controlled neurologic condition), moderate disability (PCPC = 3; impaired age-appropriate functioning, uncontrolled neurologic condition), severe disability (PCPC = 4; abnormal motor responses, including no purposeful, decorticate, or decerebrate reactions to pain), coma or vegetative state (PCPC = 5), and death (PCPC = 6).

Scoping Review

To gather additional data, we performed a scoping review, according to Preferred Reporting Items for Systematic Reviews and Meta-Analyses guidelines (*11*). In the review, we searched PubMed for articles or abstracts published during January 1, 2020–June 30, 2024. We curated English-language publications and used the following search terms: "coronavirus disease 2019 (COVID-19)" OR "SARS-CoV-2" AND (encephalitis) OR (acute fulminant cerebral edema) OR (Hemorrhagic shock and encephalopathy syndrome) OR (Acute shock and encephalopathy with multiorgan failure) NOT (autoimmune). We employed the following inclusion criteria: diagnosed cases of COVID-19, clinical courses and neuroimaging abnormalities consistent with the ASEM/AFCE diagnosis, and eligible case series, case reports, and cohort studies. Two authors (M.K. and H.S.) reviewed the articles. We standardized data extraction by using 2 categories, study characteristics (first author's name, year of publication, country of origin, study design, and sample size) and clinical details (sex, age, medical history or comorbidities, neurologic symptoms, and radiologic findings). We excluded studies that lacked sufficient information on neurologic symptoms. A single reviewer extracted data and validated it for accuracy. We sourced the flow diagram for scoping reviews, which included searches of databases, from a previous report (*9*).

Cytokine and Chemokine Profiles

Of the 25 patients in the cohort, we obtained serum samples from 9 patients with ASEM/AFCE to conduct cytokine and chemokine measurement. Among the 9 patients, 2 provided 2 samples collected at different time points, resulting in a total of 11 samples analyzed. We centrifuged blood samples immediately after collection to separate serum, which we then stored at –80°C until analysis. For all samples, we recorded the precise interval from neurologic onset to blood collection and divided samples into early-stage (≤24 hours after neurologic onset; n = 6) and late-stage (>24 hours after neurologic onset;

n = 5). For control samples (n = 14), we used samples from patients with other inflammatory neurologic diseases who had neurologic symptoms: epilepsy (n = 1), status epilepticus (n = 6), altered mental status with seronegative autoimmune encephalitis (n = 4), abnormal behavior after influenza (n = 1), and unclassified acute encephalopathy (n = 2). All controls were children <18 years of age without neurologic autoantibodies, abnormal findings on brain imaging, or cerebrospinal fluid pleocytosis. The methods used to determine neurologic autoantibodies in the controls were reported in a previous study (*12*).

We determined serum levels of cytokines and chemokines for all samples by using the Bio-Plex suspension array system with the Bio-Plex Pro Human Chemokine Panel 11-Plex (Bio-Rad Laboratories, https://www.bio-rad.com). The assays were CXC-chemokine ligand (CXCL) 13, CXCL1, interferon-gamma (IFN-γ), interleukin (IL) 10, IL-1β, IL-6, IL-8, CXCL10, chemokine ligand 2 (CCL2), macrophage migration inhibitory factor (MIF), and tumor necrosis factor α (TNF-α). We conducted all assays in duplicate and adopted the mean values for each set of results. We diluted serum 1:4 for the assay and further diluted some serum samples to fit the calibration curve if IL-6 and IL-8 levels were beyond the detection limits. We then compared the cytokine/chemokine levels between the early-stage, late-stage, and control groups.

Statistical Analysis

We evaluated cytokine and chemokine profiles by using the nonparametric Kruskal-Wallis test with post hoc Mann-Whitney U tests. We set the significance of the differences at $p<0.05$. We used Mann-Whitney U tests with Bonferroni adjustments (adjusted $\alpha = 0.016$) for multiple testing at the cytokine/chemokine levels. We performed statistical analyses by using R software version 4.3.2 (The R Project for Statistical Computing, https://www.r-project.org).

Ethics and Informed Consent

The studies involving human participants were reviewed and approved by the institutional review board of Tokyo Metropolitan Institute of Medical Science, approval nos. 20-28 (*3*) and 21-2 (*6*). Written informed consent to participate in this study was provided by the participants or their legal guardian/next of kin.

Results

Patient Cohort

The patient cohort consisted of 25 new cases of SARS-CoV-2 ASEM/AFCE: 14 from Japan, 8 from Taiwan, 2 from Singapore, and 1 from Australia. All patients were of Asian ethnicity. We compiled complete clinical characteristics of the patients (Table 1). The age at onset ranged from 10 months to 10 years (median 2 years 11 months). The male:female ratio was 1.1:1. The medical history of 20 of the 25 patients was healthy; 4 had febrile convulsions, and 1 had previous hypoxic ischemic encephalopathy and epilepsy. All but 1 patient, whose vaccination history was unknown, had not been vaccinated against SARS-CoV-2.

None of the patients had severe respiratory symptoms before neurologic onset. Fever was evident in all patients; maximum body temperature ranged from 38.3°C to 42.4°C (median 41°C) in the acute clinical course. Neurologic symptoms appeared 2–48 (median 14.5) hours after the onset of fever. The median Glasgow Coma Scale score at initial hospital visit was 4 (range 3–11) (n = 22). Clinical seizures were evident in 23 (92%) of 25 patients in our cohort, among which status epilepticus or seizure clusters were present in 16/25 (64%) patients, whereas seizures lasting <5 minutes were present in 7 (28%) patients. Diarrhea was present in 8 (32%) of the 25 patients at the onset of neurologic symptoms. Neurologic deterioration and systemic organ damage were evident in all patients, especially in the early course of ASEM/AFCE; 18 (72%) patients had shock, 14 (56%) multiorgan failure, and 13 (52%) disseminated intravascular coagulation (DIC) within 6 hours of neurologic onset (Table 2; Figure 1). Metabolic acidosis was evident in 24 (96%) of 25 patients.

Immunotherapies were given to most case-patients. Intravenous methylprednisolone (30 mg/kg) was administered in 18 (72%) cases, intravenous immunoglobulin (2 g/kg) in 14 (56%) cases, and targeted temperature management (36.0°C–36.9°C) in 17 (68%) cases. Four of 25 patients were treated with intravenous tocilizumab.

Typical brain imaging findings in ASEM/AFCE (Figure 2) show diffuse cerebral edema (DCE) that appears within 1–24 hours after neurologic onset. In some cases, initial brain imaging demonstrated moderate cerebral edema, but several hours later, severe DCE developed. Some brain images (Figure 2, panel E) were identical to those previously reported (*13*). Typical EEG abnormalities in acute illness included generalized high-amplitude slow waves or diffuse low activity.

All patients were admitted to the intensive care unit and required tracheal intubation. The duration of hospitalization ranged from 12 hours to 458 days (median 168 hours), and follow-up ranged from 1 to 350 (median 2) days after neurologic onset. The outcomes

Table 1. Clinical characteristics of patients with SARS-CoV-2 ASEM/AFCE in study of life-threatening SARS-CoV-2–associated encephalopathy and multiorgan failure in children, Asia and Oceania, 2022–2024*

Patient no.	Age	Hours from onset of fever to neurologic symptoms	GCS at onset	Brain CT/MRI	Outcome by PCPC†	Hours from onset of neurologic symptoms	
						To RA	To CA
1	10 mo	10	E1V1M1	DCE	6	<6	≥48
2	10 mo	48	NA	DCE, focal abnormality	6	NA	NA
3	1 y 6 mo	19	E4V3M4	DCE	6	NA	NA
4	1 y 10 mo	14	NA	DCE	5	≥48	–
5	2 y	16	E1V1M1	DCE	6	<6	<6
6	2 y	NA	E1V1M1	DCE	6	6–12	≥48
7	2 y 4 mo	5	E1V1M1	DCE	5	≥48	–
8	2 y 4 mo	12	E1V1M1	DCE	6	At onset	At onset
9	2 y 7 mo	12	E1V1M3	DCE, BTA	6	NA	NA
10	2 y 7 mo	24	E1V2M1	DCE	6	<6	≥48
11	2 y 8 mo	15	E1V1M3	DCE	6	6–12	≥48
12	2 y 9 mo	NA	E2V2M3	DCE	6	<6	<6
13	2 y 11 mo	27	E2V1M3	DCE	6	≥48	≥48
14	3 y 2 mo	20	E1V2M4	DCE	6	<6	<6
15	3 y 9 mo	5~10	E1V1M4	DCE, focal abnormality	6	NA	NA
16	4 y	NA	NA	DCE	6	≥48	≥48
17	4 y	NA	E1V1M1	DCE	6	<6	<6
18	6 y 7 mo	10	E3V2M5	DCE	1	–	–
19	7 y 4 mo	9.5	E1V1M4	DCE	6	NA	≥48
20	7 y 7 mo	18	E1V1M1	DCE	6	24–48	≥48
21	8 y 1 mo	20	E1V2M1	DCE	6	24–48	24–48
22	8 y 6 mo	NA	E1V1M1	DCE	6	<6	<6
23	8 y 9 mo	NA	E2V3M4	DCE	6	<6	≥48
24	8 y 9 mo	2	E1V1M1	DCE	6	<6	<6
25	10 y 2 mo	12	NA	DCE	6	6–12	≥48

*AFCE, acute fulminant cerebral edema; ASEM, acute shock with encephalopathy and multiorgan failure; BTA, bright tree appearance; CA, cardiac arrest; DCE, diffuse cerebral edema; GCS, Glasgow Coma Scale; NA, not available; PCPC, pediatric cerebral performance category; RA, respiratory arrest; –, not applicable.
†Outcome was graded as follows: presymptomatic state (PCPC = 1), mild disability (PCPC = 2), moderate disability (PCPC = 3), severe disability (PCPC = 4), coma or vegetative state (PCPC = 5), and death (PCPC = 6).

in our cohort were PCPC 1 in 1 patient (4%), PCPC 5 in 2 patients (8%), and PCPC 6 in 22 patients (88%), including 11 (44% of all 25 patients) who died within 24 hours of hospitalization. Respiratory arrests at <6 hours after neurologic onset occurred in 10 (40%) patients, and cardiac arrests at <6 hours after neurologic onset occurred in 7 (28%) patients (Figure 1).

Scoping Review

The scoping review identified 1,212 studies, and we screened 230 relevant articles for eligibility; of those, we included 7 independent studies in the review (*6*,*7*,*14*–*18*) (Figure 3). Of those, 4 case reports and 3 case series involved individualized clinical information of 12 cases and fulfilled the definition of ASEM or AFCE (Table 3). We excluded a case series from Taiwan (*8*) and a case report from Japan (*19*) from the review because they overlapped with our cohort; the duplicates were cases 5, 8, 14, 16, 17, and 25 from Taiwan and case 21 from Japan (Table 1).

For the remaining cases, age at onset ranged from 2 months to 17 years, including 9 school-aged children. The male:female ratio was 3:1. The reported cases were from India, South Korea, Tunisia, and the United States; however, the ethnicity of each patient was not identified. At least 7 of the 12 patients had status epilepticus as the first neurologic symptom.

Table 2. Frequency of shock and signs of multiorgan failure in patients with SARS-CoV-2 ASEM/AFCE in study of life-threatening SARS-CoV-2–associated encephalopathy and multiorgan failure in children, Asia and Oceania, 2022–2024*

Symptoms	No. (%) cases
Shock	24 (96)
DIC	22 (88)
Elevated AST or ALT†	25 (100)
Elevated BUN or creatinine	25 (100)
Thrombocytopenia‡	21 (84)
Reduced hemoglobin§	15 (60)
Metabolic acidosis	24 (96)

*ALT, alanine aminotransferase; AFCE, acute fulminant cerebral edema; ASEM, acute shock with encephalopathy and multiorgan failure; AST, aspartate aminotransferase; BUN, blood urea nitrogen; DIC, disseminated intravascular coagulation.
†A total of 22 patients had AST or ALT elevations with a ≥4-digit range.
‡Platelet count <150,000/μL.
§Hemoglobin level decreased by >3 g/dL from admission.

Cytokine/Chemokine Levels in Patients with SARS-CoV-2 ASEM/AFCE

Within the international cohort of SARS-CoV-2 ASEM/AFCE, we determined 11 cytokine/chemokine levels from the 9 case-patients who had given consent to provide their serum. We compared each level among early-stage samples, late-stage samples, and controls (Figure 4). The early-stage samples showed significantly higher levels of all

cytokines than did controls. The levels of CXCL8, IL-6, and IL-10 were significantly elevated in late-stage samples compared with those in controls. No cytokines were correlated with outcome, and the case-patient with a low cytokine profile was one of the few survivors (PCPC 1). That case-patient exhibited the lowest values for CXCL13, IFN-γ, IL-1β, IL-10, and IL-6 of all case-patients (Figure 5). When plotting the relationship between serum cytokine and chemokine levels and the interval between neurologic onset and blood collection, the fitted curve suggested that the levels were higher in samples collected earlier, and we observed a peak within 24 hours of onset (Appendix Figure).

Discussion

A condition in which encephalopathy develops concurrently with or shortly after a febrile infection and does not result from direct invasion of the pathogen into the brain is known as infection-triggered encephalopathy syndrome (ITES) and is distinguished from infectious and autoimmune encephalitis (*3*). ITES is an umbrella term used for several encephalopathy syndromes, each of which has specific clinical and radiologic phenotypes. ASEM and AFCE are the most severe types of ITES syndromes. ASEM is a serious condition in which the patient experiences shock and rapidly progresses to coma and multiorgan failure with progressive diffuse brain edema. ASEM was previously known as hemorrhagic shock encephalopathy syndrome and frequently affects children <1 year of age (*4*,*20*). Conversely, patients with AFCE exhibit encephalopathy and rapidly progressive cerebral edema without shock and multiorgan failure (*5*). Whether ASEM and AFCE are a continuous spectrum of clinical phenotypes with fulminant brain edema remains uncertain.

In this study, we described the clinical manifestations of 25 patients with SARS-CoV-2 ASEM/AFCE from an international cohort. Of note, our SARS-CoV-2 ASEM/AFCE cohort had an older age of onset, with 8 school-aged case-patients out of 25, compared with non–SARS-CoV-2–triggered ASEM, in which onset age has been predominantly in infants and toddlers in previous reports (*4*,*20*,*21*). That result could be attributed to the broad age at onset of SARS-CoV-2 infection.

All cohort patients with ASEM rapidly progressed to coma, hemodynamic failure, and systemic organ damage in the early stages of onset, similar to results of a previous report on non–SARS-CoV-2–triggered ASEM (*20*–*22*). In addition, more than half of our cohort exhibited shock, multiorgan failure, and DIC within 6 hours of neurologic onset. In contrast, bleeding was evident in less than half (48%) of the 25 cases. Although bleeding has been described as one of the clinical features of hemorrhagic shock encephalopathy syndrome in the past (*4*,*20*), the frequency of bleeding was not high in ASEM, and the absence of bleeding should not rule out a diagnosis of ASEM, nor should bleeding be considered essential for diagnosis. The 88% mortality rate among our patients with SARS-CoV-2 ASEM/AFCE was slightly higher than that reported in a retrospective clinical study of non–SARS-CoV-2–triggered ASEM (*22*). That high mortality rate could be attributed to the high incidence of multiorgan failure in cases of SARS-CoV-2 ASEM. However, because the case series reporting

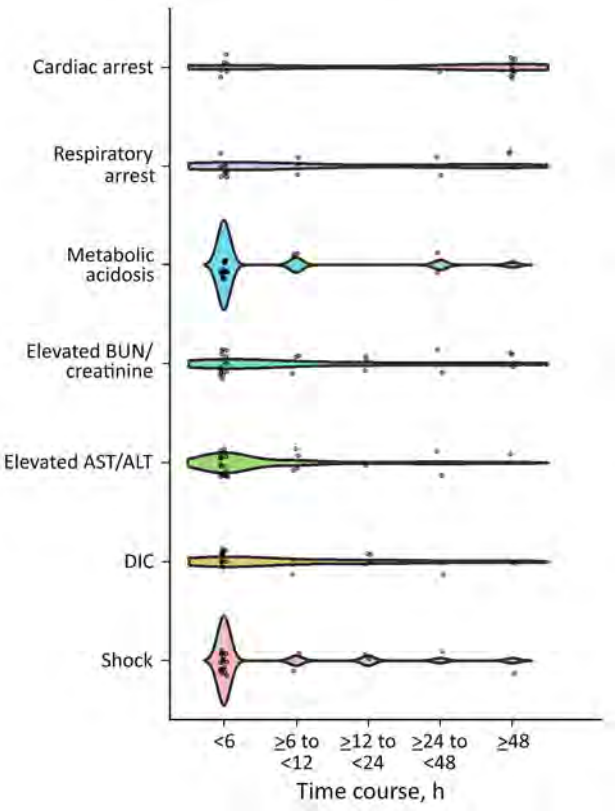

Figure 1. Time course of clinical manifestations of acute shock with encephalopathy and multiorgan failure/acute fulminant cerebral edema (ASEM/AFCE) for study of life-threatening SARS-CoV-2–associated encephalopathy and multiorgan failure in children, Asia and Oceania, 2022–2024. Violin plots show time from onset of neurologic symptoms; dots indicate cases and shading 95% CIs. Laboratory findings observed within 6 hours of neurologic onset in more than half of patients with SARS-CoV-2 ASEM/AFCE were as follows: increased hepatocellular enzymes (68%), elevated blood urea nitrogen or creatinine (56%), prolonged prothrombin time, partial thromboplastin time, thrombin time (52%), and metabolic acidosis (52%). ALT, alanine aminotransferase; AST, aspartate aminotransferase; BUN, blood urea nitrogen; DIC, disseminated intravascular coagulation.

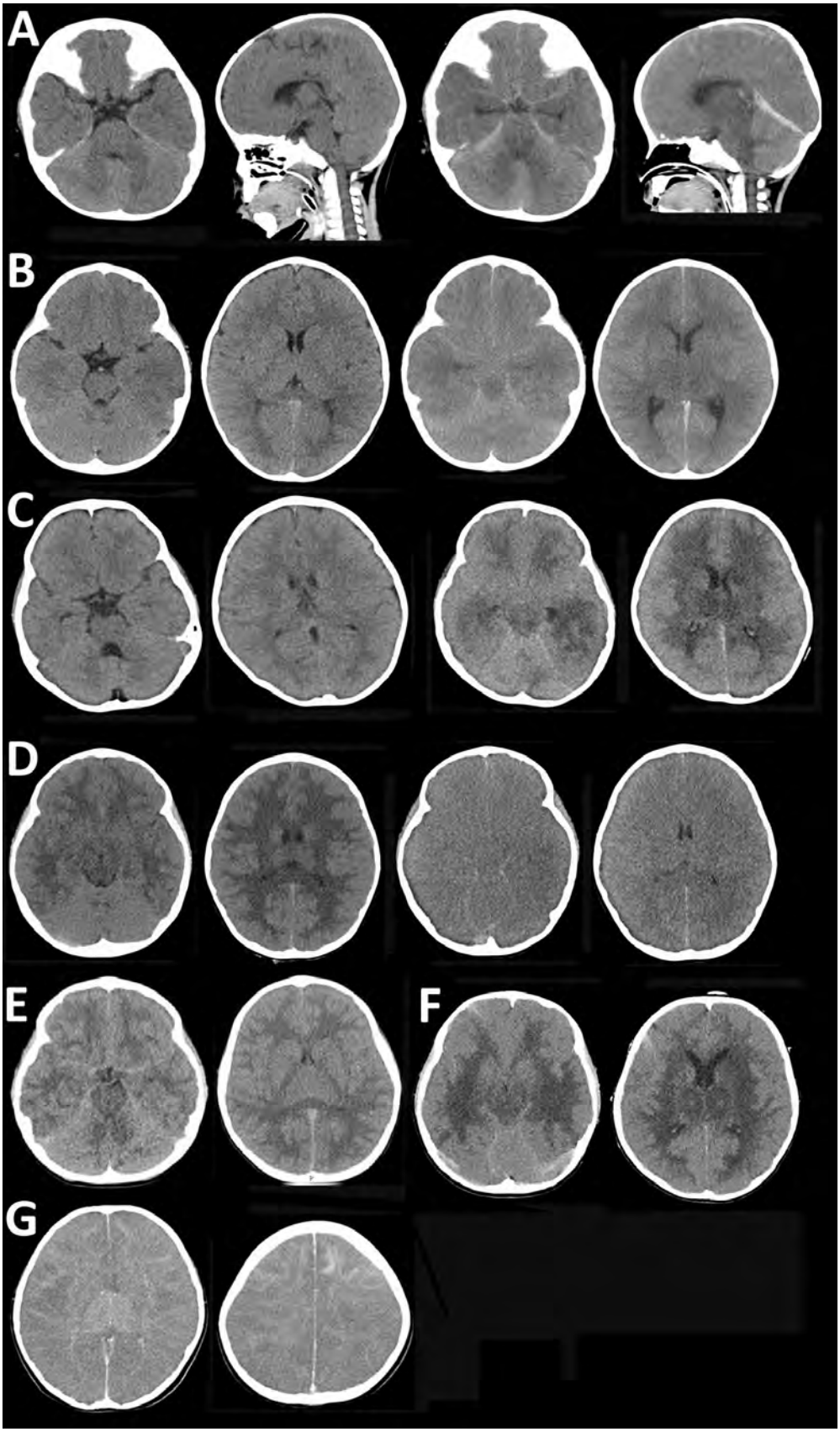

Figure 2. Brain computed tomography imaging for patients with SARS-CoV-2 acute shock with encephalopathy and multiorgan failure/ acute fulminant cerebral edema (ASEM/AFCE) for study of life-threatening SARS-CoV-2–associated encephalopathy and multiorgan failure in children, Asia and Oceania, 2022–2024. A) Case-patient 1, showing diffuse cerebral edema (DCE) within 10 hours after onset of neurologic symptoms (left 2 images) and severe DCE and herniation at 18 hours after onset (right 2 images). B) Case-patient 6, showing mild cerebral edema within 4 hours after onset (left 2 images) and severe DCE at 23 hours after onset (right 2 images). C) Case-patient 15, showing DCE 3 hours after onset (left 2 images) and severe DCE with low-density involving the bilateral cerebral white matter and thalamus at 23 hours from the onset (right 2 images). D) Case-patient 19, showing DCE with low-density lesions in the bilateral cerebral white matter within 90 minutes after onset (left 2 images) and severe DCE at 10 hours after onset (right 2 images). E) Case-patient 18, showing mild cerebral edema on day 2 of illness; the patient had no further exacerbation of DCE. F) Case-patent 20, showing DCE with bilateral low-density lesions in the thalamus (left image) and periventricular cerebral white matter within 30 hours after onset (right image). G) Case-patient 23, showing DCE within 7 hours after onset (left image) and a high density of frontal subcortical white matter (right image).

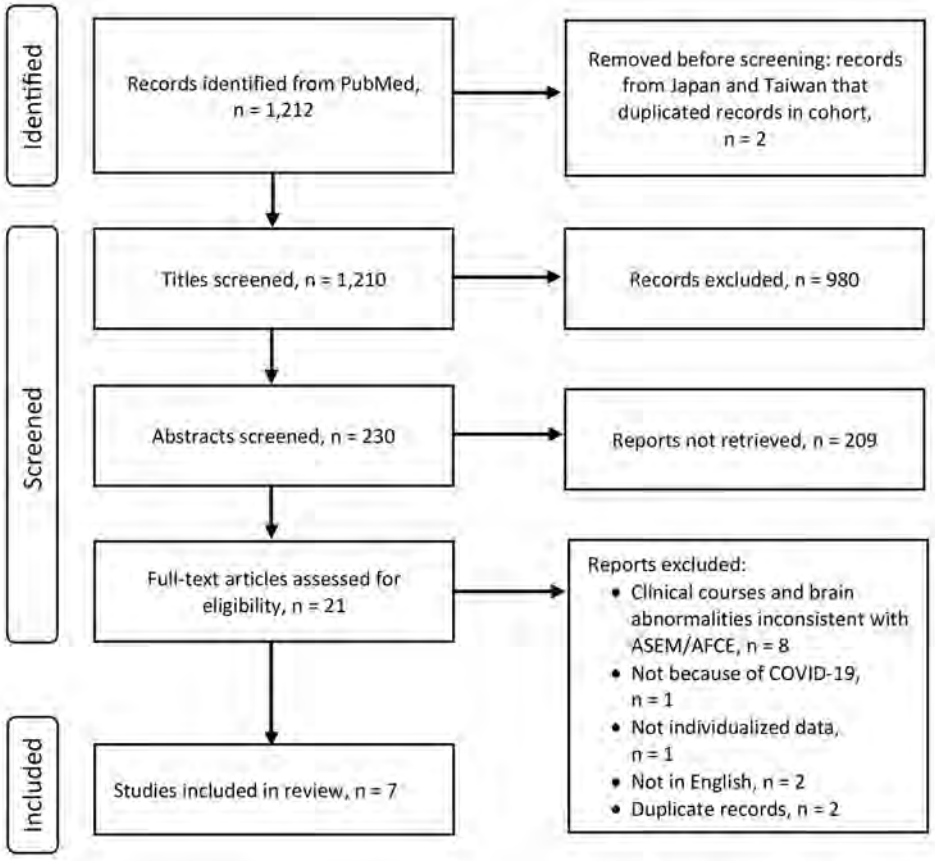

Figure 3. Flow diagram for scoping review of SARS-CoV-2 ASEM/AFCE cases from the literature via PubMed for study of life-threatening SARS-CoV-2–associated encephalopathy and multiorgan failure in children, Asia and Oceania, 2022–2024. AFCE, acute fulminant cerebral edema; ASEM, acute shock with encephalopathy and multiorgan failure.

the clinical manifestations of non–SARS-CoV-2 ASEM/AFCE involved a very small population, it remains uncertain whether prognostic differences exist. To address that question, future multicenter collaborative studies and establishment of prospective cohorts will be required for accurate comparisons.

In comparison with our cohort, the scoping review cases exhibited a similarly broad age at onset,

Table 3. Cases of SARS-CoV-2 ASE/AFCE reported in the literature from scoping review for study of life-threatening SARS-CoV-2–associated encephalopathy and multiorgan failure in children, Asia and Oceania, 2022–2024*

Country and reference	Patient age	First symptoms with fever	Brain CT/MRI	Outcome by PCPC†	Times from onset to CA
United States (*6*)	7 y	Headaches, abdominal pain, and emesis	DCE	6	NA
United States (7)	<1 y	Gastrointestinal symptoms and status epilepticus	DCE	6	<24 h
	6–12 y	Status epilepticus	DCE and herniation	6	3rd day of admission
	6–12 y	Status epilepticus	DCE and herniation	6	48 h of admission
	3–5 y	Altered awareness, seizure, vomiting, acute respiratory failure, and shock	DCE	NA	NA
United States (*14*)	8 y	Lethargy, myalgias, anorexia, and seizure	DCE	6	NA
Tunisia (*15*)	2 mo	Poor feeding and sleep, seizure, and shock	DCE	6	12 h
India (*16*)	10 y	Repetitive seizures and encephalopathy	DCE and herniation	6	14th day of admission
United States (*17*)	13–17 y	NA	NA	6	NA
	13–17 y	NA	NA	6	NA
South Korea (*18*)	11 y	Status epilepticus	DCE	6	14th day of admission
	9 y	Status epilepticus	DCE	6	NA

*AFCE, acute fulminant cerebral edema; ASEM, acute shock with encephalopathy and multiorgan failure; CA, cardiac arrest; CT, computed tomography; DCE, diffuse cerebral edema; MRI, magnetic resonance imaging; NA, not available; PCPC, pediatric cerebral performance category.
†Outcome was graded as follows: presymptomatic state (PCPC = 1), mild disability (PCPC = 2), moderate disability (PCPC = 3), severe disability (PCPC = 4), coma or vegetative state (PCPC = 5), and death (PCPC = 6).

from infancy to late childhood, and all cases had a fatal outcome. That finding might indicate a reporting bias toward severe cases in the review. Alternatively, discrepancies between our study cohort and the scoping review might reflect variations in the circulating SARS-CoV-2 strains, which could have contributed to differences in the severity of ASEM/AFCE.

In general, an ITES syndrome can be associated with a range of pathogens, although some viruses have been reported to be associated with specific encephalopathy syndromes (*10*). That fact suggests that not the infection itself but the immunologic responses of the host play a major role in determining the phenotype of ITES. To investigate the immunologic mechanisms, we also measured cytokines/chemokines in the serum samples from patients with of SARS-CoV-2 ASEM/AFCE. When we divided the samples into early-stage and late-stage according to their sampling time, the serum levels of CXCL8, CXCL10, IFN-γ, IL-1β, IL-6, IL-10, and TNF-α were the

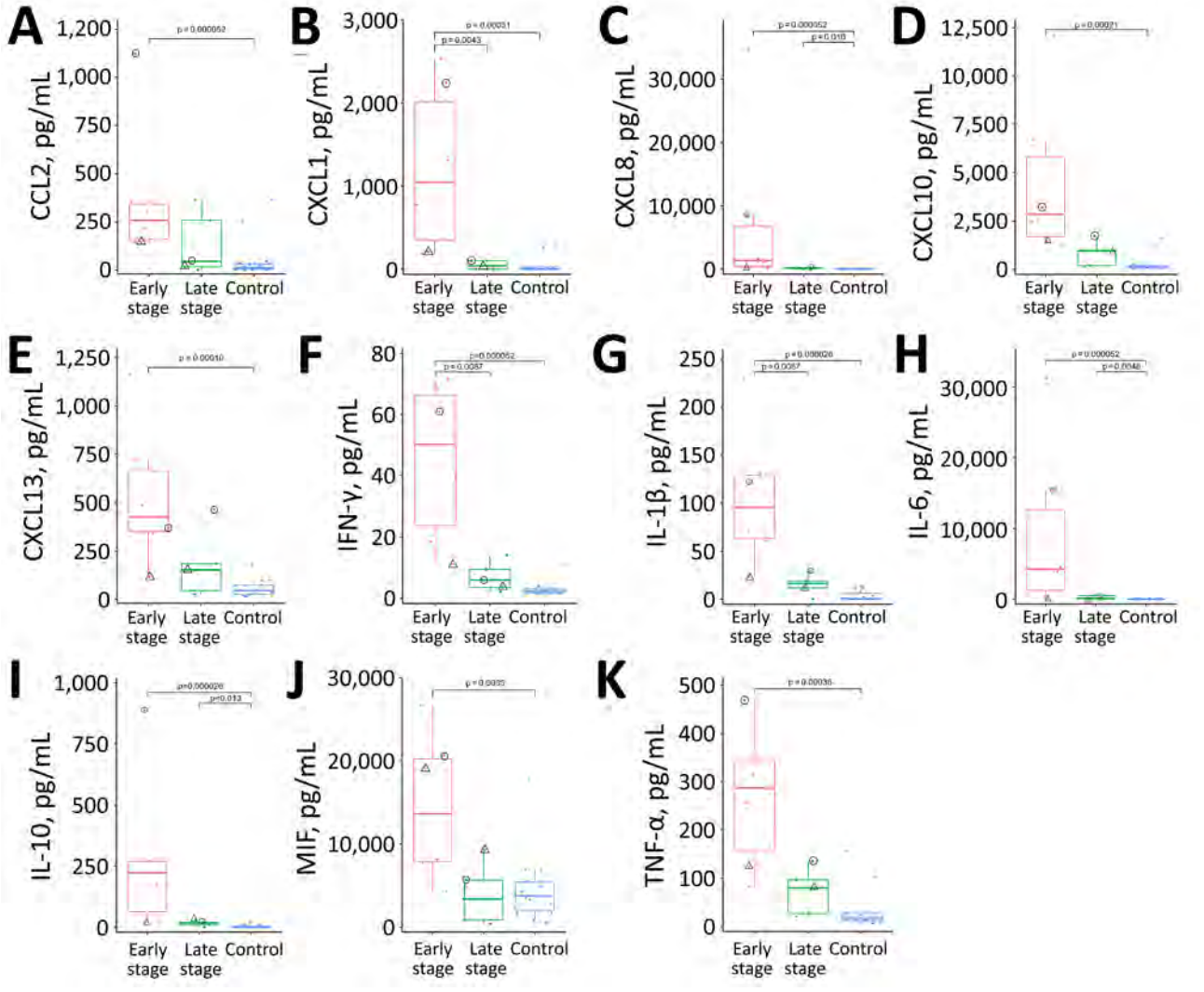

Figure 4. Cytokine and chemokine levels in serum from 9 patients with SARS-CoV-2 acute shock with encephalopathy and multiorgan failure/acute fulminant cerebral edema for study of life-threatening SARS-CoV-2–associated encephalopathy and multiorgan failure in children, Asia and Oceania, 2022–2024. Serum levels were compared among early-stage (red; ≤24 h after neurologic onset; n = 6), late-stage (green; >24 h after neurologic onset; n = 5), and controls (blue; n = 14). Samples derived from early- and late-stage samples can be compared in 2 cases; circles indicate 1 from case-patient 13 (pediatric cerebral performance category = 6), and triangles indicate 1 from case-patient 18 (pediatric cerebral performance category = 1). Each dot indicates a case-patient; horizontal lines within boxes indicate medians; box tops and bottoms indicate interquartile ranges (IQRs); whiskers indicate 1.5× IQR; outliers are values >1.5× IQR. Kruskal-Wallis p values: A) p = 0.0064; B) p = 0.0019; C) p = 0.00029; D) p = 0.00091; E) p = 0.0018; F) p = 0.00042; G) p = 0.00029; H) p = 0.00025; I) p = 0.00029; J) p = 0.016; K) p = 0.0016. CCL, CC-chemokine ligand; CXCL, CXC-chemokine ligand; IFN, interferon; IL, interleukin; MIF, macrophage migration inhibitory factor; TNF, tumor necrosis factor.

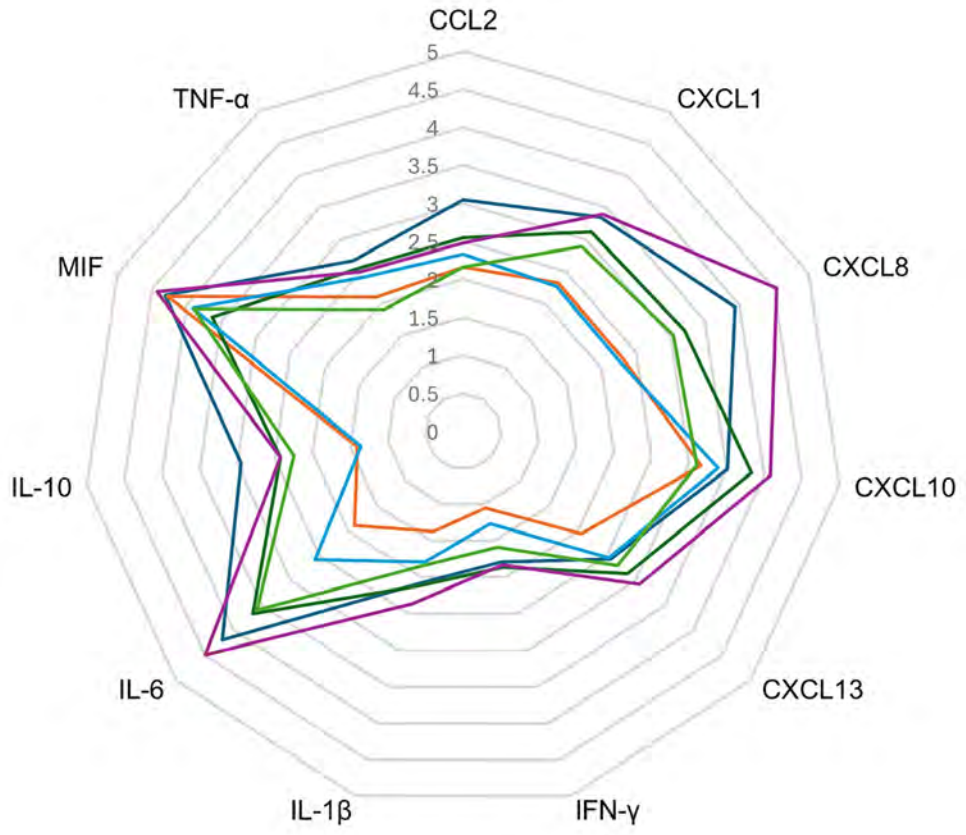

Figure 5. Cytokine and chemokine levels of serum in early illness stage of study of life-threatening SARS-CoV-2–associated encephalopathy and multiorgan failure in children, Asia and Oceania, 2022–2024. Serum levels were compared for 6 patients with early-stage SARS-CoV-2 acute shock with encephalopathy and multiorgan failure/acute fulminant cerebral edema. The values for each cytokine/chemokine are presented on a logarithmic scale; each colored line indicates results for 1 patient. The orange line indicates the case in which the pediatric cerebral performance category = 1. CCL, CC-chemokine ligand; CXCL, CXC-chemokine ligand; IFN, interferon; IL, interleukin; MIF, macrophage migration inhibitory factor; TNF, tumor necrosis factor.

highest within 24 hours after neurologic onset, which was in agreement with another study that reported serum concentrations of cytokines and chemokines with non–SARS-CoV-2–triggered ASEM (*23*). Within 24 hours of infection, the antigen-nonspecific innate immune response is generally dominant, whereas cellular immunity involving T cells would not be activated that early. In this study, most of the elevated factors were proinflammatory cytokines and chemokines. Innate immune responses are mediated by neutrophils, monocytes, dendritic cells, and natural killer cells. Human $CD14^{++}CD16^{-}$ inflammatory monocytes express the chemokine receptor CCR2 and migrate to inflammatory foci via CCL2 (*24*). Such inflammatory monocytes have the ability to produce a broad range of cytokines, including IL-1, IL-6, IL-10, CXCL8, and TNF-α, in response to stimulation (*25*). Of note, the levels of all inflammatory molecules measured in our study were markedly increased. Such a hypercytokine state causes multiorgan failure through the action of IL-1, IL-6, and TNF-α (*26*). Those findings suggest that the high mortality rate associated with SARS-CoV-2 ASEM/AFCE might be related to cytokine storm.

In contrast to the SARS-CoV-2 ASEM/AFCE cases we describe, severe cases of COVID-19 in adults tend to progress to severe acute respiratory distress syndrome and multiorgan failure after 7–10 days of COVID-19 infection (*27*,*28*). In adult cases of COVID-19 with severe acute respiratory distress syndrome and multiorgan failure, increased blood cytokine levels correlated with SARS-CoV-2 detection in the lungs (*29*), indicating that cytokines were produced locally in the lungs. Focusing on cytokine-targeted therapies, tocilizumab, an IL-6–directed therapy, was used in some cases but was not associated with improved prognosis. Rapid progression appears to be less reversible than in other ITES syndromes, such as acute necrotizing encephalopathy. Serum levels of IL-6 were increased in the very early stages of SARS-CoV-2 ASEM/AFCE, but further studies are required to explore the potential benefits of early immunotherapy and other neuroprotective measures.

The first limitation of our study was that we had insufficient clinical information and materials for the analysis because of the small sample size and large number of deaths in our cohort. Also, this multinational cohort has limited generalizability beyond Asia and Oceania. Owing to the retrospective nature of the study, we did not include pediatric cases of SARS-CoV-2 without encephalopathy or non–SARS-CoV-2 ASEM/AFCE. In our review, the details of

the treatment and the time course from the onset of neurologic symptoms to death or brain death could not be followed. Age was reported in some cases but not in others. However, this study demonstrated that emerging infections such as SARS-CoV-2 can precipitate devastating ASEM/AFCE that threatens the lives of previously healthy children. Similarly, recent reports of influenza-associated acute necrotizing encephalopathy in the United States during the 2023–2025 influenza seasons have increasingly been documented, underscoring the young age groups affected and the associated high mortality rates (*30*). In view of the serious health effects of severe ITES, particularly ASEM/AFCE, our observations highlight the urgent need to establish international multicenter registries and to implement comprehensive strategies for prevention and surveillance.

In conclusion, our study revealed the clinical features of children with SARS-CoV-2 ASEM/AFCE in patients from Asia and Oceania. Mortality rates are overwhelmingly high because of systemic organ failure, and serum cytokine/chemokine profiles exhibited the presence of hypercytokine states in the early stage of disease onset. Further studies are required to elucidate the mechanisms underlying hypercytokine states and establish treatment strategies. In the meantime, clinicians should be aware of SARS-CoV-2–associated encephalopathy cases such as those we describe and monitor at-risk patients for rapidly progressive brain edema and multiorgan failure.

Acknowledgments

We are grateful to the participants and the members of the Japanese Society of Child Neurology for their assistance in data collection for the study.

The study was promoted by the Committee of Collaborative Study Support in the Japanese Society of Child Neurology.

About the Author

Dr. Kasai is a senior researcher at Tokyo Metropolitan Institute of Medical Science, Kamikitazawa, Tokyo, Japan. Her work focuses on neuroinflammatory disease, particularly infection-triggered encephalopathy syndrome.

References

1. Sakuma H, Takanashi JI, Muramatsu K, Kondo H, Shiihara T, Suzuki M, et al.; Japanese Pediatric Neuro-COVID-19 Study Group. Severe pediatric acute encephalopathy syndromes related to SARS-CoV-2. Front Neurosci. 2023;17:1085082. https://doi.org/10.3389/fnins.2023.1085082
2. Kasai M, Sakuma H, Abe Y, Kuki I, Maegaki Y, Murayama K, et al.; Japanese Pediatric Neuro-COVID-19 Study Group. Clinical characteristics of SARS-CoV-2-associated encephalopathy in children: nationwide epidemiological study. J Neurol Sci. 2024;457:122867. https://doi.org/10.1016/j.jns.2024.122867
3. Sakuma H, Thomas T, Debinski C, Eyre M, Han VX, Jones HF, et al. International consensus definitions for infection-triggered encephalopathy syndromes. Dev Med Child Neurol. 2024;67:195–207. https://doi.org/10.1111/dmcn.16067
4. Bacon CJ, Hall SM. Haemorrhagic shock encephalopathy syndrome in the British Isles. Arch Dis Child. 1992;67:985–93. https://doi.org/10.1136/adc.67.8.985
5. Krishnan P, Glenn OA, Samuel MC, Sheriff H, Foster-Barber A, Sejvar JJ, et al. Acute fulminant cerebral edema: a newly recognized phenotype in children with suspected encephalitis. J Pediatric Infect Dis Soc. 2021;10:289–94. https://doi.org/10.1093/jpids/piaa063
6. Kim MG, Stein AA, Overby P, Kleinman G, Nuoman R, Gulko E, et al. Fatal cerebral edema in a child with COVID-19. Pediatr Neurol. 2021;114:77–8. https://doi.org/10.1016/j.pediatrneurol.2020.10.005
7. LaRovere KL, Riggs BJ, Poussaint TY, Young CC, Newhams MM, Maamari M, et al.; Overcoming COVID-19 Investigators. Neurologic involvement in children and adolescents hospitalized in the United States for COVID-19 or multisystem inflammatory syndrome. JAMA Neurol. 2021;78:536–47. https://doi.org/10.1001/jamaneurol.2021.0504
8. Lin JJ, Tu YF, Chen SJ, Kuo YT, Jeng MJ, Hsin-Ju Ko M, et al. Fatal fulminant cerebral edema in six children with SARS-CoV-2 Omicron BA.2 infection in Taiwan. J Pediatric Infect Dis Soc. 2023;12:99–103. https://doi.org/10.1093/jpids/piac116
9. Mizuguchi M, Ichiyama T, Imataka G, Okumura A, Goto T, Sakuma H, et al. Guidelines for the diagnosis and treatment of acute encephalopathy in childhood. Brain Dev. 2021;43:2–31. https://doi.org/10.1016/j.braindev.2020.08.001
10. Zaritsky A, Nadkarni V, Hazinski MF, Foltin G, Quan L, Wright J, et al. Recommended guidelines for uniform reporting of pediatric advanced life support: the pediatric Utstein style. A statement for healthcare professionals from a task force of the American Academy of Pediatrics, the American Heart Association, and the European Resuscitation Council. Pediatrics. 1995;96:765–79. https://doi.org/10.1542/peds.96.4.765
11. Page MJ, McKenzie JE, Bossuyt PM, Boutron I, Hoffmann TC, Mulrow CD, et al. The PRISMA 2020 statement: an updated guideline for reporting systematic reviews. BMJ. 2021;372:n71. https://doi.org/10.1136/bmj.n71
12. Kohyama K, Nishida H, Kaneko K, Misu T, Nakashima I, Sakuma H. Complement-dependent cytotoxicity of human autoantibodies against myelin oligodendrocyte glycoprotein. Front Neurosci. 2023;17:1014071. https://doi.org/10.3389/fnins.2023.1014071
13. Toma K, Aoki K, Kurosawa H, Nishiyama M, Maruyama A. Two cases of COVID-19-related hemorrhagic shock and encephalopathy syndrome with different outcomes. Brain Dev Case Reports. 2024;2:100024. https://doi.org/10.1016/j.bdcasr.2024.100024
14. Ninan S, Thompson P, Gershon T, Ford N, Mills W, Jewells V, et al. Fatal pediatric COVID-19 case with seizures and fulminant cerebral edema. Child Neurol Open. 2021;8:2329048X211022532. https://doi.org/10.1177/2329048X211022532

15. Abdelbari M, Tilouche S, Hannachi S, Bouguila J, Hannachi N, Boughammoura L. Fulminant encephalitis caused by SARS-CoV-2 in a two-month-old infant. Indian J Pediatr. 2023;90:101. https://doi.org/10.1007/s12098-022-04404-9
16. Botre A, Otiv M, Parekar A. Acute fulminant cerebral edema presenting as refractory status epilepticus in a SARS-CoV-2 PCR-positive child without pulmonary involvement. Indian J Pediatr. 2023;90:529. https://doi.org/10.1007/s12098-023-04510-2
17. LaRovere KL, Poussaint TY, Young CC, Newhams MM, Kucukak S, Irby K, et al.; Overcoming COVID-19 Investigators. Changes in distribution of severe neurologic involvement in US pediatric inpatients with COVID-19 or multisystem inflammatory syndrome in children in 2021 vs 2020. JAMA Neurol. 2023;80:91–8. https://doi.org/10.1001/jamaneurol.2022.3881
18. Kim M, Choi Y, Kim SY, Cho A, Kim H, Chae JH, et al. Severe neurological manifestation associated with coronavirus disease 2019 in children during the Omicron variant-predominant period. Pediatr Neurol. 2024;156:17–25. https://doi.org/10.1016/j.pediatrneurol.2024.04.004
19. Kurane K, Wakae K, Yamagishi H, Kawahara Y, Ono M, Tamura D, et al. The first case of hemorrhagic shock and encephalopathy syndrome with fulminant hypercytokinemia associated with pediatric COVID-19. Brain Dev. 2023;46:44–8. https://doi.org/10.1016/j.braindev.2023.08.008
20. Levin M, Hjelm M, Kay JD, Pincott JR, Gould JD, Dinwiddie R, et al. Haemorrhagic shock and encephalopathy: a new syndrome with a high mortality in young children. Lancet. 1983;322:64–7. https://doi.org/10.1016/S0140-6736(83)90057-0
21. Rinka H, Yoshida T, Kubota T, Tsuruwa M, Fuke A, Yoshimoto A, et al. Hemorrhagic shock and encephalopathy syndrome—the markers for an early HSES diagnosis. BMC Pediatr. 2008;8:43. https://doi.org/10.1186/1471-2431-8-43
22. Kuki I, Inoue T, Nukui M, Okazaki S, Kawawaki H, Ishikawa J, et al. Effect of higher body temperature and acute brain edema on mortality in hemorrhagic shock and encephalopathy syndrome. J Neurol Sci. 2022;439:120321. https://doi.org/10.1016/j.jns.2022.120321
23. Yamaguchi H, Nishiyama M, Tokumoto S, Ishida Y, Tomioka K, Aoki K, et al. Elevated cytokine, chemokine, and growth and differentiation factor-15 levels in hemorrhagic shock and encephalopathy syndrome: a retrospective observational study. Cytokine. 2021;137:155324. https://doi.org/10.1016/j.cyto.2020.155324
24. Shi C, Pamer EG. Monocyte recruitment during infection and inflammation. Nat Rev Immunol. 2011;11:762–74. https://doi.org/10.1038/nri3070
25. Wong KL, Tai JJ, Wong WC, Han H, Sem X, Yeap WH, et al. Gene expression profiling reveals the defining features of the classical, intermediate, and nonclassical human monocyte subsets. Blood. 2011;118:e16–31. https://doi.org/10.1182/blood-2010-12-326355
26. Karki R, Kanneganti TD. The 'cytokine storm': molecular mechanisms and therapeutic prospects. Trends Immunol. 2021;42:681–705. https://doi.org/10.1016/j.it.2021.06.001
27. Merad M, Martin JC. Pathological inflammation in patients with COVID-19: a key role for monocytes and macrophages. Nat Rev Immunol. 2020;20:355–62. https://doi.org/10.1038/s41577-020-0331-4
28. Xiang-Hua Y, Le-Min W, Ai-Bin L, Zhu G, Riquan L, Xu-You Z, et al. Severe acute respiratory syndrome and venous thromboembolism in multiple organs. Am J Respir Crit Care Med. 2010;182:436–7. https://doi.org/10.1164/ajrccm.182.3.436
29. Buszko M, Park JH, Verthelyi D, Sen R, Young HA, Rosenberg AS. The dynamic changes in cytokine responses in COVID-19: a snapshot of the current state of knowledge. Nat Immunol. 2020;21:1146–51. https://doi.org/10.1038/s41590-020-0779-1
30. Silverman A, Walsh R, Santoro JD, Thomas K, Ballinger E, Fisher KS, et al.; Influenza-Associated Acute Necrotizing Encephalopathy (IA-ANE) Working Group. Influenza-associated acute necrotizing encephalopathy in US children. JAMA. 2025;334:692–701. https://doi.org/10.1001/jama.2025.11534

Address for correspondence: Hiroshi Sakuma, Department of Brain and Neurosciences, Tokyo Metropolitan Institute of Medical Science, 2-1-6 Kamikitazawa, Setagaya-ku, Tokyo 156-8506, Japan; email: sakuma-hs@igakuken.or.jp

Predictors of Fatal Outcomes among Pediatric Patients Hospitalized for Rocky Mountain Spotted Fever, Sonora, Mexico, 2004–2024[1]

Stephanie Bellman, Kaci D. McCoy, Diana Enriquez, Pamela Romo, JongIn Hwang, Kathleen Weimer, Sarah M. Gunter, José Luis Alomía-Zegarra, Kristy O. Murray,[2] Gerardo Álvarez-Hernández[2]

The tickborne disease Rocky Mountain spotted fever (RMSF) remains life-threatening among children in northern Mexico. We retrospectively investigated 500 pediatric RMSF patients hospitalized in Sonora during 2004–2024. We analyzed clinical, laboratory, and sociodemographic data to identify predictors of fatality by using descriptive statistics and multivariable logistic regression. We found that the overall case-fatality rate was 19.8%, decreasing over time from 31.4% (2004–2013) to 14.5% (2014–2024). Fatal outcomes were associated with delayed doxycycline treatment (>5 days after symptom onset), older age, Indigenous background, and abnormal laboratory markers. Among survivors, 16% had life-altering sequelae, including amputations and neurologic deficits. Cases occurred year-round, predominantly in urban settings. Timely doxycycline administration remains a critical factor in reducing mortality rates. Vulnerable populations, including persons living in poverty, children >10 years of age, and Indigenous communities, require targeted interventions. Strengthening early diagnosis and understanding mechanisms underlying severe disease and death could improve RMSF outcomes in endemic regions.

Rocky Mountain spotted fever (RMSF) is a severe, often fatal tickborne disease caused by *Rickettsia rickettsii* bacteria (*1*). Although multiple hard tick species carry *R. rickettsii*, the brown dog tick (*Rhipicephalus sanguineus* sensu lato) has emerged as the predominant vector in the southwestern United States and in Mexico (*2*,*3*). RMSF is associated with high case-fatality rates (CFRs), particularly in communities with lower socioeconomic status where close contact with tick-infested dogs is common (*4*).

RMSF is endemic in the Americas (*1*). During 2009–2023, Mexico reported 9,153 cases of spotted fever rickettsioses (SFR), including RMSF, nearly half of which occurred in US-bordering states. The state of Sonora had the highest CFR of the region; 37.9% of patients died from their infections (*5*), exceeding the 24% CFRs in the United States in the preantibiotic era (*6*), and far exceeding current US CFR estimates of 5%–10% (*7*). Of note, in Sonora, children accounted for more than half of confirmed RMSF cases and more than one quarter of deaths (*5*).

Without prompt doxycycline treatment, RMSF can rapidly progress to multiorgan failure and death; survivors can experience life-altering sequelae, including neurologic deficits or limb amputations

Author affiliations: Emory University School of Medicine, Atlanta, Georgia, USA (S. Bellman, K.D. McCoy, J. Hwang, K. Weimer, K.O. Murray); Children's Healthcare of Atlanta, Atlanta (S. Bellman, K.D. McCoy, J. Hwang, K. Weimer, K.O. Murray); University of Sonora, Hermosillo, Mexico (D. Enriquez, P. Romo, G. Álvarez-Hernández); Baylor College of Medicine and Texas Children's Hospital, Houston, Texas, USA (S.M. Gunter); Secretaría de Salud Pública del Estado de Sonora, Hermosillo (J.L. Alomía-Zegarra); Hospital Infantil del Estado de Sonora, Hermosillo (G. Álvarez-Hernández)

DOI: https://doi.org/10.3201/eid3202.251223

[1]Preliminary results from this study were presented at the Southeastern Pediatric Research Conference; June 6, 2025; Atlanta, Georgia, USA; and at the American Society of Tropical Medicine and Hygiene Conference; November 10, 2025; Toronto, Ontario, Canada.

[2]These senior authors contributed equally to this article.

(*7*,*8*). Treatment delays of >5 days from symptom onset triple the risk for death (*8*). Early symptoms, including fever, malaise, headache, and rash, are nonspecific and resemble other diseases like dengue and COVID-19 (*9*,*10*). Diagnostic limitations further complicate timely treatment: indirect immunofluorescent antibody (IFA) testing often requires send-out testing and confirmation of paired acute and convalescent samples (*11*), which typically takes days to weeks; PCR lacks sensitivity (*12*); and immunohistochemical (IHC) staining is not widely available and requires collection of tissue, often a punch biopsy of a rash lesion (*13*).

Previous studies identified clinical predictors of fatal outcomes in children, including septic shock, acute kidney injury, neurologic complications, hemorrhages, and hemophagocytic lymphohistiocytosis (*8*,*14*,*15*). Treatment-related factors, such as mechanical ventilation, inotropic support, intravenous fluid supplementation, and delayed doxycycline administration, also contribute to adverse outcomes (*16*). Although those aspects have been researched in Sonora (*8*,*10*,*17*), how clinical manifestations, treatment, and outcomes of hospitalized pediatric patients have evolved over the past 2 decades remain unclear. We examined trends in pediatric RMSF case-patients hospitalized at Sonora's main public pediatric hospital during 2004–2024 to describe clinical characteristics and identify predictors of severe and fatal outcomes that can inform strategies to improve outcomes for children infected with RMSF.

Materials and Methods

Data Collection

We conducted a retrospective analysis of medical records from all children hospitalized with suspected SFR at the primary public pediatric referral center in the state of Sonora, Hospital Infantil del Estado de Sonora (HIES), during January 2, 2004–December 31, 2024. Case-patients included those who had RMSF or SFR diagnoses and an acute illness of <2 weeks' duration that was characterized by fever, headache or irritability, and a rash that might involve the palms and soles. We assigned patients codes A77.0 (Spotted fever due to *Rickettsia rickettsii*) or A77.9 (Spotted fever, unspecified) from the International Classification of Diseases, 10th Revision (ICD-10) (*18*), on the basis of final classification. Laboratory confirmation was established either through a single blood sample testing positive for *R. rickettsii* or *Rickettsia* spp. by PCR or by positive IgG titer >1:64 using IFA. When laboratory confirmation was not possible, we used clinical and epidemiologic criteria to support the diagnosis. We identified a total of 558 case-patients and excluded 58 case-patients for whom we were unable to confirm clinical, laboratory, or discharge diagnoses, yielding a total of 500 case-patients for analysis. Original data collection was approved by the Research Ethics Committee (registration no. 2869) of HIES (registration no. 003/23, approved June 20, 2023), and secondary analysis of de-identified data was determined to be nonhuman subjects research by the institutional review board of Emory University (Atlanta, GA, USA) on April 1, 2025.

HIES investigators trained in standardized chart review procedures and blinded to the study objectives extracted data from medical records. Extracted variables included clinical signs and symptoms, laboratory data at admission, sociodemographic variables, method of diagnostic confirmation, and factors related to medical care (e.g., day of symptom onset, day of doxycycline initiation), as well as discharge outcomes. The socioeconomic status (SES) variable represents an internal categorization by HIES, which primarily serves patients without any formal health insurance system affiliation, generally representing middle- and low-income populations. HIES classifies patients into 8 socioeconomic categories, which we dichotomized as having either sufficient or insufficient economic resources.

When available, we categorized patient weights and heights as moderately underweight if the weight-for-age was <2 SD below the median for sex and malnourished if body mass index (BMI) was <2 SD below the median for children ≥24 months of age or if weight-for-length was below the second percentile for children <24 months of age. We made those categorizations on the basis of World Health Organization International Growth Charts for children <24 months (*19*) and the US Centers for Disease Control and Prevention (CDC) Growth Charts for persons ≥24 months of age (*20*), as recommended by CDC (*21*). Because CDC charts report percentiles, we calculated the 2 SD threshold of weight by using the formula documented (*22*).

Data Analysis

We estimated annual cumulative incidence and mortality rates per million pediatric population from 2004–2024. The denominator for those calculations was the pediatric population (children 0–18 years of age) covered by the Ministry of Health, representing ≈32% of the total population. We calculated CFRs by using the number of deaths as the numerator and the

number of confirmed case-patients at HIES as the denominator. We plotted polynomial-smoothed temporal trends for those epidemiologic indicators and assessed statistical significance by using the coefficient of determination (R^2) and 95% CIs.

For statistical analysis, we primarily stratified study participants by case outcome (i.e., fatal or nonfatal) and period of occurrence (2004–2013 vs. 2014–2024). We additionally performed subanalyses, assessing disease severity by stratifying case-patients with long-term sequelae or death versus those whose disease resolved without sequelae, and among survivors, comparing those with long-term sequelae versus those without.

We used R version 4.5.0 (The R Project for Statistical Computing, https://www.r-project.org) to perform descriptive statistical analysis to evaluate the clinical characteristics of the study population. We assessed laboratory values both as continuous and categorical variables, classified as normal or abnormal on the basis of age-specific reference ranges (*23*). We used Kruskal-Wallis analysis of variance, Fisher exact test, and Pearson χ^2 test to compare differences between groups. We considered $p<0.05$ statistically significant for all predictors except clinical symptoms and laboratory values, for which we considered $p<0.001$ significant, applying a Bonferroni correction for multiple comparisons (*24*).

We conducted bivariable and multivariable logistic regression analyses to assess associations between predictors and fatality and developed a multivariable model to evaluate sociodemographic and treatment-associated factors. To decrease collinearity, we selected predictors by choosing 1 representative variable per concept by lowest p value in bivariable analysis or, if all nonsignificant, least manipulated (e.g., continuous instead of categorical age) and excluded variables with >10 missing values. We entered all candidate variables into the model and assessed collinearity by using car package version 3.1-3 (all variance inflation factor <5; https://CRAN.R-project.org/package=car), followed by backward selection using the stepAIC function from MASS package version 7.3-65 (https://CRAN.R-project.org/package=MASS) to obtain the final model with the lowest Akaike information criteria (AIC). We also calculated adjusted odds ratios (aORs) and 95% CIs.

Results

RMSF incidence at HIES rose steadily during 2004–2015, then fluctuated, with subsequent peaks in 2018 and 2022 (Figure 1, panel A). During the study period, 500 children were hospitalized with RMSF, and 372 (74.4%) had laboratory-confirmed RMSF. The overall CFR was 19.8% (99/500), decreasing from 31.4% (49/156) in 2004–2013 to 14.5% (50/344) in 2014–2024 (odds ratio [OR] 0.37 [95% CI 0.24–0.58]; $p<0.001$). CFR rose until the early 2010s, then declined modestly ($R^2 = 0.3326$), with a relative increase after 2020. Mortality rates began to decline around 2013 and then stabilized at ≈20 deaths/1 million children served by the Ministry of Health annually (Figure 1, panel B).

In addition to the high mortality rates, 16% (n = 64) of survivors experienced severe, permanent sequelae, including amputations and neurologic impairment. Those outcomes declined from 25.3% (25/99) during 2004–2013 to 13% (39/301) during 2014–2024 (OR 0.50 [95% CI 0.29–0.89]; p = 0.016). Overall, 32.7% (163/499) of case-patients experienced either death or life-altering sequelae, a rate that nearly halved from 47.4% (74/156) during 2004–2013 to 25.9% (89/343) during 2014–2024.

Case-patients were concentrated in central and southern Sonora, particularly in Hermosillo, the state capital and most populous city (Figure 2). We noted an urban predominance; 420 case-patients were from urban areas versus 80 from rural regions; however, fatality rates did not differ significantly by setting (p = 0.36) (Table 1). RMSF cases occurred year-round, and we did not note any seasonal or monthly patterns (Appendix Figure, https://wwwnc.cdc.gov/EID/article/32/2/25-1223-App1.pdf). In addition, most (93.5%) children had a documented history of tick exposure before hospitalization.

Sociodemographic Features

Slightly more case-patients were male (54%) than female (46%); we found no significant association between sex and fatality (p = 0.50) (Table 1). Most (87%) children were classified as having insufficient SES; ≈10% were of Indigenous origin, representing 10 ethnic groups, and most resided in impoverished suburban or rural communities. During 2014–2024, older age was significantly associated with higher CFR, and the median age among fatal cases was 10.3 (interquartile range [IQR] 6.9–14.2) years versus 8.5 (IQR 5.5–12.2) years in nonfatal cases (p = 0.048); that association was not observed across the full study period.

Clinical and Laboratory Features

The most common clinical features at hospital admission were fever (100%); exanthema (95%) (Figure 3, panels A, B), notably on palms (81%) or soles (77%); and headache (88%) (Appendix Table 1). Features

significantly (p<0.001 for all) associated with fatal outcomes were vomiting, petechial rash, hemorrhage, ecchymosis and necrosis (Figure 3, panels C, D), respiratory distress, pulmonary and peripheral edema, hepatomegaly, neurologic alterations (e.g., altered mental status, confusion, seizures, encephalitis, coma), hypovolemia, and shock (Appendix Table 1).

The most frequent abnormal laboratory findings, defined as values outside age-specific reference ranges (23), were procalcitonin (98%), aspartate aminotransferase (AST) (92%), lactate dehydrogenase (LDH) (91%), platelet count (85%), prothrombin time (PT) (85%), alanine aminotransferase (ALT) (81%), and serum sodium (81%) (Appendix Table 2). Nearly all laboratory parameters we assessed were significantly associated with fatality (p<0.001), including leukocytosis, neutrophilia, elevated neutrophil-to-lymphocyte ratio (NLR), thrombocytopenia, elevated procalcitonin, prolonged prothrombin time (PT) and partial thromboplastin time (PTT), elevated liver enzymes (AST, ALT, LDH), elevated creatinine, low albumin, and low total protein (Table 2). Although both fatal and nonfatal cases had many abnormal values, those values were markedly more severe in the fatal group; for example, the median platelet count was 17,000/μL in fatal cases versus 60,000/μL in nonfatal cases (reference range 150,000–450,000/μL) (Table 2).

Clinical Course and Outcomes

Children with fatal outcomes were hospitalized later, at a median of 6 (IQR 4–7) days after symptom onset, compared with 5 (IQR 3–7) days in nonfatal cases (p<0.001) (Figure 4; Appendix Table 1). Children with later hospitalization times were also significantly more likely to develop complications during hospitalization, including vascular instability, secondary

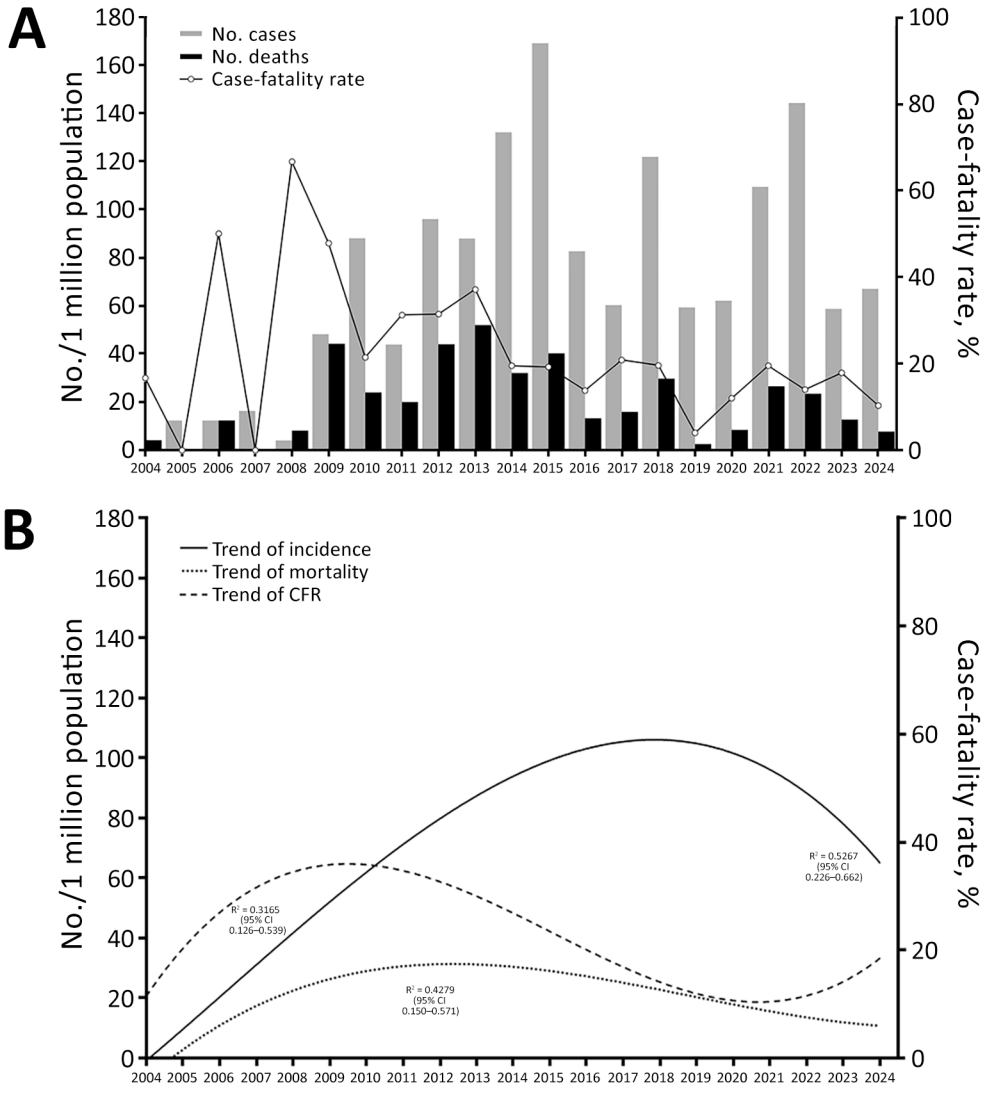

Figure 1. Incidence of cases and deaths per 1 million children and case-fatality rates over time in study of predictors of fatal outcomes among pediatric patients hospitalized for Rocky Mountain spotted fever, Sonora, Mexico, 2004–2024. A) Cumulative rates; B) polynomic trends. Scale bars for y-axes differ substantially to underscore patterns but do not permit direct comparisons.

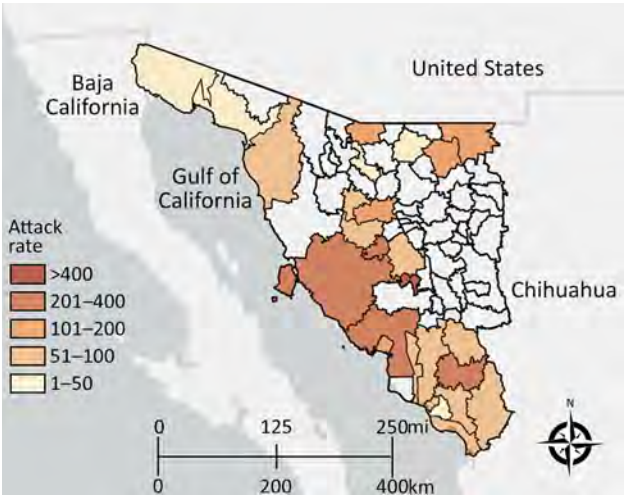

Figure 2. Attack rates by municipality of residence in study of predictors of fatal outcomes among pediatric patients hospitalized for Rocky Mountain spotted fever, Sonora, Mexico, 2004–2024. Map created by Esri ArcGIS Online (https://www.esri.com), June 2025. The map includes data from Esri, TomTom (https://www.tomtom.com), Garmin (https://www.garmin.com), Food and Agriculture Organization of the United Nations (https://www.fao.org), National Oceanic and Atmospheric Administration (https://www.noaa.gov), US Geological Survey (https://www.usgs.gov), OpenStreetMap contributors (https://www.openstreetmap.org), and the GIS User Community (https://communitymaps.arcgis.com).

bacterial infections, neurologic disturbances, respiratory distress, acute renal failure, and shock (all p<0.001) (Table 3).

Doxycycline was administered at a median of 6 (IQR 5–7) days of illness in fatal cases versus 5 (IQR 3–7) days in nonfatal cases. Delayed treatment (>5 days) was significantly associated with death (p = 0.01) (Table 3). During 2014–2024, physicians more frequently initiated doxycycline within 5 days of symptom onset than during 2004–2013 (59% vs. 50%). Overall, 98% (490/500) of children received doxycycline during hospitalization, and 55% (276/500) received it within 5 days of symptom onset. Of the 10 children who did not receive doxycycline, 9 died and 1 survived; 2 of those children (both with fatal outcomes) were from Indigenous backgrounds, and the other 8 children (7 fatal with outcomes) were non-Indigenous. Of note, 40 children died despite receiving timely treatment, representing 40% of recorded deaths.

Multivariable Model

For the multivariable model, we assessed the following variables as potential predictors for death: sex, age, urbanicity, region, exposure to ticks, SES, Indigenous background, season (fall/winter/summer/spring), days of in-hospital treatment with doxycycline, time to doxycycline treatment, number of symptomatic days before hospital arrival, treatment with doxycycline monotherapy, and multidrug therapy. The best-fit model included ethnicity, days of in-hospital doxycycline treatment, time to doxycycline treatment, and doxycycline monotherapy (Table 4). After adjusting for other predictors, both a higher number of days from symptom onset to doxycycline treatment (aOR 1.19 [95% CI 1.08–1.31]) and Indigenous background (aOR 2.84 [95% CI 1.15–6.90]) were associated with higher odds of death. In contrast, doxycycline monotherapy (intravenous or oral) was protective (aOR 0.18 [95% CI 0.08–0.38]), as was more days of in-hospital doxycycline (aOR 0.63 [95% CI 0.57–0.69]) (Table 4).

Morbidity Subanalysis

Among hospitalized RMSF survivors, 64 (16%) were discharged with long-term sequelae, including neurologic impairments, amputations, and cardiac or respiratory complications. Children with long-term sequalae were more likely to be Indigenous (p = 0.006) and have delayed doxycycline treatment (p = 0.04) than children discharged without sequelae. Children with long-term sequalae also more frequently had rash on the palms or soles, petechiae, and signs of disease progression (e.g., hepatomegaly, neurologic signs, edema, and shock) (Appendix Table 3). Laboratory abnormalities were also more common in that group, and we noted statistically significant differences in platelet count, AST, LDH, serum albumin, and total protein levels (all p<0.001) (Appendix Table 4). As in fatal cases, children who survived with sequelae had a median time to doxycycline treatment of 6 days, but children without sequalae were treated at a median of 5 days (Appendix Table 3). Analyses combining sequelae and death as adverse outcomes yielded results similar to those observed when comparing fatal to nonfatal cases.

Discussion

Our findings indicate that RMSF remains a major pediatric health concern among the population in Sonora, Mexico. Although the CFR declined to 14.5% during 2014–2024, it remains twice as high as that of neighboring Arizona, USA (7%), during 2008–2017 (*25*). However, CFR was lower than the 24.1% observed in Brazil (2007–2015) (*26*) and CFRs from other areas of Mexico, ranging from 20.2% (*8*) to 58.8% (*27*). In those regions, fatal outcomes are closely linked to a complex interplay of social and ecologic determinants, including limited access to healthcare (*28*) and high exposure to *R. sanguineus*–infected ticks,

Table 1. Sociodemographic characteristics of children in study of predictors of fatal outcomes among pediatric patients hospitalized for Rocky Mountain spotted fever, Sonora, Mexico, 2004–2024*

Characteristics	Fatal cases	Nonfatal cases	Total	p value†
Sex			500	
M	50 (50.5)	219 (54.6)	269 (53.8)	0.50
F	49 (49.5)	182 (45.4)	231 (46.2)	
Age range, y			500	
0–4	26 (26.3)	86 (21.4)	112 (22.4)	0.41
5–9	34 (34.3)	167 (41.7)	201 (40.2)	
10–14	27 (27.3)	113 (28.2)	140 (28.0)	
15–19	12 (12.1)	35 (8.7)	47 (9.4)	
Median age, y (IQR)	8.3 (4.1–12.3)	8.3 (5.3–11.6)	8.3 (5.3–11.8)	0.72
Residence			500	
Urban	80 (80.8)	340 (84.8)	420 (84.0)	0.36
Rural	19 (19.2)	61 (15.2)	80 (16.0)	
History of tick contact			492	
Y	86 (91.5)	374 (94.0)	460 (93.5)	0.36
N	8 (8.5)	24 (6.0)	32 (6.5)	
Socioeconomic status‡			499	
Insufficient	82 (82.8)	350 (87.5)	432 (86.6)	0.25
Sufficient	17 (17.2)	50 (12.5)	67 (13.4)	
Ethnicity			500	
Non-Indigenous	83 (83.8)	366 (91.3)	449 (89.8)	**0.04**
Indigenous	16 (16.2)	35 (8.7)	51 (10.2)	
Weight			260	
Underweight	3 (8.3)	17 (7.6)	20 (7.7)	0.75
BMI or weight-for-length§			260	
Malnourished	3 (3.8)	16 (7.1)	19 (7.3)	0.73

*Values are no. (%) except as indicated. Bold font indicates statistical significance (p<0.05). BMI, body mass index; IQR, interquartile range.
†Based on Fisher exact test, Pearson's χ^2, or Kruskal-Wallis analysis of variance.
‡Hospital Infantil del Estado de Sonora classifies patients into 8 socioeconomic categories, which we dichotomized as having either sufficient or insufficient economic resources.
§BMI was calculated for children ≥24 months of age; weight-for-length was calculated for children <24 months of age.

particularly among children living near large populations of free-roaming or stray dogs (*29*).

We found that one third of children in this study died or experienced long-term disability because of RMSF. That finding highlights the need to systematically incorporate severe sequelae into clinical assessments to more accurately estimate the true burden of RMSF in pediatric populations and to avoid

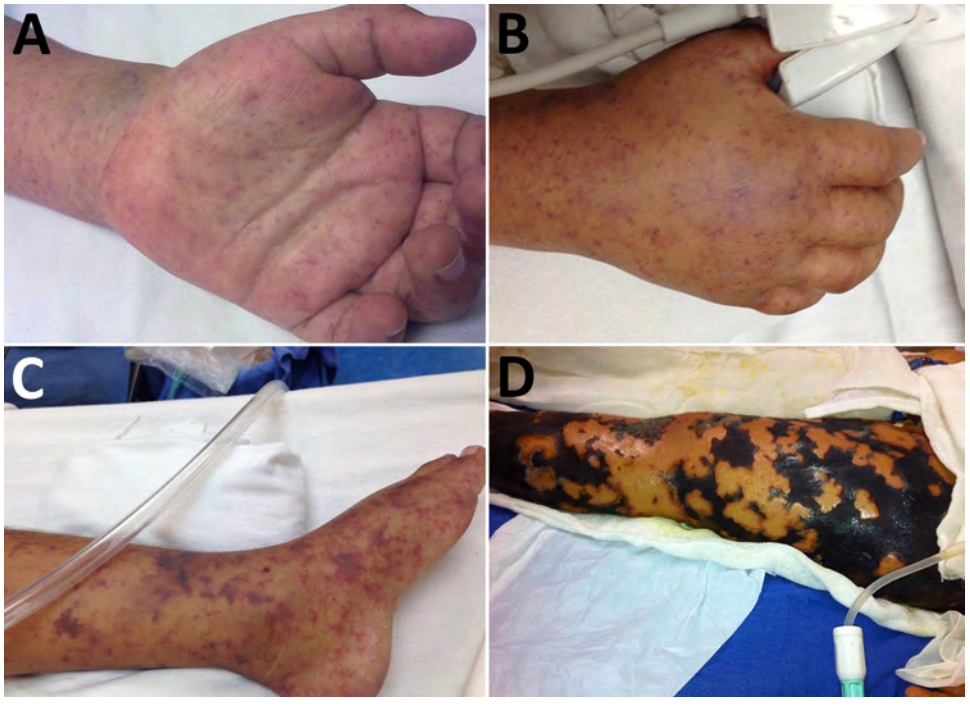

Figure 3. Clinical progress of children in in study of predictors of fatal outcomes among pediatric patients hospitalized for Rocky Mountain spotted fever, Sonora, Mexico, 2004–2024. A) Maculopapular rash on the palm of an 8-year-old child, observed on day 3 after symptom onset. B) Edema with petechia on the dorsum of the hand of a 6-year-old child, observed on day 5 after symptom onset. C) Ecchymotic patches on the foot and ankle of a 7-year-old child, observed on day 7 after symptom onset. D) Necrosis of the left lower limb in another 7-year-old child, observed on day 24 of disease progression.

Table 2. Laboratory findings at admission for fatal and nonfatal cases in study of predictors of fatal outcomes among pediatric patients hospitalized for Rocky Mountain spotted fever, Sonora, Mexico, 2004–2024*

Indicator	No. cases	Median (interquartile range)			p value†
		Fatal	Nonfatal	Total	
Hemoglobin, g/dL	497	11.3 (10.3–12.8)	11.5 (10.3–12.5)	11.4 (10.3–12.5)	0.75
Hematocrit, %	494	34.1 (30.4–37.5)	33.7 (30.4–36.9)	33.8 (30.4–37.0)	0.92
Blood leukocytes, × 10^3/μL	498	17 (10–26)	8 (6–13)	9 (6–15)	**<0.001**
Absolute lymphocyte count, × 10^3 cells/μL	475	1.8 (0.8–3.3)	1.1 (0.8–2.0)	1.2 (0.8–2.1)	0.007
Absolute neutrophil count, × 10^3 cells/μL	477	11.1 (8.1–18.8)	5.9 (4.0–9.0)	6.7 (4.3–10.5)	**<0.001**
Neutrophil-to-lymphocyte ratio	471	8 (4–15)	5 (3–9)	5 (3–9)	**<0.001**
Platelets, × 10^3 cells/μL	497	17 (10–25)	60 (27–120)	46 (20–103)	**<0.001**
Serum procalcitonin, ng/mL	337	20 (8–44)	4 (1–11)	6 (2–18)	**<0.001**
Prothrombin time, sec	488	18.0 (15.8–20.7)	15.1 (13.9–16.2)	15.5 (14.1–17.1)	**<0.001**
Partial thromboplastin time, sec	486	47 (41–56)	39 (32–43)	40 (33–45)	**<0.001**
Aspartate aminotransferase, U/L	488	253 (171–398)	115 (61–165)	132 (70–205)	**<0.001**
Alanine aminotransferase, U/L	487	83 (65–115)	55 (34–82)	61 (37–90)	**<0.001**
Lactate dehydrogenase, U/L	384	1,479 (1,055–1,928)	752 (549–998)	839 (574–1224)	**<0.001**
Serum sodium level, mq/L	492	130 (126–135)	132 (129–136)	132 (129–136)	0.003
Serum creatinine, mg/dL	451	1.5 (0.8–2.6)	0.5 (0.4–0.6)	0.6 (0.4–0.9)	**<0.001**
Serum albumin, g/dL	416	2.8 (2.4–3.1)	3.2 (2.8–3.9)	3.1 (2.7–3.8)	**<0.001**
Serum total protein, mg/dL	417	5.0 (4.3–5.8)	5.8 (5.0–6.4)	5.6 (4.9–6.3)	**<0.001**

*Bold font indicates statistical significance (p<0.001).
†Based on Kruskall-Wallis analysis of variance or Fisher exact test; statistical significance determined by Bonferroni correction.

underestimation when only considering in-hospital deaths (*30*). Our analysis also revealed a shift in the age-related risk for death and that children >10 years of age had increased fatality rates during the last decade of the study period. Historically, children <10 years of age were considered the most vulnerable to severe RMSF outcomes (*31*). Although the reasons for the shift remain unclear, increased awareness and clinician training, particularly regarding doxycycline safety in young children, might partially explain the trend. Further research is needed to explore specific vulnerabilities to RMSF among adolescents.

We also found significant associations between Indigenous background and negative outcomes, including both death and long-term sequelae. That finding could partially be related to lack of doxycycline administration among the population because a greater percentage of Indigenous versus non-Indigenous children (3.9% vs. 1.8%) received no doxycycline treatment. That disparity also could reflect a range of factors not fully captured in our dataset. Although Indigenous populations in Mexico have historically faced systemic inequities in health access and social services (*32*), further research should explore additional contributors to poor outcomes in that population, such as the regional presence of highly virulent *R. rickettsii* genetic clades (e.g., Taiaçu and Sheila Smith) (*33*), glucose-6-phosphate dehydrogenase deficiency (*34*), barriers within primary or nonreferral healthcare systems, and social determinants related to language, beliefs, and cultural practices (*3*,*28*,*35*). Those factors are particularly relevant given the annual migration of ≈160,000 agricultural workers, many from diverse Indigenous communities, from southern to northwest Mexico (*36*), including RMSF-endemic areas of Sonora.

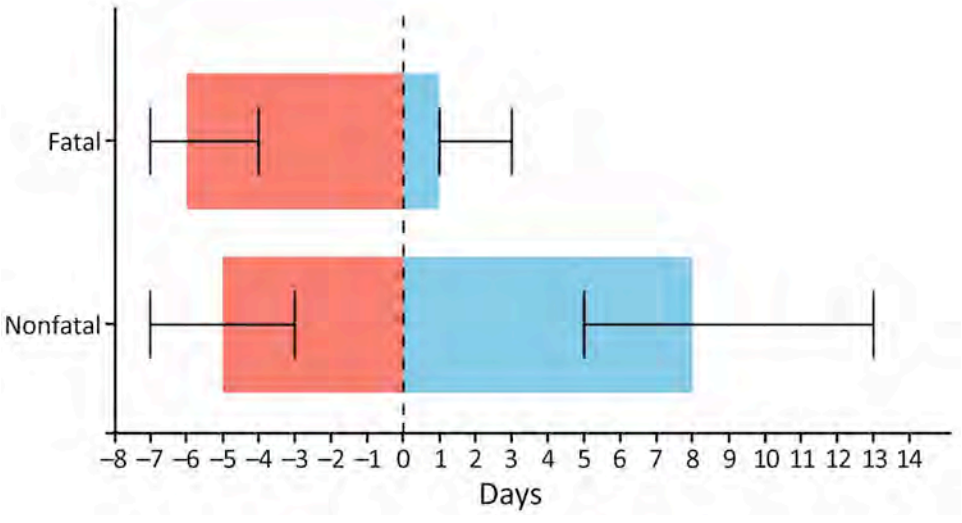

Figure 4. Analysis of days from symptom onset to hospitalization and length of hospital stay as predictors of fatal outcomes among pediatric patients hospitalized for Rocky Mountain spotted fever, Sonora, Mexico, 2004–2024. Horizontal bars represent median time from symptom onset to hospitalization (red bars) and length of hospital stay (blue bars) for fatal and nonfatal cases; whiskers indicate 95% CIs. Vertical dotted line indicates day of hospital admission.

Table 3. Treatment and outcomes for fatal and nonfatal cases in study of predictors of fatal outcomes among pediatric patients hospitalized for Rocky Mountain spotted fever, Sonora, Mexico, 2004–2024*

Characteristic	No. cases	No. (%) cases			p value†
		Fatal	Nonfatal cases	Total	
Doxycycline initiated	500				**0.01**
≤5 days		40 (40.4)	236 (58.9)	276 (55.2)	
≥6 days		50 (50.5)	164 (40.9)	214 (42.8)	
Not treated		9 (9.1)	1 (0.2)	10 (2.0)	
Clinical complications‡					
Vascular§	496	80 (83.3)	106 (26.5)	186 (37.5)	**<0.001**
Bacterial¶	494	72 (75.0)	141 (35.4)	213 (43.1)	**<0.001**
Neurologic#	461	14 (21.5)	58 (14.6)	72 (15.6)	0.19
Acute respiratory distress syndrome	500	63 (63.6)	89 (22.2)	152 (30.4)	**<0.001**
Acute renal failure	499	60 (61.2)	27 (6.7)	87 (17.4)	**<0.001**
Shock	500	79 (79.8)	135 (33.7)	214 (42.8)	**<0.001**

*Bold font indicates statistical significance (p<0.05).
†Based on Fisher exact or Pearson χ^2 test.
‡Patients could have >1 complication.
§Including hemorrhage, disseminated intravascular coagulation, necrosis, edema of target organs (brain, lung), and others.
¶Including nosocomial pneumonia, meningitis/encephalitis, septic hepatitis, bacterial endocarditis, and others.
#Including neuromuscular disturbances, neuropsychiatric alterations, speech disorders, cerebral palsy, hepatic encephalopathy, and others.

Although 53% of RMSF cases occurred during July–October, Sonora's warmest months, we observed no clear seasonal pattern in incidence or mortality rates, consistent with previous reports (*37*,*38*). Therefore, clinicians should maintain a high index of suspicion for RMSF year-round to ensure timely diagnosis and treatment (*39*). Furthermore, our findings indicate that RMSF in this pediatric population primarily occurs in urban foci, contrasting with the historically rural and suburban distribution of the disease (*40*,*41*). In both the southwestern United States and in Mexico, RMSF is strongly associated with large populations of tick-infested stray and domestic dogs, often concentrated in densely populated, low-income areas, thereby enabling exposure and transmission (*29*,*42*).

The most frequently observed clinical symptoms (fever, rash, and headache) were highly nonspecific, underscoring challenges clinicians face in establishing timely diagnosis and treatment. That finding highlights the urgent need for rapid and reliable diagnostic tools to support early clinical decision-making and prevent disease progression. Currently available methods for confirming RMSF, such as IFA, PCR, and IHC, are valuable for epidemiologic purposes but have limited clinical efficacy because of methodologic constraints and the need for specialized personnel and infrastructure (*43*,*44*). Therefore, strengthening laboratory capacity and developing new rapid diagnostics are essential not only for enhancing RMSF surveillance but also to guide clinical decision-making and improve outcomes in resource-limited settings (*5*,*7*,*28*).

We found that symptoms associated with fatal RMSF outcomes were predominantly related to disruptions in coagulation, vascular permeability, and neurologic function. Those clinical manifestations were supported by abnormal laboratory findings, such as thrombocytopenia, hyponatremia, and elevated liver enzymes and creatinine, consistent with previous studies (*8*,*16*,*27*,*45*). Although many laboratory abnormalities were noted in all case-patients, elevated neutrophil counts, increased NLR (*46*), prolonged PTT, elevated creatinine, hypoalbuminemia, and low total protein were significantly more frequent and severe in fatal cases (p<0.001) (Table 2; Appendix Table 2). Although recognized in other disease contexts (*47*), some of those biomarkers have not been consistently emphasized in the RMSF literature, suggesting their potential as underrecognized indicators of severe and fatal outcomes.

Comparing the clinical manifestations of fatal versus nonfatal cases and survivors with sequalae versus those who fully recovered, several notable trends emerged. As expected, laboratory

Table 4. Sociodemographic and treatment predictors of fatal outcomes among pediatric patients hospitalized for Rocky Mountain spotted fever, Sonora, Mexico, 2004–2024*

Characteristic	β coefficient	SE	aOR (95% CI)†
Intercept	0.13	0.35	1.14 (0.58–2.25)
Ethnicity‡	1.04	0.45	2.84 (1.15–6.90)
Days of in-hospital doxycycline treatment	−0.46	0.05	0.63 (0.57–0.69)
Days from symptom onset to doxycycline treatment	0.17	0.05	1.19 (1.08–1.31)
Treatment with IV or oral doxycycline monotherapy§	−1.71	0.40	0.18 (0.08–0.38)

*Results of logistic multivariable analysis. aOR, adjusted odds ratio; IV, intravenous.
†Accounting for all the variables included in the final model. Ten observations excluded due to missing data.
‡Referent was non-Indigenous.
§Referent was no dose of doxycycline or inclusion of other antibiotics in treatment course.

abnormalities increased with disease severity. Platelet counts were markedly lower in fatal cases (median 17,000/μL) and in survivors with sequelae (median 22,000/μL) compared with fully recovered survivors (median 72,000/μL) (reference range 150,000–450,000/μL), suggesting platelet count could serve as a key marker of RMSF severity. Children discharged with sequelae and those who died also experienced significantly more severe symptoms and complications (e.g., edema, hemorrhage, shock) during hospitalization ($p<0.001$). Of note, case-patients who died more often experienced vomiting and showed substantial differences in PT, PTT, and NLR than those who survived, patterns not observed when comparing surviving case-patients with and without sequalae. Those findings could aid in clinical stratification of disease severity and identifying predictors of fatal outcomes.

Most of the statistically significant clinical signs we identified reflect the severity and rapid progression of RMSF, typically emerging after the fifth day of illness. That delayed clinical manifestation hindered timely intervention and increased the risk for fatal outcomes (*48*), underscoring the need for predictive tools to identify high-risk patients earlier. We propose developing a composite clinical severity score or a machine learning–based algorithm integrating early clinical indicators (e.g., vital signs, basic laboratory parameters, epidemiologic risk factors) to stratify patients at initial examination. Those tools should be built using retrospective clinical data and prospectively validated to ensure rigor and ethical application. Their implementation in endemic areas could substantially improve early diagnosis, guide timely treatment, and reduce RMSF-related fatality.

Our findings reinforce that early doxycycline initiation is critical for avoiding severe outcomes; we found administration beyond 5 days after symptom onset was a strong predictor of death, consistent with previous reports (*3*,*8*). That finding is particularly concerning because during the first decade of our study, half of case-patients received doxycycline after the 5-day threshold. Although the percentage receiving doxycycline >5 days after symptom onset declined to 41% during 2014–2024, delays remained common. Educational efforts targeting healthcare providers and community members appear to have improved timely doxycycline administration, especially in younger children (*39*); nevertheless, further action is needed to improve early recognition and treatment across all ages. Timeliness was also limited by delayed hospital arrival; median time from symptom onset to hospital arrival was 5 days, leaving a narrow window for intervention. Although whether case-patients sought care or received treatment before HIES admission is unclear, the need for 2 key strategies is evident: increasing awareness among primary care providers to initiate doxycycline earlier or refer patients to hospital care without delay, and implementing community-based programs encouraging caregivers to seek immediate care for children with suspected RMSF (*5*,*28*).

The first limitation of this retrospective study is the possibility for selection bias because the cohort included only patients treated at HIES, which primarily treats uninsured and severely ill patients, potentially limiting generalizability to the broader pediatric population affected by RMSF in Sonora. Second, information bias is also a concern because of variability in medical record quality and absence of prehospital care data, and because 25.5% (128/500) of case-patients were clinically diagnosed without laboratory confirmation. As described previously, laboratory confirmation is a pervasive problem for SFR globally, especially in resource-limited settings. Although laboratory confirmation is preferred to validate SFR cases (*49*), clinical manifestations of our identified case-patients aligned with studies published by CDC (*2*,*7*), supporting our conclusions of SFR diagnosis. Those limitations preclude causal inference; rather, our aim was to identify major predictors of fatal outcomes in pediatric RMSF and improve our understanding of its clinical and epidemiologic profile.

In summary, RMSF remains a major cause of severe pediatric illness and death in Sonora. Further research is needed to elucidate host, pathogen, and environmental determinants of RMSF-related mortality and long-term sequelae, especially among low-income communities, children >10 years, and Indigenous populations. Continued investment in diagnostic testing, education, and prevention is essential for reducing the burden of this treatable disease.

Acknowledgments

We thank Christopher Paddock for his helpful expertise on RMSF and Grace Gombolay for her feedback on the clinical interpretation of results.

About the Author

Dr. Bellman is a physician-scientist in training and postdoctoral researcher at Emory University and Children's Healthcare of Atlanta. Her main interests include understanding the ecology and epidemiology of emerging infectious diseases and vectorborne diseases, and improving diagnostics for neglected tropical diseases.

References

1. Dantas-Torres F. Rocky Mountain spotted fever. Lancet Infect Dis. 2007;7:724–32. https://doi.org/10.1016/S1473-3099(07)70261-X
2. Demma LJ, Traeger MS, Nicholson WL, Paddock CD, Blau DM, Eremeeva ME, et al. Rocky Mountain spotted fever from an unexpected tick vector in Arizona. N Engl J Med. 2005;353:587–94. https://doi.org/10.1056/NEJMoa050043
3. Álvarez-Hernández G, Roldán JFG, Milan NSH, Lash RR, Behravesh CB, Paddock CD. Rocky Mountain spotted fever in Mexico: past, present, and future. Lancet Infect Dis. 2017;17:e189–96. https://doi.org/10.1016/S1473-3099(17)30173-1
4. Foley J, Tinoco-Gracia L, Rodriguez-Lomelí M, Estrada-Guzmán J, Fierro M, Mattar-Lopez E, et al. Unbiased assessment of abundance of *Rhipicephalus sanguineus* sensu lato ticks, canine exposure to spotted fever group *Rickettsia*, and risk factors in Mexicali, México. Am J Trop Med Hyg. 2019;101:22–32. https://doi.org/10.4269/ajtmh.18-0878
5. Álvarez-Hernández G, López-Ridaura R, Cortés-Alcalá R, García Rodríguez G, Calleja-López JRT, Rivera-Rosas CN, et al. Rocky Mountain spotted fever in Mexico: a call to action. Am J Trop Med Hyg. 2024;111:1070–7. https://doi.org/10.4269/ajtmh.24-0265
6. Dahlgren FS, Holman RC, Paddock CD, Callinan LS, McQuiston JH. Fatal Rocky Mountain spotted fever in the United States, 1999–2007. Am J Trop Med Hyg. 2012;86:713–9. https://doi.org/10.4269/ajtmh.2012.11-0453
7. Biggs HM, Behravesh CB, Bradley KK, Dahlgren FS, Drexler NA, Dumler JS, et al. Diagnosis and management of tickborne rickettsial diseases: Rocky Mountain spotted fever and other spotted fever group rickettsioses, ehrlichioses, and anaplasmosis—United States. MMWR Recomm Rep. 2016;65:1–44. https://doi.org/10.15585/mmwr.rr6502a1
8. Alvarez-Hernandez G, Murillo-Benitez C, Candia-Plata Mdel C, Moro M. Clinical profile and predictors of fatal Rocky Mountain spotted fever in children from Sonora, Mexico. Pediatr Infect Dis J. 2015;34:125–30. https://doi.org/10.1097/INF.0000000000000496
9. Mora JD, Licona-Enríquez JD, Álvarez-López DI, Aguilar-León DE, Álvarez-Hernández G. Clinical features of patients with Rocky Mountain spotted fever, dengue and chikungunya infection [in Spanish]. Gac Med Mex. 2021;157:58–63. https://doi.org/10.24875/GMM.20000105
10. Álvarez-Hernández G, Rivera-Rosas CN, Calleja-López JRT, Álvarez-Meza JB, Candia-Plata MDC, Cruz-Loustaunau D, et al. A comparison of the clinical and epidemiological profile of Rocky Mountain spotted fever with dengue and COVID-19 in hospitalized children, Sonora, México, 2015–2022. Trop Med Infect Dis. 2025;10:20. https://doi.org/10.3390/tropicalmed10010020
11. McQuiston JH, Wiedeman C, Singleton J, Carpenter LR, McElroy K, Mosites E, et al. Inadequacy of IgM antibody tests for diagnosis of Rocky Mountain spotted fever. Am J Trop Med Hyg. 2014;91:767–70. https://doi.org/10.4269/ajtmh.14-0123
12. Chung IH, Robinson LK, Stewart-Juba JJ, Dasch GA, Kato CY. Analytically sensitive *Rickettsia* species detection for laboratory diagnosis. Am J Trop Med Hyg. 2022;106:1352–7. https://doi.org/10.4269/ajtmh.21-0757
13. Paddock CD, Greer PW, Ferebee TL, Singleton J Jr, McKechnie DB, Treadwell TA, et al. Hidden mortality attributable to Rocky Mountain spotted fever: immunohistochemical detection of fatal, serologically unconfirmed disease. J Infect Dis. 1999;179:1469–76. https://doi.org/10.1086/314776
14. Nogueira Angerami R, Oliveira Morais E, Katz G, Jacintho da Silva L. Brazilian spotted fever in the paediatric age-segment in the state of São Paulo, southeastern Brazil, 2003–2006. Clin Microbiol Infect. 2009;15(Suppl 2):205–6. https://doi.org/10.1111/j.1469-0691.2008.02728.x
15. Hosahalli Vasanna S, Lim PPC, Khan TS, Dalal J. Secondary hemophagocytic lymphohistiocytosis associated with Rocky Mountain spotted fever in a toddler: a case report. eJHaem. 2022;3:463–6. https://doi.org/10.1002/jha2.405
16. Buckingham SC, Marshall GS, Schutze GE, Woods CR, Jackson MA, Patterson LE, et al.; Tick-borne Infections in Children Study Group. Clinical and laboratory features, hospital course, and outcome of Rocky Mountain spotted fever in children. J Pediatr. 2007;150:180-4–184.e1. https://doi.org/10.1016/j.jpeds.2006.11.023
17. Álvarez-Hernández G, Candia-Plata MC, Delgado-de la Mora J, Acuña-Meléndrez NH, Vargas-Ortega AP, Licona-Enríquez JD. Rocky Mountain spotted fever in Mexican children: clinical and mortality factors [in Spanish]. Salud Publica Mex. 2016;58:385–92.
18. World Health Organization. The ICD-10 classification of mental and behavioural disorders: diagnostic criteria for research. Geneva: The Organization; 1993.
19. World Health Organization. Nutrition and Food Safety (NFS). WHO child growth standards: growth velocity based on weight, length and head circumference: methods and development, 1st ed. Geneva: The Organization; 2009.
20. Kuczmarski RJ, Ogden CL, Guo SS, Grummer-Strawn LM, Flegal KM, Mei Z, et al. 2000 CDC growth charts for the United States: methods and development. Vital Health Stat 11. 2002;246:1–190.
21. Grummer-Strawn LM, Reinold C, Krebs NF; Centers for Disease Control and Prevention. Use of World Health Organization and CDC growth charts for children aged 0–59 months in the United States. MMWR Recomm Rep. 2010;59:1–15.
22. Flegal KM, Cole TJ. Construction of LMS parameters for the Centers for Disease Control and Prevention 2000 growth charts. Natl Health Stat Report. 2013;63:1–3.
23. Children's Hospital of Philadelphia Pathology & Laboratory Medicine. Laboratory reference ranges [cited 2025 Aug 5]. https://www.chop.edu/sites/default/files/2024-06/chop-labs-reference-ranges.pdf
24. Armstrong RA. When to use the Bonferroni correction. Ophthalmic Physiol Opt. 2014;34:502–8. https://doi.org/10.1111/opo.12131
25. Centers for Disease Control and Prevention. Data and statistics on spotted fever rickettsiosis [cited 2025 Aug 5]. https://www.cdc.gov/rocky-mountain-spotted-fever/data-research/facts-stats/index.html
26. de Oliveira SV, Guimarães JN, Reckziegel GC, Neves BM, Araújo-Vilges KM, Fonseca LX, et al. An update on the epidemiological situation of spotted fever in Brazil. J Venom Anim Toxins Incl Trop Dis. 2016;22:22. https://doi.org/10.1186/s40409-016-0077-4
27. Estrada-Mendizabal RJ, Tamez-Rivera O, Vela EH, Blanco-Murillo P, Alanis-Garza C, Flores-Gouyonnet J, et al. Rickettsial disease outbreak, Mexico, 2022. Emerg Infect Dis. 2023;29:1944–7. https://doi.org/10.3201/eid2909.230344
28. Álvarez-Hernández G, Paddock CD, Walker DH, Valenzuela JG, Calleja-López JRT, Rivera-Rosas CN, et al. Rocky Mountain spotted fever is a neglected tropical disease in Latin America. PLoS Negl Trop Dis. 2024;18:e0012276. https://doi.org/10.1371/journal.pntd.0012276
29. Foley J, López-Pérez AM, Álvarez-Hernández G, Labruna MB, Angerami RN, Zazueta OE, et al. A wolf at the door: the

ecology, epidemiology, and emergence of community- and urban-level Rocky Mountain spotted fever in the Americas. Am J Vet Res. 2025;86:12. https://doi.org/10.2460/ajvr.24.11.0368
30. Laupland KB, Pasquill K, Parfitt EC, Dagasso G, Gupta K, Steele L. Inhospital death is a biased measure of fatal outcome from bloodstream infection. Clin Epidemiol. 2019;11:47–52. https://doi.org/10.2147/CLEP.S187381
31. Openshaw JJ, Swerdlow DL, Krebs JW, Holman RC, Mandel E, Harvey A, et al. Rocky Mountain spotted fever in the United States, 2000–2007: interpreting contemporary increases in incidence. Am J Trop Med Hyg. 2010;83:174–82. https://doi.org/10.4269/ajtmh.2010.09-0752
32. Pelcastre-Villafuerte BE, Meneses-Navarro S, Sánchez-Domínguez M, Meléndez-Navarro D, Freyermuth-Encis G. Health conditions and use of services among indigenous peoples of Mexico [in Spanish]. Salud Publica Mex. 2020;62:810–9. https://doi.org/10.21149/11861
33. Brito-Lorán CB, Araiza-Rodríguez A, Garcés-Ayala F, Contreras-Pérez CU, Montes-Colima NA, López-Martínez I, et al. Analysis of Rocky Mountain spotted fever cases in northern Mexico reveals genetic variability of *Rickettsia rickettsii* and the different distribution of genotypes. I nt Microbiol. 2023;27:689–95. https://doi.org/10.1007/s10123-023-00424-3
34. Walker DH, Kirkman HN. Rocky Mountain spotted fever and deficiency in glucose-6-phosphate dehydrogenase. J Infect Dis. 1980;142:771. https://doi.org/10.1093/infdis/142.5.771
35. Alvarez-Hernandez G, Drexler N, Paddock CD, Licona-Enriquez JD, la Mora JD, Straily A, et al. Community-based prevention of epidemic Rocky Mountain spotted fever among minority populations in Sonora, Mexico, using a One Health approach. Trans R Soc Trop Med Hyg. 2020;114:293–300. https://doi.org/10.1093/trstmh/trz114
36. Velasco L, Coubes ML, Contreras OF. The vulnerability of migrant farmworkers and COVID-19 [in Spanish] [cited 2025 Aug 5]. https://www.colef.mx/noticia/la-vulnerabilidad-de-los-jornaleros-agricolas-migrantes-y-el-covid-19
37. Zazueta OE, Armstrong PA, Márquez-Elguea A, Hernández Milán NS, Peterson AE, Ovalle-Marroquín DF, et al. Rocky Mountain spotted fever in a large metropolitan venter, Mexico–United States border, 2009–2019. Emerg Infect Dis. 2021;27:1567–76. https://doi.org/10.3201/eid2706.191662
38. Álvarez-López DI, Ochoa-Mora E, Nichols Heitman K, Binder AM, Álvarez-Hernández G, Armstrong PA. Epidemiology and clinical features of Rocky Mountain spotted fever from enhanced surveillance, Sonora, Mexico: 2015–2018. Am J Trop Med Hyg. 2021;104:190–7. https://doi.org/10.4269/ajtmh.20-0854
39. Alvarez-Hernandez G, Ernst K, Acuña-Melendrez NH, Vargas-Ortega AP, Candia-Plata MDC. Medical knowledge related to Rocky Mountain spotted fever in Sonora, Mexico. Trans R Soc Trop Med Hyg. 2018;112:109–14. https://doi.org/10.1093/trstmh/try030
40. Bustamante ME, Varela G. A new rickettsiosis in Mexico. Existence of American spotted fever in the states of Sinaloa and Sonora [in Spanish]. Rev Inst Salubr Enferm Trop. 1943;4:189–211.
41. Bustamante ME, Varela G. Characteristics of Rocky Mountain spotted fever in Sonora and Sinaloa, Mexico (study of 12 cases and 2 strains) [in Spanish]. Rev Inst Salubr Enferm Trop. 1944;5:129–34.
42. Tinoco-Gracia L, Quiroz-Romero H, Quintero-Martínez MT, Rentería-Evangelista TB, González-Medina Y, Barreras-Serrano A, et al. Prevalence of *Rhipicephalus sanguineus* ticks on dogs in a region on the Mexico-USA border. Vet Rec. 2009;164:59–61. https://doi.org/10.1136/vr.164.2.59
43. Paddock CD. Perspectives on the laboratory diagnosis of rickettsial diseases in the 21st century. Acta Med Costarric. 2013;55:13–24.
44. Stewart AG, Stewart AGA. An update on the laboratory diagnosis of *Rickettsia* spp. infection. Pathogens. 2021;10:1319. https://doi.org/10.3390/pathogens10101319
45. Regan JJ, Traeger MS, Humpherys D, Mahoney DL, Martinez M, Emerson GL, et al. Risk factors for fatal outcome from Rocky Mountain spotted fever in a highly endemic area—Arizona, 2002–2011. Clin Infect Dis. 2015;60:1659–66. https://doi.org/10.1093/cid/civ116
46. Buonacera A, Stancanelli B, Colaci M, Malatino L. Neutrophil to lymphocyte ratio: an emerging marker of the relationships between the immune system and diseases. Int J Mol Sci. 2022;23:3636. https://doi.org/10.3390/ijms23073636
47. Jiang J, Liu R, Yu X, Yang R, Xu H, Mao Z, et al. The neutrophil-lymphocyte count ratio as a diagnostic marker for bacteraemia: a systematic review and meta-analysis. Am J Emerg Med. 2019;37:1482–9. https://doi.org/10.1016/j.ajem.2018.10.057
48. Paddock CD, Alvarez-Hernandez G. *Rickettsia rickettsii* (Rocky Mountain spotted fever). In: Long SS, Long SS, Prober GC, Fischer M, Kimberlin D, editors. Principles and practice of pediatric infectious diseases, sixth edition. Philadelphia: Elsevier; 2023. p. 971–975.
49. Centers for Disease Control and Prevention. National Notifiable Diseases Surveillance System. Spotted fever rickettsiosis (including Rocky Mountain spotted fever) (SFR, including RMSF) 2020 case definition [cited 2025 Nov 24]. https://ndc.services.cdc.gov/case-definitions/spotted-fever-rickettsiosis-2020

Address for correspondence: Kristy O. Murray, Department of Pediatrics, Emory University School of Medicine, and Children's Healthcare of Atlanta, 2015 Uppergate Dr, Atlanta, GA 30322, USA; email: kristy.murray@emory.edu

Leptotrombidium imphalum Chiggers as Vector for Scrub Typhus in Human Settlements, India, 2022–2023

Carol S. Devamani, Neal Alexander, Rawadee Kumlert, Benjamin L. Makepeace, Serge Morand, Mary Cameron, Alexandr A. Stekolnikov, Winsley Rose, Daniel Chandramohan, Punam Mangtani, Kundavaram P.P. Abhilash, Wolf-Peter Schmidt

Scrub typhus is a common bacterial infection in many parts of Asia. The causative agent, *Orientia tsutsugamushi*, is transmitted by trombiculid mite (chigger) larvae that require small mammals as maintaining hosts. We studied the prevalence of *O. tsutsugamushi* infection in mites and small mammals in villages and land surrounding them in South India to determine high-risk settings. We identified 12,431 mite larvae on 883 small mammals, 32% of which were bandicoot rats, 31% black rats, and 31% Asian house shrews. *Leptotrombidium imphalum* was the most common mite species and the only species associated with *O. tsutsugamushi* infection (prevalence 3.6%). *Orientia* infection increased with mite population size on a host. Host numbers, the *L. imphalum* index, and the prevalence of *Orientia* infection in chiggers were considerably higher within human settlements than in surrounding fields, suggesting that most human scrub typhus infection occurs inside villages rather than during agricultural work.

Scrub typhus is caused by intracellular bacteria of the genus *Orientia* (family Rickettsiaceae, order Rickettsiales) (*1*). Scrub typhus, caused by *O. tsutsugamushi*, occurs predominantly in South Asia, East Asia, and Southeast Asia (*2*). Severe infection is characterized by acute respiratory distress syndrome, shock, renal failure, and meningoencephalitis (*3*). *Orientia* bacteria are transmitted by the bite of trombiculid mite larvae (chiggers) (*4*) that use small mammals such as rodents and shrews as their primary maintaining hosts (*4*). Humans are regarded as accidental hosts. The India subcontinent is a region marked by a high occurrence of scrub typhus, accounting for up to 35% of hospital admissions for fever (*3*,*5*–*9*).

Groups regarded at risk for scrub typhus, including farmers and military personnel, are thought to acquire infected chiggers in agricultural fields and within disturbed ecosystems such as forest edges (*4*). However, agricultural and other outdoor activities were only weakly associated with scrub typhus in rural settings in South India (*10*,*11*). That finding was confirmed in a cohort study on risk factors for scrub typhus in the state of Tamil Nadu, in which agricultural activities, taking animals for grazing, firewood collection, and open defecation did not increase the risk for scrub typhus (*12*). Furthermore, persons residing at the edge of a village were not at a higher risk than those in the village center. To better understand scrub typhus transmission in South India, we trapped small mammals in highly endemic villages to estimate parameters of scrub typhus ecology.

Methods

We conducted our study in the context of a human cohort study on scrub typhus in 32,279 persons of all ages living in 37 scrub typhus–endemic villages in Vellore and Ranipet, 2 districts of Tamil Nadu (*13*). Study villages had an average size of ≈225 households; mean household size was 4.0. Approximately 55% of the population practiced part-time

Author affiliations: Christian Medical College, Vellore, India (C.S. Devamani, W. Rose, K.P.P. Abhilash); London School of Hygiene and Tropical Medicine, London, UK (N. Alexander, M. Cameron, D. Chandramohan, P. Mangtani, W.-P. Schmidt); Ministry of Public Health, Nonthaburi, Thailand (R. Kumlert); University of Liverpool, Liverpool, UK (B.L. Makepeace); Centre National de la Recherche Scientifique, France–Kasetsart University and Mahidol University, Bangkok, Thailand (S. Morand); Zoological Institute of the Russian Academy of Sciences, St. Petersburg, Russia (A.A. Stekolnikov)

DOI: https://doi.org/10.3201/eid3202.251170

or full-time agriculture. The Institutional Animal Ethics Committee of the Christian Medical College Vellore (Ref 09/2019) and the Animal Welfare and Ethical Review Board of the London School of Hygiene and Tropical Medicine (Ref 2019-10) approved the study. We followed institutional and national (India and United Kingdom) standards of animal care and use.

Trapping of Small Mammals

For logistical reasons, we included in this study 25 of the 37 villages in the human cohort study that were within 45 minutes driving distance from the study center. We conducted trapping continuously during August 2022–September 2023, visiting each of the 25 villages twice. We aimed to visit each village once in the rainy season (approximately June–December) and once in the dry season (January–May). At each village visit, we set traps for 4 consecutive nights, Mondays through Thursdays, choosing different trap locations at each of the 2 visits. We used locally available single-capture cage traps, 27 cm × 15 cm × 12.5 cm, that contained a bowl of water and coconut and peanut butter as bait. We set traps in 3 different habitats: village center, village edge, and fields surrounding the village (Appendix Figure 1, https://wwwnc.cdc.gov/EID/article/32/2/25-1170-App1.pdf). We used Google Maps (https://www.google.com/maps) to visualize geographic village centers with households closest to the center chosen for trapping within the household compound but outside the house. We chose the 2 edges of the village nearest the village center and selected households located at the edge for trapping within the compound. We allowed for some flexibility in selecting the village edge to account for unevenly shaped village borders and access to surrounding fields.

We set traps in the field at ≥50 m from the village edge, measured from the houses on the village edge selected for trapping; we determined locations of the traps by the presence of trees to which traps were chained to reduce loss. Because success was highest in the center and lowest in the field, we set 4 traps in the center, 6 traps at the edge, and 10 traps in the fields to achieve similar catches in all 3 habitats. Traps were open during the night and closed during the day to reduce catching nontarget animals. Each morning, we inspected traps for catches and brought captured target animals (small mammals) to the study center inside the cage in an air-conditioned vehicle. At the study center, we euthanized the animals by carbon dioxide inhalation, then measured body, tail, hindfoot, and ear length for species identification, using published guidance (*14*). We inspected animals for any visible ectoparasites. We clipped their ears at the base and stored them in absolute ethanol at −70°C. For animals on which we found mite colonies on their hindlegs, we clipped and stored the hindlegs. We dissected the animals and removed spleen tissue for immediate storage at −70°C without ethanol (*15*).

Chigger Enumeration and Identification

We examined ears and legs of each animal under a stereomicroscope (StereoBlue EVO; Euromex, https://www.euromex.com). We enumerated chiggers on ears and legs separately; because the overall number found was large, we used samples of chiggers for species identification and molecular analysis. We selected up to 10 chiggers from each ear or leg for mounting on microscopy slides, using Hoyer medium for morphologic identification, and placed up to 20 in an Eppendorf tube in absolute ethanol for molecular analysis. To ensure that chigger species on slides and in Eppendorf tubes were approximately comparable, we alternately chose chiggers for slide mounting or molecular analysis in groups of up to 5. In shrews, we found more chiggers on hindlegs than ears. In those cases, we used chiggers from legs for mounting and for PCR; we counted chiggers found on ears but did not further process them.

We identified chiggers under a light microscope (iScope; Euromex) using a key for chigger mites in India (*16*). We confirmed identification of species from the genus *Leptotrombidium* and related genera using published keys (*17*,*18*).

DNA Extraction and Molecular Analysis

We extracted DNA from chiggers and spleen tissue using a DNeasy Blood & Tissue Kit (QIAGEN, https://www.qiagen.com). We used quantitative PCR to detect *O. tsutsugamushi* targeting the 47-kDa protein gene as previously described (*19*). For each morphologically identified rodent species, we selected 2 representative specimens for molecular barcoding (Appendix).

Statistical Analysis

We calculated the proportion of small mammals infested with chiggers by mammal and chigger species, as well as the chigger index (i.e., the mean number of chiggers per host) (*4*). To account for the sampling process of selecting a subset of chiggers for identification, we calculated the chigger index for different mammal and chigger species by extrapolation from the species composition observed for different

locations on a host (each of 2 ears and hindlegs). We averaged the proportions of each chigger species from different locations on the same host and weighted the averages by the total number of chiggers on that location (mounted or not). We then applied the weighted average proportions to the total number of chiggers found on that host to arrive at the species-specific chigger index.

Similarly, we estimated the number of chiggers of each species in a pool undergoing PCR from the proportion of microscopically identified chiggers of that species at the same location from which chiggers for the PCR pool were selected. We calculated the association between the estimated number of chiggers of 1 species in the pool and *O. tsutsugamushi* PCR positivity of the same pool using generalized linear models (binomial family, identity link). We explored effect modification by habitat as a 3-category variable (village center, edge, field) using likelihood ratio tests. We estimated the prevalence of *O. tsutsugamushi* in individual chiggers, *p*, on the basis of pool size and pool positivity using complementary log-log models based on the formula (*20*)

$$P_{pool} = 1 - (1 - p)^s$$

where P_{pool} is the proportion of pools that are positive for *O. tsutsugamushi* and *s* is the pool size (Appendix).

We estimated the association between the total number of *Leptotrombidium imphalum* chiggers on a host and the probability of *O. tsutsugamushi* PCR positivity of the chigger pool from the same host using logistic regression with PCR positivity as outcome and the estimated number of chiggers (chigger index) as explanatory variable, modeled as cubic splines with knots at 0, 100, and 200 chiggers. We resolved a pronounced right skew in the chigger index by applying the 4th root, and we adjusted for pool size because small mammals with a high chigger index tended to have larger pool sizes. We explored the association between chigger index and the probability of the spleen sample being PCR positive for *O. tsutsugamushi*. We expressed clustering of trap success and *Orientia* infection prevalence within villages as the intraclass correlation coefficient (ICC).

Results

Small Mammal Trapping by Habitat and Season

We trapped 883 small mammals during 9,496 trap nights, an overall trap success of 9.3% (Table 1). Trap success was 20.3% in the village center (314 during 1,545 trap nights), 16.6% on the village edge (297/1,794) and 4.4% in the fields (272/6,152). There was some degree of clustering of the overall trap success within villages (ICC = 0.011; p = 0.001).

The greater bandicoot rat (*Bandicota indica*), the black rat (*Rattus rattus*), and the Asian house shrew (*Suncus murinus*) accounted for most of the trapped mammals, followed by mouse species (*Mus* spp.), three-striped Indian palm squirrel (*Funambulus palmarum*), Indian gerbil (*Tatera indica*), and Asian gray mongoose (*Urva edwardsii*). The bandicoot rats (GenBank accession no. PV918832) predominantly displayed an unusual tail to head/body ratio >1 (Appendix Figure 3). One mouse specimen (GenBank accession no. PV915568) showed 99.7% sequence identity with *M. saxicola* (GenBank accession no. MN964116). A further *Mus* specimen (accession no. PV915577) showed 98.3% identity with *M. terricolor* (accession no. KY018920). Greater bandicoot rats predominated in human habitats, whereas black rats, Indian gerbils, mice, and squirrels were more commonly trapped in the fields (Table 1). Asian house shrews were common in all 3 habitats.

In the fields, small mammal trapping showed pronounced seasonal variation with a low in the dry season and a high in October and November (Figure 1); we observed strong correlation between trappings and monthly human scrub typhus cases (r = 0.80). Trappings in village edge (r = −0.48) and center (r = −0.37) tended to be inversely correlated with scrub typhus cases.

Table 1. Small mammal distribution by habitat in study of *Leptotrombidium imphalum* chiggers as vector for scrub typhus in human settlements, India, 2022–2023

Animal	No. (%) animals			
	Village center	Village edge	Field	Total
Greater bandicoot rat, *Bandicota indica*	156 (49.4)	105 (35.4)	23 (8.5)	284 (32.2)
Black rat, *Rattus rattus*	79 (25.0)	85 (28.6)	113 (41.9)	277 (31.4)
Asian house shrew, *Suncus murinus*	80 (25.3)	102 (34.3)	91 (33.7)	273 (30.9)
Mouse, *Mus* spp.	1 (0.3)	0	21 (7.8)	22 (2.5)
Three-striped Indian palm squirrel, *Funambulus palmarum*	0	2 (0.7)	12 (4.4)	14 (1.6)
Indian gerbil, *Tatera indica*	0	3 (1.0)	9 (3.3)	12 (1.4)
Asian gray mongoose, *Urva edwardsii*	0	0	1 (0.4)	1 (0.1)
Total	316 (100.0)	297 (100.0)	270 (100.0)	883 (100.0)

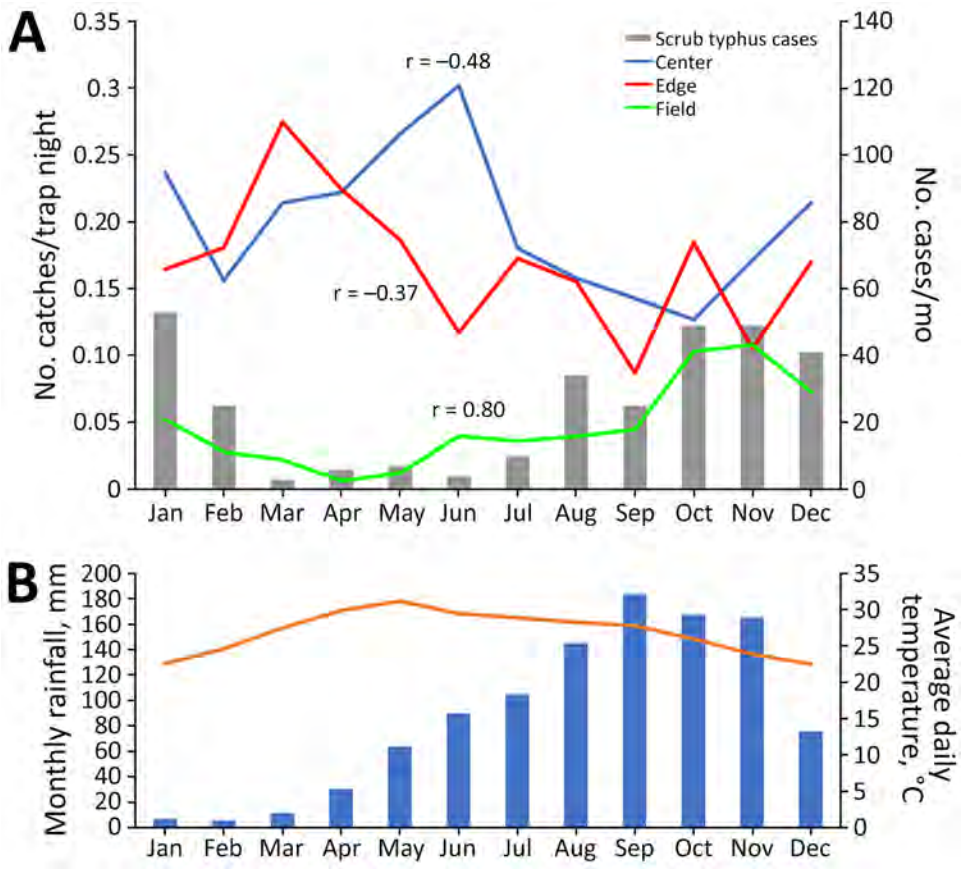

Figure 1. Correlation of trapping success with seasonal characteristics in study of *Leptotrombidium imphalum* chiggers as vector for scrub typhus in human settlements, India, 2022–2023. A) Monthly small mammal catches per trap night, by habitat (center of village, edge of village, or field outside village), compared with numbers of monthly human scrub typhus cases. Case numbers adapted from Devamani et al. (*13*). B) Monthly rainfall (blue bars) and average daily temperature (orange line) 1991–2021. Source: India Meteorological Department (https://mausam.imd.gov.in). Scales for the y-axes differ substantially to underscore patterns but do not permit direct comparisons.

Chigger Species by Host, Habitat, and Season

We collected 90,377 chiggers; of those, we identified 12,431 morphologically under the microscope and placed 10,740 in 759 pools for PCR analysis. *L. imphalum* was the most common chigger species, followed by *Ericotrombidium bhattipadense* and *Schoengastiella ligula* (Table 2). The *L. imphalum* indices were highest on Indian gerbils and house shrews. Otherwise, *L. imphalum* chiggers did not show a strong host preference, whereas *E. bhattipadense* and *S. ligula* chiggers had a strong host preference for *B. indica* rats. *Trombicula hypodermata* chiggers were found mainly on shrews, whereas *Microtrombicula kajutekrii* was mostly on black rats and *Schoengastia tuberculata* on bandicoot rats. One species of *Hypotrombidium* chiggers and 1 species of *Walchia* chiggers could not be identified to species level (Appendix Figures 4–7).

The total chigger index, as well as the indices for *L. imphalum*, *E. bhattipadense*, and *S. ligula* chiggers, were far higher in the village center and edge than in the fields (Figure 2). The *L. imphalum* index correlated moderately with monthly scrub typhus cases (r = 0.51) (Figure 3), whereas the *E. bhattipadense* index showed a strong negative correlation with scrub typhus, peaking in the hot months of April–July (r = −0.78). The *S. ligula* index showed no association (r = 0.08).

O. tsutsugamushi Infection by Chigger and Host Species

By real-time PCR, 122/759 pools (16.1%) tested positive for *O. tsutsugamushi* (Table 3). The coefficients indicate the change in the prevalence of positivity by PCR as a function of the expected number of chiggers of each species per pool, the latter extrapolated from the proportion of each chigger species among specimens examined by microscopy from the same ear or leg. Each additional *L. imphalum* chigger expected to be in a pool was associated with a 2.2% percentage point increase in the PCR pool positivity. By contrast, an increase in the number of most other chigger species was associated with a decreased probability of PCR positivity. *Schoengastia tuberculata* was associated with an increased PCR positivity, but with a wide confidence interval. *L. imphalum* chiggers were found concurrent with *S. tuberculata* in 9/13 locations where *S. tuberculata* was found on slides.

The percentage point increase in PCR positivity with each additional expected *L. imphalum* chigger

was higher in the village center (+2.8%, 95% CI 2.0%–3.5%) and edge (+2.4, 95% CI 1.6%–3.1%) than in the field (+1.2%, 95% CI 0.5%–2.0%), with evidence for effect modification (p = 0.018). The overall prevalence of infection with *O. tsutsugamushi* among individual *L. imphalum* chiggers was 3.6%. The prevalence was 2.3 times higher in the village center (4.5%; prevalence ratio 2.3, 95% CI 1.3–4.1) and 2.2 times higher in the village edge (4.2%; prevalence ratio 2.2, 95% CI 1.2–3.8) than in the fields (1.9%). The prevalence of infection in chigger pools was highest in those from house shrews (29%), followed by bandicoot rats (14.3%) and black rats (8.5%) (Table 4).

We observed considerable clustering of chigger pool positivity within villages (ICC = 0.09; p<0.001), but no evidence of correlation between trap success and pool positivity by habitat (r = −0.09 for village center, r = −0.08 for edge, and r = −0.07 for fields).

We performed real-time PCR on spleen tissue of 874 small mammals, of which 99 (11.3%, 95% CI

Table 2. Chiggers identified by host species in study of *Leptotrombidium imphalum* chiggers as vector for scrub typhus in human settlements, India, 2022–2023*

Chigger species	Black rat, n = 277	Greater bandicoot rat, n = 284	Indian gerbil, n = 12	Mouse, n = 22	Three-striped Indian palm squirrel, n = 14	Asian house shrew, n = 273	Asian gray mongoose, n = 1	Total, n = 883
L. imphalum	769 (48.7)	967 (59.9)	80 (75.0)	6 (13.6)	20 (35.7)	2,470 (75.1)	7 (100.0)	4,319 (59.8)
Chigger index (SD)	11.7 (26.5)	34.3 (55.8)	59.9 (91.1)	0.9 (3.3)	3.7 (6.8)	53.9 (74.4)	14.2 (NA)	32.3 (58)
Leptotrombidium sp.	2 (0.7)	0	0	0	1 (7.1)	1 (0.4)	0	4 (0.5)
Chigger index (SD)	0.04 (0.5)	0	0	0	0.15 (0.5)	0.01 (0.2)	0	0.02 (0.3)
Ericotrombidium bhattipadense	1,098 (63.2)	2,348 (90.1)	4 (16.7)	18 (4.5)	25 (57.1)	665 (51.3)	1 (100.0)	4,159 (66.0)
Chigger index (SD)	13.8 (24.4)	83 (85.3)	0.7 (1.6)	2.4 (11.3)	4.7 (6.2)	12.9 (30.1)	2.8 (NA)	35.2 (62.4)
Hypotrombidium sp.	360 (27.1)	134 (18.7)	8 (16.7)	3 (9.1)	122 (78.6)	5 (0.7)	0	632 (16.4)
Chigger index (SD)	6 (21.8)	5.2 (17.7)	1.4 (3.8)	0.3 (1)	37.7 (50.5)	0.1 (0.8)	0	4.2 (17.7)
Ericotrombidium or *Hypotrombidium* sp.	13 (1.4)	8 (1.4)	0	0	0	0	0	21 (0.9)
Chigger index (SD)	0.2 (2.1)	0.2 (2.8)	0	0	0	0	NA	0.1 (2)
Trombicula hypodermata	1 (0.4)	3 (1.1)	0	0	0	165 (19.4)	0	169 (6.5)
Chigger index (SD)	0.02 (0.3)	0.1 (0.8)	0	0	0	2.4 (6.6)	NA	0.8 (3.9)
Microtrombicula kajutekrii	519 (27.4)	2 (0.4)	0	1 (4.5)	0	0	0	522 (8.8)
Chigger index (SD)	5.7 (17.2)	0.01 (0.1)	0	0.05 (0.2)	0	0	NA	1.8 (10)
Schoengastia tuberculata	9 (1.8)	33 (5.3)	0	0	0	0	0	42 (2.3)
Chigger index (SD)	0.1 (1.4)	0.9 (4.5)	0	0	0	0	NA	0.3 (2.7)
S. ligula	271 (22.7)	1,826 (76.4)	37 (50.0)	2 (4.5)	0	12 (2.6)	0	2,148 (33.3)
Chigger index (SD)	3.4 (13.7)	71.9 (112.1)	7.4 (14.6)	0.3 (1.5)	0	0.1 (1)	NA	24.3 (71.9)
S. liota	0	0	2 (16.7)	0	0	6 (1.1)	0	8 (0.6)
Chigger index (SD)	0	0	0.45 (1.1)	0	0	0.03 (0.3)	NA	0.02 (0.2)
S. punctata	1 (0.4)	0	0	0	0	18 (4.4)	0	19 (1.5)
Chigger index (SD)	0.04 (0.6)	0	0	0	0	0.3 (1.9)	NA	0.1 (1.1)
S. ralagea	7 (1.1)	13 (4.2)	0	0	0	173 (15.4)	0	193 (6.5)
Chigger index (SD)	0 (0.4)	0.7 (4)	0	0	0	6.6 (45.7)	NA	2.3 (25.6)
S. argalea	0	0	1 (8.3)	0	0	3 (0.7)	0	4 (0.3)
Chigger index (SD)	0	0	0.2 (0.7)	0	0	0.04 (0.6)	NA	0 (0.3)
S. ceylonica	20 (1.1)	1 (0.4)	5 (8.3)	53 (40.9)	0	0	0	79 (1.6)
Chigger index (SD)	0.1 (1.7)	0.03 (0.6)	1.8 (6.3)	6.2 (17.3)	0	0	NA	0.2 (3.1)
S. bengalensis	0	1 (0.4)	0	0	0	23 (5.9)	0	24 (1.9)
Chigger index (SD)	0	0.01 (0.2)	0	0	0	0.23 (1.2)	NA	0.07 (0.7)
S. singularis	0	0	40 (41.7)	0	0	0	0	40 (0.6)
Chigger index (SD)	0	0	28.8 (51.8)	0	0	0	NA	0.4 (6.7)
Walchia sp.	0	0	0	8 (18.2)	0	37 (9.2)	0	45 (3.3)
Chigger index (SD)	0	0	0	0.8 (2.2)	0	0.3 (1.7)	NA	0.1 (1)
Gahrliepia khandalaensis	0	1 (0.4)	0	0	0	2 (0.4)	0	3 (0.2)
Chigger index (SD)	0	0.01 (0.1)	0	0	0	0.04 (0.6)	NA	0.01 (0.3)
Total	3,070 (92.1)	5,337 (99.3)	177 (100.0)	91 (63.6)	168 (92.9)	3,580 (91.2)	8 (100.0)	12,431 (93.5)
Chigger index (SD)	41.4 (50.2)	196.4 (148.3)	100.7 (106.4)	11 (22.6)	46.2 (49.5)	77 (98.1)	17 (NA)	102.4 (124.4)

*Chigger species and total values are no. chiggers (% infestation). Chigger index is mean number of chiggers per host. NA, not applicable.

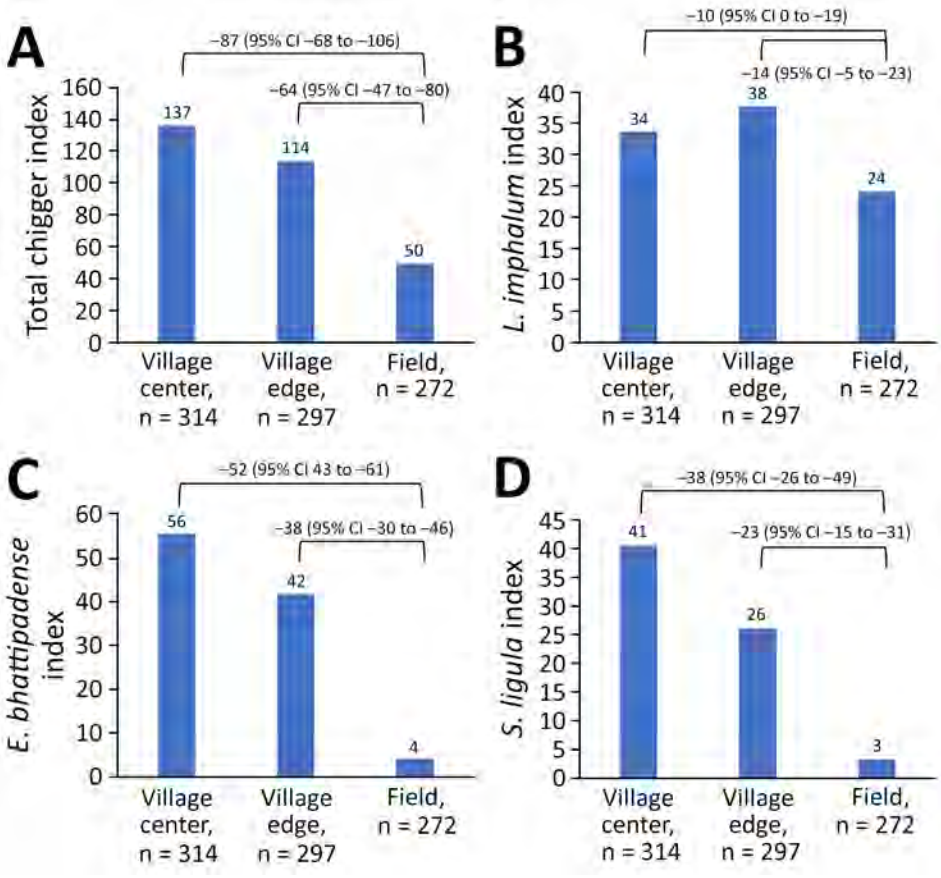

Figure 2. Differences in chigger index by habitat in study of *Leptotrombidium imphalum* chiggers as vector for scrub typhus in human settlements, India, 2022–2023. Chigger index is mean number of chiggers per host. Values above bars indicate chigger index; values above brackets indicate differences and 95% CIs. A) Total chigger index. B) Index for *L. imphalum* chiggers. C) Index for *Ericotrombidium bhattipadense* chiggers. D) Index for *Schoengastiella ligula* chiggers.

9.3%–13.6%) tested positive for *O. tsutsugamushi* (Table 5). The prevalence of infection in spleen tissue was higher in small mammals caught in the field (15.2%) than in those caught at the village edge (10.3%) and center (8.9%; p = 0.019 by score test for trend), in contrast to infection in chiggers by location. The high prevalence of *Orientia* infection in spleen tissue of shrews in the fields (31%) is a

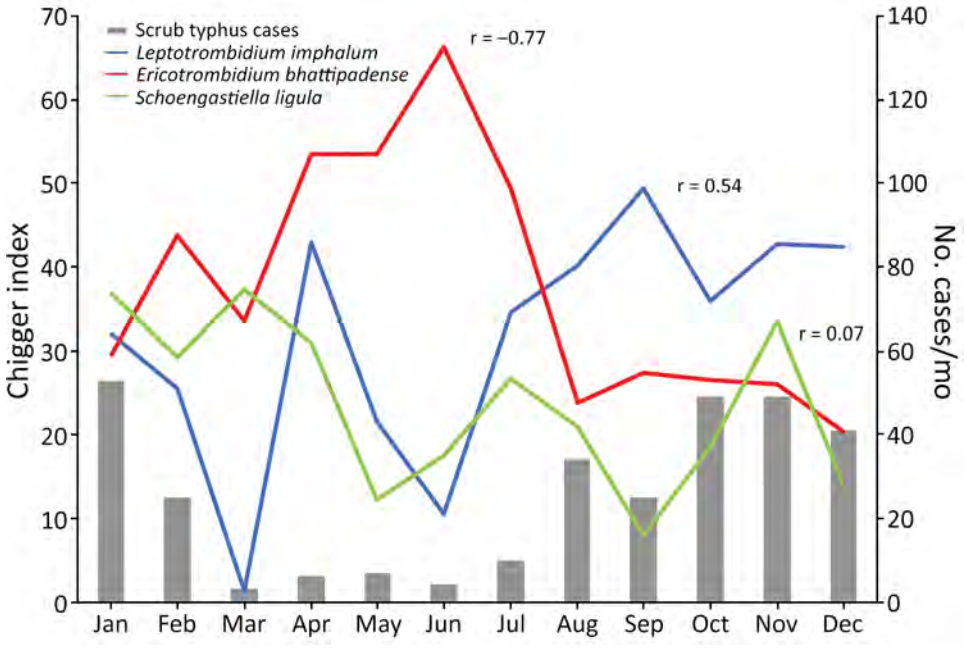

Figure 3. Chigger index by month in study of *Leptotrombidium imphalum* chiggers as vector for scrub typhus in human settlements, India, 2022–2023. Chigger index is mean number of chiggers per host; r is correlation coefficient between chigger index for each species and monthly human scrub typhus cases. Case numbers adapted from Devamani et al. (*13*).

Table 3. Molecular detection of *O. tsutsugamushi* in chigger mite pools in study of *Leptotrombidium imphalum* chiggers as vector for scrub typhus in human settlements, India, 2022–2023*

Chigger species	No. pools expected to contain species, N = 759	Coefficient (95% CI)
L. imphalum	415	2.2% (1.7%–2.6%)
Ericotrombidium bhattipadense	470	−0.3% (−0.7% to 0.1%)
Hypotrombidium sp.	103	−0.4% (−1.2% to 0.4%)
Schoengastia tuberculata	13	2.4% (−2.9% to 7.7%)
Schoengastiella ligula	231	−0.5% (−0.9% to 0.0%)
Schoengastiella ralagea	41	0.4% (−1.5% to 2.2%)
Any *Schoengastiella* sp.	290	−0.5% (−0.9% to 0.1%)
Microtrombicula kajutekrii	65	−0.9% (−2.3% to 0.5%)
Trombicula hypodermata	41	−0.3% (−2.3% to 1.7%)
Walchia sp.	12	NA

*Coefficient is the absolute change in probability of PCR positivity of a pool per additional chigger of a given species. NA, not applicable.

likely cause of the trend (Table 5). Conversely, despite high prevalence of infection in chigger pools from bandicoot rats, the prevalence of infection in spleen tissue was 2.5%.

Adjusted for pool size, the prevalence of *Orientia* infection in chigger PCR pools increased with the estimated *L. imphalum* index on small mammals, leveling off at an index of ≈200 (Figure 4, panel A). By contrast, the association between the estimated *L. imphalum* index and prevalence of spleen tissue infection sharply plateaued at an *L. imphalum* index of ≈60 (Figure 4, panel B).

Discussion

In this setting in South India where scrub typhus is a major public health problem (*13*), chigger numbers found on small mammals and the prevalence of *O. tsutsugamushi* infection in chiggers were higher within human settlements than in the land surrounding them. Several findings point to the peridomestic environment as a high-risk setting for infestation with *O. tsutsugamushi*–infected chigger mites. Trap success of small mammals, a proxy for density, was 4–5 times higher in village centers and edges than in the fields. Furthermore, chigger indices were higher in those locations, presumably because mite larvae more frequently encounter small mammals as suitable hosts (*21*), which they require to develop into the nymph and adult stages. *L. imphalum* chiggers, which have been implicated as a vector for scrub typhus in other foci across Asia (*22*,*23*), might be the dominant and perhaps only vector for scrub typhus in our setting. Of note, the estimated prevalence of *O. tsutsugamushi* infection in *L. imphalum* chiggers was more than twice as high in village center and edge than in the fields. Even when adjusting for pool size, a higher *L. imphalum* index, a potential marker of trombiculid mite density in the environment, was associated with a higher prevalence of infection in chigger pools (Figure 4, panel A). Our data suggest that, through mechanisms such as acquisition of infection from the host (*24*), cofeeding of chiggers (*25*,*26*), or horizontal transmission during other life stages, a high population density of *Leptotrombidium* mites may promote *Orientia* infection in the vector. Conclusive evidence only exists for vertical transmission (*24*,*27*).

A study in Yunnan, China, revealed close association between human habitats and *Leptotrombidium deliense* chiggers (*28*); that study and others from Thailand (*29*,*30*) found a low chigger species diversity in human settlements compared with less disturbed ecosystems. The occurrence of 1 *Leptotrombidium* chigger species, *L. imphalum*, in our study stands in contrast to earlier work from South India, which suggested a high *Leptotrombidium* chigger species diversity and an absence of *L. imphalum* chiggers in comparable settings (*31*–*33*). Future studies could include molecular barcoding to distinguish between

Table 4. Molecular detection of *Orientia tsutsugamushi* in chigger mite pools in study of *Leptotrombidium imphalum* chiggers as vector for scrub typhus in human settlements, India, 2022–2023

Small mammal species	Prevalence in chigger pool, no. positive/no. tested (%)			
	Village center	Village edge	Field	Total
Black rat, *Rattus rattus*	8/61 (13.1)	3/76 (4)	9/98 (9.2)	20/235 (8.5)
Greater bandicoot rat, *Bandicota indica*	17/153 (11.1)	22/104 (21.2)	1/23 (4.4)	40/280 (14.3)
Indian gerbil, *Tatera indica*	0/0	0/3 (0)	0/9 (0)	0/12 (0)
Mouse, *Mus* spp.	0/0	0/9 (0)	0/8 (0)	0/17 (0)
Three-striped Indian palm squirrel, *Funambulus palmarum*	0/0	1/2 (50)	0/11 (0)	1/13 (7.7)
Asian house shrew, *Suncus murinus*	21/68 (30.9)	28/85 (32.9)	12/56 (21.4)	61/209 (29.2)
Asian gray mongoose, *Urva edwardsii*	0/0	0/0	0/1 (0)	0/1 (0)
Total	46/283 (16.3)	54/270 (20.0)	22/206 (10.7)	122/759 (16.1)

Table 5. Molecular detection of *Orientia tsutsugamushi* in small mammal spleen tissue in study of *Leptotrombidium imphalum* chiggers as vector for scrub typhus in human settlements, India, 2022–2023

	Prevalence in spleen tissue, no. positive/no. tested (%)			
Small mammal species	Village center	Village edge	Field	Total
Black rat, *Rattus rattus*	9/79 (11.4)	9/82 (11)	9/112 (8)	27/273 (9.9)
Greater bandicoot rat, *Bandicota indica*	4/156 (2.6)	2/103 (1.9)	1/24 (4.2)	7/283 (2.5)
Indian gerbil, *Tatera indica*	0/0	1/3 (33.3)	3/9 (33.3)	4/12 (33.3)
Mouse, *Mus* spp.	0/1 (0)	0/0	0/21 (0)	0/22 (0)
Three-striped Indian palm squirrel, *Funambulus palmarum*	0/0	0/1 (0)	0/12 (0)	0/13 (0)
Asian house shrew, *Suncus murinus*	15/78 (19.2)	18/101 (17.8)	28/91 (30.8)	61/270 (22.6)
Asian gray mongoose, *Urva edwardsii*	0/0	0/0	0/1 (0)	0/1 (0)
Total	28/314 (8.9)	30/290 (10.3)	41/270 (15.2)	99/874 (11.3)

morphologically similar species (*34*). In general, vector studies involving small mammals trapped in the peridomestic environment in South India have demonstrated high prevalence of *Leptotrombidium* infestation (*33*,*35*,*36*). Our study confirms that chigger mites regularly infest highly synanthropic small mammals, thus increasing the likelihood of infestation of humans.

As observed in earlier studies from India (*36*,*37*), *S. murinus* shrews carry large numbers of *Leptotrombidium* spp. chiggers (Table 2) and could play an important role in maintaining scrub typhus transmission. Bandicoot rats had lower *L. imphalum* indices than did the shrews but were highly synanthropic (Table 1) and likely to substantially contribute to *L. imphalum* density in villages. By contrast, the prevalence of infection in host spleen tissue plateaued at relatively low *L. imphalum* indices (Figure 4, panel B), suggesting that high exposure to *O. tsutsugamushi* might strengthen the immune response

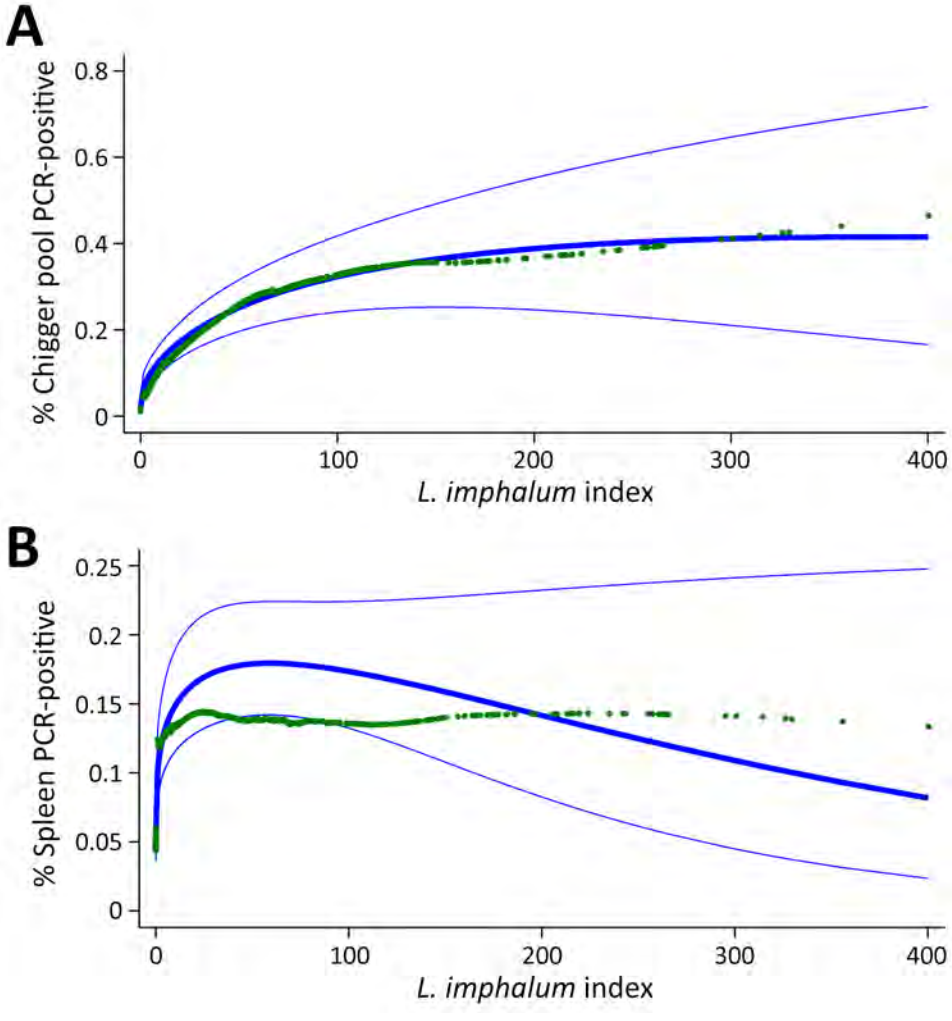

Figure 4. Association between *Leptotrombidium imphalum* index and the prevalence of *Orientia* infection in study of *L. imphalum* chiggers as vector for scrub typhus in human settlements, India, 2022–2023. A) Association between prevalence in the chigger pool collected from the host and chigger index. B) Association between prevalence determined from host spleen tissue and chigger index. Blue lines show predicted prevalence (thick) with 95% CI (thin). Green markers show locally weighted scatterplot smoothing of *Orientia* prevalence by *L. imphalum* index using a bandwidth of 0.4.

to the pathogen in hosts and enable them to rapidly clear the infection. The higher prevalence of *Orientia* infection in spleen tissue from hosts trapped in the field, compared with those from center and edge locations (Table 5), was driven by the high infection prevalence in house shrews, which might be less able to clear the infection than bandicoot rats.

Previous work has discussed causes of the strong seasonality of human scrub typhus in most settings (*4*,*38*). We found a strong correlation between human scrub typhus and trap success in the fields but not in village edge and center (Figure 1). The *L. imphalum* index correlated moderately with human scrub typhus, as in a study from Puducherry in South India (*37*). Small mammal trappings within villages increased in the dry season, inversely to human scrub typhus, suggesting that hosts may prefer the village environment in the dry season. Similarly, infestation with *E. bhattipadense*, the dominant chigger in the village center, correlated inversely with human scrub typhus. Trombiculid mites are able to complete their life cycle within burrows (*39*), perhaps independently of seasonal changes in temperature and humidity. Therefore, chigger numbers on small mammals may not accurately reflect human exposure to chiggers. Further, small mammals, in particular Asian house shrews (*40*), can have large home ranges (*4*) and can move between village and field (i.e., the trap location may be far away from the place where chiggers are acquired). Collecting questing chiggers in the environment may provide further insights, for example, by using the black plating method (*41*) in village center, edge, and field to estimate the risk for human exposure in each habitat, ideally complemented by human behavior studies with possible use of tracking devices. Such studies might also investigate the marked clustering of *Orientia* infection in chiggers we observed in our study and the observed variation in human scrub typhus risk and associated risk factors among study villages (*12*).

The seasonality of small mammal trappings might also be influenced by changes in food availability, especially in the dry season, when the baited traps could be more attractive. The bait used in this study, coconut with peanut butter, might attract host species differently. For example, Indian gerbils, common rodents in the Indian subcontinent that cause extensive crop damage (*42*), were caught in small numbers in this study. Given that it was the host with the highest *L. imphalum* index (Table 2), our results might have underestimated its role as a maintaining host of *L. imphalum* chiggers. Our study confirmed the utility of genetic barcoding in identifying common host species presenting with unusual morphology (Appendix Figure 3).

We based the species-specific chigger index on a relatively small sample of ≤20 mites per host undergoing morphologic identification. Furthermore, we included different mites for morphologic identification and *O. tsutsugamushi* detection using PCR, then estimated infection prevalence using regression models. Our approach does not rule out *Orientia* infection of a mite species at a very low prevalence. Ideally, the same chigger morphologically identified under the microscope would have been used for PCR, potentially following methods described previously (*43*), but that was not feasible given the large number of chiggers processed.

In conclusion, this study corroborates studies in South India suggesting human settlements as the setting in which most infestation with chigger mites infected with *O. tsutsugamushi* occurs (*10*–*12*,*35*). Our findings suggest a causal chain involving large numbers of small mammals in human settlements, enabling high trombiculid mite densities (*21*) and large populations of chigger mites, which might encourage the spread of *O. tsutsugamushi* within the vector population (*25*,*26*) and cause a high risk for human scrub typhus infection.

Acknowledgments

We thank the residents of the participating villages in Vellore and Ranipet districts of Tamil Nadu, India for their support.

The study was supported by the Medical Research Council, UK (grant reference MR/S023275/1). A.A.S. was supported by the Ministry of Science and Higher Education of the Russian Federation (cooperative agreement no. 125013001089-0).

About the Author

Dr. Devamani works as a doctor of community medicine at the Christian Medical College of Vellore. Her research interests include the epidemiology of rickettsial infections and fever etiology in rural settings.

References

1. Tamura A, Ohashi N, Urakami H, Miyamura S. Classification of *Rickettsia tsutsugamushi* in a new genus, *Orientia* gen. nov., as *Orientia tsutsugamushi* comb. nov. Int J Syst Bacteriol. 1995;45:589–91. https://doi.org/10.1099/00207713-45-3-589
2. Kelly DJ, Fuerst PA, Ching WM, Richards AL. Scrub typhus: the geographic distribution of phenotypic and genotypic variants of *Orientia tsutsugamushi*. Clin Infect Dis. 2009;48(Suppl 3):S203–30. https://doi.org/10.1086/596576

3. Abhilash KP, Jeevan JA, Mitra S, Paul N, Murugan TP, Rangaraj A, et al. Acute undifferentiated febrile illness in patients presenting to a tertiary care hospital in South India: clinical spectrum and outcome. J Glob Infect Dis. 2016;8:147–54. https://doi.org/10.4103/0974-777X.192966
4. Elliott I, Pearson I, Dahal P, Thomas NV, Roberts T, Newton PN. Scrub typhus ecology: a systematic review of *Orientia* in vectors and hosts. Parasit Vectors. 2019;12:513. https://doi.org/10.1186/s13071-019-3751-x
5. Behera B, Biswal M, Das RR, Dey A, Jena J, Dhal S, et al. Clinico-epidemiological analysis of scrub typhus in hospitalised patients presenting with acute undifferentiated febrile illness: a hospital-based study from eastern India. Indian J Med Microbiol. 2019;37:278–80. https://doi.org/10.4103/ijmm.IJMM_19_147
6. Bonell A, Lubell Y, Newton PN, Crump JA, Paris DH. Estimating the burden of scrub typhus: a systematic review. PLoS Negl Trop Dis. 2017;11:e0005838. https://doi.org/10.1371/journal.pntd.0005838
7. Devamani CS, Prakash JAJ, Alexander N, Suzuki M, Schmidt WP. Hospitalisations and outpatient visits for undifferentiated fever attributable to scrub typhus in rural South India: retrospective cohort and nested case-control study. PLoS Negl Trop Dis. 2019;13:e0007160. https://doi.org/10.1371/journal.pntd.0007160
8. Roopa KS, Karthika K, Sugumar M, Bammigatti C, Shamanna SB, Harish BN. Serodiagnosis of scrub typhus at a tertiary care hospital from southern India. J Clin Diagn Res. 2015;9:DC05–07. https://doi.org/10.7860/JCDR/2015/15871.6759
9. Devasagayam E, Dayanand D, Kundu D, Kamath MS, Kirubakaran R, Varghese GM. The burden of scrub typhus in India: a systematic review. PLoS Negl Trop Dis. 2021;15:e0009619. https://doi.org/10.1371/journal.pntd.0009619
10. Trowbridge P, P D, Premkumar PS, Varghese GM. Prevalence and risk factors for scrub typhus in South India. Trop Med Int Health. 2017;22:576–82. https://doi.org/10.1111/tmi.12853
11. Devamani CS, Schmidt WP, Ariyoshi K, Anitha A, Kalaimani S, Prakash JAJ. Risk factors for scrub typhus, murine typhus, and spotted fever seropositivity in urban areas, rural plains, and peri-forest hill villages in South India: a cross-sectional study. Am J Trop Med Hyg. 2020;103:238–48. https://doi.org/10.4269/ajtmh.19-0642
12. Schmidt WP, Alexander N, Rose W, Chandramohan D, Cameron M, Abhilash K, et al. Risk factors for scrub typhus infection in South India: population-based cohort study. Epidemiol Infect. 2025;153:e102. https://doi.org/10.1017/S0950268825100484
13. Devamani C, Alexander N, Chandramohan D, Stenos J, Cameron M, Abhilash KPP, et al. Incidence of scrub typhus in rural South India. N Engl J Med. 2025;392:1089–99. https://doi.org/10.1056/NEJMoa2408645
14. Agrawal VC. Taxonomic studies on Indian *Muridae* and *Hystricidae*. Kolkata: Zoological Survey of India; 2000.
15. CERoPath. Community ecology of rodents and their pathogens in southeast Asia. 2024 [cited 2025 Jul 15]. http://www.ceropath.org
16. Fernandes S, Kulkarni SM. Studies on the Trombiculid mite fauna of India. Kolkata: Zoological Survey of India; 2003.
17. Stekolnikov AA. *Leptotrombidium* (Acari: Trombiculidae) of the world. Zootaxa. 2013;3728:1–173. https://doi.org/10.11646/zootaxa.3728.1.1
18. Vercammen-Grandjean PH, Langston R. The chigger mites of the world. Volume III. *Leptotrombidium* complex. San Francisco: George Williams Hooper Foundation, UCSF Reprographics Department; 1976.
19. Jiang J, Chan TC, Temenak JJ, Dasch GA, Ching WM, Richards AL. Development of a quantitative real-time polymerase chain reaction assay specific for *Orientia tsutsugamushi*. Am J Trop Med Hyg. 2004;70:351–6. https://doi.org/10.4269/ajtmh.2004.70.351
20. Katholi CR, Toé L, Merriweather A, Unnasch TR. Determining the prevalence of *Onchocerca volvulus* infection in vector populations by polymerase chain reaction screening of pools of black flies. J Infect Dis. 1995;172:1414–7. https://doi.org/10.1093/infdis/172.5.1414
21. Patterson JE, Ruckstuhl KE. Parasite infection and host group size: a meta-analytical review. Parasitology. 2013;140:803–13. https://doi.org/10.1017/S0031182012002259
22. Liu QY, Fan R, Song WY, Peng PY, Zhao YF, Jin DC, et al. The distribution and host-association of the vector chigger species *Leptotrombidium imphalum* in southwest China. Insects. 2024;15:504. https://doi.org/10.3390/insects15070504
23. Tanskul P, Linthicum KJ. Redescription of *Leptotrombidium* (*Leptotrombidium*) *imphalum* (Acari: Trombiculidae), with observations on bionomics and medical importance in northern Thailand. J Med Entomol. 1999;36:88–91. https://doi.org/10.1093/jmedent/36.1.88
24. Traub R, Wisseman CL Jr, Jones MR, O'Keefe JJ. The acquisition of *Rickettsia tsutsugamushi* by chiggers (trombiculid mites) during the feeding process. Ann N Y Acad Sci. 1975;266:91–114. https://doi.org/10.1111/j.1749-6632.1975.tb35091.x
25. Frances SP, Watcharapichat P, Phulsuksombati D, Tanskul P. Transmission of *Orientia tsutsugamushi*, the aetiological agent for scrub typhus, to co-feeding mites. Parasitology. 2000;120:601–7. https://doi.org/10.1017/S0031182099005909
26. Takhampunya R, Korkusol A, Promsathaporn S, Tippayachai B, Leepitakrat S, Richards AL, et al. Heterogeneity of *Orientia tsutsugamushi* genotypes in field-collected trombiculid mites from wild-caught small mammals in Thailand. PLoS Negl Trop Dis. 2018;12:e0006632. https://doi.org/10.1371/journal.pntd.0006632
27. Frances SP, Watcharapichat P, Phulsuksombati D. Vertical transmission of *Orientia tsutsugamushi* in two lines of naturally infected *Leptotrombidium deliense* (Acari: Trombiculidae). J Med Entomol. 2001;38:17–21. https://doi.org/10.1603/0022-2585-38.1.17
28. Liu RJ, Guo XG, Zhao CF, Zhao YF, Peng PY, Jin DC. An ecological survey of chiggers (Acariformes: Trombiculidae) associated with small mammals in an epidemic focus of scrub typhus on the China–Myanmar border in southwest China. Insects. 2024;15:812. https://doi.org/10.3390/insects15100812
29. Chaisiri K, Gill AC, Stekolnikov AA, Hinjoy S, McGarry JW, Darby AC, et al. Ecological and microbiological diversity of chigger mites, including vectors of scrub typhus, on small mammals across stratified habitats in Thailand. Anim Microbiome. 2019;1:18. https://doi.org/10.1186/s42523-019-0019-x
30. Wulandhari SA, Paladsing Y, Saesim W, Charoennitiwat V, Sonthayanon P, Kumlert R, et al. High prevalence and low diversity of chigger infestation in small mammals found in Bangkok metropolitan parks. Med Vet Entomol. 2021;35:534–46. https://doi.org/10.1111/mve.12531
31. Govindarajan R, Sankar SG, Kumar MS, Rajamannar V, Krishnamoorthi R, Anand AAP, et al. Molecular detection of *Orientia tsutsugamushi* in ectoparasites & their small mammal

hosts captured from scrub typhus endemic areas in Madurai district, India. Indian J Med Res. 2024;159:180–92. https://doi.org/10.4103/ijmr.ijmr_3530_21
32. Paulraj PS, Renu G, Ranganathan K, Veeramanoharan R, Kumar A. Ectoparasites diversity on rodents and shrews at scrub typhus endemic Vellore district of Tamil Nadu, India. J Arthropod Borne Dis. 2022;16:51–60. https://doi.org/10.18502/jad.v16i1.11192
33. Prakash JAJ, Kamarasu K, Samuel PP, Govindarajan R, Govindasamy P, Johnson LA, et al. Detection of *Orientia tsutsugamushi* in novel trombiculid mite species in northern Tamil Nadu, India: use of targeting the multicopy *traD* gene. J Med Entomol. 2022;59:693–9. https://doi.org/10.1093/jme/tjab180
34. Rajasegaran P, Tan KK, Khoo JJ, Mansor MS, Ahmad Khusaini MKS, AbuBakar S, et al. Molecular species delimitation analysis of *Leptotrombidium* spp. and other chigger species parasitizing birds in Malaysia. J Med Entomol. 2025;62:1175–91. https://doi.org/10.1093/jme/tjaf078
35. Rose W, Kang G, Verghese VP, Candassamy S, Samuel P, Prakash JJA, et al. Risk factors for acquisition of scrub typhus in children admitted to a tertiary centre and its surrounding districts in South India: a case–control study. BMC Infect Dis. 2019;19:665. https://doi.org/10.1186/s12879-019-4299-2
36. Sadanandane C, Elango A, Panneer D, Mary KA, Kumar NP, Paily KP, et al. Seasonal abundance of *Leptotrombidium deliense*, the vector of scrub typhus, in areas reporting acute encephalitis syndrome in Gorakhpur district, Uttar Pradesh, India. Exp Appl Acarol. 2021;84:795–808. https://doi.org/10.1007/s10493-021-00650-2
37. Candasamy S, Ayyanar E, Paily K, Karthikeyan PA, Sundararajan A, Purushothaman J. Abundance & distribution of trombiculid mites & *Orientia tsutsugamushi*, the vectors & pathogen of scrub typhus in rodents & shrews collected from Puducherry & Tamil Nadu, India. Indian J Med Res. 2016; 144:893–900. https://doi.org/10.4103/ijmr.IJMR_1390_15
38. Elliott I, Thangnimitchok N, Chaisiri K, Wangrangsimakul T, Jaiboon P, Day NPJ, et al. *Orientia tsutsugamushi* dynamics in vectors and hosts: ecology and risk factors for foci of scrub typhus transmission in northern Thailand. Parasit Vectors. 2021;14:540. https://doi.org/10.1186/s13071-021-05042-4
39. Traub R, Wisseman CL Jr. Ecological considerations in scrub typhus. 2. Vector species. Bull World Health Organ. 1968;39:219–30.
40. Nakamoto A, Nakanishi N. Home range, habitat selection, and activity of male Asian house shrews, *Suncus murinus*, on Okinawa-Jima Island. Mammal Study. 2013;38:147–53. https://doi.org/10.3106/041.038.0303
41. Jones BM. A method for studying the distribution and bionomics of trombiculid mites (Acarina: Trombidiidae). Parasitology. 1950;40:1–13. https://doi.org/10.1017/S0031182000017819
42. Munawar N, Mahmood T, Akrim F, Fatima H, Farooq M, Irshad N, et al. Small rodent communities and their associated damage to wheat-groundnut agriculture systems. Braz J Biol. 2024;84:e254445. https://doi.org/10.1590/1519-6984.254445
43. Kumlert R, Chaisiri K, Anantatat T, Stekolnikov AA, Morand S, Prasartvit A, et al. Autofluorescence microscopy for paired-matched morphological and molecular identification of individual chigger mites (Acari: Trombiculidae), the vectors of scrub typhus. PLoS One. 2018;13:e0193163. https://doi.org/10.1371/journal.pone.0193163

Address for correspondence: Wolf-Peter Schmidt, Department for Disease Control, London School of Hygiene and Tropical Medicine, Keppel St, WC1E 7HT London, UK; email: Wolf-Peter.Schmidt@lshtm.ac.uk

Using Routine Surveillance Data to Assess Dengue Virus Transmission Risk in Travelers Returning to the United States

Kristyna Rysava,[1] Zachary J. Madewell,[1] Maile B. Thayer, Liliana Sánchez-González, Kamalich Muniz-Rodriguez, Ashley Brown, Julie Thwing, Laura E. Adams, Gabriela Paz-Bailey, Michael A. Johansson

Dengue virus poses a growing global health threat, yet inconsistent local surveillance limits global risk assessments. We analyzed 10,530 travel-associated dengue cases among US travelers reported to ArboNET during January 2010–April 2024, involving travel to 128 countries. By using negative binomial and Poisson models, we developed country-specific thresholds (75th, 80th, 90th percentiles) to identify elevated travel-associated dengue risk. We applied a ≥10-case threshold in a 3-month period to improve specificity. The final dual-criteria method accurately identified high-risk periods, including sustained transmission in countries with limited official reporting, such as Cuba in 2022–2023. Threshold comparisons revealed a tradeoff between early detection and overclassification, whereas real-time and retrospective assessments revealed consistent high-risk signals. This traveler-based approach offers a timely, complementary method for travel-associated dengue risk detection, although timeliness might be reduced if reporting delays increase beyond our observations. Our findings support integrating travel surveillance into global dengue monitoring and preparedness efforts.

Dengue is a mosquitoborne viral disease of major public health concern, particularly in tropical and subtropical regions (*1*). Four dengue virus (DENV) serotypes, transmitted primarily by *Aedes* spp. mosquitoes, can cause repeat infections; secondary infections might be associated with more severe disease (*2*,*3*). An estimated 60%–80% of all DENV infections are asymptomatic or subclinical, complicating surveillance and control (*4*,*5*).

Dengue incidence has increased globally in recent decades, and nearly half the world's population now lives in areas at risk (*6*–*8*). International travel further contributes to dengue burden, as infected travelers introduce dengue to new areas. Genomic and routine surveillance data indicate that DENV serotypes have moved repeatedly between regions, including introductions to and from the Caribbean that contributed to transmission across the Americas (*9*,*10*). Most evidence on viral spread comes from national surveillance systems, but travel-based surveillance data can provide complementary insights into DENV exposure risk, particularly where local data are limited or delayed, by detecting introductions or exportations through infected travelers. Traditional surveillance depends on timely case reporting, laboratory confirmation, and consistent national data sharing, all of which vary widely by country and can delay recognition of emerging outbreaks. Traveler-based surveillance, although influenced by who travels and where, can provide near–real-time indication of international transmission patterns that might otherwise go undetected. Integrating local and traveler-based surveillance streams can enhance detection of DENV exposure risk: local data reflect population-level risk, whereas traveler data capture exportation risk and can provide early warning where national reporting is incomplete. The concurrent emergence of other *Aedes*-borne viruses, such as chikungunya and Zika, has further highlighted the role of human mobility in arbovirus spread (*11*,*12*). Global dengue surveillance and the identification of high-transmission periods have become increasingly critical as international connectivity grows.

Author affiliations: University of Warwick, Warwick, UK (K. Rysava); Centers for Disease Control and Prevention, San Juan, Puerto Rico, USA (Z.J. Madewell, M.B. Thayer, L. Sánchez-González, K. Muniz-Rodriguez, L.E. Adams, G. Paz-Bailey, M.A. Johansson); Centers for Disease Control and Prevention, Atlanta, Georgia, USA (A. Brown, J. Thwing)

DOI: https://doi.org/10.3201/eid3202.251217

[1]These first authors contributed equally to this article.

To increase awareness of global health risks, the US Centers for Disease Control and Prevention (CDC) issues Travel Health Notices (THNs) to advise travelers, clinicians, and public health professionals about disease outbreaks or other health concerns. THNs might be triggered by outbreaks, disease occurrence in new locations, or large events such as natural disasters or mass-gatherings and take into consideration both risk and the availability of preventive measures (*13*). Dengue THNs support both pretravel counseling and posttravel clinical evaluation: they inform travelers about destinations with elevated risk and help clinicians consider dengue in returned travelers with fever. That role has become more necessary with the recent rise in travel-associated dengue; 3,742 cases were reported in 2024, far exceeding the previous peak of 1,474 cases in 2019 (*14*,*15*). Historically, new THNs have relied on outbreak declarations or detailed national surveillance data to confirm that case numbers exceed historical levels. However, dengue surveillance varies widely by country, with differing testing practices, laboratory capacity, and public data availability, creating challenges for timely warnings.

To help address those gaps in surveillance, we developed a new approach to assess DENV incidence levels in other countries by using routine surveillance data from travelers returning to the United States. This approach leverages dengue cases reported to ArboNET, the national arboviral surveillance system, to establish baseline dengue activity in US travelers and detect deviations that indicate increased transmission (*16*). We used regression models and percentile-based thresholds, combined with a case-count criterion, to identify sustained periods of elevated risk by country and to support more timely, reproducible guidance for both pretravel risk communication and posttravel clinical decision-making.

Methods

Data Sources

For this study, we used dengue case data among travelers returning to the United States reported to ArboNET during January 2010–April 2024 (*16*). ArboNET is a national CDC surveillance system that monitors locally acquired and travel-associated arboviral diseases. Dengue is a nationally notifiable disease; state health departments receive reports from clinicians and laboratories, conduct case investigations, and submit data to CDC. ArboNET data are reviewed and updated continuously. Routine analyses and data pulls occur at least monthly to support surveillance and decision-making.

Countries of exposure are identified through public health investigations on the basis of travel history 14 days before symptom onset. For this analysis, we included all countries identified as exposure locations for ≥2 US travel-associated dengue cases during the study period. ArboNET includes the country of exposure, date of symptom onset, and US state of residence. All analyses were based solely on dengue cases in US travelers.

Statistical Analysis

To identify elevated incidence periods in travelers, we fit country-specific regression models to monthly dengue case counts from January 2010–April 2024. Models included the month of symptom onset to capture seasonal variation and US state of residence to account for differences in reporting. We used negative binomial or Poisson regression, depending on the variance-to-mean ratio of case counts. For each country, we estimated the modeled distribution of expected monthly case counts and classified incidence as high (above the selected threshold), medium (between the median and the threshold), or low (below the median).

Sensitivity of Risk Warning Thresholds Analysis

We evaluated percentile thresholds at the 75th, 80th, and 90th levels because those thresholds are commonly used in outbreak detection algorithms to balance sensitivity and specificity: lower percentiles provide earlier signals, whereas higher percentiles provide more conservative classifications (*17*). For each threshold, we quantified how often country-months were flagged as high risk and the duration of consecutive high-risk periods (mean, median, and maximum). Our analysis focused on 27 countries that reported >2 travel-associated dengue cases in 2014, the year with the median number of travel-associated cases across the study period, to ensure sufficient data for comparison. Those analyses evaluated the sensitivity of risk warnings to threshold selection, balancing timeliness and specificity.

Real-Time Versus Retrospective Risk Assessments

To assess the effect of reporting delays on threshold classifications, we compared country-specific real-time case data (cases reported at the time of risk assessment) with complete retrospective data (full case data as of April 2024). For each country, we compared the duration of consecutive months with high-risk warnings under each percentile threshold in both datasets.

Case Count Thresholds Assessment

Our objective was not to redefine CDC's existing ≥10-case threshold for THNs but to embed it within

a transparent, reproducible modeling framework by using percentile-based thresholds accounting for seasonal and historical variation. To refine alert criteria, we assessed a dual-criteria rule requiring both exceedance of the 80th percentile threshold and ≥10 travel-associated dengue cases in a 3-month window. The ≥10-case criterion reflects internal CDC THN practice and is a pragmatic cutoff for distinguishing sustained transmission from isolated events. We applied that dual rule across all country-months and compared the number and duration of alerts generated by the threshold-only versus dual-criteria approaches.

Final Alert Criteria for THNs

On the basis of those analyses, the final criteria we used to classify country-months as high dengue risk were exceeding the 80th percentile of the modeled distribution of historical travel-associated dengue case counts and reporting ≥10 travel-associated dengue cases in the prior 3 months (Appendix Figures 1, 2, http://wwwnc.cdc.gov/EID/article/32/2/25-1217-App1.pdf). This dual-criterion approach distinguishes sustained incidence from isolated spikes, especially in countries with low traveler volume. The 3-month window reflects ongoing elevation in dengue risk, accommodates reporting delays, and aligns with the monthly review cycle used for CDC THNs. We classified a country as high-risk for a given month if both criteria were met during any of the preceding 3 months. We completed all analyses by using R version 4.4.0 (The R Project for Statistical Computing, https://www.r-project.org).

Results

Dataset Overview

ArboNET recorded 10,530 travel-associated dengue cases during January 2010–April 2024, involving travel to 128 countries (Appendix Table 1). During 2010–2023, the overall median delay between symptom onset and reporting date was 1.3 months (interquartile range [IQR] 0.7–2.7) (Appendix Figure 3), ranging from 1.9 months (IQR 1.1–3.9) during 2010–2019 to 2.8 months (IQR 1.3–10.3) in 2020–2021 and 1.3 months (IQR 0.9–2.2) in 2022–2023. Real-time data missed a median of 25% (IQR 15%–39%) of retrospective high-risk months across countries, with country-specific proportions ranging from 0% (e.g., Barbados, Jamaica, Peru) to 100% (Kenya) (Appendix Table 2).

Temporal Patterns

We observed clear seasonal fluctuations in dengue cases among US travelers, stratified by country, which were reflected in the estimated thresholds. By using an 80th percentile threshold derived from retrospective models, we found that some countries experienced sustained high risk over multiple years, whereas others had more sporadic elevations (Figure 1; Appendix Figures 4, 5). Costa Rica (58 months), Haiti (57 months), Mexico (44 months), Dominican Republic (41 months), and the Philippines (41 months) had the most months retrospectively classified as high-risk, indicating frequent and prolonged traveler-associated incidence. Cuba demonstrated a more recent pattern, with 36 high-risk months from late 2018 to early 2024, including the highest number of traveler cases in a single month, 241 cases in August 2022. India (40 months), Thailand (37 months), Jamaica (36 months), Brazil (31 months), and Honduras (30 months) also demonstrated persistent incidence. In contrast, some countries had more sporadic dengue incidence with fewer high-risk months, such as French Polynesia (13 months), Ecuador (5 months), Peru (5 months), and Sri Lanka (5 months), reflecting short-lived increases in cases among travelers.

Sensitivity of Risk Warning Thresholds and the Duration of Risk Warnings

We found that by applying the threshold-only approach, the frequency of high-risk months increased with lower percentile thresholds (Figure 2; Appendix Figure 6). Some countries, such as India and the Philippines, had substantially fewer high-risk months at the 90th percentile than at the 75th percentile, whereas countries including Guatemala and Jamaica showed more stable patterns and were less sensitive to threshold choice.

The median duration of elevated-risk warnings, which we defined as consecutive months classified as high risk on the basis of threshold exceedance alone, was 5 months at the 80th percentile (Appendix Figure 6). At the 90th percentile, the median warning duration was 3 months, whereas at the 75th percentile it also reached 5 months. Cuba had the longest warning durations, a median of 15.5 months and a maximum of 30 months at the 80th percentile, reflecting prolonged high-risk periods. India (median 12 months) and Mexico (median 6 months) also showed extended warnings. Sri Lanka, Malaysia, and Ecuador had consistently short warning durations (3–4 months), indicating more transient activity or lower traveler volume.

Threshold choice also influenced the overall frequency of high-risk months. Across all countries, we classified a median of 33% (IQR 11%–46%) of months as high risk at the 75th percentile, compared with 29%

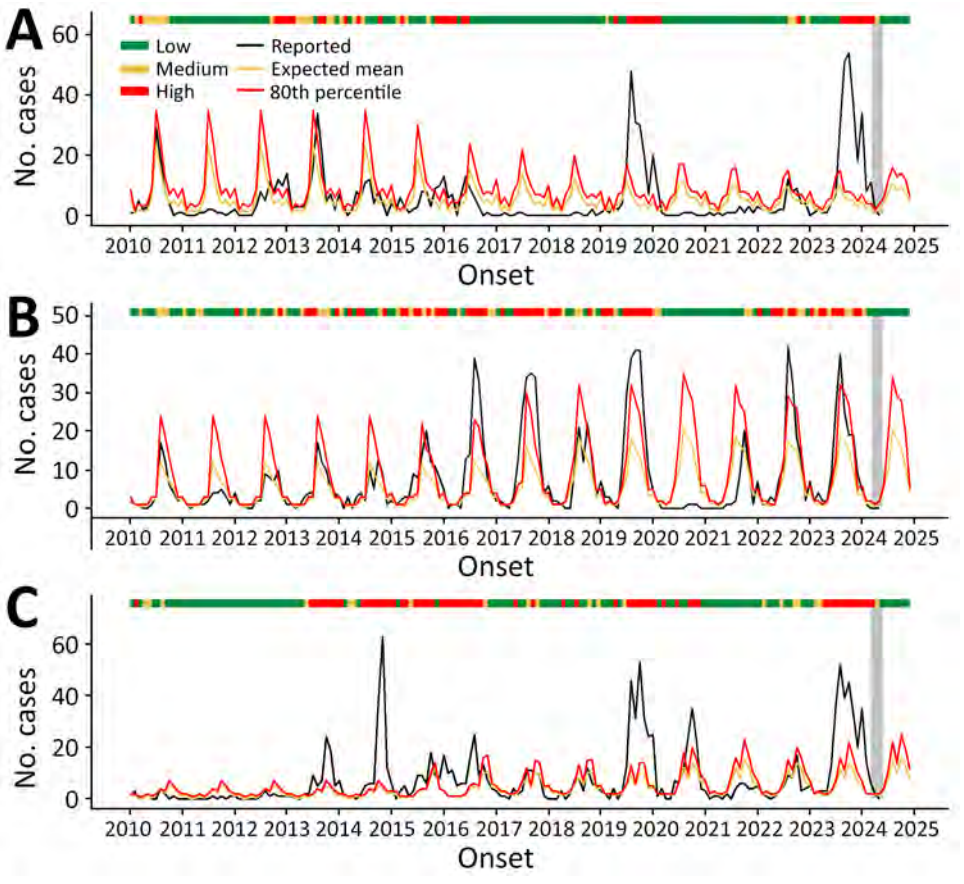

Figure 1. Temporal patterns and modeled transmission classification levels on the basis of percentile thresholds for dengue cases in travelers returning to the United States from the Dominican Republic (A), India (B), and Mexico (C), 2010–2024. Black line represents monthly dengue cases reported in US travelers. Yellow line represents expected mean number of cases on the basis of the fitted model. Red line represents the 80th percentile of the fitted distribution. Risk levels were categorized as low (green bar), medium (yellow bar), or high (red bar). We made those classifications on the basis of modeled case counts and did not incorporate the ≥10-case count criterion used in the Travel Health Notice classification. The most recent months of reported data at the time of analysis are shaded in gray to indicate periods of incomplete reporting. All 3 countries showed strong seasonal patterns and multiple sustained periods where traveler case counts exceeded the 80th percentile, reflected in frequent high-risk classifications, particularly during recent years (2022–2024).

(IQR 11%–42%) at the 80th percentile and 19% (IQR 9%–25%) at the 90th percentile (Appendix Table 3), demonstrating that stricter cutoffs reduced the proportion of months flagged as elevated risk.

Assessment of Risk Levels with Real-time Data

When we compared real-time and retrospective data, we found the average number of months that dengue cases crossed the threshold was similar (Figure 2; Appendix Figure 6). However, differences emerged by country and threshold level. Honduras, Guatemala, and Jamaica showed little change in the number of high-risk months when using real-time data versus retrospective data. In contrast, fewer months were flagged by using real-time (compared with retrospective) data for Brazil, Dominican Republic, Haiti, India, and the Philippines, particularly at the 80th and 90th percentiles, indicating reduced sensitivity to sustained transmission when relying only on contemporaneous reports. Some countries, including Barbados and Colombia, had high-risk periods identified only in the retrospective assessment, not detected in real-time, across all 3 thresholds, underscoring the effect of reporting delays and gaps (Appendix Figure 6).

Although the number of months crossing the threshold was generally consistent, the mean duration of outbreak warnings on the basis of real-time data was shorter than for retrospective data (Figures 2; Appendix Figure 6). For instance, at the 80th percentile threshold, the median warning duration was 3 months for real-time data (IQR 3.0–6.0), compared with 4.5 months for retrospective data (IQR 3.0–7.0) among countries with ≥2 dengue cases in 2014. The narrower IQR in real-time data suggests that incomplete reporting can interrupt otherwise continuous outbreaks, effectively chopping longer episodes into shorter ones and reducing sensitivity to sustained transmission, especially where healthcare-seeking and reporting practices vary.

Addition of Case Count Thresholds

Applying the dual-criteria rule, which required both threshold exceedance and ≥10 cases in a 3-month period, reduced the number of THN alerts by 52.8%

from 714 to 337. The magnitude of reduction varied by country (Figures 3, 4). In higher-volume origins such as Cuba and Mexico, most high-risk months also met the ≥10-case criterion, whereas in others, such as Thailand, Colombia, and Malaysia, many threshold-exceedance months did not meet the case-count criterion.

To contextualize alert frequency by country, we also visualized total travel-associated case volume alongside alert months (Figure 4). Countries with higher dual-criteria alert frequencies generally correspond with higher traveler case volumes. For example, Cuba reported 1,609 travel-associated dengue cases and met both criteria in 52 months, whereas countries such as Singapore, Kenya, and China had both low case counts and few or no alert months.

Final Criteria and Application to Travel Health Notices

We applied the final dual-criteria alert approach to identify country-months with sustained dengue incidence relevant to US travelers beginning in 2024. We then compared monthly traveler-based alerts to historical CDC THNs. The new method identified substantially more high-risk periods than THNs issued during the same interval (Appendix Figure 7). Although THNs often captured isolated or short-lived signals, typically 1- or 2-month spans, the new criteria consistently flagged longer durations of elevated incidence. From mid-2023 to early 2024, Brazil, Costa Rica, Cuba, Dominican Republic, Guatemala, Jamaica, and Mexico all experienced extended multi-month periods flagged by the new method, whereas corresponding THNs were limited or absent. For example, no THNs were issued for Brazil or Costa Rica despite 6–10 consecutive months meeting both incidence and case-volume criteria. Some official outbreak notifications during the study period were not captured by the final alert criteria (Appendix Figure 7), reflecting the inherent limitations of relying solely on traveler-based data.

Discussion

This study demonstrates that national surveillance for travel-associated dengue can detect periods of heightened dengue activity and provide early warning of increased incidence in international destinations. We identified seasonal patterns by country and derived country-specific thresholds that account for expected trends. We also detected high dengue incidence in countries with limited public reporting, such as Cuba, where sustained activity was evident from late 2018 to early 2024, highlighting the added value of traveler-based surveillance. Outbreak detection varied by percentile threshold, with the 80th percentile providing a useful balance between sensitivity and specificity. When we compared real-time with retrospective data there were generally consistent elevated-risk detections, although reporting delays shortened the apparent duration of warnings for some countries. When we applied a minimum case count threshold (≥10 cases in 3 months) we noted an increased specificity while maintaining sensitivity, minimizing low-volume anomalies and consistently identifying prolonged high-risk periods aligned with known outbreaks.

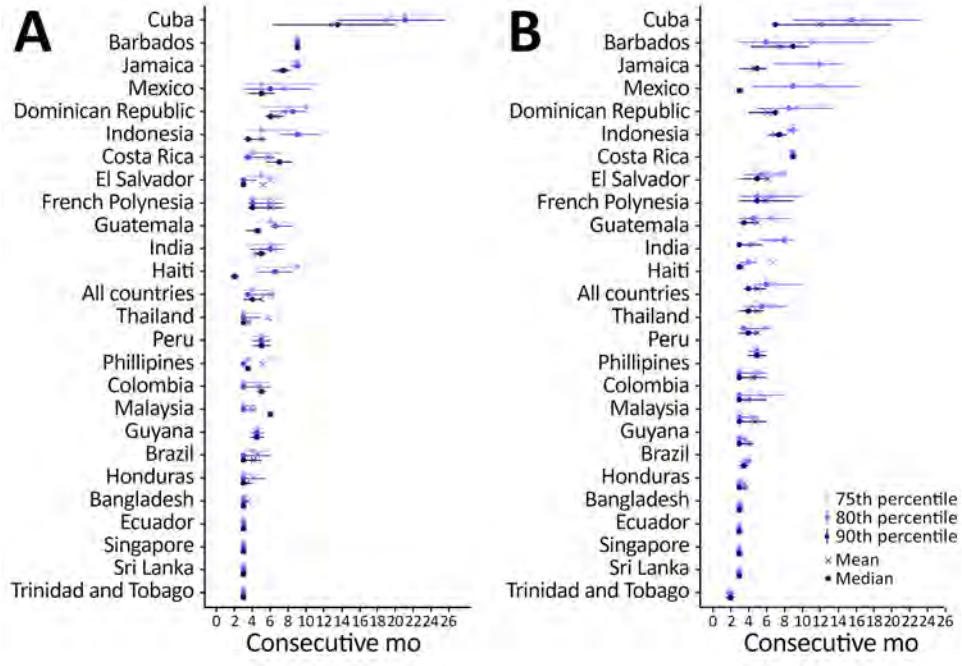

Figure 2. Duration of dengue outbreak warnings by country of exposure for travelers returning to the United States, based on different percentile thresholds in retrospective and real-time datasets, 2010–2024. A) Retrospective (complete) ArboNET data. B) Real-time data available at each monthly timepoint. Panels show the distribution of consecutive months classified as high-risk for dengue based solely on the 75th, 80th, and 90th percentile thresholds. Horizontal lines represent the interquartile range of outbreak duration for each country; median and mean warning lengths are indicated.

Figure 3. Monthly dengue risk classifications among travelers returning to the United States, by country, by using real-time data and dual-alert criteria, 2014–2024. Each tile represents 1 country-month and is colored according to the criteria met: dark green for months that met both criteria (dengue case counts exceeded the 80th percentile threshold and met the ≥10 case-criterion in the previous 3-month window), yellow for months exceeding the 80th percentile threshold only, and light green for months meeting the ≥10-case criterion but below the transmission threshold. Blank tiles indicate months that met neither criterion. The high transmission threshold was based on the 80th percentile of modeled country-specific traveler case distributions (real-time or annually updated). Countries are ordered by the total number of months that met both criteria.

Changes in dengue incidence patterns inferred from traveler data depend on factors including the number of travelers, travel routes, and individual prevention measures, which are difficult to quantify. Because ArboNET did not capture the total number of US travelers to each country, we could not calculate incidence rates or directly adjust for traveler volume. Instead, we analyzed trends in absolute case counts by using thresholds that incorporate historical and seasonal patterns, providing a practical and interpretable approach in the absence of denominator data. Traveler-based data also do not necessarily mirror local transmission intensity. Countries with inadequate reporting systems might appear to have few outbreaks in official statistics while traveler data reveal ongoing transmission; conversely, concentrated tourism in low-risk areas might yield lower traveler risk than national averages suggest. Those discrepancies underscore both the value and limitations of using travelers as a proxy for local populations. Because of those limitations, this framework is intended as guidance for US travelers and health practitioners and as a complement, not a replacement, to in-country surveillance.

Our findings indicate that traveler cases can reliably capture seasonal trends and detect increases above expected levels. Seasonal patterns aligned with known dengue transmission seasons across multiple countries, and stronger signals were found in destinations frequently visited by US travelers, including the Caribbean, Mexico, and Central America. Fewer cases were detected from more distant dengue-endemic countries, such as Singapore and Kenya, likely reflecting lower US traveler volume. India was an exception of note, with clear seasonal trends and high-incidence months consistently detected across 14 years, likely reflecting substantial travel between the United States and India (*18*). Although a single traveler population will not provide equal indicators of risk for all countries, traveler-based thresholds remain highly relevant for informing US THNs and could be adapted by other countries by using their own traveler surveillance data.

Our results support using traveler-based dengue surveillance as one component of a broader decision-making framework for timely risk communication through THNs. The 2023 spike in cases among

travelers from Costa Rica, Dominican Republic, Honduras, Jamaica, and Mexico, all surpassing the 80th percentile, highlights the need for timely, country-specific THNs. In contrast, some destinations did not reach high-risk thresholds, either because of better-controlled transmission or lower traveler volume, enabling more targeted responses rather than uniform interventions. Operationally, traveler-based surveillance could be used as a routine supplement to THN reviews, flagging destinations that exceed traveler-based thresholds even when local reporting is incomplete. Integration into dashboards or automated alerting systems would enable CDC and partner agencies to cross-check traveler signals against official reports, strengthening risk communication for travelers and clinicians.

Despite improved specificity and sensitivity, the final alert criteria did not capture several official

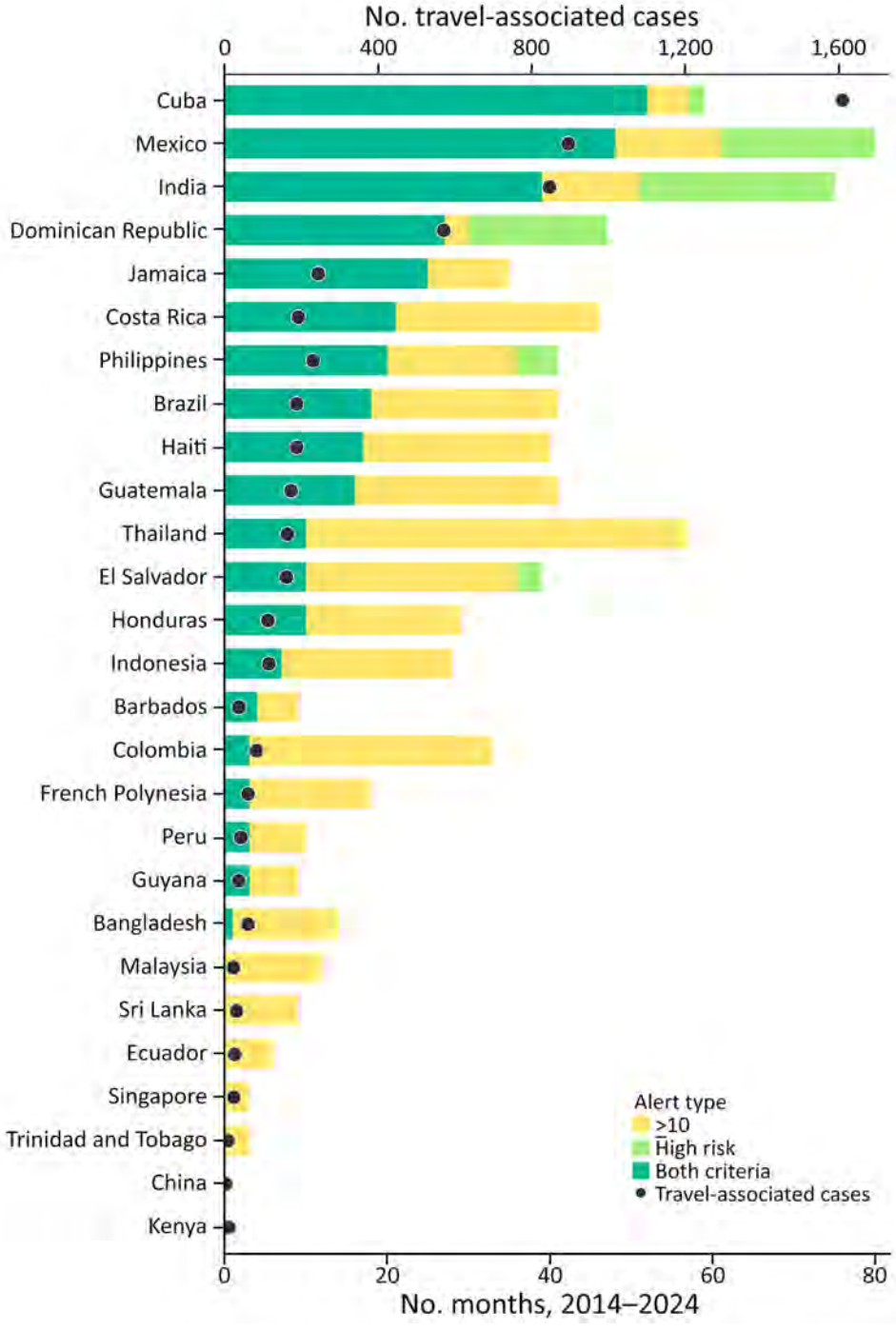

Figure 4. Travel-associated dengue case volume and number of alert months among travelers returning to the United States, by country, 2014–2024. Stacked bars represent the number of months each country was classified as meeting both criteria (teal), exceeding the 80th percentile threshold only (yellow), or meeting the ≥10-case criterion only (light green); categories are mutually exclusive, as in Figure 3. Dots indicate the total number of travel-associated dengue cases reported from each country over the same period. The secondary y-axis reflects case counts scaled to align with the alert-month axis.

outbreak notifications, underscoring a crucial limitation of traveler-based surveillance. Traveler data should not be used alone to infer local incidence; integrating multiple surveillance sources remains essential for comprehensive global dengue risk monitoring. In countries with sparse traveler data, alerts could be improved by combining traveler-based signals with regional context, historical travel volume, or syndromic surveillance from other sources. Linking traveler thresholds with airline passenger data or mobility datasets might also strengthen interpretability when case numbers are low.

Although traveler-based surveillance offers advantages in sensitivity and timeliness, particularly for sustained transmission that might be underreported locally, it is not intended to replace existing systems. Official publications and outbreak alerts remain critical for identifying emerging risks, as in-country surveillance, when available, provides the most reliable indicator of disease trends. Traveler-based data can nonetheless serve as an early warning system where official dengue reporting is incomplete or delayed (*9*,*19*,*20*). This approach aligns with the World Health Organization's International Health Regulations, which emphasize early detection and rapid response to public health threats of international concern (*21*,*22*), and illustrates how model-based approaches can be integrated with traditional surveillance to support more complete risk assessment.

A key insight from our study is that real-time and retrospective data produced similar outbreak warnings, suggesting the traveler-based threshold approach is robust to moderate reporting delays. Further improvements in real-time data collection and reporting, through better coordination among clinicians, laboratories, and public health agencies at state and federal levels, would still enhance the timeliness of outbreak alerts and public health responses (*17*,*23*).

The first limitation of our study is that dengue case detection in travelers depends on healthcare-seeking behavior and diagnostic practices in the United States, and many infections are likely underreported; we assume underreporting is relatively consistent over time, enabling reliable trend analysis. Second, traveler data might not fully reflect transmission in origin-country populations because findings depend on where travelers go and how travel volume changes, including in response to mass gatherings or other events. Without data on total US travelers by destination, we cannot calculate incidence rates or separate changes in transmission from changes in travel volume. Although such events could drive short-term increases, our dual-criteria approach reduces the effect of transient spikes by focusing on sustained incidence and still provides useful information for travelers visiting elevated-risk locations. Third, thresholds are based on reported case counts, which are subject to underreporting and variable healthcare-seeking behavior in both origin countries and the United States. If surveillance systems capture only 10%–30% of symptomatic dengue infections, then true incidence is substantially higher than observed, but thresholds should still capture relative deviations from baseline, which is the primary goal for outbreak detection. Fourth, reporting delays in ArboNET, median 1.3 months during 2010–2023, limit real-time utility because some cases are not available until weeks after onset, and reporting lag remains a constraint on timeliness. Fifth, the approach may be less sensitive in destinations infrequently visited by US travelers, limiting generalizability, although it could be adapted by other countries using their own traveler surveillance. Finally, transmission dynamics evolve over time, and growing global dengue incidence will require periodic updates of warning thresholds, with more frequent updates during major epidemics or when real-time decision-making is needed.

In conclusion, travel-associated dengue surveillance provides a practical, timely complement to national systems, particularly for travelers visiting high or emerging dengue-risk regions. Our dual-criteria method offers a transparent framework that can be adapted by other countries by using traveler or sentinel surveillance data. Future work should validate thresholds against independent datasets, explore integration with mobility and genomic data, and assess cost-effectiveness for real-time implementation. Embedding traveler-based analyses into existing decision-making frameworks, such as CDC's THN process and the World Health Organization's International Health Regulations, could strengthen global preparedness and support more timely, targeted responses to dengue outbreaks.

About the Author

Dr. Rysava is a disease ecologist and epidemiology modeler at The Zeeman Institute for Systems Biology & Infectious Disease Epidemiology Research at the University of Warwick, United Kingdom. Her main research interests include understanding ecological, environmental, and social determinants driving disease dynamics, focused on applications in health policy. Dr. Madewell is an epidemiologist with the Dengue Branch of the Centers for Disease Control and Prevention, in San Juan, Puerto Rico. His primary research interests include epidemiologic study and modeling of infectious diseases.

References

1. Paz-Bailey G, Adams LE, Deen J, Anderson KB, Katzelnick LC. Dengue. Lancet. 2024;403:667–82. https://doi.org/10.1016/S0140-6736(23)02576-X
2. St John AL, Rathore APS. Adaptive immune responses to primary and secondary dengue virus infections. Nat Rev Immunol. 2019;19:218–30. https://doi.org/10.1038/s41577-019-0123-x
3. Murphy BR, Whitehead SS. Immune response to dengue virus and prospects for a vaccine. Annu Rev Immunol. 2011;29:587–619. https://doi.org/10.1146/annurev-immunol-031210-101315
4. Montoya M, Gresh L, Mercado JC, Williams KL, Vargas MJ, Gutierrez G, et al. Symptomatic versus inapparent outcome in repeat dengue virus infections is influenced by the time interval between infections and study year. PLoS Negl Trop Dis. 2013;7:e2357. https://doi.org/10.1371/journal.pntd.0002357
5. Anderson KB, Gibbons RV, Cummings DA, Nisalak A, Green S, Libraty DH, et al. A shorter time interval between first and second dengue infections is associated with protection from clinical illness in a school-based cohort in Thailand. J Infect Dis. 2014;209:360–8. https://doi.org/10.1093/infdis/jit436
6. Bhatt S, Gething PW, Brady OJ, Messina JP, Farlow AW, Moyes CL, et al. The global distribution and burden of dengue. Nature. 2013;496:504–7. https://doi.org/10.1038/nature12060
7. Cattarino L, Rodriguez-Barraquer I, Imai N, Cummings DAT, Ferguson NM. Mapping global variation in dengue transmission intensity. Sci Transl Med. 2020;12:eaax4144. https://doi.org/10.1126/scitranslmed.aax4144
8. Ware-Gilmore F, Rodriguez DM, Ryff Mph K, Torres JM, Velez MP, Torres-Toro CT, et al. Dengue outbreak and response—Puerto Rico, 2024. MMWR Morb Mortal Wkly Rep. 2025;74:54–60. https://doi.org/10.15585/mmwr.mm7405a1
9. Taylor-Salmon E, Hill V, Paul LM, Koch RT, Breban MI, Chaguza C, et al. Travel surveillance uncovers dengue virus dynamics and introductions in the Caribbean. Nat Commun. 2024;15:3508. https://doi.org/10.1038/s41467-024-47774-8
10. Messina JP, Brady OJ, Scott TW, Zou C, Pigott DM, Duda KA, et al. Global spread of dengue virus types: mapping the 70 year history. Trends Microbiol. 2014;22:138–46. https://doi.org/10.1016/j.tim.2013.12.011
11. Stoddard ST, Forshey BM, Morrison AC, Paz-Soldan VA, Vazquez-Prokopec GM, Astete H, et al. House-to-house human movement drives dengue virus transmission. Proc Natl Acad Sci U S A. 2013;110:994–9. https://doi.org/10.1073/pnas.1213349110
12. Wesolowski A, Qureshi T, Boni MF, Sundsøy PR, Johansson MA, Rasheed SB, et al. Impact of human mobility on the emergence of dengue epidemics in Pakistan. Proc Natl Acad Sci U S A. 2015;112:11887–92. https://doi.org/10.1073/pnas.1504964112
13. Centers for Disease Control and Prevention. Travel Health Notices. 2024 [cited 2024 Aug 27]. https://wwwnc.cdc.gov/travel/notices
14. Wong JM, Rivera A, Volkman HR, Torres-Velasquez B, Rodriguez DM, Paz-Bailey G, et al. Travel-associated dengue cases—United States, 2010–2021. MMWR Morb Mortal Wkly Rep. 2023;72:821–6. https://doi.org/10.15585/mmwr.mm7230a3
15. Centers for Disease Control and Prevention. Dengue: historic data (2010–2024). 2025 [cited 2025 Jun 6]. https://www.cdc.gov/dengue/data-research/facts-stats/historic-data.html
16. Centers for Disease Control and Prevention. ArboNET. 2024 [cited 2024 Aug 19]. https://www.cdc.gov/mosquitoes/php/arbonet
17. Thayer MB, Marzan-Rodriguez M, Torres Aponte J, Rivera A, Rodriguez DM, Madewell ZJ, et al. Dengue epidemic alert thresholds for surveillance and decision-making in Puerto Rico: development and prospective application of an early warning system using routine surveillance data. BMJ Open. 2025;15:e106182. https://doi.org/10.1136/bmjopen-2025-106182
18. International Trade Administration. December and annual 2024 total international travel volume to and from the United States. 2025 [cited 2025 Jul 28]. https://www.trade.gov/feature-article/december-and-annual-2024-total-international-travel-volume
19. Cordes KM, Cookson ST, Boyd AT, Hardy C, Malik MR, Mala P, et al. Real-time surveillance in emergencies using the early warning alert and response network. Emerg Infect Dis. 2017;23:S131–7. https://doi.org/10.3201/eid2313.170446
20. Meckawy R, Stuckler D, Mehta A, Al-Ahdal T, Doebbeling BN. Effectiveness of early warning systems in the detection of infectious diseases outbreaks: a systematic review. BMC Public Health. 2022;22:2216. https://doi.org/10.1186/s12889-022-14625-4
21. World Health Organization. International health regulations. 2024 [cited 2024 Aug 23]. https://www.who.int/health-topics/international-health-regulations
22. Cramer EY, Ray EL, Lopez VK, Bracher J, Brennen A, Castro Rivadeneira AJ, et al. Evaluation of individual and ensemble probabilistic forecasts of COVID-19 mortality in the United States. Proc Natl Acad Sci U S A. 2022;119:e2113561119. https://doi.org/10.1073/pnas.2113561119
23. Charniga K, Madewell ZJ, Masters NB, Asher J, Nakazawa Y, Spicknall IH. Nowcasting and forecasting the 2022 U.S. mpox outbreak: support for public health decision making and lessons learned. Epidemics. 2024;47:100755. https://doi.org/10.1016/j.epidem.2024.100755

Address for correspondence: Zachary J. Madewell, Centers for Disease Control and Prevention, 1324 Cañada St, San Juan, PR 00920-3860, USA; email: ock0@cdc.gov

Pulmonary Complications in Fatal Yellow Fever, Brazil, 2017–2019

Amaro N. Duarte-Neto, Katia C. Dantas, Suzette C. Ferreira, Fernando R. Giugni, Marielton P. Cunha, Shahab Z. Pour, Felipe L. Ledesma, Yeh-Li Ho, Ana C.S. Nastri, Cinthya S.C. Borges, Fernanda A. Rodrigues, Ceila M.S. Malaque, Jaques Sztajnbok, Thais Mauad, Luiz F.F. Silva, Paulo H.N. Saldiva, Marisa Dolhnikoff

Yellow fever (YF) mainly causes severe hepatitis; data on pulmonary pathology remain limited. We investigated respiratory tract pathology in 73 fatal YF cases during the 2017–2019 epidemic in São Paulo, Brazil. All patients died from YF-related fulminant hepatitis. Autopsies revealed frequent tracheitis (91%), pulmonary edema and hemorrhage (100%), diffuse alveolar damage (84%), secondary pneumonia (84%), and bronchoaspiration (60%). Microabscesses, thrombi, and hemophagocytosis were also observed. In 5 cases of vaccine-associated viscerotropic disease, hemorrhage and diffuse alveolar damage were prominent. We detected antigens of YF virus in all cases and viral RNA in 94%. Molecular analysis identified bacterial and fungal pathogens in pneumonia, including gram-negative bacilli, *Candida* spp., and *Aspergillus* spp. Electron microscopy did not reveal viral particles in 3 examined cases. Our findings underscore the respiratory tract involvement in severe YF and could help guide diagnosis, intensive care, and public health preparedness in future outbreaks.

Yellow fever (YF) is a mosquitoborne, flavivirus-induced hemorrhagic fever with a high case-fatality rate. The disease is endemic in tropical regions of South America and sub-Saharan Africa, with sporadic epidemics (*1*,*2*).

Since the end of 2016, YF has reemerged in Brazil, affecting areas not previously considered to be at risk outside the Amazon Basin, the region in Brazil endemic for the disease (*3*). During 2017–2019, a total of 696 cases of YF were reported in the state of São Paulo, with 232 deaths (mortality rate 33.3%) (*4*–*6*). Several factors are likely to have contributed to the recent expansion of YF in Brazil toward the southeast region. In São Paulo state, the vector, *Aedes aegypti* mosquitoes, has reached near-universal distribution, infesting ≈93.6% of municipalities. That pattern is exacerbated during warmer and wetter periods, such as El Niño events, and is strongly associated with urban density and inadequate infrastructure. Other contributing factors include the increase in neotropical nonhuman primates as susceptible amplifier hosts of YF virus (YFV), low vaccination coverage of susceptible persons living close to the forest, and viral factors. Molecular sequencing and phylogenetic studies have demonstrated that the South American genotype I, lineage 1E, is the strain of YFV involved in recent Brazil epidemics; some mutations are potentially influencing viral replication and fitness (*3*–*5*).

The clinical picture of YF is classified in 5 periods: the incubation period, after the bite of an infected mosquito; the period of infection, which coincides with viremia, with influenza-like symptoms; the period of remission, in which the patient has a slight improvement in symptoms and might progress to cure, and in which serum YFV IgM neutralizing antibodies appear; the period of intoxication, with variable severity, characterized by recurrence of fever, signs and symptoms of an acute hepatitis, oliguria, and hemorrhagic phenomena; and finally, the period of convalescence, with complete resolution of symptoms and laboratory alterations (*2*,*7*).

The pathology of severe YF, first described in the 19th Century, consists of midzonal hepatitis as the main lesion; it is characterized by apoptotic and steatotic hepatocytes associated with visceral edema and hemorrhagic phenomena, which lead to death (*8*,*9*). However, studies conducted during the 2017–2019 YF

Author affiliations: Universidade de São Paulo, São Paulo, São Paulo, Brazil (A.N. Duarte-Neto, K.C. Dantas, F.R. Giugni, M.P. Cunha, S.Z. Pour, F.L. Ledesma, Y.-L. Ho, A.C.S. Nastri, F.A. Rodrigues, T. Mauad, L.F.F. Silva, P.H.N. Saldiva, M. Dolhnikoff); Fundação Pró-Sangue Hemocentro de São Paulo, São Paulo (S.C. Ferreira); Instituto Adolfo Lutz, São Paulo (C.S.C. Borges); Instituto de Infectologia Emílio Ribas, São Paulo (C.M.S. Malaque, J. Sztajnbok).

DOI: https://doi.org/10.3201/eid3202.250530

epidemic in Brazil have broadened our understanding of the disease (*7*,*10*–*16*). Those investigations have provided new insights into the molecular characteristics of circulating YFV strains; emerging clinical manifestations including seizures, pancreatitis, refractory acidosis, and late-onset hepatitis recurrence in convalescent patients; the kinetics of serum YFV RNA detected by reverse transcription PCR (RT-PCR); mortality predictors and prognostic biomarkers; and novel therapeutic strategies such as hemodialysis and plasma exchange. In addition, new data on the pathology of YF have been described. Our group has previously demonstrated YFV replication in various body systems (*5*), characterization of YFV-infected liver grafts in cases undergoing liver transplantation for YFV fulminant hepatitis (*17*), ultrasound-guided minimally invasive tissue sampling as an equivalent alternative to conventional autopsy for the postmortem diagnosis of YF (*9*), and a detailed description of cardiac and endothelial pathology in YF (*18*).

Although YFV is considered a hepatotropic virus, the systemic effects of severe YF are not yet well understood. One of the most intriguing findings from our autopsy cohort of fatal YF cases is pulmonary injury. In previous studies describing the first 20 cases, we reported severe pneumonia caused by bacteria and filamentous fungi in 12 cases, in addition to alveolar edema and hemorrhage in all 20 (*9*,*17*). To understand the role of the respiratory tract in the pathology of severe or fatal YF, we described the tracheal and pulmonary pathological changes in 73 fatal cases, their association with clinical and laboratory features, and molecular findings.

Methods

Study and Autopsy Protocols

This autopsy-based case series study was conducted during the seasonal period of 2017–2019 YF epidemic. This report is part of a project approved by Hospital das Clínicas da Faculdade de Medicina da Universidade de São Paulo (HCFMUSP) Ethical Committee (process no. 2·669·963). That hospital and Emílio Ribas Institute of Infectious Diseases are referral hospitals for YF cases in the state of São Paulo, Brazil; all YF cases were referred to them. The committee recommended autopsy upon patient death; all autopsies were performed with the written consent of first-degree relatives.

We used the definition from the Brazil Ministry of Health and local public health authorities to diagnose YF (*6*,*7*,*10*). Confirmed cases had a compatible clinical manifestation and laboratory confirmation by ≥1 method: positive serum IgM, detection of YFV RNA by RT-PCR in blood samples, and histopathology compatible for YF hepatitis with YF antigen detectable in tissues by immunohistochemistry (*6*,*7*,*10*,*11*). We excluded other causes of hepatic failure (Appendix, https://wwwnc.cdc.gov/EID/article/32/2/25-0530-App1.pdf). We classified the YF vaccine–associated viscerotropic disease (YEL-AVD) as level 1 of diagnostic certainty (*19*).

We collected demographic and clinical data from patients' records; data included sex (assigned at birth), age, previous medical history, and clinical and laboratory results during hospitalization. We performed autopsies in accordance with Letulle's technique and examined all organs (*9*). From each patient we collected ≥10 lung samples, including 1 peripheric (with pleural tissue) and 1 from the central area of each pulmonary lobe. In 57 (78%) cases, we took trachea samples. We fixed tissue samples in buffered 10% formalin, embedded them in paraffin sections, and used hematoxylin and eosin (HE) stain. We performed additional stains in pulmonary sections with histologic signs of infections. A pathologist specializing in autopsy and infectious diseases and several pulmonary pathologists reviewed the histopathology of all samples; we resolved disagreements by consensus.

Molecular Diagnosis and Sequencing

We collected a total of 73 lung tissue samples during autopsy and used specific primers and probes in quantitative RT-PCR to detect YFV RNA (*5*,*9*,*17*). We performed nested PCR in frozen lung samples for fungi and bacteria detection. We Sanger sequenced samples of lung tissue in which fungi and bacteria were detected (Appendix).

Immunohistochemistry

Selected pulmonary cuts without extensive pneumonia underwent immunohistochemistry reactions for detecting YFV antigens. We used a primary antibody, a polyclonal anti-YFV mouse ascitic fluid specific to the virus, originally standardized for ELISA and validated for formalin-fixed paraffin-embedded tissues in our laboratories at the optimized dilution of 1:20,000 (*9*,*17*). In the validation procedures, we tested YFV primary antibody on YFV-infected liver samples confirmed by PCR and serology and in negative cases with different liver diseases for specificity (Appendix). We considered samples positive for YFV if chromogen stained the cytoplasm of hepatocytes, Kupffer cells, or inflammatory cells in the liver. All YF-negative cases had a negative reaction for YFV

antigens in the liver. We also tested for vascular cell adhesion molecule (VCAM, mouse monoclonal, clone E10; Santa Cruz Biotechnology, Inc., https://www.scbt.com) at 1:100 dilution and VIII factor of coagulation (polyclonal IH, 760–2642; Roche, https://www.roche.com). We have not performed immunohistochemistry reactions to detect YFV antigens on tracheal sections.

Electron Microscopy

We collected 3 lung tissue samples from different cases and fixed them in 3% glutaraldehyde for examination. We fixed and processed samples as previously described (*17*). We analyzed the thin sections under a transmission electron microscope (Philips Tecnai 10, 80kV; Thermo Fisher Scientific, https://www.thermofisher.com).

Results

During 2017–2019, a total of 696 cases of YF were reported in the state of São Paulo; 232 (33.3%) cases resulted in death. Of those, 84 cases were referred for autopsy at the central morgue in São Paulo to determine cause of death; YF was excluded as the cause in 9 cases and confirmed in 73 cases. The main cause of death was fulminant YF-related hepatitis in all 73 cases. The immediate causes of death were as follows: pulmonary hemorrhage in 28 cases (38.4%), intraabdominal hemorrhage in 26 (35.6%), sepsis due to intestinal ischemia in 6 (8.2%), cerebral event (hemorrhage or herniation) in 6 (8.2%), necrohemorrhagic pancreatitis in 4 (5.5%), and sepsis due to bronchopneumonia in 3 cases (4.1%). Therefore, for 31 (42.4%) cases, the immediate cause of death was pneumonia or hemorrhage in the respiratory tract. The time from death to autopsy was 6 hours to 44 hours 19 minutes (median 14 hours 50 minutes).

Clinical Characteristics and Laboratory Results

Of the 73 confirmed cases of YF, we classified 68 (93.2%) cases as wild-type YF, and 5 (6.8%) cases as YEL-AVD (Table 1). Sixty-two (84.9%) of the 73 patients were male and 11 (15.1%) female; median age was 48 (34–60) years. The most common underlying conditions were arterial hypertension (28.8%), diabetes (11%), alcohol use (50.7%), and smoking (37.0%). The median duration of hospitalization was 5 days, and the median interval from symptoms to death was 9 days. Four patients underwent liver transplantation for YF-fulminant hepatitis. Secondary infection was diagnosed clinically in 56 (76.7%) cases, mostly through blood cultures. All patients underwent mechanical ventilation and experienced shock, requiring vasopressors. Initial laboratory results showed neutrophilia (median 4,466 cells/μL, reference range 1,592-4,350 cells/μL), lymphopenia (median 675 cells/μL, reference range 1,120–2,946 cells/μL), and ratio of the partial pressure of oxygen in arterial blood to inspired oxygen (PaO_2/FiO_2) >300 mm Hg (reference threshold >400 mm Hg). During hospitalization, 36 (56%) cases had PaO_2/FiO_2 <200, and 12 (19%) cases had PaO_2/FiO_2 <100.

Pathology

All case-patients had visible signs of liver failure (jaundice, cavitary effusions, visceral congestion, edema, and hemorrhage) (Table 2). Gastrointestinal hemorrhages with signs of mesenteric ischemia and acute tubular necrosis were universal in variable degrees. The livers from all cases were steatotic with typical microscopic findings of YF hepatitis: midzonal hepatitis with steatotic and apoptotic hepatocytes, scarce inflammatory reaction, and positive expression of YFV antigens in degenerated hepatocytes and hepatic mononuclear cells. The main immediate cause of death was shock caused by hemorrhages in the gastrointestinal and respiratory tracts, refractory acidosis, and sepsis. At the respiratory tract, the main tracheal changes were congestion in 72 cases (99%), hemorrhage in 58 (79%), and ulceration in 41 (56%). Tracheal samples were available for 57 cases and showed tracheitis (91%), mucosal necrosis (45%), and microorganisms (35%) through histochemical stains. The lungs were heavier than normal; cut surfaces showed edema and hemorrhages, diffusely in both lungs, from all cases (Table 2). We observed friable cut surfaces mainly in middle and inferior pulmonary fields in cases with pneumonia (Figure 1). We noted macroscopic thrombi in 2 cases.

The main microscopic findings were alveolar edema in 72 (99%) cases, alveolar hemorrhage in 66 (90%) cases, and secondary suppurative pneumonia in 61 (84%) cases; pneumonia was bilateral in 49 (67%) cases, with microabscesses in 23 (32%) cases, and associated with signs of bronchoaspiration (alimentary vegetal material in pulmonary tissue) in 44 (60%) cases (Figure 2). Gram-negative bacilli were detectable in 59 (81%) cases, yeasts in 27 (37%) cases, hyphomycetes in 9 (12%) cases, and gram-positive cocci in 6 (8%) cases. The yeasts had morphologic aspects compatible with *Candida* spp.; most hyphae had morphology compatible with *Aspergillus* spp. One case had hyphae resembling *Mucorales* spp. Fungal pneumonia was associated with angioinvasion, tissue necrosis, cellular debris, and scarce inflammatory reaction surrounding the fungal forms. We found

septic pulmonary vasculitis in 13 (21.3%) cases: in 1 (7.7%) case from gram-positive cocci, in 2 (15.3%) from gram-negative bacilli, in 2 (15.3%) from yeasts, and in 8 (80%) from hyphomycetes (Figures 2, 3). Septal capillaries showed increased numbers of circulating megakaryocytes in 67 (92%) cases and fibrinoid necrosis in 42 (58%) cases. We observed microscopic thrombi in 23 (32%) cases and diffuse alveolar damage (DAD) in 61 (84%) cases, mainly in the exudative phase (Figure 2). All patients with PaO_2/FiO_2 ratio <300 had DAD. We observed hemophagocytosis in the intraalveolar macrophages or the intrapulmonary lymph nodes in 16 (22%) cases. One case showed a calcified primary complex at the hilum and another an isolated cryptococcoma. We observed no viral cytopathic effect.

Table 1. Clinical characteristics of patients in study of severe YF, Brazil, 2017–2019*

Characteristic	Wild-type YF, n = 68	YEL-AVD, n = 5	Total YF, n = 73
Sex			
M	59 (86.8)	3 (60.0)	62 (84.9)
F	9 (13.2)	2 (40.0)	11 (15.1)
Age, y (range)	49 (35.5–60)	37 (32–49)	48 (34–60)
Previous medical condition			
Hypertension	19 (27.9)	2 (40.0)	21 (28.8)
Diabetes	8 (11.8)	0	8 (11.0)
Heart disease	5 (7.4)	0	5 (6.8)
Asthma/COPD	4 (5.9)	0	4 (5.5)
Habits			
Alcoholism	36 (52.9)	1 (20.0)	37 (50.7)
Smoking	26 (38.2)	1 (20.0)	27 (37.0)
Illicit drug use	11 (16.2)	0	11 (15.1)
Diagnostic criteria for YF			
Clinical criteria	68 (100)	5 (100)	73 (100)
Epidemiologic criteria	68 (100)	5 (100)	73 (100)
Live near to epizootic areas	46 (63)	NA	46 (63)
Travel to epizootic areas	35 (48)	NA	35 (48)
Serology, IgM, n = 47	37 (80)	NA	37 (80)
Time interval, d (range)			
Symptoms to hospitalization	4 (3–6)	5 (4–7)	4 (3–6)
Symptoms to death	9 (7–11)	8 (7–11)	9 (7–11)
Hospitalization to death	5 (3–6)	3 (2–5)	5 (3–6)
Intubation to death	2 (1–4)	2 (1–5)	2 (1–4)
Respiratory symptoms at admission			
Hemoptysis	6 (8.9)	1 (20)	7 (9.6)
Tachypnea	6 (8.9)	1 (20)	7 (9.6)
Cough	2 (3)	1 (20)	3 (4.1)
In-hospital events and interventions			
Shock or vasopressor use	68 (100)	5 (100)	73 (100)
Dialysis	58 (85.3)	4 (80.0)	62 (84.9)
Mechanical ventilation	68 (100)	5 (100)	73 (100)
Liver transplant for YF hepatitis	4 (5.9)	0	4 (5.5)
Secondary infection	53 (77.9)	3 (60.0)	56 (76.7)
Clinical diagnosis of pneumonia	5 (7)	0	5 (7)
SAPS 3, no. (range)	62 (31–104)	0	62 (31–104)
Vaccine status			
YF vaccine	9 (13.2)	5 (100)	14 (19.2)
Vaccination >10 d before symptoms	2 (2.9)	0	2 (2.7)
Laboratory tests, no. (range)	n = 64	n = 0	n = 64
Initial absolute neutrophil count, cells/μL	4,466 (2,433–6,633)		4,466 (2,433–6,633)
Initial lymphocyte count, cells/μL	675 (440–1,095)		675 (440–1,095)
Aspartate aminotransferase, U/L†	14,829 (3,523–75,000)		14,829 (3,523–75,000)
Alanine aminotransferase, U/L‡	6,074 (1,758–14,998)		6,074 (1,758–14,998)
Direct bilirubin, mg/dL§	7.26 (3.06–31.67)		7.26 (3.06–31.67)
Initial PaO_2/FiO_2 ratio	380 (281–471)		380 (281–471)
PaO_2/FiO_2 ratio during hospitalization, no. positive/no. tested (%)			
Moderate or severe, <200	36/64 (56)		36/64 (56)
Severe, <100	12/64 (19)		12/64 (19)

*Values are no. (%) except as indicated. COPD, chronic obstructive pulmonary disease; NA, not applicable; PaO_2/FiO_2, ratio of the partial pressure of oxygen in arterial blood to the inspired oxygen; SAPS 3, Simplified Acute Physiology Score III; YF, yellow fever; YEL-AVD, yellow fever vaccine–associated viscerotropic disease.
†Reference range 10–40 U/L.
‡Reference range 4–36 U/L.
§Reference value<0.3 mg/dL.

Table 2. Pulmonary findings in study of severe YF, Brazil, 2017–2019*

Characteristic	Wild-type YF, n = 68	YEL-AVD, n = 5	Total YF, n = 73
Pleural effusion			
Any effusion	18 (26)	2 (40)	20 (27)
Serous effusion	13 (19)	2 (40)	15 (21)
Hemorrhagic effusion	5 (7)	0	5 (7)
Volume, mL (range)	550 (400–1,000)	400 (300–500)	500 (400–950)
Pleuritis	38 (52)		38 (52)
Tracheal macroscopy			
Mucosal congestion	67 (99)	5 (100)	72 (99)
Mucosal edema	67 (99)	5 (100)	72 (99)
Mucosal ulceration	40 (59)	1 (20)	41 (56)
Mucosal hemorrhages	55 (81)	3 (60)	58 (79)
Tracheal histology	n = 54	n = 3	n = 57
Tracheitis	51 (94)	1 (33)	52 (91)
Squamous metaplasia	24 (44)	0	24 (42)
Necrotizing tracheitis	33 (61)	0	33 (45)
Infectious microorganism	19 (35)	1 (20)	20 (35)
Pulmonary macroscopic findings			
Right lung weight, g (range)†	758 (634–952)	752 (633–895)	755 (635–944)
Left lung weight, g (range)‡	658 (544–848)	534 (378–707)	654 (531–826)
Pulmonary cut surface with edema and hemorrhages	68 (100)	5 (100)	73 (100)
Friable pulmonary cut surface	59 (87)	2 (40)	61 (84)
Pulmonary microscopic findings			
Alveolar edema§	67 (99)	5 (100)	72 (99)
Mild	6 (9)	0	6 (8)
Moderate	36 (53)	1 (20)	37 (51)
Severe	25 (37)	4 (80)	29 (40)
Alveolar hemorrhage§	61 (90)	5 (100)	66 (90)
Mild	28 (41)	3 (60)	31 (42)
Moderate	25 (37)	1 (20)	26 (36)
Severe	8 (12)	1 (20)	9 (12)
Interstitial perivascular or peribronchial hemorrhage	51 (70)		51 (70)
Secondary pneumonia§	59 (87)	2 (40)	61 (84)
Mild	29 (43)	1 (20)	30 (41)
Moderate	17 (25)	0	17 (23)
Severe	13 (19)	1 (20)	14 (19)
Bilateral	47 (69)	2 (40)	49 (67)
Micro abscesses	22 (32)	1 (20)	23 (32)
Bronchoaspiration	42 (62)	2 (40)	44 (60)
Gram-positive cocci	5 (7)	1 (20)	6 (8)
Bacilli	55 (81)	4 (80)	59 (81)
Yeasts	23 (34)	4 (80)	27 (37)
Hyphae	8 (12)	1 (20)	9 (12)
Diffuse alveolar damage§	57 (84)	4 (80)	61 (84)
Mild	46 (68)	4 (80)	50 (68)
Moderate	11 (16)	0	11 (15)
Severe	0	0	0
Proliferative	4 (6)	0	4 (5)
Increased siderophages in the alveolar space	65 (96)	5 (100)	70 (96)
Increased megakaryocytes in the pulmonary parenchyma	62 (91)	5 (100)	67 (92)
Fibrin and fibrinoid endothelial necrosis	40 (59)	2 (40)	42 (58)
Pulmonary thrombi	22 (32)	1 (20)	23 (32)
Macroscopic thrombi	2	0	2
Microscopic thrombi	22	1	23 (32)
Hemophagocytosis¶	14 (21)	2 (40)	16 (22)
Bone marrow emboli	4 (5.5)	0	4 (5.5)
Emphysema	37	0	37 (50.7)
Foci of mononuclear perivascular infiltrate	68	5	73 (100)
Quantitative RT-PCR for YF	N = 61	N = 4	N = 65
Positive	57 (93)	4 (100)	61 (94)
Cycle threshold (range)	28 (26–32)	23 (22–32)	28 (26–32)

*Values are no. (%) except as indicated. RT-PCR, reverse transcription PCR; YF, yellow fever; YEL-AVD, yellow fever vaccine–associated viscerotropic disease.
†Mean reference weight is 465 g.
‡Mean reference weight is 400 g.
§Mild, present in 1%–25% of the histological sample; moderate, present in 25%–50%; severe, present in >50%.
¶Alveolar macrophages or in macrophages within the sinuses of intrapulmonary lymph nodes.

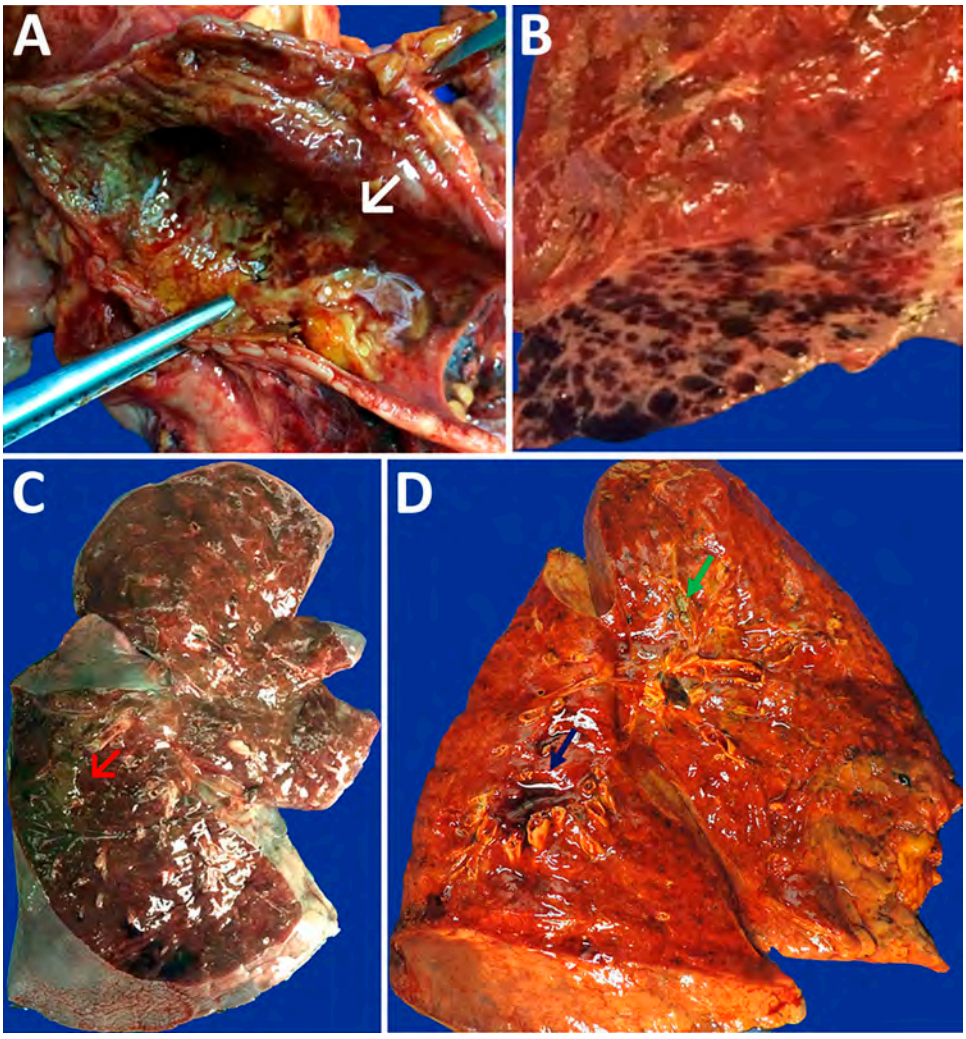

Figure 1. Macroscopic images of respiratory tract from patients with fatal yellow fever, São Paulo, Brazil, 2017–2019. A) Hemorrhagic necrosis of tracheal mucosa, covered with a thick whitish exudate (arrow), caused by *Candida* spp. invasive infection. B) Petechial pleural hemorrhage. C) Intense parenchymal edema and hemorrhage in the right lung, with massive gastrointestinal content aspiration in the posterior side (red arrow). D) Right lung with icterus, edema, hemorrhage, perivascular hemorrhage (blue arrow), and whitish exudate within bronchus (green arrow) caused by *Aspergillus* spp. infection.

All cases had an increased expression of VIII coagulation factor and VCAM in the pulmonary vessels (Figure 3). All 3 cases examined by EM of the lung tissue showed altered endothelial cells cytoplasmatic pseudopods in the pulmonary septa, intravascular fibrin, and intraalveolar or intravascular bacilli (Figure 3). YFV particles were not found. All cases had positive YFV antigens in pulmonary tissue, staining the cytoplasm of scattered endothelial cells from septal capillaries and interstitial inflammatory cells (Figure 3).

Molecular Analysis in Fresh Frozen Lung Tissue

We detected YFV RNA in 61 (94%) cases of the lung tissue samples analyzed. In addition, Sanger sequencing of 48 tissue samples enabled us to identify secondary bacterial and fungal infections in samples collected during autopsy (Tables 3–5). The sequences obtained in this study have been deposited in GenBank (Tables 3–5). Bacterial infections were detected in 41 cases (85.4%), fungal infections in 21 cases (43.7%), and mixed infections in 14 cases (29%). The bacterial genera most frequently associated with pneumonia in those 41 cases were *Enhydrobacter* in 13 (31.7%) cases, *Klebsiella* in 9 (22%) cases, *Acinetobacter* in 5 (12.3%) cases, and *Pseudomonas* in 3 (7.3%) cases (Appendix Table). The most prevalent fungal genera in those 21 cases were *Candida* in 10 (47.6%) cases, *Aspergillus* in 4 (19%), and *Trichosporon* in 2 (9.5%). We were unable to detect the presence of microorganisms by nested PCR in 25 cases. Among 48 PCR-positive cases, histological correlation was absent in 1 (*Cladosporium sphaerospermum*, not visualized in a case with pneumonia). In 47 cases, PCR findings matched histopathology: 43 with complete correlation, 3 with partial correlation (≥1 agent identified within pneumonia), and 1 case corresponding to terminal aspiration rather than pneumonia.

Discussion

In this study, we describe results of the autopsies of patients who died of severe YF, focusing on

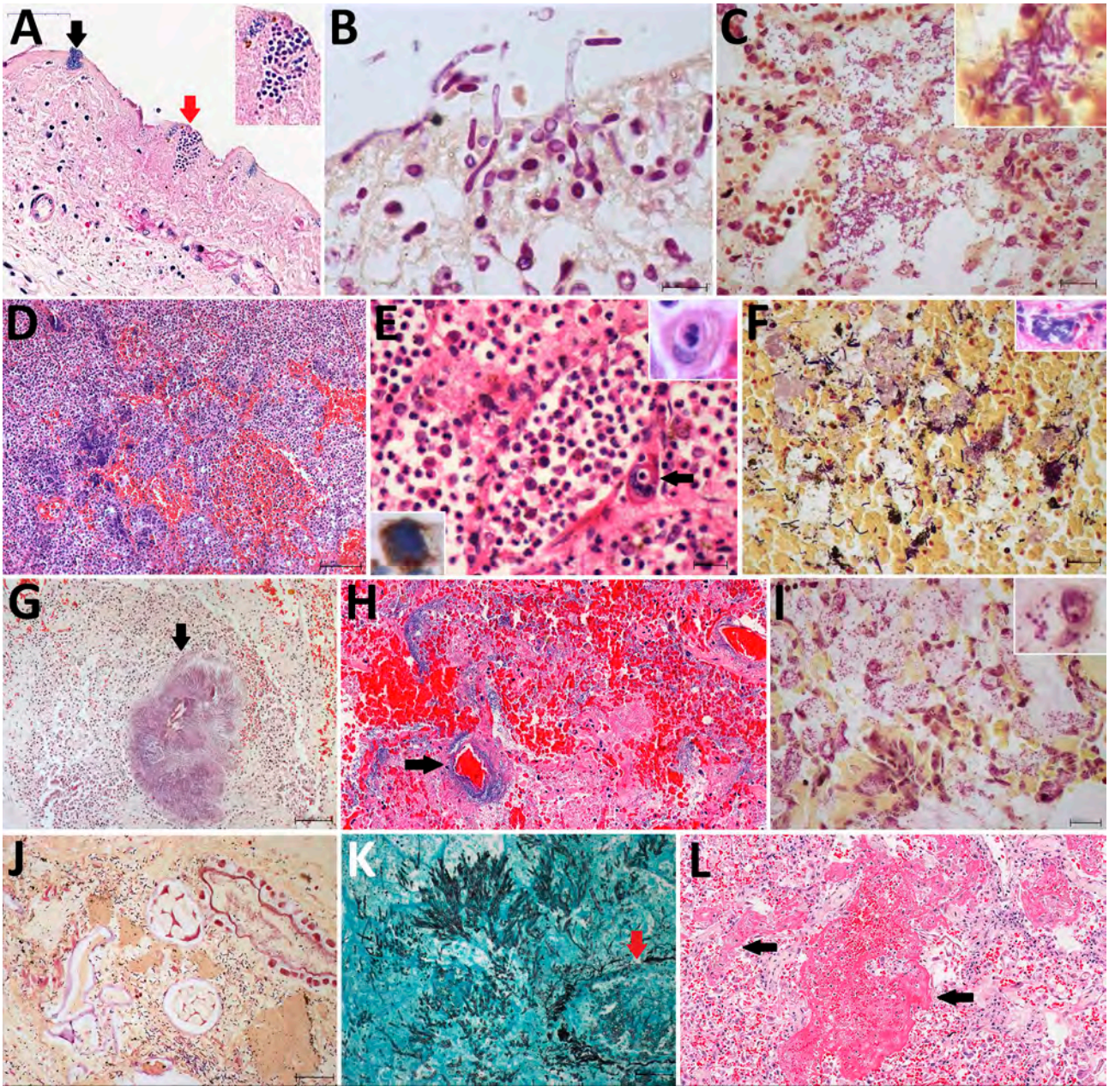

Figure 2. Pulmonary microscopic findings in patients with fatal yellow fever, São Paulo, Brazil, 2017–2019. A) Tracheal necrosis associated with bacilli (black arrow) and yeasts (inset and red arrow). Hematoxylin and eosin (HE) stain; scale bar = 50 μm. B) *Candida albicans* pseudohyphae and hyphae invading necrotic tracheal mucosa. Gram stain in immersion oil; scale bar = 10 μm. C) Bronchopneumonia associated with gram-negative bacilli. Gram stain; scale bar = 20 μm. D) Hemorrhagic pneumonia with microabscess composed of macrophages, neutrophils and colonies of coccus. HE stain; scale bar = 100 μm. E) Suppurative pneumonia showing hemophagocytosis (right inset) and a megakaryocyte in a septal vessel (arrow), with emperipolesis. HE stain; scale bar = 20 μm. Left inset: megakaryocyte labeled by VIII factor antigen detected by immunohistochemistry. Peroxidase stain. F) Polymicrobial aspirative pneumonia with gram-positive cocci and gram-positive and gram-negative bacilli with different morphologies; the inset shows a colony of bacilli in a septal vessel corresponding to agonal bacteremia. Gram stain; scale bar = 20 μm. Inset: HE stain. G) *Actynomyces granule* (arrow) with degenerated squamous cells in the center in an area of aspirative pneumonia. HE stain; scale bar = 100 μm. H) *Pseudomonas* hemorrhagic pneumonia, with numerous bacilli surrounding a septal vessel (arrow). HE stain; scale bar = 50 μm. I) *Mycoplasma salivarium pneumonia*, showing tiny gram-negative bacilli (inset) in the cytoplasm of intrabronchial macrophages. Gram stain; scale bar = 20 μm. J) Bronchoaspiration of vegetal alimentary material, associated with gram-negative bacilli, in the alveolar space. Gram stain; scale bar = 20 μm. K) Pulmonary angioinvasive aspergillosis, with typical hyphae invading pulmonary vessel (arrow), with associated necrosis and mild neutrophilic reaction. Grocott-Gomori methenamine silver stain; scale bar = 20 μm. L) Exudative diffuse alveolar damage, with congestion, alveolar edema, and hyaline membranes (arrow). HE stain; scale bar = 100 μm. Insets: original magnification ×400.

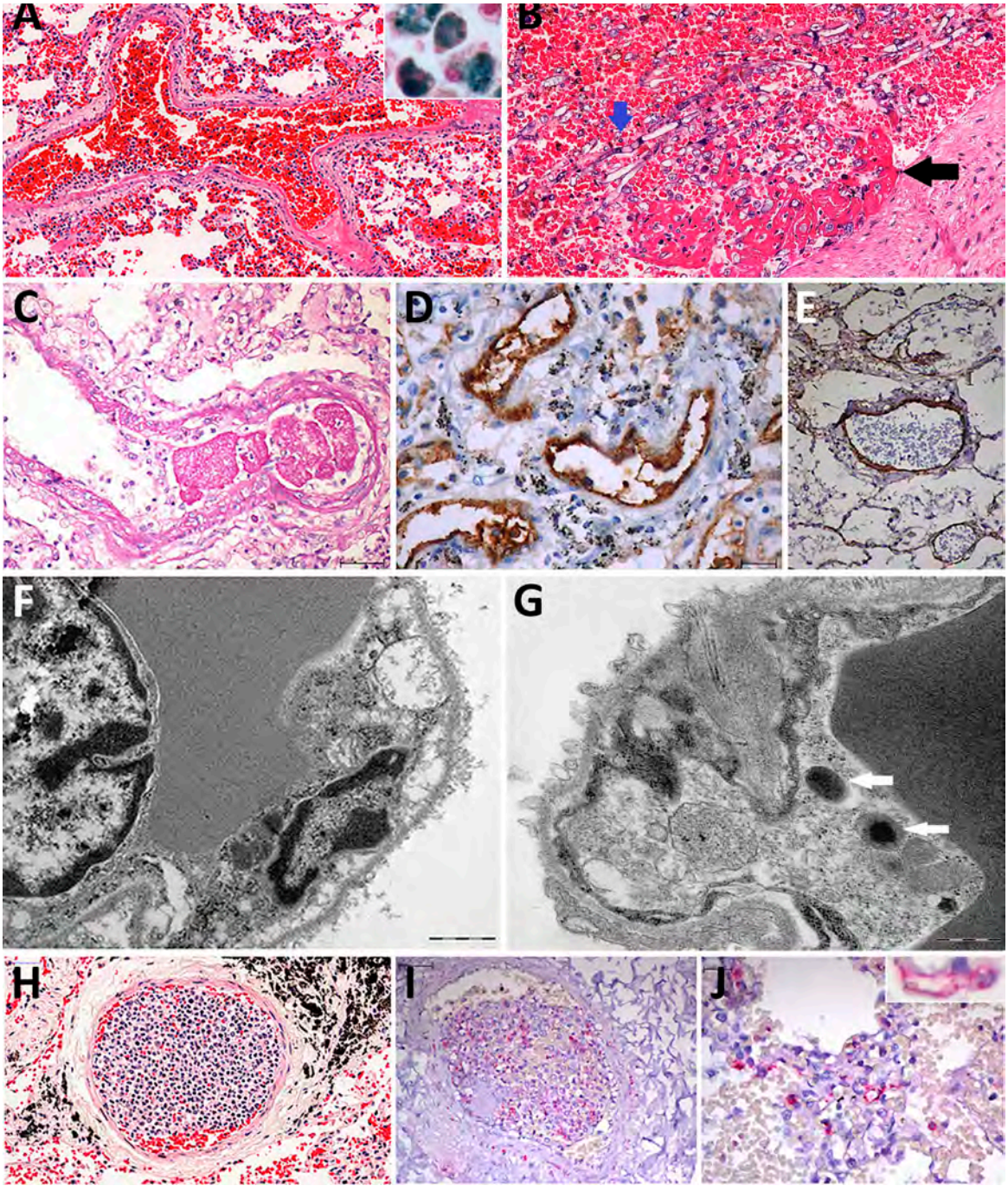

Figure 3. Pulmonary vascular damage in fatal yellow fever cases, 2017–2019 epidemic, São Paulo, Brazil. A) Medium-sized artery with fibrinoid necrosis of the endothelial layer, marginated leukocytes, wall edema, septal congestion, alveolar hemorrhage. Hematoxylin and eosin (HE) stain; scale bar 50 μm. Inset shows group of hemosiderin-laden alveolar macrophages stained for iron. Perls stain; original magnification ×200. B) Pulmonary artery showing angioinvasion by Aspergillus spp. forming fibrinous thrombus on the endothelial vascular layer (black arrow). HE stain; scale bar = 50 μm. C) A small fibrin clot and the artery fibrinoid necrosis and wall edema. Periodic acid–Schiff stain; scale bar = 50 μm. D) Positive detection of VIII coagulation factor in the entire wall of pulmonary arteries. Peroxidase stain; scale bar = 20 μm. E) The VCAM is detected in the endothelial and muscular pulmonary artery layers. Peroxidase stain; scale bar = 20 μm. F) Septal capillaries showing mitochondrial dilation with loss of cristae. Ultrathin section; scale bar = 1 μm. G) Bacilli (arrows) within septal pulmonary vessel. Ultrathin section; scale bar = 500 nm. H) Histologic leukostasis in a septal pulmonary artery, showing immature myeloid cells, lymphocytes, and neutrophils. HE stain; scale bar = 50 μm. I) Intravascular cells expressing yellow fever virus antigens in their cytoplasm. Alkaline phosphatase stain; scale bar = 50 μm. J) The yellow fever virus antigen is detected in the cytoplasm of septal endothelial cells (inset; original magnification ×400) and in interstitial and alveolar inflammatory cells. Alkaline phosphatase stain; scale bar = 20 μm.

pathologic findings in the respiratory tract. The classic pulmonary findings in YF (*8*,*20*), such as edema and alveolar hemorrhage, were very frequent as expected; however, we also observed a high incidence (84%) of extensive pneumonia caused by bacterial and fungal microorganisms, associated with exudative diffuse alveolar damage, which certainly contributed to the fatal outcomes. We also discovered an unexpected and frequent finding of infectious necrotizing tracheitis, which supports the rationale that inhalation or aspiration are the main routes of respiratory infection in those cases. Of note, few patients (7%) had clinical suspicion of pneumonia during their intensive care stay. Some of them had a clinical diagnosis of sepsis, albeit with a poorly defined site, mainly based on persistent fever, clinical deterioration, and progressive neutrophilia with left deviation and elevated serum C-reactive protein. The difficulty in determining the primary site of infection was multifactorial: rapid clinical progression and hemorrhagic phenomena, making diagnostic procedures such as bronchoalveolar lavage and chest tomography difficult; use of broad-spectrum antimicrobial drugs as prophylaxis for infections associated with acute liver failure, rendering cultures negative; pulmonary hemorrhage masking new infiltrates associated with pneumonia on chest radiographs taken in bed; misattribution of septic signs to YFV infection; and finally, little understanding of the disease, which was previously uncommon in urban centers in southeastern Brazil (*1*–*6*).

The respiratory secondary infections we described are not usually reported in YF autopsies, although they are a common cause of infection and death in patients with acute liver failure of other etiologies (*20*–*25*). Our data are the result of thorough

Table 3. Characteristics of yellow fever cases with bacterial infections in the lung, Brazil, 2017–2019*

Pathogen	GenBank accession no.	YFV type	Gram stain
Enhydrobacter aerosaccus	MN436791	Sylvatic	Negative
	MN439924	Sylvatic	Negative
	MN44786	Sylvatic	Negative
	MN447222	Sylvatic	Negative
	MN447318	Sylvatic	Negative
	MN447732	Sylvatic	Negative
	MN431431	Sylvatic	Negative
	MN441757	Negative	Negative
	MN44855	Sylvatic	Negative
	MN445607	Vaccinal	Negative
	MN447234	Sylvatic	Negative
	MN447305	Sylvatic	Negative
	MN447407	Sylvatic	Negative
Klebsiella pneumoniae	MN437654	Sylvatic	Negative
	MN44823	Sylvatic	Negative
	MN447127	Sylvatic	Negative
	MN526933	Sylvatic	Negative
	MN447416	Sylvatic	Negative
	MN447588	Sylvatic	Negative
	MN447652	Sylvatic	Negative
	MN447666	Sylvatic	Negative
	MN442076	Vaccinal	Negative
Acinetobacter baumannii	MN428414	Sylvatic	Negative
	MN435153	Sylvatic	Negative
	MN431185	Sylvatic	Negative
	MN447636	Sylvatic	Negative
Acinetobacter sp.	MN445371	Sylvatic	Negative
Pseudomonas aeruginosa	MN429315	Sylvatic	Negative
P. baetica	MN447128	Sylvatic	Negative
	MN447668	Sylvatic	Negative
Escherichia coli	MN436844	Sylvatic	Negative
	MN437322	Sylvatic	Negative
Mycoplasma salivarium	MN447214	Sylvatic	
M. orale	MN447304	Sylvatic	
Moraxella osloensis	MN445979	Vaccinal	Negative
	MN437656	Sylvatic	Negative
Streptococcus pneumoniae	MN431202	Sylvatic	Positive
Serratia marcescens	MN431240	Sylvatic	Negative
Cronobacter dublinensis	MN431459	Sylvatic	Negative
Simiduia agarivorans	MN447394	Sylvatic	Negative
Enterobacter asburiae	MN430860	Sylvatic	Negative

*A total of 41 bacterial infections represented 56.75% of study cases. YFV, yellow fever virus.

Table 4. Characteristics of 21 yellow fever cases with fungal infections in the lung, Brazil, 2017–2019*

Pathogen	GenBank accession no.	YFV type
Nakaseomyces glabratus†	MN473880	Sylvatic
	MN475751	Sylvatic
	MN477933	Sylvatic
	MN475749	Sylvatic
Candida albicans	MN473077	Sylvatic
	MN475275	Sylvatic
	MN477032	Sylvatic
C. tropicalis	MN477465	Sylvatic
	MN475173	Vaccinal
C. parapsilosis	MN477247	Sylvatic
Aspergillus fumigatus	MN474008	Sylvatic
	MN475197	Sylvatic
	MN477796	Sylvatic
A. flavus	MN477210	Sylvatic
Trichosporon faecale	MN472741	Sylvatic
T. asahii	MN475174	Vaccinal
Didymella glomerata	MN472927	Sylvatic
	MN472744	Vaccinal
Debaryomyces hansenii	MN472906	Sylvatic
Cladosporium sphaerospermum	MN476933	Sylvatic
Apiotrichum domesticum	MN477197	Sylvatic

*A total of 21 fungal infections represented 28.4% of study cases. YFV, yellow fever virus.
†Formerly known as *Candida glabrata*.

macroscopic examination in the autopsy room and extensive lung sampling for microscopy and molecular analysis. In addition, the minimally invasive tissue sampling protocol we used during the 2017–2019 YF epidemic was also successful in diagnosing pneumonia at postmortem examination in these cases (*9*).

The pattern of tracheitis and pneumonia observed at autopsy shows aspirative, nosocomial, and opportunistic elements (*25*,*26*). In the pathogenesis of the aspirative and nosocomial elements, massive gram-negative bacilli (including nonfermenting bacilli and Enterobacteriaceae) from the gastrointestinal flora colonized and infected the upper and lower airways of patients with severe YF. The uncontrollable vomiting associated with hepatic coma and gastrointestinal bleeding and ischemia might have caused bronchoaspiration. Other predisposing factors are the presence of an endotracheal tube and mechanical ventilation and the selective pressure of broad-spectrum antimicrobial drugs prescribed for prophylaxis in fulminant hepatitis for opportunistic nonfermenting gram-negative bacilli (e.g., *Enhydrobacter*, *Klebsiella*, *Acinetobacter*, and *Pseudomonas*) and non-*albicans* strains of *Candida* spp. The presence of the endotracheal tube might have caused the unusual finding of ulcerative tracheitis; however, our intensive care unit staff follows standard protocols to avoid endotracheal tube–related injuries, which are also rare in our autopsy routine (*7*,*11*,*13*,*25*,*26*).

Another element that we highlighted was an intense and systemic immune dysfunction in severe YF cases, which probably also lowered the immunity of the respiratory mucosal barrier, predisposing case-patients to invasive infections by bacteria and fungi, including *Aspergillus* spp., commonly described in severely lymphopenic or neutropenic patients. That opportunistic element is supported by evidence: peripheral lymphopenia (Table 1), an increase in inflammatory cytokines similar to that seen in patients with lethal bacterial sepsis, lymphoid depletion, and hemophagocytosis in secondary lymphoid organs, including the intrapulmonary lymph nodes, spleen, and bone marrow (*7*,*9*,*10*,*17*,*18*).

Disseminated angioinvasive infections by hyphomycetes in cases with severe YF, involving the lungs and other organs, have been reported previously in humans and neotropical nonhuman primates, which suggests a direct effect of YFV on lymphoid organs

Table 5. Cases of severe yellow fever with bacterial and fungal co-infections in the same case, detected in the lung tissue by nested RT-PCR and genomic sequencing, Brazil, 2017–2019*

		Bacteria			Fungus	
Case no.	YFV type	Organism	GenBank accession no.	Gram stain	Organism	GenBank accession no.
1	Sylvatic	*Pseudomonas aeruginosa*	MN429315	Negative	*Nakaseomyces glabratus*†	MN473880
2	Sylvatic	*Streptococcus pneumoniae*	MN431202	Positive	*Debaryomyces hansenii*	MN472906
3	Sylvatic	*Enhydrobacter aerosaccus*	MN44786	Negative	*Aspergillus fumigatus*	MN474008
4	Sylvatic	*P. aeruginosa*	MN447128	Negative	*A. fumigatus*	MN475197
5	Sylvatic	*Mycoplasma salivarium*	MN447214		*Candida albicans*	MN475275
6	Sylvatic	*Klebsiella pneumoniae*	MN447588	Negative	*Apiotrichum domesticum*	MN477197
7	Sylvatic	*K. pneumoniae*	MN447652	Negative	*N. glabratus*†	MN477933
8	Sylvatic	*Enterobacter asburiae*	MN430860	Negative	*Trichosporon faecale*	MN472741
9	Vaccinal	*Moraxella osloensis*	MN445979	Negative	*Trichosporon asahii*	MN475174
10	Vaccinal	*E. aerosaccus*	MN445607	Negative	*Candida tropicalis*	MN475173
11	Sylvatic	*E. aerosaccus*	MN447234	Negative	*N. glabratus*†	MN475749
12	Sylvatic	*E. aerosaccus*	MN447407	Negative	*C. albicans*	MN477032
13	Sylvatic	*Acinetobacter baumannii*	MN447636	Negative	*Candida parapsilosis*	MN477247
14	Sylvatic	*K. pneumoniae*	MN447416	Negative	*A. fumigatus*	MN477796

*YFV, yellow fever virus
†Formerly *Candida glabrata*.

regardless of the host and independent of intensive treatment (*21*,*22*,*27*). Further analysis focusing on the airway mucosal immunity would clarify some gaps in the host immune response in severe YF.

We detected YFV RNA in 94% of the lung samples by RT-PCR and YFV antigens in all cases by immunohistochemistry in endothelial and inflammatory cells. Those findings corroborate that YFV induces systemic vascular damage associated with hemorrhagic phenomena (*2*,*7*,*8*). It is possible that pulmonary edema and hemorrhage represent the alterations most directly associated with YFV-induced vasculopathy. However, we propose the extensive pneumonia observed in our cases, with consequent sepsis, exacerbates the vascular damage initiated by the YFV. Moreover, pneumonia induces exudative diffuse alveolar damage, leading to hypoxemia and consequent respiratory failure, adding more vascular damage. One striking finding was thrombosis in the pulmonary vasculature, which appeared to be recent and have little organization on histology, mainly affecting small and medium-sized vessels. We observed macroscopic thrombi in 2 cases, suggesting that thrombosis is mainly formed in the intrapulmonary bed, triggered by intense inflammation in the lung tissue, rather than by thromboembolism. Some cases also had fungal angioinvasion and septic vasculitis (Table 2; Figures 2, 3). We observed a complex coagulopathy in fatal cases of YF. Higher levels of D-dimer in those cases than in survivors did not seem to be related only to liver failure, as observed in an experimental model of YFV infection, which suggests a concurrent consumptive coagulopathy in severe YF (*28*). Pulmonary vascular thrombosis could explain the increase in serum D-dimer; other possible sources are intestinal ischemia and hemophagocytes, which should also be investigated in severe YF (*9*,*17*,*29*).

We found a similar pattern of secondary infections, vasculopathy, and evidence of direct YFV damage in hearts from the same YF autopsy cohort (*18*). We also observed in the hearts from YF case-patients an increased in situ expression of inflammatory cytokines and markers of endothelial damage, similar to those who died of bacterial sepsis and septic shock (*18*). Our results support the concept that the period of intoxication is characterized by sepsis in those with a fatal outcome.

Our results are somewhat related to those of a previous study in the city of São Paulo during the same epidemic, which showed that, in 76 patients with symptomatic YF, markers of death included neutrophilia ≥4,000 cells/mL, older age, high aspartate transaminase, and high viral load at hospital admission (*10*). Other studies from the clinical cohort of YF cases have shown that YFV proteins nonstructural 1, syndecan 1, and angiopoietin 2 were higher at hospital admission in patients with a fatal outcome than in those who survived and in normal controls without heart infection (*15*,*16*). Those markers were also high in the hearts of the cases in our study but similar to those observed in sepsis (*18*). Of note, our autopsy series includes most of the fatal cases reported in our clinical cohort study and in other clinical studies from the 2017–2019 YF epidemics in São Paulo (*7*,*11*,*13*). We believe that those markers reflect not only an intense viral infection with extensive liver necrosis but also an ongoing sepsis originating from the respiratory tract and also from bacterial translocation associated with intestinal ischemia that aggravates the systemic inflammatory response and endothelial damage induced by YFV and determines the fatal fate of some patients during the period of intoxication (*29*). All those processes are interconnected in a complex way (Figure 4).

A limitation of this study is that few pathogens were recovered in culture before death, and therefore, little correlation can be made with histologic or molecular postmortem results. However, we saw great correlation between the PCR results and the histopathologic study with ancillary histochemical stains in our study. We performed the treatments and postmortem examinations within a single institution, which ensured consistency of results and standardized clinical and pathologic protocols. Nonetheless, the single-site nature of the study might limit the generalizability of our findings to resource-limited settings where YF is endemic.

In conclusion, severe YF is a complex, systemic viral disease that affects other organs in addition to the liver. The respiratory tract is affected both by YFV, as evidenced by the detection of viral antigens and RNA in the lung parenchyma, and by secondary infections (tracheitis and pneumonia) of a multifactorial nature, which amplify the initial systemic inflammatory response, endothelial damage, and coagulopathy caused by YFV. Secondary sepsis and DAD exacerbate the intoxication phase of YF and lead patients to unfavorable outcomes. Our findings could guide the management of severe YF and help to establish preventive measures for bronchoaspiration and for the diagnosis and treatment of secondary respiratory infections. This study demonstrates the role of autopsy in better understanding the pathogenesis of infectious diseases

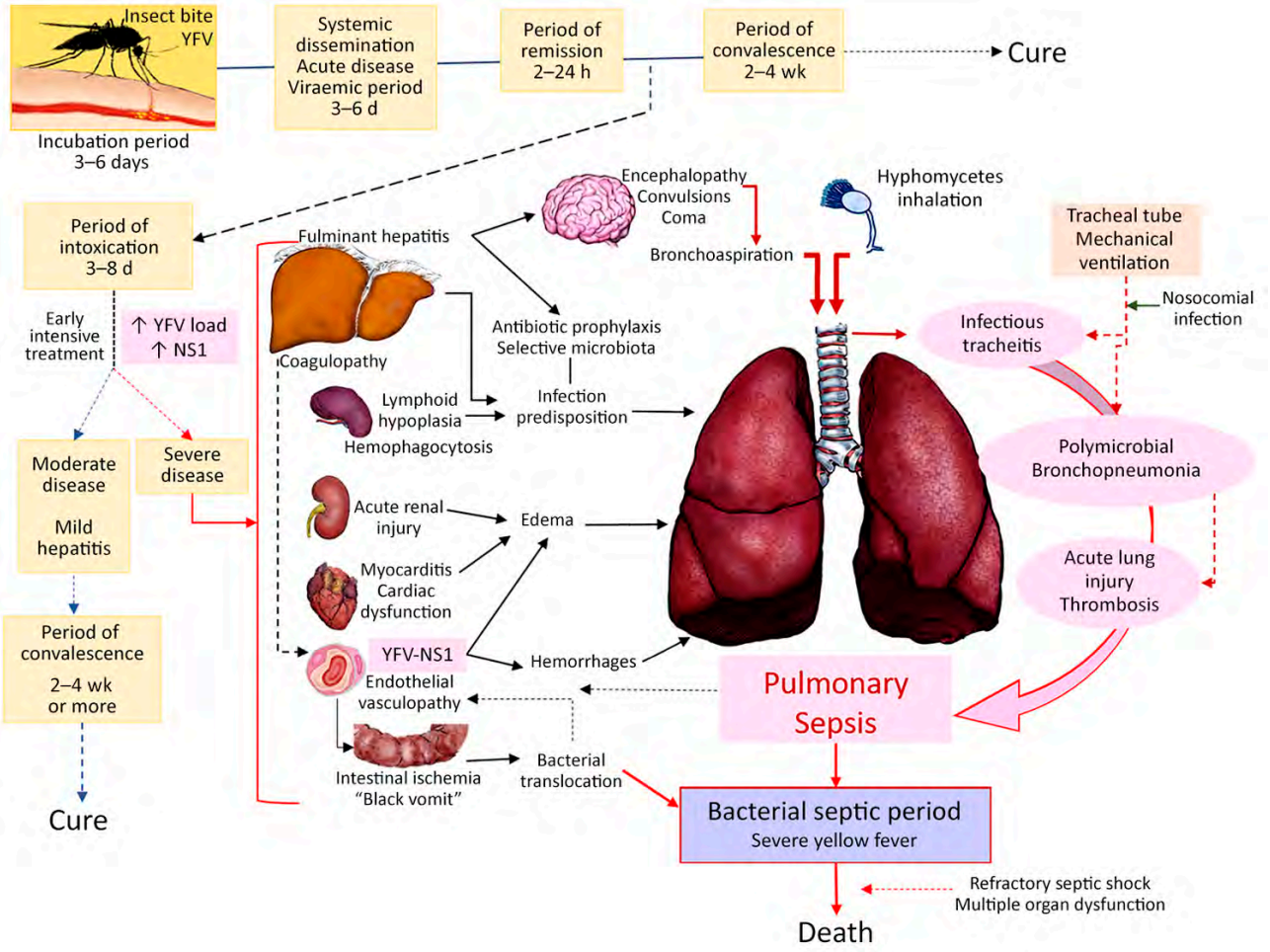

Figure 4. Proposal for the pathogenesis of respiratory tract involvement in fatal yellow fever, 2017–2019, epidemic, São Paulo, Brazil. After the mosquito bite with inoculation of YFV virions into the skin, there is a systemic spread of YFV with viremia that lasts for 5–7 days. The virus replicates in the blood, liver, spleen, kidneys, heart, brain, lungs, and other internal organs, and patients have nonspecific viral symptoms. After that is the toxemic phase, which is more severe in those with higher YFV-RNA load and higher YFV-NS1, with hepatitis, acute renal injury, immune dysfunction (lymphoid hypoplasia and hemophagocytosis), myocarditis, and systemic vascular damage. The lungs are affected in a multifactorial way. The acute liver failure due to YF-fulminant hepatitis and immune dysfunction predisposes to secondary infection. In particular, hepatic encephalopathy leads to aspiration of gastrointestinal microbiota (bacilli and *Candida* spp.) or inhalation of ubiquitous filamentous fungi that cause polymicrobial pneumonia and acute lung injury. The tracheal tube exerts mechanical damage to the tracheal mucosa, producing acute tracheitis associated with the aspirated flora, with ulceration and mucosal necrosis. Acute renal and myocardial dysfunction by YFV contribute to pulmonary edema. The endothelial injury also contributes to pulmonary edema which, in association with liver failure coagulopathy, leads to pulmonary hemorrhage. Acute lung injury caused by pneumonia, edema, and hemorrhage plus intestinal bacterial translocation in severe cases, presumed by evidence of intestinal ischemia and severe liver damage at autopsy, lead to bacterial sepsis, which amplifies the initial endothelial dysfunction generated by YFV, causing refractory shock and subsequent death. NS, nonstructural protein; YFV, yellow fever virus.

during epidemics, especially at a time when arboviruses are reemerging, as seen in Brazil in 2024 with the catastrophic dengue epidemic and the spread of Oropouche fever and in 2025 with a new epidemic of YF in the state of São Paulo (*30*,*31*).

Acknowledgments

We thank all health workers who provided care to patients with severe yellow fever and all who took part in the HCFMUSP–Yellow Fever Crisis Committee during the epidemic season, all medical residents from the pathology department of FMUSP who participated in the autopsy procedures, and technicians who work at our histotechnical laboratory. We thank Arthur Medeiros for the drawings in Figure 4.

This study has received funding from Fundação de Amparo à Pesquisa do Estado de São Paulo (grant no.

2013/17159-2); Bill and Melinda Gates Foundation (grant no. INV-002396); Conselho Nacional de Desenvolvimento Científico e Tecnológico (CNPQ): Bolsa de produtividade em pesquisa (no. 304987/2017-4 for M.D.) and Projeto PREPARE (no. 445484/2023-3); and Universidade de São Paulo (process no. 22.1.09345.01.2). F.R.G. received a grant from Coordenação de Aperfeiçoamento de Pessoal de Nível Superior (Programa Demanda Social, no. 88887.629398/2021-00).

The authors declare that no artificial intelligence technologies were used in the writing process or in in any part of this study. No medical writer or editor was involved in the preparation of this manuscript.

Author contributions: A.N.D.N.: conceptualization, data curation, literature review, writing (original draft), visualization, formal analysis, methodology, project administration. K.C.D.: writing (review and editing), data curation, visualization, formal analysis, methodology, investigation, validation. S.C.F.: writing (review and editing), investigation, formal analysis. F.R.G.: writing (review and editing), investigation, formal analysis. M.P.C.: writing (review and editing), investigation, formal analysis. S.Z.P.: writing (review and editing), investigation, formal analysis. F.L.L.: writing (review and editing), investigation, formal analysis. H.Y.L.: writing (review and editing), formal analysis, patient care. A.C.S.N.: writing (review and editing), formal analysis, patient care. C.S.C.B.: writing (review and editing), investigation, formal analysis. F.A.R.: writing (review and editing), investigation, formal analysis. C.E.M.: writing (review and editing), investigation, patient care. J.S.: writing (review and editing), formal analysis, patient care. T.M.: writing (review and editing), formal analysis. L.F.F.S.: writing (review and editing), resources. P.H.N.S.: writing (review and editing), supervision, funding acquisition. M.D.: conceptualization, writing (review and editing), supervision, funding acquisition, project administration. A.N.D.N., K.D., and M.D. have directly accessed and verified the underlying data reported in the manuscript. All authors read and approved the final version of the manuscript.

About the Author

Prof. Duarte-Neto is an infectious diseases physician, pathologist, and associate professor in the department of pathology at the University of São Paulo, Brazil. His research focuses on autopsy and infectious disease pathology, with an emphasis on emerging infections. He currently leads a project on epidemic preparedness in anatomical pathology in São Paulo.

References

1. The Lancet. Yellow fever: a major threat to public health. Lancet. 2018;391:402. https://doi.org/10.1016/S0140-6736(18)30152-1
2. Douam F, Ploss A. Yellow fever virus: knowledge gaps impeding the fight against an old foe. Trends Microbiol. 2018;26:913–28. https://doi.org/10.1016/j.tim.2018.05.012
3. Possas C, Lourenço-de-Oliveira R, Tauil PL, Pinheiro FP, Pissinatti A, Cunha RVD, et al. Yellow fever outbreak in Brazil: the puzzle of rapid viral spread and challenges for immunisation. Mem Inst Oswaldo Cruz. 2018;113:e180278. https://doi.org/10.1590/0074-02760180278
4. Cunha MS, da Costa AC, de Azevedo Fernandes NCC, Guerra JM, Dos Santos FCP, Nogueira JS, et al. Epizootics due to yellow fever virus in São Paulo State, Brazil: viral dissemination to new areas (2016–2017). Sci Rep. 2019;9:5474. https://doi.org/10.1038/s41598-019-41950-3
5. Cunha MDP, Duarte-Neto AN, Pour SZ, Pereira BBS, Ho YL, Perondi B, et al. Phylogeographic patterns of the yellow fever virus around the metropolitan region of São Paulo, Brazil, 2016–2019. PLoS Negl Trop Dis. 2022;16:e0010705. https://doi.org/10.1371/journal.pntd.0010705
6. Secretaria da Saúde—Governo do Estado de São Paulo. Statistical data [in Portuguese] [cited 2025 Apr 7]. http://saude.sp.gov.br/cve-centro-de-vigilancia-epidemiologica-prof.-alexandre-vranjac/areas-de-vigilancia/doencas-de-transmissao-por-vetores-e-zoonoses/agravos/febre-amarela/dados-estatisticos
7. Ho YL, Joelsons D, Leite GFC, Malbouisson LMS, Song ATW, Perondi B, et al.; Hospital das Clínicas Yellow Fever Assistance Group. Severe yellow fever in Brazil: clinical characteristics and management. J Travel Med. 2019;26:taz040. https://doi.org/10.1093/jtm/taz040
8. De Brito T, Siqueira SA, Santos RT, Nassar ES, Coimbra TL, Alves VA. Human fatal yellow fever: immunohistochemical detection of viral antigens in the liver, kidney and heart. Pathol Res Pract. 1992;188:177–81. https://doi.org/10.1016/S0344-0338(11)81176-3
9. Duarte-Neto AN, Monteiro RAA, Johnsson J, Cunha MDP, Pour SZ, Saraiva AC, et al. Ultrasound-guided minimally invasive autopsy as a tool for rapid post-mortem diagnosis in the 2018 Sao Paulo yellow fever epidemic: correlation with conventional autopsy. PLoS Negl Trop Dis. 2019;13:e0007625. https://doi.org/10.1371/journal.pntd.0007625
10. Kallas EG, D'Elia Zanella LGFAB, Moreira CHV, Buccheri R, Diniz GBF, Castiñeiras ACP, et al. Predictors of mortality in patients with yellow fever: an observational cohort study. Lancet Infect Dis. 2019;19:750–8. https://doi.org/10.1016/S1473-3099(19)30125-2
11. Ribeiro AF, Cavalin RF, Abdul Hamid Suleiman JM, Alves da Costa J, Januaria de Vasconcelos M, Sant'Ana Málaque CM, et al. Yellow fever: factors associated with death in a hospital of reference in infectious diseases, São Paulo, Brazil, 2018. Am J Trop Med Hyg. 2019;101:180–8. https://doi.org/10.4269/ajtmh.18-0882
12. Casadio LVB, Salles APM, Malta FM, Leite GF, Ho YL, Gomes-Gouvêa MS, et al. Lipase and factor V (but not viral load) are prognostic factors for the evolution of severe yellow fever cases. Mem Inst Oswaldo Cruz. 2019;114:e190033. https://doi.org/10.1590/0074-02760190033
13. Arantes MF, Seabra VF, Lins PRG, Rodrigues CE, Reichert BV, Silveira MAD, et al. Risk factors for acute kidney injury and death in patients infected with the yellow fever virus during the 2018 outbreak in São Paulo, Brazil.

Kidney Int Rep. 2022;7:601–9. https://doi.org/10.1016/j.ekir.2021.12.021
14. Casadio L, Nastri AC, Malta FM, Araujo J, Silva JB, Salomao J, et al. Late-onset relapsing hepatitis associated with yellow fever. N Engl J Med. 2020;382:2059–61. https://doi.org/10.1056/NEJMc1913036
15. van de Weg CAM, Thomazella MV, Marmorato MP, Correia CA, Dias JZC, Maestri A, et al. Levels of angiopoietin 2 are predictive for mortality in patients infected with yellow fever virus. J Infect Dis. 2024;230:e60–4. https://doi.org/10.1093/infdis/jiad389
16. de Sousa FTG, Warnes CM, Manuli ER, Tjang LV, Carneiro PH, Maria de Oliveira Pinto L, et al. Yellow fever disease severity and endothelial dysfunction are associated with elevated serum levels of viral NS1 protein and syndecan-1. EBioMedicine. 2024;109:105409. https://doi.org/10.1016/j.ebiom.2024.105409
17. Duarte-Neto AN, Cunha MDP, Marcilio I, Song ATW, de Martino RB, Ho YL, et al. Yellow fever and orthotopic liver transplantation: new insights from the autopsy room for an old but re-emerging disease. Histopathology. 2019;75:638–48. https://doi.org/10.1111/his.13904
18. Giugni FR, Aiello VD, Faria CS, Pour SZ, Cunha MDP, Giugni MV, et al. Understanding yellow fever-associated myocardial injury: an autopsy study. EBioMedicine. 2023;96:104810. https://doi.org/10.1016/j.ebiom.2023.104810
19. Gershman MD, Staples JE, Bentsi-Enchill AD, Breugelmans JG, Brito GS, Bastos Camacho LA, et al.; Brighton Collaboration Viscerotropic Disease Working Group. Viscerotropic disease: case definition and guidelines for collection, analysis, and presentation of immunization safety data. Vaccine. 2012;30:5038–58. https://doi.org/10.1016/j.vaccine.2012.04.067
20. Noguchi H. Etiology of yellow fever: I. Symptomatology and pathological findings of the yellow fever prevalent in Guayaquil. J Exp Med. 1919;29:547–64. https://doi.org/10.1084/jem.29.6.547
21. Maciel GVR, Tavares MCF, Pereira LS, Silva GLC, de Oliveira NR, Paulino Jr. E, et al. Disseminated mycosis in a patient with yellow fever. Autops Case Rep. 2018;8:e2018038. https://doi.org/10.4322/acr.2018.038
22. Centers for Disease Control and Prevention. Fatal yellow fever in a traveler returning from Venezuela, 1999. MMWR Morb Mortal Wkly Rep. 2000;49:303–5.
23. Fabro AT, Engelman GG, Ferreira NN, Velloni JMF, Espósito DLA, da Fonseca BAL, et al. Yellow fever–induced acute lung injury. Am J Respir Crit Care Med. 2019;200:250–2. https://doi.org/10.1164/rccm.201711-2267IM
24. Vasconcelos DB, Falcão LFM, da Ponte LCT, Lima CP, Bezerra PG, Silva AG, et al. New insights into the mechanism of immune-mediated tissue injury in yellow fever: the role of immunopathological and endothelial alterations in the human lung parenchyma. Viruses. 2022;14:2379. https://doi.org/10.3390/v14112379
25. Maiwall R, Kulkarni AV, Arab JP, Piano S. Acute liver failure. Lancet. 2024;404:789–802. https://doi.org/10.1016/S0140-6736(24)00693-7
26. Craven DE, Hjalmarson KI. Ventilator-associated tracheobronchitis and pneumonia: thinking outside the box. Clin Infect Dis. 2010;51(Suppl 1):S59–66. https://doi.org/10.1086/653051
27. Guerra JM, Ferreira CSDS, Díaz-Delgado J, Alves ES, Machado G, Santos WJ, et al. Concurrent yellow fever and pulmonary aspergillosis due to *Aspergillus fumigatus* in a free-ranging howler monkey (*Alouatta* sp). J Med Primatol. 2021;50:201–4. https://doi.org/10.1111/jmp.12522
28. Bailey AL, Kang LI, de Assis Barros D'Elia Zanella LGF, Silveira CGT, Ho YL, Foquet L, et al. Consumptive coagulopathy of severe yellow fever occurs independently of hepatocellular tropism and massive hepatic injury. Proc Natl Acad Sci U S A. 2020;117:32648–56. https://doi.org/10.1073/pnas.2014096117
29. Thomazella MV, Qiu X, Silveira CGT, Correia CA, Marmorato MP, Sanson E, et al. Mesenteric ischemia and bacterial translocation precipitate the intoxication phase of yellow fever. J Infect Dis. 2025;jiaf483. https://doi.org/10.1093/infdis/jiaf483
30. The Lancet. Dengue: the threat to health now and in the future. Lancet. 2024;404:311. https://doi.org/10.1016/S0140-6736(24)01542-3
31. Scachetti GC, Forato J, Claro IM, Hua X, Salgado BB, Vieira A, et al. Re-emergence of Oropouche virus between 2023 and 2024 in Brazil: an observational epidemiological study. Lancet Infect Dis. 2025;25:166–75. https://doi.org/10.1016/S1473-3099(24)00619-4

Address for correspondence: Amaro Nunes Duarte-Neto, Departamento de Patologia, Faculdade de Medicina, Universidade de São Paulo, Av. Dr. Arnaldo no. 455, sala 1149, Cerqueira Cesar, 01246903, São Paulo, SP Brazil; email: amaro.ndneto@hc.fm.usp.br

Characteristics and Transmission Dynamics of Global Travel-Related Mpox Cases Caused by Clade Ib Monkeypox Virus

Henry Laurenson-Schafer,[1] Martina McMenamin,[1] Lennox Kesington Ebbarnezh, Ioannis Karagiannis, Viema Biaukula, Rosamund Lewis, Masaya Kato, Michel Muteba, Jeremias D. Naiene, Felix Sanni, Tshewang Dorji, Lorenzo Subissi, Marc-Alain Widdowson, WHO Mpox Collaborative Surveillance Group[2] Ana Hoxha, Olivier le Polain de Waroux;

We examined 89 travel-related clade Ib monkeypox virus cases detected in 33 countries during August 2024–July 2025. Most cases were among men; approximately one third led to secondary transmission. Secondary transmission risk was highest among sexual, then household, contacts. Those groups should be the focus of response strategies and interventions.

In September 2023, an outbreak of a new strain of monkeypox virus (MPXV) emerged in the nonendemic Sud-Kivu province of the Democratic Republic of the Congo (DRC); the outbreak was driven by sustained human-to-human transmission (*1*). Mpox cases previously reported in the DRC described outbreaks linked to zoonotic spillover in forested areas (*2*). The sustained human-to-human transmission in the 2023 outbreak led to proposed designation of a new MPXV subclade, clade Ib (*1*). Subsequent spread to countries neighboring the DRC (*3*) prompted the World Health Organization (WHO) to declare a second public health emergency of international concern for mpox on August 14, 2024 (*4*). We collated data from travel-related cases and their contacts reported to WHO or published seperately to describe transmission dynamics, estimate secondary attack rates (SAR), and help define risk factors for clade Ib MPXV infection.

The Study

By June 19, 2025, MPXV clade Ib had been reported from 14 countries in Africa. Travel-related cases, as defined by WHO (*5*), were reported from 19 countries outside of Africa and led to secondary cases in 8 of the destination countries.

We used case data that was shared with WHO under the provisions of the International Health Regulations (2005) (*6*) or published separately. We collated data from 127 mpox cases, 124 confirmed and 3 suspected; 89 were travel-related, 34 were secondary, and 4 were unlinked. Of the 89 travel-related cases, 70 case-patients reported having been exposed in Africa and 18 outside Africa; 1 had unknown exposure origin (Figure 1). All imported cases were among adults, except 1 of unknown age (missing data); 88 cases had data on sex available, 67 (76%) were men and 21 (24%) were women; 25 travel-related cases led to 34 secondary cases in the country of notification, including cases among 6 men, 19 women, and 6 children (≤17 years of age). Among secondary cases, 15/25 (60%) adults reported sexual contact or likely

Author affiliations: World Health Organization (WHO) Health Emergencies Programme, Geneva, Switzerland (H. Laurenson-Schafer, M. McMenamin, L.K. Ebbarnezh, R. Lewis, L. Subissi, A. Hoxha, O. le Polain de Waroux); WHO Health Emergencies Programme, Regional Office for the European Region, Copenhagen, Denmark (I. Karagiannis, M.-A. Widdowson); WHO Health Emergencies Programme, Regional Office for the Western Pacific Region, Manila, Philippines (V. Biaukula); WHO Health Emergencies Programme, Regional Office for the South-East Asian Region, New Delhi, India (M. Kato); WHO Health Emergencies Programme, Regional Office for Africa, Brazzaville, Republic of the Congo (M. Muteba, F. Sanni); WHO Health Emergencies Programme, Regional Office for the Eastern Mediterranean Region, Cairo, Egypt (J.D. Naiene); WHO Health Emergencies Programme, Regional Office for the Americas, Washington, DC, USA (T. Dorji)

DOI: https://doi.org/10.3201/eid3202.251530

[1]These first authors contributed equally to this article.

[2]Members of this group are listed at the end of this article.

sexual contact between the index case (i.e., unspecified contact with the index case and partners).

Of the 33 secondary cases with data available for both index and secondary cases, most (73%) resulted from men, who transmitted MPXV to mostly women and children, followed by women (21%), who infected mostly men and other women. Secondarily infected children (6%) infected 1 child and 1 man (Figure 2, panel A). Using 14 case pairs, we estimated that the mean serial interval (SI) for infection was 12 (95% CI 4–27) days. We estimated that the SI for sexual and likely sexual contact was 9 (95% CI 5–14) days, which was shorter than the SI for nonsexual household contact, 15 (95% CI 8–29) days (Figure 2, panel B), raw data boxplots. That SI difference could partly be because of the shorter incubation period and higher infectious dose for sexual transmission (*7*; F.K. Kaiser et al., unpub. data., https://doi.org/10.1101/2025.08.14.669880).

Contact data were available from 50 cases, and we were able to disaggregate risk status of contacts for 32 of those cases. We defined high-risk contacts as household members, sexual contacts, or both. When no further information was available, we relied on reporting countries' definitions of high-risk contacts. Using those data, we identified a total of 74 high-risk contacts from 33 cases, 1 of which did not have enough information available to disaggregate further into contact type (Figure 2, panel C). Of the 25 travel-related index cases from whom secondary transmission was reported, a median of 1 (range 1–4) secondary case occurred. We estimated the SAR for household contacts was 17% (95% CI 8%–31%) and for sexual contacts was 73% (95% CI 39%–94%) (Figure 2, panel D). No secondary cases were reported among community contacts or contacts in healthcare settings.

The first limitation of our analysis is the small sample size because information was missing for some cases. Second, the sexual contact SAR is primarily limited to transmission between spouses or partners, and the high estimate might reflect repeated sexual exposure, prolonged close contact within the household, or both, together with a possible underreporting of sexual contacts outside the household. Finally, travel-associated cases could be missed, especially in countries where mpox is strongly stigmatized, and our estimates might not be generalizable beyond the settings described.

Conclusions

Our results highlight that close contact is a key driver of MPXV clade Ib outbreaks and show that sexual contact carried the highest transmission risk, followed by household contact. We found no evidence of transmission beyond settings involving close and prolonged contact in the available data. Other studies

Figure 1. Transmission dynamics among global travel-related mpox cases caused by clade Ib monkeypox virus. Yellow dots represent country of exposure; arrows represent direction of travel for mpox cases reported as of June 19, 2025. Some of the cases included in the article are not shown because the exact country of exposure was not known. Data source: World Health Organization (WHO); produced by WHO Health Emergencies Programme;

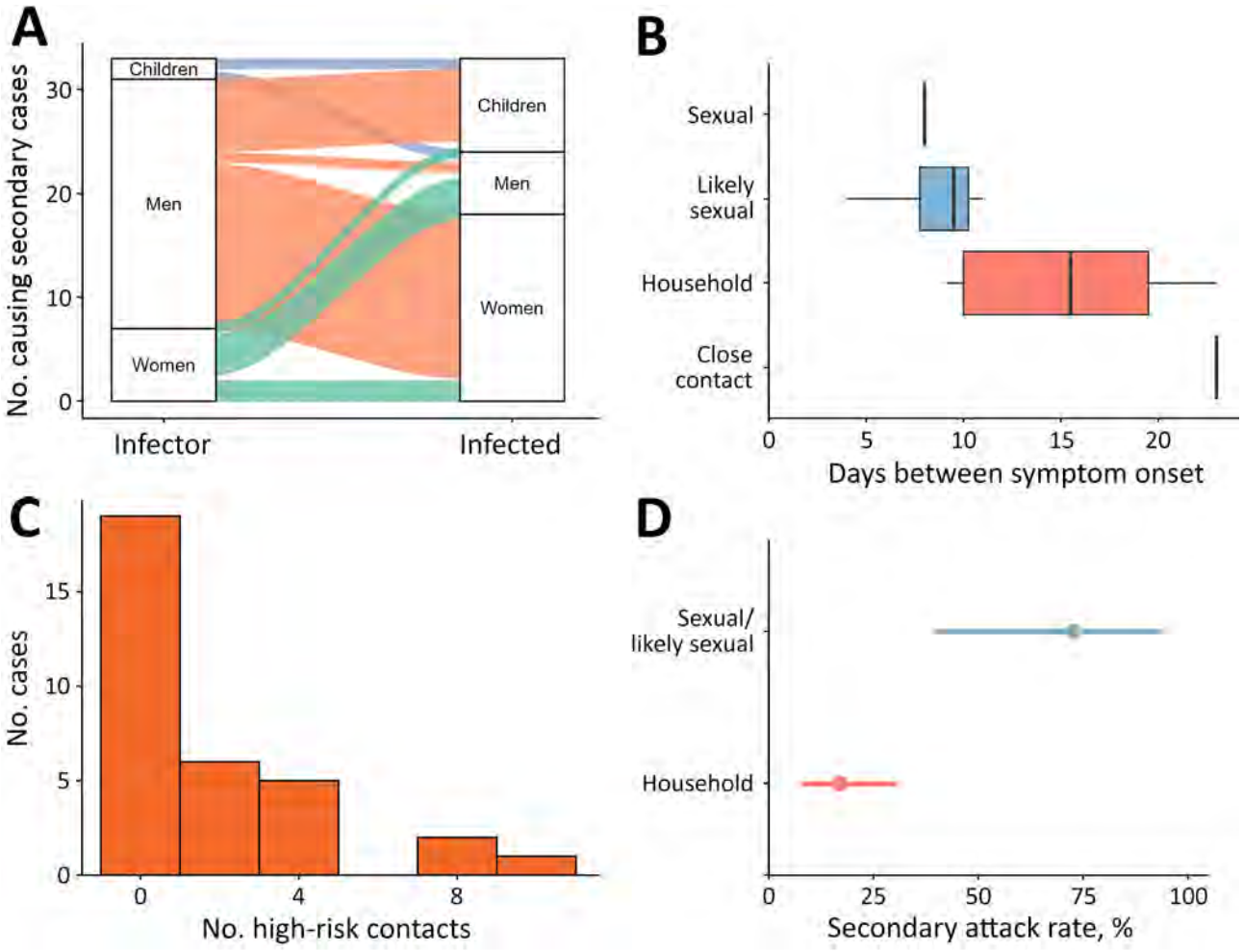

Figure 2. Characteristics and transmission dynamics among global travel-related mpox cases caused by clade Ib monkeypox virus. A) Sankey diagram of secondary transmission events among 33 transmission events and secondarily infected persons. Index cases causing multiple secondary cases were counted per secondary case. Children are persons ≤17 years of age. B) Box and whisker plot representing the serial interval for symptom onset by reported contact type for 14 case–contact pairs. Close contact is physical nonsexual interaction between the index and secondary case. Box left and right edges represent first and third quartiles, vertical lines indicate medians, and whiskers represent ranges. C) Number of high-risk contacts per each imported MPXV clade Ib case with available data among 33 high-risk contacts. D) Secondary attack rate (with 95% CIs) by reported contact type. Household contacts represent 8 secondary cases from 47 contacts; sexual contacts represent 8 secondary cases from 11 contacts.

have also acknowledged the role of sexual contact as the most efficient MPXV transmission route (*8*,*9*). Of note, secondary household cases were identified during the MPXV clade Ib outbreak reported here, but during the 2022–23 clade IIb outbreak, such events were rare; before August 2024, WHO recorded only 15 (0.2%) of 7,794 mpox cases in children <15 years of age among those exposed in the household (data not shown). Whether that disparity reflects differences in household and social contact structures or intrinsic viral properties remains unclear. The higher risk associated with sexual exposure and household contact should inform response strategies and priority interventions for populations most at risk.

WHO Mpox Collaborative Surveillance Group: Steve Kerr (CPC Analytics, Berlin); Yurie Izawa (WHO Health Emergencies Programme, Headquarters, Geneva, Switzerland); Esther Muwanguzi, Sara Hollis, Penelope Gorton (WHO Health Emergencies Programme, Regional Office for Africa, Brazzaville, the Republic of Congo); Mahmoud Hassan, Shaza Mohammed, Sherein Elnossery, Basant Mohamed (WHO Health Emergencies Programme, Regional Office for the Eastern Mediterranean Region, Cairo, Egypt); Jeffrey Pires, Kareena Hundal, Nhu Nguyen Tran Minh (WHO Health Emergencies Programme, Regional Office for the European Region, Copenhagen, Denmark); Rajkrishna Ravikumar, Christian Hertlein, Silvano Barbosa De Oliveira (WHO Health Emergencies

Programme, Regional Office for the Americas, Washington DC, United States of America); Stefany Ildefonso Acuna, Pavana Murthy, Pushpa Ranjan Wijesinghe, Manish Kakkar (WHO Health Emergencies Programme, Regional Office the South-East Asian Region, New Delhi, India); Tika Ram, Sean Casey, and Chen Zhongdan (WHO Health Emergencies Programme, Regional Office for the Western Pacific Region, Manila, Philippines).

Acknowledgments

We acknowledge all WHO Member States and their health workers for engaging in the response and reporting case-based information to WHO and other regional institutions, in line with temporary recommendations issued by the WHO Director-General under the Public Health Emergency of International Concern within the framework of the International Health Regulations (2005).

About the Author

Dr. Laurenson-Schafer is a data analyst for health emergencies working in the Epidemiology and Analytics for Response Unit within WHO's Health Emergencies Programme., Geneva, Switzerland. His research interests focus on the use of data science in the context of disease surveillance, outbreak and emergency response, and humanitarian settings. Dr. McMenamin is a data scientist in the Epidemiology and Analytics for Response Unit within WHO's Health Emergencies Programme in Geneva. Her research interests focus on outbreak analytics and surveillance in emergency response.

References

1. Masirika LM, Udahemuka JC, Schuele L, Nieuwenhuijse DF, Ndishimye P, Boter M, et al. Epidemiological and genomic evolution of the ongoing outbreak of clade Ib mpox virus in the eastern Democratic Republic of the Congo. Nat Med. 2025;31:1459–63. https://doi.org/10.1038/s41591-025-03582-1
2. Kinganda-Lusamaki E, Amuri-Aziza A, Fernandez-Nuñez N, Makangara-Cigolo JC, Pratt C, Vakaniaki EH, et al. Clade I mpox virus genomic diversity in the Democratic Republic of the Congo, 2018–2024: predominance of zoonotic transmission. Cell. 2025;188:4–14.e6. https://doi.org/10.1016/j.cell.2024.10.017
3. World Health Organization. Mpox—African Region [cited 2025 Sep 11]. https://www.who.int/emergencies/disease-outbreak-news/item/2024-DON528
4. World Health Organization. First meeting of the International Health Regulations (2005) Emergency Committee regarding the upsurge of mpox 2024 [cited 2025 Sep 11]. https://www.who.int/news/item/19-08-2024-first-meeting-of-the-international-health-regulations-(2005)-emergency-committee-regarding-the-upsurge-of-mpox-2024
5. World Health Organization. Surveillance, case investigation and contact tracing for mpox: interim guidance, 27 November 2024 [cited 2025 Sep 17]. https://www.who.int/publications/i/item/B09169
6. World Health Organization. International health regulations (2005), as amended in 2014, 2022, and 2024 [cited 2025 Sep 17]. https://apps.who.int/gb/bd/pdf_files/IHR_2014-2022-2024-en.pdf.
7. Perez-Saez J, Bugeme PM, O'Driscoll M, Bugale PK, Mukika TF, Bugwaja L, et al. Incubation periods of mpox virus clade Ib. Ann Intern Med. 2025 Dec 9 [Epub ahead of print]. https://doi.org/10.7326/ANNALS-25-01016
8. Mutuku P, Abade A, Owiny M, Irura Z, Roba A, Limo H, et al. Clade Ib mpox outbreak—Kenya, July 2024–February 2025. MMWR Morb Mortal Wkly Rep. 2025;74:379–84. https://doi.org/10.15585/mmwr.mm7422a2
9. Packer S, Patrzylas P, Merrick R, Sawyer C, McAuley A, Crowe W, et al. Mpox in UK households: estimating secondary attack rates and factors associated with transmission, May–November 2022. Epidemiol Infect. 2024;152:e113. https://doi.org/10.1017/S0950268824000864

Address for correspondence: Ana Hoxha, World Health Organization, Avenue Appia 20, 1211 Geneva, Switzerland; email: hoxhaa@who.int

Rabies Reemergence, Central Europe, 2022–2024

Emmanuelle Robardet, Marcin Smreczak, Anna Orłowska, Peter Malik, Alexandra Nándori, Zuzana Dirbáková, Rastislav Odaloš, Oleksii Rudoi, Ivan Polupan, Oxana Groza, Serghei Arseniev, Florica Barbuceanu, Vlad Vuta, Evelyne Picard-Meyer

Oral rabies vaccination campaigns helped eliminate rabies from parts of Europe, but rabies appears to be reemerging. We analyzed 2022–2024 data, which demonstrated reemergence of 2 virus variants; both were detected in Ukraine, Moldova, Poland, and Romania. Our findings highlight the need to strengthen rabies control efforts in the region.

Rabies had been eliminated from Western and Central Europe through regular implementation of oral rabies vaccination (ORV) campaigns among red foxes (*Vulpes vulpes*), the primary disease reservoir (*1*). Those campaigns, initiated over large and continuous areas since the 1990s, were typically conducted twice a year, in spring and autumn, and used an average bait density of 20–25 baits/km^2 (*1*).

The year 2020 was considered pivotal in the elimination of the classic *Lyssavirus rabies* virus (RABV) because, until that date, only sporadic cases were detected at the eastern border of the European Union in the previous 3 years (*1*). The European Commission Animal Disease Information System (https://webgate.ec.europa.eu/tracesnt/adis/public/notification) reported 8 cases/year in 2017 and 2018, mainly in wildlife, then 5 cases in 2019, including 4 wildlife cases. Although 12 cases were detected in Poland in 2020 (6 among wildlife and 6 among domestic animals), the rabies situation in Poland greatly deteriorated in 2021. Rabies was reported in the central part of Mazowieckie voivodeship, Poland (*2*), a region that had been free of sylvatic rabies, for 17 years (*2*). The outbreak escalated through the end of 2021; a total of 113 cases were reported, 103 among wildlife (mainly foxes), and 10 among domestic animals (Figure 1). Isolate analysis revealed that all the cases were caused by a single Central Europe (CE) RABV variant (*2*) (Figure 2). Poland implemented ORV campaigns that controlled the outbreak, and continued surveillance detected no cases after 2022.

A second major outbreak occurred in Central Europe in 2022, affecting Romania, Hungary, and Slovakia, then another in Poland in 2023 (*3*). Hungary and Slovakia had maintained a rabies-free status (according to the World Organisation for Animal Health self-declaration of rabies-free status that comply with Article 8.14.2 or 8.14.4 of the Terrestrial Animal Health Code) for several years but saw a resurgence of the disease in 2022, mainly near the eastern borders with Ukraine (*3*). During that outbreak, the North Eastern Europe (NEE) variant, previously detected in Poland, Slovakia, and Baltic countries (*4*), was identified. At that time, no recently published data identified variants circulating in Russia, Belarus, or Ukraine, making it difficult to compare variants and follow the geographic evolution of rabies. We analyzed RABV strains from Central Europe to assess migration of virus variants between countries during 2022–2024.

Author affiliations: ANSES, Nancy Laboratory for Rabies and Wildlife, European Union Reference Laboratory for Rabies, Bâtiment H, Technopôle Agricole et Vétérinaire, Malzéville, France (E. Robardet, E. Picard-Meyer); National Veterinary Research Institute, National Reference Laboratory for Rabies, Pulawy, Poland (M. Smreczak, A. Orłowska); National Food Chain Safety Office Veterinary Diagnostic Directorate, National Reference Laboratory for Rabies, Budapest, Hungary (P. Malik, A. Nándori); State Veterinary and Food Institute, Veterinary Institute Zvolen, Zvolen, Slovakia (Z. Dirbáková, R. Odaloš); The State Scientific and Research Institute of Laboratory Diagnostics and Veterinary Sanitary Expertise, Kyiv, Ukraine (O. Rudoï, I. Polupan); Republican Centre for Veterinary Diagnoses, Chisinau, Moldova (O. Grozda, S. Arseniev); Faculty of Veterinary Medicine, Splaiul Independentei, Bucharest (F. Barbuceanu); Institute for Diagnosis and Animal Health, National Reference Laboratory for Rabies and World Organisation for Animal Health Reference Laboratory for Rabies, Bucharest, Romania (F. Barbuceanu, V. Vuta)

DOI: https://doi.org/10.3201/eid3202.251597

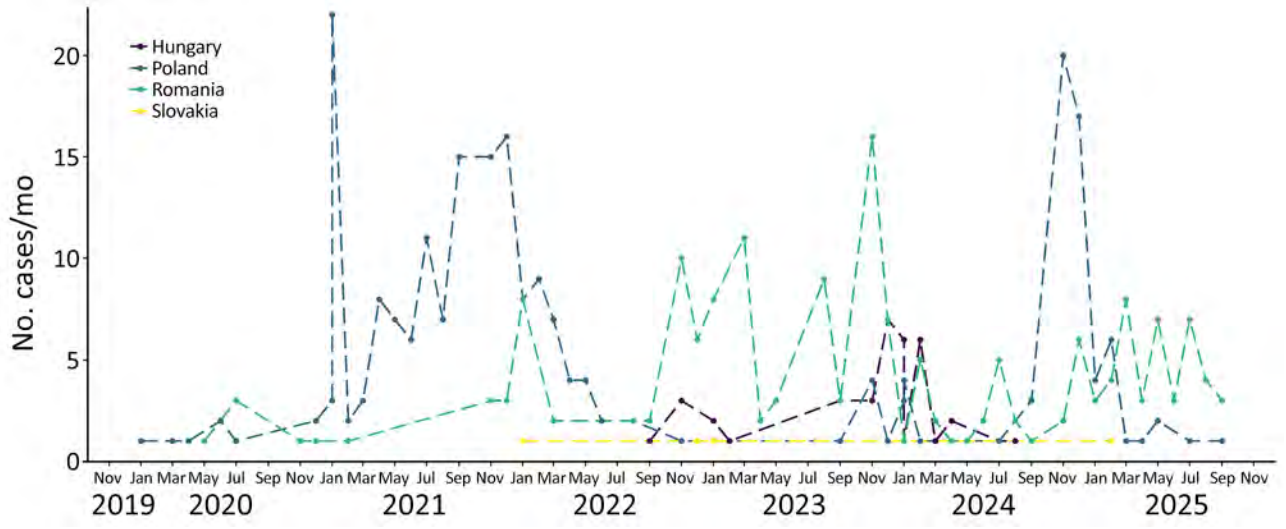

Figure 1. Distribution of detected rabies cases in wild and domestic animals from study of rabies reemergence, Central Europe, 2022–2024. The graph shows increases in rabies cases in Hungary, Poland, Romania, and Slovakia from the end of 2019 through September 2025.

The Study

We used rabies surveillance data from the Animal Disease Information System of the European Food Safety Commission (https://food.ec.europa.eu/animals/animal-diseases/animal-disease-information-system-adis_en#animal-disease-information) to document rabies case numbers. Since 2021, countries in the European Union have systematically identified RABV isolate strains by using Sanger sequencing of the full-length nucleoprotein (N) gene (1,353-bp) (Appendix 1, https://wwwnc.cdc.gov/EID/article/32/2/25-1597-App1.xlsx), according to a method described in 2023 (*3*).

Our phylogenetic analysis revealed the C variant in Poland in February 2024 and in Romania in August 2024 (Figure 2), although that variant is typically found in eastern Turkey, Georgia, Kazakhstan, Ukraine, and Russia (*4*,*5*). The number of related C variant cases then increased in Poland through the end of 2024, and we identified a single isolate from Romania in the same year. All other cases for which sequence data were available were the NEE variant.

The C variant includes viruses circulating in the steppe and forest-steppe regions of Russia from near its border with Europe to Tuva Province, as well as in Kazakhstan (*5*). The phylogeny shows that the C

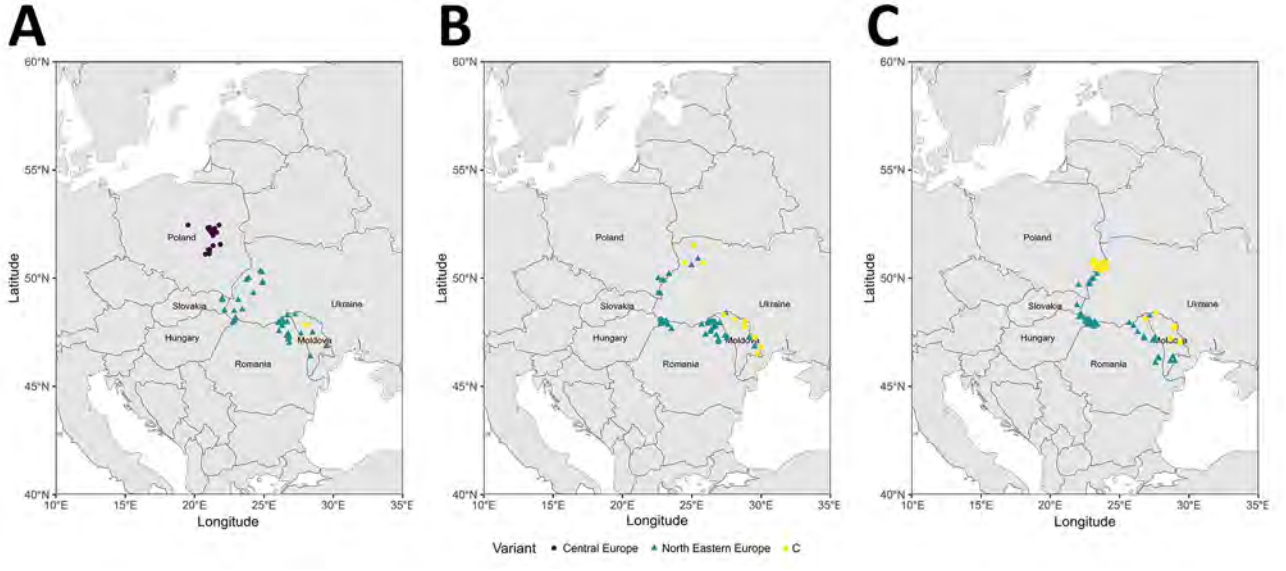

Figure 2. Spatial evolution of the different virus variants identified in a study of rabies reemergence, Central Europe, 2022–2024. A) 2022; B) 2023; C) 2024. For Ukraine and Moldova, only a few cases detected on their western borders have been sequenced; not all positive cases are noted.

variant is spatially and genetically distinct from the NEE, CE, Eastern Europe (EE), and Western Europe (WE) variants (Appendix 2 Figure, https://wwwnc.cdc.gov/EID/article/32/2/25-1597-App1.pdf).

The NEE variant probably has the largest geographic range because that lineage has been detected in the Baltic region, Romania, Moldova, Poland, and Ukraine (*3*,*5*–*7*) and was the representative variant during the 2022 outbreak in Central Europe (*3*). The CE variant, initially isolated mainly in west and south Poland, eastern Germany, the Czech Republic, and Slovenia (*4*), was the variant involved in the 2021 outbreak in Poland (*2*). The EE variant has been shown to have a similar geographic distribution to the WE variant (Serbia, Bosnia and Herzegovina, Slovenia, Croatia, and Hungary) (*4*), and cases were also detected in northern Macedonia during 2011–2012 (*8*). The WE variant, previously detected in France, Italy, Slovenia, Croatia, Montenegro, and Bosnia and Herzegovina (*4*), was last reported during 2010–2011 (*9*), and could now be extinct.

A study of the full N gene from isolates collected during 2009–2022 from 13 regions of Russia near the border with Europe found that isolates belonged to variants C or D (*10*), as previously reported (*5*). That study also highlighted the predominance of C over D isolates and that variant C apparently replaced variant D in many regions (*10*). During 2002–2014, variant C was detected in the Baltic region (*11*), Ukraine (*12*), and Poland, which had 8 rabies cases along the border with Belarus during 2008–2014 (M. Smreczak, unpub. data). The C variant has not been previously isolated in Romania (*13*).

Using information on reported rabies cases, we calculated the distance to the nearest border for cases detected during January 2023–September 2025. Those calculations revealed that most rabies cases in Hungary, Poland, Romania, and Slovakia were located ≤50 km from borders with Ukraine or Moldova (mean 21.8, SD ±24.9 km) (Figure 3). That distance appears to have remained unchanged over time, suggesting that the extent of the RABV infection might be stable in the region.

In Europe, the oral vaccination of wildlife reservoirs has proven to be the only effective measure to eliminate rabies (*14*). Since 2021, Western and Central Europe have experienced rabies challenges in the form of several distinct outbreaks, and the NEE variant has affected several countries at nearly the same time and remains active (*2*,*3*). The number of vaccinated regions in Ukraine has been increasing yearly since 2023, from 4 regions in 2023 to 14 in 2024 and 21 in 2025 (*15*). Although aerial ORV distribution is known to be more effective, manual distribution is used in Moldova and Ukraine because of local constraints. Given the rapid turnover of red fox populations, any interruption in ORV programs, as in Romania, likely will to lead to a drastic decline in vaccination coverage, which could enable RABV to spread more easily. Indeed, Romania reported an endemic human rabies case in 2025 caused by a free-roaming dog, but no endemic human cases had been reported in the European Union since 2012 (https://who-rabies-bulletin.org/news/tragic-human-rabies-case-romania). In 2024, two human rabies cases were notified in Ukraine, and 1 case was reported during the first quarter of 2025 (*15*). Those recent dramatic cases illustrate the need to redouble awareness and surveillance efforts to evaluate the infected areas and implement adequate ORV programs to avoid silent extension. Biologics can also be used as preventive measures, such as vaccinating humans and domestic species at risk when the reservoir is infected and untreated, or by administering postexposure prophylaxis.

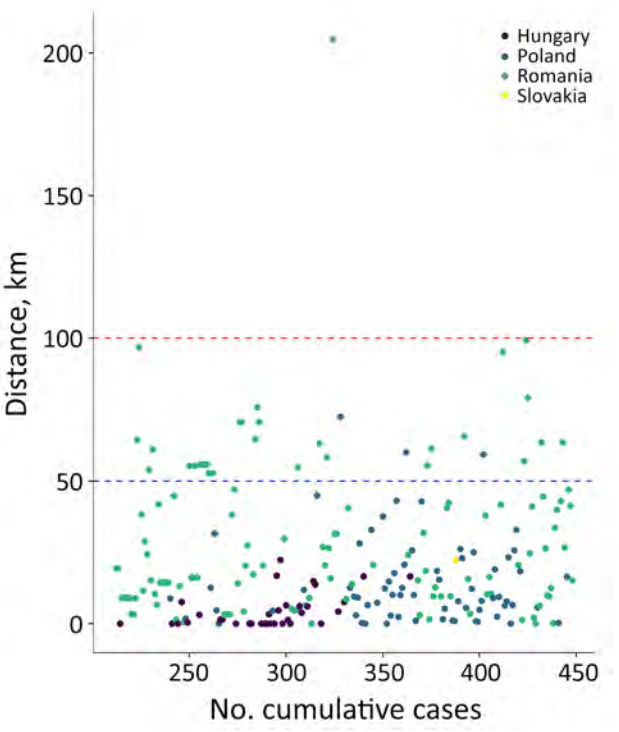

Figure 3. Distance from Ukraine and Moldova of cases detected in Hungary, Poland, Romania and Slovakia, January 2023–September 2025. Most cases were located ≤50 km from borders with Ukraine or Moldova (blue dashed line); almost all were <100 km from the border (red dashed line).

Conclusions

Through close and continuous cooperation between national reference laboratories for rabies and the

extensive sequencing of the entire N gene of all rabies isolates since 2021, we detected the C variant and mapped its spread in Central Europe during 2024, reflecting a constant westward infection pressure and a fragile zoonotic situation. The ongoing war in the region is disrupting the organization of human societies and is affecting wildlife through the destruction of habitat and food resources. The effects of armed conflict on the spread of zoonoses, including rabies, should be assessed and given greater consideration. To overcome the worrying setback in rabies elimination in this part of Europe, regular, large-scale, and effective rabies vaccination campaigns need to be maintained and cross-border cooperation between countries needs to be strengthened.

Acknowledgments

We thank the European Union Reference Laboratory staff involved in this study, particularly C. Carvalho and J.L. Schereffer for their support in conducting molecular laboratory analyses. We also thank everyone who contributed directly or indirectly to national rabies surveillance programs, which consequently made this study possible.

Prior to submission, the nucleic acid sequence data found and presented in the reported study were deposited in GenBank. Accession numbers are provided (Appendix 1 Table 2, https://wwwnc.cdc.gov/EID/article/32/2/25-1597-App1.xlsx).

This article is based on a jointly funded program to control and eradicate rabies in wildlife, so no ethical approval was required. According to Regulation (EU) 2016/429-EN-EUR-Lex, rabies is a classified B-listed disease that must be monitored and controlled in all member states to eradicate it throughout the European Union. This work was funded by the European Commission and by the national reference laboratories for rabies in Hungary, Poland, Romania, and Slovakia.

About the Author

Dr. Robardet is a scientific manager in the field of animal health epidemiology at the ANSES Nancy Laboratory for Rabies and Wildlife (LRFSN), Malzéville, France, and oversees the European Union Reference Laboratory. Her research interests include rabies surveillance and control, as well as epidemiologic understanding of lyssaviruses transmission.

References

1. Robardet E, Bosnjak D, Englund L, Demetriou P, Rosado Martín P, Cliquet F. Zero endemic cases of wildlife rabies (classical rabies virus, RABV) in the European Union by 2020: an achievable goal. Trop Med Infect Dis. 2019;4:124. https://doi.org/10.3390/tropicalmed4040124
2. Smreczak M, Orłowska A, Trębas P, Stolarek A, Freuling C, Müller T. Re-emergence of rabies in Mazowieckie voivodeship, Poland, 2021. Zoonoses Public Health. 2023;70:111–6. https://doi.org/10.1111/zph.13005
3. Robardet E, Smreczak M, Orlowska A, Malik P, Nándori A, Dirbáková Z, et al. Two sylvatic rabies re-emergences in central-eastern Europe over the 2021–2022 period: an unprecedented situation in recent years. Transbound Emerg Dis. 2023;2023:5589201. https://doi.org/10.1155/2023/5589201
4. Bourhy H, Kissi B, Audry L, Smreczak M, Sadkowska-Todys M, Kulonen K, et al. Ecology and evolution of rabies virus in Europe. J Gen Virol. 1999; 80:2545–57. https://doi.org/10.1099/0022-1317-80-10-2545
5. Kuzmin IV, Botvinkin AD, McElhinney LM, Smith JS, Orciari LA, Hughes GJ, et al. Molecular epidemiology of terrestrial rabies in the former Soviet Union. J Wildl Dis. 2004;40:617–31. https://doi.org/10.7589/0090-3558-40.4.617
6. Dascalu MA, Picard-Meyer E, Robardet E, Servat A, Arseniev S, Groza O, et al. Whole genome sequencing and phylogenetic characterisation of rabies virus strains from Moldova and north-eastern Romania. PLoS Negl Trop Dis. 2023;17:e0011446. https://doi.org/10.1371/journal.pntd.0011446
7. Orłowska A, Żmudziński JF. Molecular epidemiology of rabies virus in Poland. Arch Virol. 2014;159:2043–50. https://doi.org/10.1007/s00705-014-2045-z
8. Picard-Meyer E, Mrenoshki S, Milicevic V, Ilieva D, Cvetkovikj I, Cvetkovikj A, et al. Molecular characterisation of rabies virus strains in the Republic of Macedonia. Arch Virol. 2013;158:237–40. https://doi.org/10.1007/s00705-012-1466-9
9. Černe D, Hostnik P, Toplak I. The successful elimination of sylvatic rabies using oral vaccination of foxes in Slovenia. Viruses. 2021;13:405. https://doi.org/10.3390/v13030405
10. Chupin SA, Chernysheva EV, Metlin AE. Genetic characterization of the rabies virus field isolates detected in Russian Federation within the period 2008–2011 [in Russian]. Vopr Virusol. 2013;58:44–9.
11. Picard-Meyer E, Robardet E, Moroz D, Trotsenko Z, Drozhzhe Z, Biarnais M, et al. Molecular epidemiology of rabies in Ukraine. Arch Virol. 2012;157:1689–98. https://doi.org/10.1007/s00705-012-1351-6
12. Turcitu MA, Barboi G, Vuta V, Mihai I, Boncea D, Dumitrescu F, et al. Molecular epidemiology of rabies virus in Romania provides evidence for a high degree of heterogeneity and virus diversity. Virus Res. 2010;150:28–33. https://doi.org/10.1016/j.virusres.2010.02.008
13. World Health Organization. WHO expert consultation on rabies: WHO TRS no. 1012. Geneva: The Organization; 2018.
14. Robardet E, Picard-Meyer E, Dobroštana M, Jaceviciene I, Mähar K, Zita M, et al. Rabies in the Baltic states: decoding a process of elimination and control. PLoS Negl Trop Dis. 2016;10:e0004432. https://doi.org/10.1371/journal.pntd.0004432
15. Mandyhra S. Epidemic situation on rabies in Ukraine, 2020–2024. Presented at: EURL Rabies Workshop; June 10–11, 2025; Maisons-Alfort, France.

Address for correspondence: Emmanuelle Robardet, ANSES, Nancy Laboratory for Rabies and Wildlife, EURL for Rabies, Bâtiment H, Technopôle Agricole et Vétérinaire, CS 40 009, 54220 Malzéville CEDEX, France; email: emmanuelle.robardet@anses.fr

Desulfovibrio Bacteremia in Patients with Abdominal Infections, Japan, 2020–2025

Naoki Watanabe,[1] Tomohisa Watari, Yoshihito Otsuka

We reviewed 8 episodes of *Desulfovibrio* bacteremia in Japan (2020–2025) and confirmed 4 species by 16S rRNA gene and whole-genome sequencing. We detected β-lactamase genes in 2 *D. desulfuricans* (bla_{DES-1}-like), 1 *D. falkowii* (bla_{MUN-1}), and 2 *D. fairfieldensis* (bla_{CfiA}-like). Mass spectometry failed to identify *D. falkowii* or *D. legallii*.

Desulfovibrio species bacteria are gram-negative, sulfate-reducing, obligately anaerobic curved or spiral rods that inhabit aquatic and soil environments, as well as the gastrointestinal tracts of humans and animals (*1*,*2*). Reported manifestations include bacteremia and intraabdominal infections, such as abscesses and cholecystitis (*2*). Several *Desulfovibrio* species have been implicated in human disease, including *D. desulfuricans*, *D. fairfieldensis*, *D. vulgaris*, and *D. piger* (*3*,*4*). *D. desulfuricans* is the most commonly reported species in *Desulfovibrio* bacteremia, which can result from translocation from the gastrointestinal tract (*2*). Species-level identification can be challenging in clinical laboratories. Routine matrix-assisted laser desorption/ionization time-of-flight (MALDI-TOF) mass spectrometry libraries might lack reference spectra for less commonly recognized species (*5*). As a result, routine identification may be uncertain, even at the genus level.

The optimal therapy for *Desulfovibrio* infections has not been determined as of January 2026. Reported isolates often show low MICs for metronidazole, whereas MICs for some β-lactams can be high; extended-spectrum β-lactamases, such as DES-1, have been described in *D. desulfuricans* (*6*,*7*). Species-resolved antimicrobial susceptibility data and resistance determinants remain limited beyond those for *D. desulfuricans* and *D. fairfieldensis*. We describe 8 episodes of *Desulfovibrio* bacteremia associated with abdominal infection in Japan and assess the limits of routine identification, confirming species by 16S rRNA gene and whole-genome sequencing. We also summarize patient characteristics, outcomes, antimicrobial MICs, and β-lactamase genes.

The Study

We retrospectively reviewed clinical and laboratory data in cases of *Desulfovibrio* bacteremia at Kameda Medical Center, a tertiary-care hospital in Kamogawa, Japan, during January 2020–June 2025; we included episodes in which *Desulfovibrio* spp. were isolated from blood cultures. We considered all positive blood culture bottles collected during the same clinical episode as 1 case. We counted a new episode only when it was clearly associated with new symptoms or signs, a new anatomic focus, or resolution of a previous episode. We assessed outcomes during hospitalization, which we defined as the period from initiation of antimicrobial therapy through hospital discharge. The ethics committee of Kameda Medical Center approved the study (approval no. 25-061) and waived the requirement for informed consent because of the retrospective study design and use of deidentified data.

We processed blood cultures with the BACTEC FX system (Becton, Dickinson and Company, https://www.bd.com) and incubated them at 35°C for ≤7 days in accordance with our routine protocol. We defined the time to positivity as the interval from the start of incubation to the first instrument-flagged positive bottle. We performed routine identification by MALDI-TOF mass spectrometry and a desulfoviridin assay. We performed species identification with a MALDI Biotyper using the MBT Compass Library version 13 (Bruker Daltonics GmbH, https://www.bruker.com). We considered scores ≥2.0 as species-level identifications and scores <2.0 as uncertain.

Author affiliation: Kameda Medical Center, Kamogawa, Japan

DOI: https://doi.org/10.3201/eid3202.251581

[1]Current affiliation: Hirosaki University, Hirosaki, Japan.

Table 1. Patient characteristics and clinical course of *Desulfovibrio* bacteremia in patients with abdominal infections, Japan, 2020–2025

Case no.	Age, y/sex	Clinical diagnosis	Underlying conditions	Time to positivity, d	Source control	Antimicrobial therapy (duration, d)*	Outcome at discharge
1†	80s/M	Ischemic colitis, bowel obstruction	Atrial fibrillation; hypertension	4	Yes (surgery)	Ampicillin/sulbactam (9), then amoxicillin/clavulanate (7)	Recovered
2	70s/M	Ischemic colitis, septic shock	Intravascular large B cell lymphoma; chronic hepatitis B; hypertension	5	No	Piperacillin/tazobactam, vancomycin, and micafungin (3), then piperacillin/tazobactam (11)	Recovered
3	80s/F	Adhesive small-bowel obstruction; hemorrhagic cystitis	Ureteral cancer; severe aortic stenosis; paroxysmal atrial fibrillation	6	No	Cefotiam (5), then ampicillin/sulbactam (14)	Recovered
4	60s/F	Perianal abscess	Rectal cancer; prior venous thromboembolism; recent colostomy	6	Yes (surgery)	Piperacillin/tazobactam (30), then piperacillin and metronidazole (3)	Recovered
5	80s/M	Psoas abscess; catheter-associated urinary tract infection	Aortic stenosis/aortic regurgitation; atrial fibrillation; heart failure	3	No	Cefepime and vancomycin (7)	Died
6	90s/M	Colonic diverticulitis; acute enteritis	None	3	No	Piperacillin/tazobactam (duration not recorded)	Transferred
7	70s/M	Febrile illness, unknown origin	Hypertension	6	No	None	Not applicable‡
8	70s/M	Colonic diverticulitis	Hypertension	4	No	Amoxicillin/clavulanate (10)	Recovered

*Antimicrobial agents are listed as the drugs used for the longest duration. When the regimen changed, the initial regimen is listed first, followed by subsequent therapy.
†Polymicrobial episode with co-pathogen *Parabacteroides goldsteinii*.
‡Indicates an episode of uncertain clinical significance that was not managed as clinically significant bacteremia. The patient declined further evaluation and was confirmed to be alive at ≈1-y follow-up.

We confirmed species by 16S rRNA gene and whole-genome sequencing (Appendix Tables 1, 2, https://wwwnc.cdc.gov/EID/article/32/2/25-1581-App1.pdf). For whole-genome sequencing, we generated paired-end reads on an Illumina MiSeq instrument (Illumina, https://www.illumina.com), assembled reads de novo, evaluated assembly quality, and assigned species by comparing average nucleotide identity with type strains and reference genomes. We identified antimicrobial drug resistance determinants from draft assemblies and determined antimicrobial drug susceptibility by microdilution in Brucella broth

Table 2. Characteristics of *Desulfovibrio* isolates in patients with abdominal infections, Japan, 2020–2025*

Case no.	Confirmed species (method)	MALDI-TOF MS primary result (score)	MIC, μg/mL					β-lactamase genes detected
			SAM	TZP	FOX	CRO	MTZ	
1	*D. legallii* (WGS/ANI)	Uncertain (<2.0)	≤0.5	>64	>32	4	≤0.5	None
2	*D. fairfieldensis* (WGS/ANI)	*D. fairfieldensis* (2.4)	16	>64	>32	>32	≤0.5	*bla*$_{CfiA}$-like
3	*D. falkowii* (WGS/ANI)	Uncertain (<2.0)	≤0.5	64	>32	8	≤0.5	None
4	*D. fairfieldensis* (WGS/ANI)	*D. fairfieldensis* (2.4)	8	>64	>32	>32	≤0.5	*bla*$_{CfiA}$-like
5	*D. falkowii* (WGS/ANI)	Uncertain (<2.0)	4	64	>32	>32	≤0.5	*bla*$_{MUN-1}$
6	*D. desulfuricans* (WGS/ANI)	*D. desulfuricans* (2.1)	1	32	>32	32	≤0.5	*bla*$_{DES-1}$-like
7†	*D. legallii* (16S)	Uncertain (<2.0)	1	64	>32	8	≤0.5	Not determined
8	*D. desulfuricans* (WGS/ANI)	*D. desulfuricans* (2.1)	2	64	>32	>32	≤0.5	*bla*$_{DES-1}$-like

*MICs were determined by broth microdilution in *Brucella* broth under anaerobic conditions. Resistance genes were identified in draft genomes by using AMRFinderPlus (https://github.com/ncbi/amr). ANI, average nucleotide identity; CRO, ceftriaxone; FOX, cefoxitin; MALDI-TOF MS, matrix-assisted laser desorption/ionization time-of-flight mass spectrometry; MTZ, metronidazole; SAM, ampicillin/sulbactam; TZP, piperacillin/tazobactam; WGS, whole-genome sequencing.
†For case 7, β-lactamase gene detection was not determined because the genome assembly did not meet completeness criteria.

on dry plates (Eiken Chemical, https://www.eiken.co.jp) incubated anaerobically at 35°C–37°C for 48–96 hours. (Appendix).

We identified 8 episodes of *Desulfovibrio* bacteremia among 4,431 patients with positive blood cultures (0.2% [95% CI 0.1%–0.4%]). All patients were ≥65 years of age (median 81 years; interquartile range 77–86 years); the presumed source in 7 episodes was abdominal infection (Table 1). The primary initial symptoms were fever (4/8) and abdominal symptoms (5/8) (Appendix Table 3). Median time to positivity was 4.1 days (range 2.9–5.5 days), and 3 episodes became positive on incubation day 6 (Table 1). We assessed outcomes at discharge; 1 patient died. Case 7 was considered of uncertain clinical significance because symptoms had resolved without antimicrobial therapy by the time of culture notification and the patient declined further evaluation; he was later confirmed to be alive when he returned for care for an unrelated illness ≈1 year later.

We identified 2 isolates each of *D. desulfuricans*, *D. fairfieldensis*, *D. falkowii*, and *D. legallii* (Table 2). Gram stains from anaerobic blood culture bottles showed curved gram-negative rods (Figure 1). The desulfoviridin assay was positive for all isolates. Seven isolates passed genome quality thresholds and were assigned to species by average nucleotide identity and digital DNA–DNA hybridization (Figure 2; Appendix Tables 4–8). The remaining isolate was identified as *D. legallii* by 16S rRNA gene sequencing because its genome assembly did not meet completeness criteria. Previous reports emphasized *D. desulfuricans* and *D. fairfieldensis* as predominant causes of bacteremia (*2*), whereas our series also included *D. falkowii* and *D. legallii*. Bacteremia caused by *D. falkowii* or *D. legallii* has been reported infrequently (*5*,*8*). MALDI-TOF mass spectrometry did not identify *D. falkowii* or *D. legallii* (Table 2); that finding was consistent with a previous report of *D. legallii* bacteremia in which MALDI-TOF mass spectrometry failed to identify the species (*5*). Sequence data are available in DDBJ/GenBank under BioProject PRJDB35884 (Appendix Table 9).

Antimicrobial susceptibility testing by broth microdilution showed low MICs for ampicillin/sulbactam

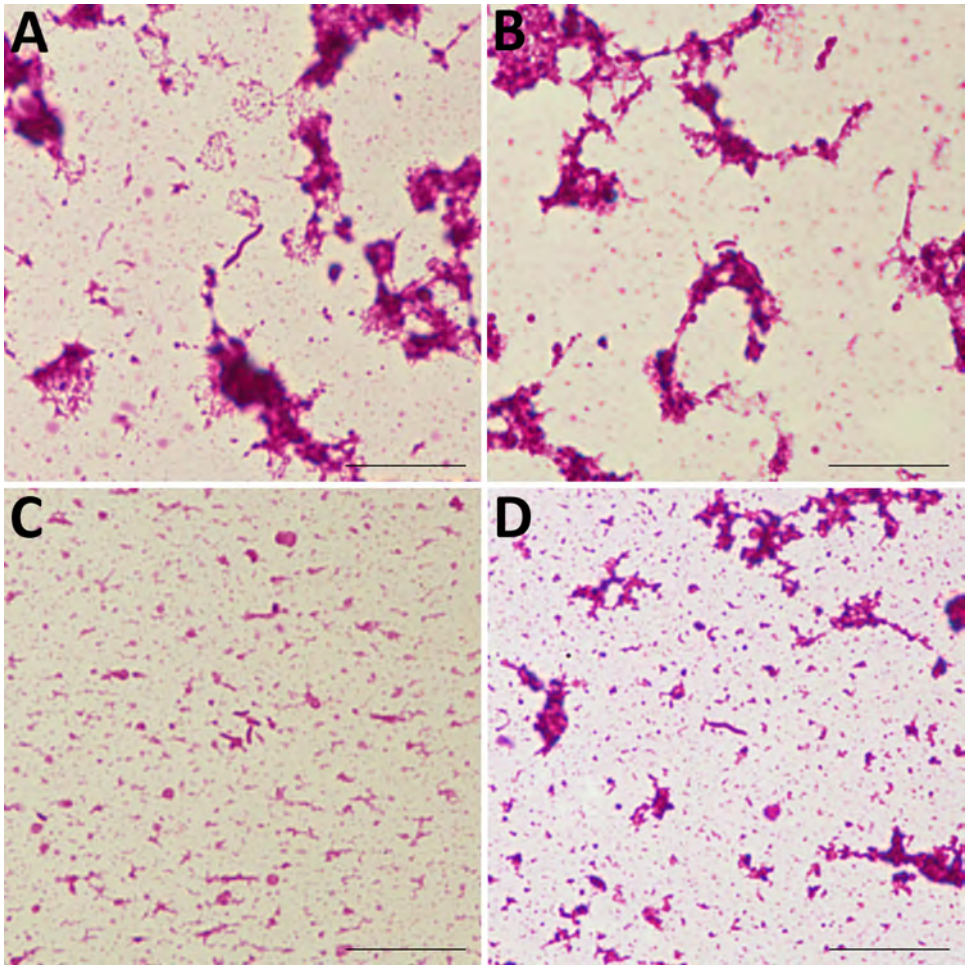

Figure 1. Gram-stained smear from a positive anaerobic blood-culture bottle in a study of *Desulfovibrio* bacteremia at a tertiary-care hospital in Japan, 2020–2025. A) *D. desulfuricans* spiral form; B) *D. desulfuricans* curved form; C) *D. falkowii* curved form; D) *D. legallii* spiral form. Curved or spiral gram-negative rods are visible. Images were acquired using a 100× oil-immersion objective. Scale bars indicate 10 μm.

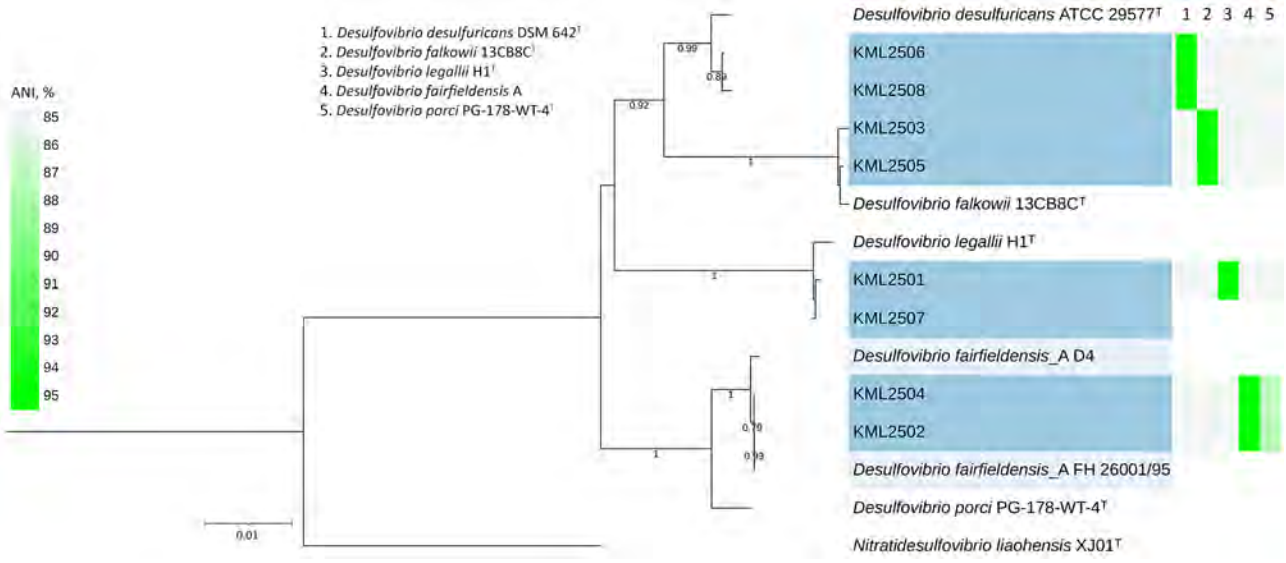

Figure 2. Phylogenetic tree of 8 *Desulfovibrio* isolates from study of *Desulfovibrio* bacteremia at a tertiary-care hospital in Japan, 2020–2025. Tree is based on 16S rRNA gene sequences and ANI heatmap and dendrogram comparing study isolates (numbers at left, defined in the key) with type or reference genomes. Cells are colored by ANI (%) on a fluorescent-green gradient; higher identity appears brighter. Blue shading indicates study isolates. Light blue shading indicates previously reported *D. fairfieldensis* isolates (FH 26001/95 and D4). Superscript T indicates type strains. Scale bar indicates number of substitutions per site. ANI, average nucleotide identity.

and metronidazole (Table 2; Appendix Table 10). Piperacillin/tazobactam MICs were 32 to >64 μg/mL for all isolates (Table 2), consistent with previous observations (*6*,*9*). We did not perform Etest susceptibility testing (bioMérieux, https://www.biomerieux.com), so could not assess agreement with broth microdilution MICs. Five isolates had ceftriaxone MICs ≥32 μg/mL and carried β-lactamase genes, including $bla_{\text{DES-1}}$-like, $bla_{\text{MUN-1}}$, or bla_{CfiA}-like (Table 2), suggesting that β-lactamase activity contributes to elevated ceftriaxone MICs in some isolates. DES-1 has been described in *D. desulfuricans* (*7*). MUN-1 is an Ambler class A extended-spectrum β-lactamase (*10*). CfiA-family class B metallo-β-lactamases have been described in the *Bacteroides fragilis* group (*11*). *D. falkowii* isolate KML2505 carried $bla_{\text{MUN-1}}$ with 100% identity and 100% coverage to reference isolate WP_206340447.1. *D. desulfuricans* isolates KML2506 and KML2508 each carried DES-family class A β-lactamases ($bla_{\text{DES-1}}$-like) with 81%–82% identity and 100% coverage to the closest reference WP_063860095.1 isolate. In addition, *D. fairfieldensis* isolates KML2502 and KML2504 harbored subclass B1 metallo-β-lactamase homologs (bla_{CfiA}-like) with 47% identity and 94% coverage to the closest reference, WP_005808062.1.

Conclusions

In this case series, *Desulfovibrio* bacteremia was associated with multiple species, including *D. desulfuricans*, *D. fairfieldensis*, *D. falkowii*, and *D. legallii*, suggesting broader species diversity than previously appreciated. Antimicrobial drug susceptibility testing showed low MICs for metronidazole and ampicillin/sulbactam, whereas MICs for piperacillin/tazobactam were high in all isolates. Routine MALDI-TOF mass spectrometry did not identify *D. falkowii* or *D. legallii* bacteria. Curved gram-negative rods in anaerobic blood culture bottles and a positive desulfoviridin assay may prompt suspicion for *Desulfovibrio* infection, which can guide empiric therapy while confirmatory identification is pending.

This article was preprinted at https://doi.org/10.1101/2025.09.26.25336699.

Acknowledgments

We thank Wataru Hayashi for advice on whole-genome sequencing analysis.

We used ChatGPT (model GPT-5.2) to assist with English-language editing. All authors reviewed and approved the final text and take full responsibility for its content.

About the Author

Dr. Watanabe is a lecturer in the Department of Bioscience and Laboratory Medicine at Hirosaki University, Hirosaki, Japan. At the time of this work, he was a clinical laboratory technologist in the Department of Clinical Laboratory at Kameda Medical Center, Kamogawa, Japan. His research interests include diagnostic microbiology, bloodstream infections, and antimicrobial resistance.

References

1. Postgate JR, Campbell LL. Classification of *Desulfovibrio* species, the nonsporulating sulfate-reducing bacteria. Bacteriol Rev. 1966;30:732–8. https://doi.org/10.1128/br.30.4.732-738.1966
2. Goldstein EJC, Citron DM, Peraino VA, Cross SA. *Desulfovibrio desulfuricans* bacteremia and review of human *Desulfovibrio* infections. J Clin Microbiol. 2003;41:2752–4. https://doi.org/10.1128/JCM.41.6.2752-2754.2003
3. Warren YA, Citron DM, Merriam CV, Goldstein EJC. Biochemical differentiation and comparison of *Desulfovibrio* species and other phenotypically similar genera. J Clin Microbiol. 2005;43:4041–5. https://doi.org/10.1128/JCM.43.8.4041-4045.2005
4. Yamaizumi K, Kyotani M, Kenzaka T. Bacteremia caused by *Desulfovibrio desulfuricans* with the intestinal tract as the portal of entry: two case reports and a literature review. BMC Infect Dis. 2024;24:725. https://doi.org/10.1186/s12879-024-09623-3
5. Kobayashi S, Hayashi M, Yaguchi T, Taguchi J, Oshima R, Hosokawa T, et al. The first case of bacteremia caused by *Desulfovibrio legallii*. J Infect Chemother. 2025;31:102762. https://doi.org/10.1016/j.jiac.2025.102762
6. Lozniewski A, Labia R, Haristoy X, Mory F. Antimicrobial susceptibilities of clinical *Desulfovibrio* isolates. Antimicrob Agents Chemother. 2001;45:2933–5. https://doi.org/10.1128/AAC.45.10.2933-2935.2001
7. Morin AS, Poirel L, Mory F, Labia R, Nordmann P. Biochemical-genetic analysis and distribution of DES-1, an Ambler class A extended-spectrum β-lactamase from *Desulfovibrio desulfuricans*. Antimicrob Agents Chemother. 2002;46:3215–22. https://doi.org/10.1128/AAC.46.10.3215-3222.2002
8. Hosoda T, Suzuki M, Matsuno T, Matsui K, Ohyama K, Doi Y. Limitations of MALDI-TOF MS in identifying anaerobic bacteremia: challenges in polymicrobial infections and the role of whole-genome sequencing. Microbiol Spectr. 2025;13:e0101425. https://doi.org/10.1128/spectrum.01014-25
9. Nakao K, Tanaka K, Ichiishi S, Mikamo H, Shibata T, Watanabe K. Susceptibilities of 23 *Desulfovibrio* isolates from humans. Antimicrob Agents Chemother. 2009;53:5308–11. https://doi.org/10.1128/AAC.00630-09
10. Gschwind R, Petitjean M, Fournier C, Lao J, Clermont O, Nordmann P, et al. Inter-phylum circulation of a beta-lactamase-encoding gene: a rare but observable event. Antimicrob Agents Chemother. 2024;68:e0145923. https://doi.org/10.1128/aac.01459-23
11. Walsh TR, Toleman MA, Poirel L, Nordmann P. Metallo-β-lactamases: the quiet before the storm? Clin Microbiol Rev. 2005;18:306–25. https://doi.org/10.1128/CMR.18.2.306-325.2005

Address for correspondence: Naoki Watanabe, Kameda Medical Center, 296-0044, Higashi-cho 929, Kamogawa, Chiba, Japan; email: m57hfh25@gmail.com

etymologia revisited

Petri Dish
[pe'tre 'dish]

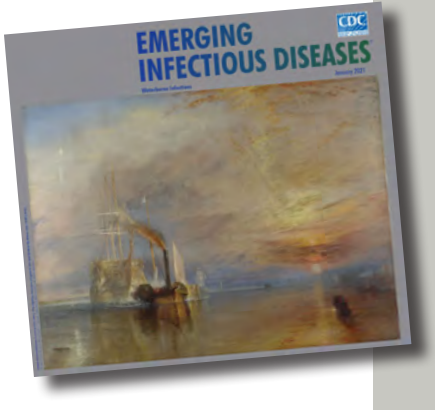

Originally published in January 2021

The Petri dish is named after the German inventor and bacteriologist Julius Richard Petri (1852–1921). In 1887, as an assistant to fellow German physician and pioneering microbiologist Robert Koch (1843–1910), Petri published a paper titled "A minor modification of the plating technique of Koch." This seemingly modest improvement (a slightly larger glass lid), Petri explained, reduced contamination from airborne germs in comparison with Koch's bell jar.

References

1 Central Sheet for Bacteriology and Parasite Science [in German]. Biodiversity Heritage Library. Volume 1, 1887 [cited 2020 Aug 25]. https://www.biodiversitylibrary.org/item/210666#page/313/mode/1up
2. Petri JR. A minor modification of the plating technique of Koch [in German]. Cent für Bacteriol und Parasitenkd. 1887;1:279–80.
3. Shama G. The "Petri" dish: a case of simultaneous invention in bacteriology. Endeavour. 2019;43:11–6. DOIExternal
4. The big story: the Petri dish. The Biomedical Scientist. Institute of Biomedical Science [cited 2020 Aug 25]. https://thebiomedicalscientist.net/science/big-story-petri-dish

https://wwwnc.cdc.gov/eid/article/27/1/et-2701_article

Retail Milk Monitoring of Influenza A(H5N1) in Dairy Cattle, United States, 2024–2025

Natalie N. Tarbuck, John Franks, Jeremy C. Jones, Ahmed Kandeil, Jennifer DeBeauchamp, Lance Miller, Thomas Fabrizio, Karlie Woodard, Hannah J. Cochran, Madison C. Owsiany, Bryant M. Foreman, James F. Lowe, Richard J. Webby, Andrew S. Bowman

US retail milk monitoring during April 13–May 3, 2024, identified influenza A(H5N1) viral RNA in 36% of retail milk samples, indicating widespread undetected infections in US dairy cows. After federal initiatives, reported infections more closely aligned with findings in retail milk during December 27, 2024–January 29, 2025, reflecting improved detection and control.

The emergence of influenza A virus (IAV) (H5N1) in dairy cows, first reported in March 2024, was unprecedented. Because dairy cows were not considered a typical host for IAV, initial identification was delayed after reports of nonspecific illness in lactating cattle in Texas, USA. After that initial detection, the virus was soon identified in dairy cows in several other US states, likely enabled by cattle movements (*1*–*3*). Considering the threat H5N1 posed to dairy cows, other livestock operations, and public health, the US Department of Agriculture issued federal orders requiring mandatory testing before interstate movement of animals and implementing a national testing strategy of raw, unpasteurized milk to monitor and control the outbreak. Given that H5N1 viral RNA has been detected in retail milk products (*4*), we used retail milk monitoring in this study to assess whether federal control measures are working to identify and mitigate influenza A(H5N1) in dairy herds.

Author affiliations: The Ohio State University College of Veterinary Medicine, Columbus, Ohio, USA (N.N. Tarbuck, H.J. Cochran, M.C. Owsiany, B.M. Foreman, A.S. Bowman); St. Jude Children's Research Hospital, Memphis, Tennessee, USA (J. Franks, J.C. Jones, A. Kandeil, J. DeBeauchamp, L. Miller, T. Fabrizio, K. Woodard, R.J. Webby); University of Illinois College of Veterinary Medicine, Urbana, Illinois, USA (J.F. Lowe)

DOI: https://doi.org/10.3201/eid3202.251332

The Study

We conducted retail milk surveillance at 2 key timepoints in the influenza A(H5N1) outbreak in dairy cows. During April 13–May 3, 2024, we purchased 168 unique pasteurized milk samples from retail stores in 13 US states. During December 27, 2024–January 29, 2025, we expanded our surveillance to include 477 (469 pasteurized and 8 raw) unique milk samples purchased from retail stores in 25 US states. To better assess the geographic extent of the outbreak, we included a mix of states with confirmed H5N1 virus–infected dairy herds and states without known infected dairy herds. To reduce duplication of samples tested, we selected unique milk samples by choosing different milk plant codes and expiration dates. We identified states with IAV viral nucleic acid–positive retail milk on the basis of the location of the milk plant, rather than where the milk was purchased.

We screened retail milk samples for the presence of influenza A viral nucleic acid using real-time quantitative PCR. We extracted RNA from retail milk using the MagMAX viral/pathogen II nucleic acid isolation kit (Thermo Fisher Scientific, https://www.thermofisher.com) or the QIAGEN RNeasy Mini Kit (QIAGEN, https://www.qiagen.com), according to manufacturer instructions. We quantified the noninfectious viral load using the VetMAX-Gold SIV Detection Kit (Thermo Fisher Scientific), which was applied to bovine milk samples outside its US Department of Agriculture license. We shipped a separate aliquot of retail milk that had never been freeze-thawed to St. Jude Children's Research Hospital (Memphis, TN, USA) for confirmation of subtype and virus viability experiments (Appendix, https://wwwnc.cdc.gov/EID/article/32/2/25-1332-App1.pdf). We ran each sample in triplicate (influenza H5b) with primers and probe sequences designed by the Centers for

Disease Control and Prevention and acquired through the International Reagent Resource (https://www.internationalreagentresource.org). Reactions were performed on the ABI 7500 FAST Real-Time PCR system (Thermo Fisher Scientific).

On April 12, 2024, only 29 infected dairy herds had been reported (*3*), although we hypothesized the outbreak was more widespread. Despite the relatively small number of infected dairy herds reported, we detected IAV in 36.3% (61/168) of pasteurized retail milk samples during April 13–May 3, 2024 (Table), including in 5 states (AR, IN, MN, MO, OK) where no outbreak in dairy cows was reported at the time sampling was initiated (Figure). We found no evidence of viable virus in IAV-positive retail milk samples, as determined by in vitro cell passaging and mouse inoculation with pasteurized milk (Appendix Figure), consistent with findings that pasteurization is effective (*4*,*5*). During December 27, 2024–January 29, 2025, we expanded our surveillance but detected IAV in only 6.9% (33/477) of retail milk samples collected, all of which were processed in California (Table). We confirmed nearly all (96.8%; 91/94) of the IAV-positive retail milk samples in this study as influenza A(H5); the remaining samples were likely untyped because of limited viral RNA or sensitivity of H5 assay.

Conclusions

The US dairy industry consists of 9.3 million cows that produce >226 billion pounds of milk annually (*6*). Shortly after the first report of influenza A(H5N1) in dairy cows, <0.1% of US dairy herds were reported as H5N1-positive, yet we detected IAV nucleic acid in 36% of retail milk samples (Figure). Our study revealed that early in the outbreak, the influenza A(H5N1) virus was more widespread than reported; the prevalence of IAV-positive retail milk was markedly higher than that of infected herds reported. Given the size of the US dairy industry, the high prevalence and low cycle threshold values detected in retail milk during April 13–May 3, 2024, suggest that a substantial number of infected cows were actively shedding virus into the milk supply, and many infections were going undetected because of limited surveillance. Those undetected cases are further supported by phylogenetic analyses that indicate that a single spillover event of influenza A(H5N1) from wild birds to dairy cows likely occurred in late 2023 and went undetected for several months (*2*), enabling opportunities for cattle movement and widespread transmission. Because initial infections were identified through passive surveillance and testing of clinically affected animals, the true extent of spread was underestimated. Those findings emphasize the importance of active surveillance and federal orders that expanded testing and reporting of influenza A(H5N1) in livestock and milk.

After the federal order on April 24, 2024, mandating premovement testing of lactating dairy cattle before interstate movement, and the subsequent implementation of the National Milk Testing Strategy on December 6, 2024 (*7*), the number of reported infected herds has grown tremendously, which is expected with increased surveillance efforts. To date, >1,000 infected herds have been reported across the United States (*3*), most of which were concentrated in California. Of note, 225 infected herds were reported in California in December (*3*), just before our second study period **(**December 27, 2024–January 29, 2025) (Figure). That report aligns more closely with patterns in our retail milk surveillance, which found IAV-positive retail milk only in California, underscoring the effectiveness of the federal orders. Those surveillance efforts not only appeared to improve

Table. Estimated influenza A virus prevalence in retail milk by state and study period in study of retail milk monitoring of influenza A(H5N1) in dairy cattle, United States, 2024–2025*

State	No. positive/no. tested (%)	
	Period 1	Period 2
Arizona	0/5	0/15
Arkansas	3/3 (100)	0/5
California	0/3	33/55 (60)
Colorado	5/20 (25)	0/23
Connecticut		0/2
Florida		0/24
Georgia	0/1	0/3
Idaho		0/7
Illinois		0/21
Indiana	2/21 (9.5)	0/31
Iowa		0/34
Kansas	12/15 (80)	0/5
Kentucky	0/1	0/6
Maryland	0/1	0/1
Massachusetts		0/2
Michigan	5/16 (31.3)	0/28
Minnesota	1/7 (14.3)	0/25
Missouri	1/5 (20)	0/24
Nebraska	0/4	0/9
New Jersey		0/5
New York	0/10	0/23
North Carolina		0/5
Ohio	2/18 (11.1)	0/25
Oklahoma	3/3 (100)	0/12
Pennsylvania		0/15
South Dakota		0/2
Tennessee		0/4
Texas	27/33 (81.8)	0/21
Utah		0/20
Virginia	0/2	0/13
Wisconsin		0/12
Total	61/168 (36.3)	33/477 (6.9)

*The number of states included in surveillance increased from period 1 to period 2. Period 1, March 25–May 3, 2024; period 2, December 9, 2024–January 29, 2025.

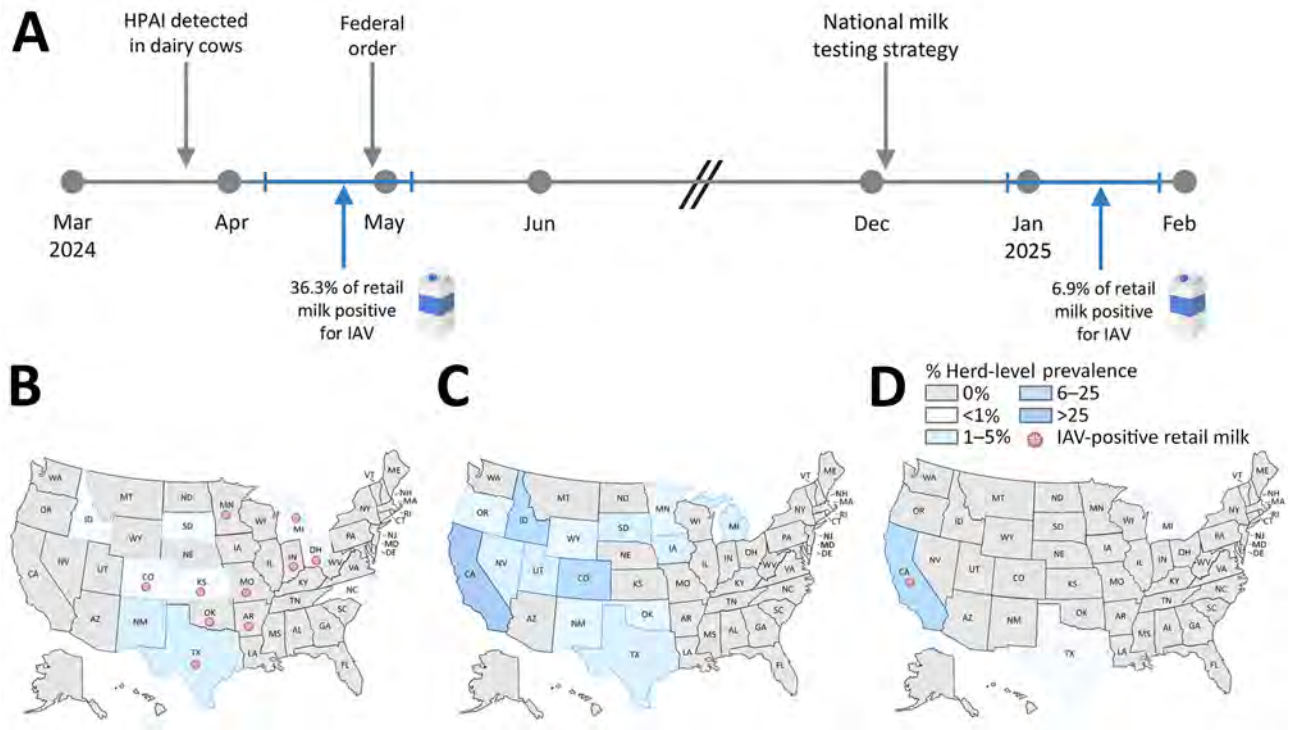

Figure. Timeline and geographic distribution of influenza A(H5N1) outbreaks in dairy cattle herds in study of retail milk monitoring of influenza A(H5N1) in dairy cattle, United States, 2024–2025. A) Timeline of detections and federal interventions. B–D) Locations of confirmed H5N1 outbreaks in dairy herds, standardized as the prevalence of infected herds relative to the total number of herds per state, on the basis of 2022 US Department of Agriculture (USDA) Census of Agriculture data (*6*). B) USDA reported outbreaks (n = 36), March 25–May 3, 2024; C) USDA reported outbreaks (n = 701), May 4–December 8, 2024); D) USDA reported outbreaks (n = 218), December 9, 2024–January 29, 2025. The red virion marks the state of processing plants where influenza A virus–positive retail milk was identified. Maps were generated using BioRender (https://BioRender.com). HPAI, highly pathogenic avian influenza; IAV, influenza A virus.

the identification of infected herds but also demonstrated more limited distribution. Taken together, our findings suggest that early in the outbreak, cases in US dairy herds were widespread and went undetected, but federal regulations have since improved detection and worked to control the spread of H5N1 virus in dairy herds. Further, the role of natural immunity from prior infections must also be considered as a factor limiting transmission, yet the duration of such immunity and its ability to prevent reinfection remain unclear. Of note, despite those combined measures, the virus has not been eliminated from dairy herds (*3*).

Retail milk testing is an imperfect solution to gaps in surveillance (*4*,*8*). Because retail milk represents a composite sample derived from multiple cows and processed in bulk, it limits the ability to identify the source of H5N1 virus–infected cows and pinpoint more granular viral evolution. In addition, the location of milk processing plants provides limited geographic resolution, because milk might be transported across state lines after collection from farms before processing. Active surveillance programs are critical in cattle and other livestock, wild birds, and humans at the frontline of exposure. Evidence of 2 additional spillover events of the H5N1D1.1 genotype, identified through the National Milk Testing Strategy (*9*,*10*), highlights the complexity and uncertainty in current transmission pathways. However, those spillover events also highlight the importance of current surveillance strategies in place to identify infected herds and new evolutionary trajectories.

Acknowledgments

We thank our collaborators who submitted milk samples from across the country, thereby expanding the geographic scope of our surveillance.

This work was supported by the Centers of Excellence for Influenza Research and Response, National Institute of Allergy and Infectious Diseases, National Institutes of Health, Department of Health and Human Services (contract no. 75N93021C00016, St. Jude Center of Excellence for Influenza Research and Response).

About the Author

Ms. Tarbuck is a PhD student in the College of Veterinary Medicine Comparative Biomedical Sciences program at The Ohio State University. Her research interests include the epidemiology of zoonotic diseases at the human-animal interface.

References

1. Burrough ER, Magstadt DR, Petersen B, Timmermans SJ, Gauger PC, Zhang J, et al. Highly pathogenic avian influenza A(H5N1) clade 2.3.4.4b virus infection in domestic dairy cattle and cats, United States, 2024. Emerg Infect Dis. 2024;30:1335–43. https://doi.org/10.3201/eid3007.240508
2. Nguyen TQ, Hutter CR, Markin A, Thomas M, Lantz K, Killian ML, et al. Emergence and interstate spread of highly pathogenic avian influenza A(H5N1) in dairy cattle in the United States. Science. 2025;388:eadq0900. https://doi.org/10.1126/science.adq0900
3. Animal and Plant Health Inspection Service. HPAI confirmed cases in livestock [cited 2025 Dec 14]. https://www.aphis.usda.gov/livestock-poultry-disease/avian/avian-influenza/hpai-detections/hpai-confirmed-cases-livestock
4. Spackman E, Jones DR, McCoig AM, Colonius TJ, Goraichuk IV, Suarez DL. Characterization of highly pathogenic avian influenza virus in retail dairy products in the US. J Virol. 2024;98:e0088124. https://doi.org/10.1128/jvi.00881-24
5. Spackman E, Anderson N, Walker S, Suarez DL, Jones DR, McCoig A, et al. Inactivation of highly pathogenic avian influenza virus with high-temperature short time continuous flow pasteurization and virus detection in bulk milk tanks. J Food Prot. 2024;87:100349. https://doi.org/10.1016/j.jfp.2024.100349
6. US Department of Agriculture National Agricultural Statistics Services. Quick stats [cited 2025 Jul 1]. https://quickstats.nass.usda.gov
7. Animal and Plant Health Inspection Service. Federal orders [cited 2025 Apr 19]. https://www.aphis.usda.gov/livestock-poultry-disease/avian/avian-influenza/hpai-detections/livestock/federal-order
8. Wallace HL, Wight J, Baz M, Dowding B, Flamand L, Hobman T, et al. Longitudinal screening of retail milk from Canadian provinces reveals no detections of influenza A virus RNA (April-July 2024): leveraging a newly established pan-Canadian network for responding to emerging viruses. Can J Microbiol. 2025;71:1–7. https://doi.org/10.1139/cjm-2024-0120
9. Animal and Plant Health Inspection Service. APHIS confirms D1.1 genotype in dairy cattle in Nevada [cited 2025 Apr 21]. https://www.aphis.usda.gov/news/program-update/aphis-confirms-d11-genotype-dairy-cattle-nevada-0
10. Animal and Plant Health Inspection Service. APHIS identifies third HPAI spillover in dairy cattle [cited 2025 Oct 27]. https://www.aphis.usda.gov/news/program-update/aphis-identifies-third-hpai-spillover-dairy-cattle

Address for correspondence: Andrew S. Bowman, The Ohio State University, 1920 Coffey Rd, Columbus OH, 43210, USA; email: bowman.214@osu.edu

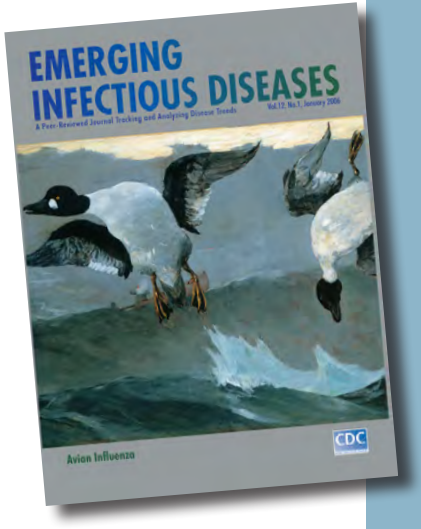

Originally published in January 2006

etymologia revisited

Influenza

[in''floo-en'zə]

An acute viral infection of the respiratory tract. From Latin influentia, "to flow into"; in medieval times, intangible fluid given off by stars was believed to affect humans. The Italian influenza referred to any disease outbreak thought to be influenced by stars. In 1743, what Italians called an influenza di catarro ("epidemic of catarrh") spread across Europe, and the disease came to be known in English as simply "influenza."

References

Dorland's illustrated medical dictionary. 30th ed. Philadelphia: Saunders; 2003; and Quinion M. World wide words. 1998 Jan 3 [cited 2005 Dec 5]. http://www.worldwidewords.org/topicalwords/tw-inf1.htm

Genomic Analysis of Doxycycline Resistance–Associated 16S rRNA Mutations in *Treponema pallidum* Subspecies *pallidum*

George S. Long, Mackenzie Neale, Thomas Braukmann, Vanessa Tran, Nishant Singh, Vanessa Allen, Muhammad Morshed, Jessica Minion, Paul Van Caeseele, Maud Vallée, Todd Hatchette, Samir N. Patel, Raymond S.W. Tsang, Venkata R. Duvvuri

We inspected 16S rRNA sequences of 784 publicly available *Treponema pallidum* subspecies *pallidum* genomes and 17 new *T. pallidum* subsp. *pallidum* genomes from Canada for putative mutations associated with doxycycline resistance. Variants were detected in 9 non-Canada genomes. These findings establish a global genomic baseline for monitoring doxycycline resistance in syphilis.

Treponema pallidum subspecies *pallidum* (TPA) is the causative agent of syphilis, a sexually transmitted infection (STI) that is on the rise globally. The incidence rate in Canada has increased by 77% since 2018, reaching 30.5 cases of syphilis/100,000 persons as of 2023 (*1*). Although syphilis is traditionally treated with benzathine penicillin G, recent shortages have hampered treatment (*2*). In Canada, doxycycline is the recommended alternative treatment for primary, secondary, and early latent syphilis in nonpregnant adults who are allergic to penicillin. Doxycycline is also an effective preexposure and postexposure prophylactic for bacterial STIs (*3*); however, treatment failures have been reported in cases of secondary and early latent syphilis (*4*).

Concerns have been raised about the mass use of doxycycline as a prophylactic in at-risk communities (*3*) despite its demonstrated effectiveness. The primary concern is the potential selection for doxycycline-resistant sexually transmitted bacteria and alterations to the gut microflora (*3*). Those worries stem from the fact that some doxycycline resistance mechanisms, such as Tet efflux pumps (*5*), are horizontally transferred through plasmids or transposons and thus render future treatments for unrelated infections less effective. Other routes to resistance, such as ribosomal mutations to the 16S rRNA gene (*5*–*8*), are possible. In *T. pallidum*, doxycycline resistance is hypothesized to occur through mutations in the 16S rRNA genes because the pathogen is believed to rarely undergo recombination (*9*,*10*). In light of that factor, a previous study demonstrated that repeated exposure to doxycycline did not significantly increase resistance (*11*). A recent genomic analysis (*12*) identified a mutational triplet at positions 965–967 (*E. coli* numbering) in the 16S rRNA gene of *Treponema* and *Spirochaeta*, which might warrant continued surveillance and further investigation for their potential role in tetracycline resistance.

The goal of this study was to characterize 17 newly sequenced TPA genomes from Canada and monitor antimicrobial resistance (AMR), with a focus on doxycycline. This analysis also includes 784

Author affiliations: Public Health Ontario, Toronto, Ontario, Canada (G.S. Long, T. Braukmann, V. Tran, N. Singh, V. Allen, S.N. Patel, V.R. Duvvuri); Public Health Agency of Canada, Winnipeg, Manitoba, Canada (M. Neale, R.S.W. Tsang); University of Toronto, Toronto (T. Braukmann, V. Tran, V. Allen, S.N. Patel, V.R. Duvvuri); Sinai Health and University Health Network, Toronto (V. Allen); British Columbia Centre for Disease Control, Vancouver, British Columbia, Canada (M. Morshed); University of British Columbia, Vancouver (M. Morshed); Roy Romanow Provincial Laboratory, Regina, Saskatchewan, Canada (J. Minion); University of Saskatchewan, Regina (J. Minion); Cadham Provincial Laboratory, Winnipeg (P. Van Caeseele); University of Manitoba, Winnipeg (P. Van Caeseele); Laboratoire de Santé Publique du Québec, Sainte-Anne-de-Bellevue, Quebec, Canada (M. Vallée); Dalhousie University, Halifax, Nova Scotia, Canada (T. Hatchette); York University, Toronto (V.R. Duvvuri)

DOI: https://doi.org/10.3201/eid3202.251060

Table 1. Demographic and genomic features of 17 *Treponema pallidum* samples from adults in Canada collected during 2016–2024 used in genomic analysis of doxycycline resistance–associated 16S rRNA mutations in *T. pallidum* subsp. *pallidum**

Sample	GenBank or BioSample accession no.	Year	Province	Lineage		Macrolide resistant
				MLST	PopPUNK	
MB1	CP191228	2016	Manitoba	SS14	SS14	Y
SK1	CP191227	2023	Saskatchewan	SS14	SS14	Y
CDN1	SAMN49899419	2016	Manitoba	SS14	SS14	Y
CDN2	SAMN49899420	2022	Manitoba	SS14	SS14	Y
CDN3	SAMN49899421	2024	British Columbia	SS14	SS14	Y
CDN4	SAMN49899422	2024	British Columbia	Unknown	SS14	Y
CDN5	SAMN49899423	2024	Saskatchewan	SS14	SS14	Y
CDN6	SAMN49899424	2024	Saskatchewan	SS14	SS14	Y
CDN7	SAMN49899425	2024	Saskatchewan	SS14	SS14	Y
CDN8	SAMN49899426	2024	Saskatchewan	SS14	SS14	N
CDN9	SAMN49899427	2024	Saskatchewan	Unknown	Nichols	Y
CDN10	SAMN49899428	2024	Saskatchewan	SS14	SS14	Y
CDN11	SAMN49899429	2024	Saskatchewan	SS14	SS14	Y
CDN12	SAMN49899430	2024	Québec	SS14	SS14	Y
CDN13	SAMN49899431	2024	Québec	SS14	SS14	Y
CDN14	SAMN49899432	2024	Saskatchewan	SS14	SS14	Y
CDN15	SAMN49899433	2024	Nova Scotia	Nichols	Nichols	Y

*The TPA lineages were identified with both MLST and PopPUNK (*14*,*15*) (Appendix, https://wwwnc.cdc.gov/EID/article/32/2/25-1060-App1.pdf). Macrolide resistance was identified on the basis of single-nucleotide polymorphisms in the 23S rRNA gene (*13*). Samples were obtained from adults (18–64 years of age), apart from 2 (BC1 and BC2) that did not contain any identifying information.

previously published global TPA genomes and sequencing libraries from the National Center for Biotechnology Information (NCBI) GenBank and Sequence Read Archives (Appendix, https://wwwnc.cdc.gov/EID/article/32/2/25-1060-App1.pdf). We investigated mutations associated with tetracycline-resistant *Cutibacterium acnes*, *Escherichia coli*, and *Helicobacter pylori* (*6*–*8*) and translated those resistance-associated positions to the 16S rRNA coordinate system of TPA to support future research and public health genomic surveillance. We also investigated macrolide resistance by analyzing known mutations in the 23S rRNA gene (*13*). This project received ethics review clearance from Health Canada and Public Health Agency of Canada's Research Ethics Borad (file no. REB 2023-012P).

The Study

We conducted genome enrichment of the study genomes by using Agilent SureSelect protocol (https://www.agilent.com) before sequencing. Lineage classification using both the 3-gene multilocus sequence typing (MLST) scheme (*14*) and the core genome lineages generated with PopPUNK (*15*) confirmed that the strains were part of the TPA subspecies. Most (15/17) of the TPA genomes belonged to the SS14 lineage; the remaining genomes belonged to the Nichols lineage (Table 1; Appendix Figures 1–4). Core genome–based classification outperformed the MLST because it successfully identified the lineages of all 17 samples, whereas MLST failed for 2 samples.

Most genomes from Canada were sampled in Saskatchewan in 2024 during a provincewide syphilis outbreak in the Prairies (Table 1). Those samples were geographically dispersed, likely suggesting multiple independent transmission events; however, detailed sexual contact tracing information is not available. We used the additional 784 TPA genomes from public databases (505 genomes from GenBank, 279 de novo assembled from data in previous studies [Appendix]) to determine the breadth of the mutational landscape of the 16S rRNA gene.

We retrieved reference sequences of 16S rRNA genes from *C. acnes* (NR_040847.1:1–1486), *E. coli* (U00096.1:4166659–8200), *H. pylori* (CP003904.1:1512657–1157), and TPA (Nichols lineage: NC_010741.1:231287–2831 and SS14 lineage: NC_021508.1:231297–2845) from NCBI and aligned them using MAFFT to translate known tetracycline resistance–associated mutation sites (*6*–*8*,*11*) (Table 2) to the TPA coordinate system. Specifically, the mutation at position 1032 in *C. acnes* corresponds to position

Table 2. 16S rRNA mutations related to tetracycline resistance in genomic analysis of doxycycline resistance-associated 16S rRNA mutations in *Treponema pallidum* subsp. *pallidum**

Species	Resistance mutations using *E. coli* (U00096.1) coordinates	Species-specific coordinates	Reference
Escherichia coli	A964G, G1053A, C1054T, A1055G	A966G, G1056A, C1057T, A1058G	(*8*)
Cutibacterium acnes	G1058C	G1032C	(*7*)
Helicobacter pylori	A965G, A965G & A967C, A965G & G966T, A967C	A930G, A930G & A932C, A930G & G931T, A932C	(*6*)

*Ampersands in the resistance mutations column indicate multi-allele resistance variants.

Table 3. Conversion of key tetracycline-related mutations to 16S coordinates in *Treponema pallidum* subsp. *pallidum* in genomic analysis of doxycycline resistance–associated 16S rRNA mutations in *T. pallidum* subsp. *pallidum**

TPA	Position	964	965	966	967	968	969	970	971	1054	1055	1056	1057	1058	1059	1060	1061	1062
	Nichols	C	G	A	T	G	A	T	A	C	T	G	C	A	T	G	G	C
	SS14	C	G	A	T	G	A	T	A	C	T	G	C	A	T	G	G	C
C. acnes	Position	935	936	937	938	939	940	941	942	1025	1026	1027	1028	1029	1030	1031	1032	1033
	WT	C	G	A	T	G	C	A	A	G	T	G	C	A	T	G	G*	C
	Hypothetical AMR strain	C	G	A	T	G	C	A	A	G	T	G	C	A	T	G	c	C
E. coli	Position	962	963	964	965	966	967	968	969	1051	1052	1053	1054	1055	1056	1057	1058	1059
	WT	C	G	A*	T	G	C	A	A	C	T	G*	C*	A*	T	G	G	C
	Hypothetical AMR strain	C	G	g	T	G	C	A	A	C	T	a	t	g	T	G	G	C
H. pylori	Position	927	928	929	930	931	932	933	934	1021	1022	1023	1024	1025	1026	1027	1028	1029
	WT	C	G	A	A*	G*	A*	T	A	C	T	G	C	A	C	G	G	C
	Hypothetical AMR strain	C	G	A	g	t	c	T	A	C	T	G	C	A	C	G	G	C

*Alignment of 16S genes from *E. coli* (U00096.1, 4166659–4168200), *C. acnes* (NR_040847.1, 1–1486), *H. pylori* (CP003904.1, 1512657–1511157), and TPA (Nichols lineage: NC_010741.1:231287–232831 and SS14 lineage: NC_021508.1:231297–232845). Columns in gray indicate sites related to tetracycline resistance whereas cells with an asterisk reveal the reference bacteria and nucleotide. Lowercase letters indicate a mutation in comparison to the WT sequence. The final coordinates reported in this dispatch are for the TPA 16S rRNA gene. Flanking sites are shown to give additional context. AMR, antimicrobial resistant; TPA, *Treponema pallidum* subsp. *pallidum*; WT, wild type.

1061 in TPA; the *E. coli* mutation at position 964 aligns to position 966 and the *E. coli* mutation at position 1053–1055 aligns to positions 1056–1058 in TPA. Similarly, the *H. pylori* resistance–associated triplet at positions 965–967 (*6*,*11*) maps to 967–969 in TPA (Table 3). The coordinates of the reported mutational triplet in *T. pallidum* at positions 965–967 appear to be relative to *E. coli* (*11*), because the mutational triplet was identified at positions 967–969 in our reference strains. We manually inspected known tetracycline resistance–associated positions (Table 2) for mutations (Appendix).

Alignment of the 16S rRNA genes also revealed that the single-nucleotide polymorphisms (SNPs) associated with doxycycline resistance in *C. acnes* and *E. coli* share the same wild-type background as TPA (Table 2). Because a single mutation at those sites can potentially cause doxycycline resistance (*7*,*8*), similar mutations could possibly exert comparable effects in TPA. In contrast, resistance-associated mutations in *H. pylori* arise from a unique wild-type background relative to *C. acnes*, *E. coli*, and TPA. If the composition of the nucleotide triplet is key to conferring doxycycline resistance, then 3 of the 4 known resistance alleles will require 2 nucleotide substitutions in TPA. The only *H. pylori* resistance allele that requires a single mutation in TPA is gGA (T967G) (*6*).

Of the 784 global TPA genomes, 9 contained a heterozygous G/T allele at position 968 (*4*). That mutation is not sufficient to cause resistance; however, it does bring the strains within a single SNP of the gtA allele in *H. pylori* (*6*). Those 9 TPA genomes were collected during 2013–2019 from the United Kingdom (n = 6), Australia (n = 1), and Hungary (n = 1) and were mostly part of the SS14 lineage (7/9) (Table 4). In contrast, the 17 Canada TPA genomes contained no mutations in the 16S rRNA gene compared with the reference strains.

We called the 16S rRNA variants using a diploid model for TPA to account for the presence of 2 gene copies. To confirm that those findings were not methodological artifacts, we analyzed the 23S rRNA gene and found it to be duplicated. Specifically, we investigated the A2058G and A2059G SNPs in *E. coli* (*13*) that correspond to positions 2106 and 2107 in TPA.

Table 4. Geographic and genomic details of *Treponema pallidum* subsp. *pallidum* strains with a mutation at doxycycline-associated 16S rRNA site 968 used in genomic analysis of doxycycline resistance–associated 16S rRNA mutations in *T. pallidum* subsp. *pallidum**

NCBI Sequence Read Archive accession no.	Lineage	Collection date	Country	16S rRNA: 968
ERR7123576	Nichols	Unknown	Unknown	G/T
ERR3684613	SS14	2013	United Kingdom	G/T
ERR3684456	SS14	2016	United Kingdom	G/T
ERR4045387	SS14	2016	United Kingdom	G/T
ERR3684510	SS14	2016	United Kingdom	G/T
ERR3684626	SS14	2016	United Kingdom	G/T
ERR3684512	SS14	2017	United Kingdom	G/T
ERR5210563	Nichols	2018	Hungary	G/T
ERR5210581	SS14	2019	Australia	G/T

*G/T indicates a heterozygous allele. NCBI, National Center for Biotechnology Information.

We detected macrolide resistance in 94% (16/17) (Table 1) of the Canada genomes through a A2106G mutation and in ≈66% (514/784) of the publicly available TPA genomes, supporting the robustness of those AMR findings.

Conclusions

The increasing use of doxycycline as a prophylactic for syphilis presents a growing risk for the emergence of AMR. Given the genetic stability of *T. pallidum* (*10*), genomic surveillance programs should prioritize monitoring positions 966–969, 1056–1058, and 1061 (TPA numbering) of the 16S rRNA genes, because those sites could serve as early indicators of emerging doxycycline resistance (*6*–*9*,*11*). Their relationship to doxycycline resistance in TPA remains theoretical and based on comparative genomics (*5*–*7*); in vitro phenotypic validation will be essential to determine their functional significance (*11*). Future analyses must account for the presence of 2 copies of the 16S rRNA gene in TPA, because heterozygous alleles could attenuate the phenotypic expression of doxycycline resistance. Nevertheless, our work establishes a global baseline for 16S rRNA diversity in TPA, simplifying future doxycycline resistance surveillance.

Acknowledgements

We acknowledge the NML-Branch DNA Core facility for providing DNA sequencing services for this project.

G.S.L., T.B., N.S., M.M., S.N.P., R.T.S.W., and V.R.D. received funding from the Genomics Research and Development Initiative (GRDI-8, 2023–2025) in support of syphilis research. G.S.L. and V.R.D. also gratefully acknowledge postdoctoral funding support from the McLaughlin Centre, University of Toronto.

About the Author

Dr. Long is a McLaughlin Centre Postdoctoral Scholar at Public Health Ontario, Canada. His research focuses on infectious diseases, with interests at the intersection of genomic surveillance, bioinformatics, pangenomes, and phylodynamic modeling.

References

1. Public Health Agency of Canada. Infectious syphilis and congenital syphilis in Canada, 2023 [cited 2025 Jun 23]. https://www.canada.ca/en/public-health/services/reports-publications/canada-communicable-disease-report-ccdr/monthly-issue/2025-51/issue-2-3-february-march-2025/infectious-congenital-syphilis-2023.html
2. Cato K, Chuang E, Connolly KL, Deal C, Hiltke T. Summary of the National Institute of Allergy and Infectious Diseases workshop on alternative therapies to penicillin for the treatment of syphilis. Sex Transm Dis. 2025;52:201–10. https://doi.org/10.1097/OLQ.0000000000002113
3. Hazra A, McNulty MC, Pyra M, Pagkas-Bather J, Gutierrez JI, Pickett J, et al. Filling in the gaps: updates on doxycycline prophylaxis for bacterial sexually transmitted infections. Clin Infect Dis. 2024:ciae062. https://doi.org/10.1093/cid/ciae062
4. Dai T, Qu R, Liu J, Zhou P, Wang Q. Efficacy of doxycycline in the treatment of syphilis. Antimicrob Agents Chemother. 2016;61:e01092-16. https://doi.org/10.1128/AAC.01092-16
5. Grossman TH. Tetracycline antibiotics and resistance. Cold Spring Harb Perspect Med. 2016;6:a025387. https://doi.org/10.1101/cshperspect.a025387
6. Dailidiene D, Bertoli MT, Miciuleviciene J, Mukhopadhyay AK, Dailide G, Pascasio MA, et al. Emergence of tetracycline resistance in *Helicobacter pylori*: multiple mutational changes in 16S ribosomal DNA and other genetic loci. Antimicrob Agents Chemother. 2002;46:3940–6. https://doi.org/10.1128/AAC.46.12.3940-3946.2002
7. Ross JI, Eady EA, Cove JH, Cunliffe WJ. 16S rRNA mutation associated with tetracycline resistance in a gram-positive bacterium. Antimicrob Agents Chemother. 1998;42:1702–5. https://doi.org/10.1128/AAC.42.7.1702
8. Yassin A, Fredrick K, Mankin AS. Deleterious mutations in small subunit ribosomal RNA identify functional sites and potential targets for antibiotics. Proc Natl Acad Sci U S A. 2005;102:16620–5. https://doi.org/10.1073/pnas.0508444102
9. Stamm LV. Global challenge of antibiotic-resistant *Treponema pallidum*. Antimicrob Agents Chemother. 2010;54:583–9. https://doi.org/10.1128/AAC.01095-09
10. Lieberman NAP, Lin MJ, Xie H, Shrestha L, Nguyen T, Huang ML, et al. *Treponema pallidum* genome sequencing from six continents reveals variability in vaccine candidate genes and dominance of Nichols clade strains in Madagascar. PLoS Negl Trop Dis. 2021;15:e0010063.
11. Tantalo LC, Luetkemeyer AF, Lieberman NAP, Nunley BE, Avendaño C, Greninger AL, et al. In vitro exposure of *Treponema pallidum* to subbactericidal doxycycline did not induce resistance: implications for doxycycline postexposure prophylaxis. J Infect Dis. 2025;231:729–33. https://doi.org/10.1093/infdis/jiae381
12. Manoharan-Basil SS, Gestels Z, Abdellati S, de Block T, Vanbaelen T, De Baetselier I, et al. Putative mutations associated with tetracycline resistance detected in *Treponema* spp.: an analysis of 4,355 Spirochaetales genomes. Access Microbiol. 2025;7:000963.v4.
13. Stamm LV, Bergen HL. A point mutation associated with bacterial macrolide resistance is present in both 23S rRNA genes of an erythromycin-resistant *Treponema pallidum* clinical isolate. Antimicrob Agents Chemother. 2000;44:806–7. https://doi.org/10.1128/AAC.44.3.806-807.2000
14. Grillová L, Bawa T, Mikalová L, Gayet-Ageron A, Nieselt K, Strouhal M, et al. Molecular characterization of *Treponema pallidum* subsp. *pallidum* in Switzerland and France with a new multilocus sequence typing scheme. PLOS ONE. 2018;13:e0200773.
15. Long G, Singh N, Patel S, Braukmann T, Tsang RSW, Duvvuri VR. Integrated genomic approaches improve *Treponema pallidum* phylogenetics and lineage classification. Can J Microbiol. 2025;71:1–11. https://doi.org/10.1139/cjm-2025-0021

Address for correspondence: Venkata R. Duvvuri, Public Health Ontario, 661 University Ave, Ste 1701, Toronto, ON M5G 1M1, Canada; email: venkata.duvvuri@oahpp.ca

Effectiveness of RSV Vaccines against RSV-Associated Thromboembolic Events

Ryan E. Wiegand, Heng-Ming Sung, Yue Zhang, Andrea Chavez, Amber Kautz, Josephine Mak, Morgan Najdowski, Yangping Chen, Yenlin Lai, Yixin Jiao, Yoganand Chillarige, Ruth Link-Gelles, Amanda B. Payne

We evaluated effectiveness of respiratory syncytial virus (RSV) vaccines against RSV-associated thromboembolic events among community-dwelling Medicare fee-for-service beneficiaries ≥65 years of age in the United States enrolled during October 1, 2023–March 30, 2024. RSV vaccines protected against RSV-associated thromboembolic events (effectiveness 79% [95% CI 74%–83%]) in the same season as vaccine receipt.

Respiratory virus infections, including respiratory syncytial virus (RSV) infections, have been associated with increased risk for myocardial infarction (*1*), ischemic stroke (*2*), and venous thromboembolism (*3*). In 1 US-based surveillance network, ≈22% of adults ≥50 years of age who were hospitalized with RSV experienced an acute cardiac event (*4*).

In June 2023, the Advisory Committee on Immunization Practices recommended a single dose of RSV vaccine for adults ≥60 years of age to be determined on the basis of shared clinical decision making (*5*). RSV vaccines have reduced the likelihood of RSV-associated hospitalizations in immunocompetent and immunocompromised adults ≥60 years of age and have reduced RSV-associated emergency department visits in immunocompetent adults ≥60 years of age by 70%–80% (*6*). Our goal was to evaluate the effectiveness of a single dose of RSV vaccine against RSV-associated thromboembolic events in community-dwelling Medicare beneficiaries ≥65 years of age during the same season as RSV vaccine receipt. Understanding the effectiveness of RSV vaccines against RSV-associated thromboembolic events could guide policy makers, clinicians, and patients on how to reduce the risk for serious cardiovascular outcomes caused by RSV.

Author affiliations: Centers for Disease Control and Prevention, Atlanta, Georgia, USA (R.E. Wiegand, A. Kautz, J. Mak, M. Najdowski, R. Link-Gelles, A.B. Payne); Acumen LLC, Burlingame, California, USA (H.-M. Sung, Y. Zhang, A. Chavez, Y. Chen, Y. Lai, Y. Jiao, Y. Chillarige); General Dynamics Information Technology, Atlanta (A. Kautz); Eagle Health Analytics, San Antonio, Texas, USA (M. Najdowski); US Public Health Service Commissioned Corps, Rockville, Maryland, USA (R. Link-Gelles)

DOI: https://doi.org/10.3201/eid3202.251520

The Study

Medicare fee-for-service beneficiaries ≥65 years of age on September 10, 2023 (index date), were eligible for inclusion in a retrospective cohort provided they met all inclusion and exclusion criteria (Appendix, https://wwwnc.cdc.gov/EID/article/32/2/25-1520-App1.pdf). Follow-up time began on October 1, 2023, and ended on the date when a beneficiary experienced an RSV-associated thromboembolic event, another censoring event (Appendix), or the end of study (March 30, 2024), whichever came first.

An RSV-associated thromboembolic event consisted of a myocardial infarction, ischemic stroke, or venous thromboembolism (Appendix Table 2) 7 days before to 30 days after an RSV diagnosis (Appendix Table 1). We identified RSV vaccine doses through Medicare Part D claims by using National Drug Code Directory codes (Appendix Table 3). A beneficiary was unvaccinated for RSV until they received an RSV vaccine dose and was vaccinated for RSV starting at 14 days after the RSV vaccine administration date. We excluded the period from vaccine receipt through day 13 after receipt.

Multivariable Cox proportional hazards models in R version 4.4.0 (The R Project for Statistical Computing, https://www.r-project.org) estimated vaccine effectiveness (VE) against RSV-associated thromboembolic events. RSV vaccination was a time-dependent covariate. The model adjusted results for age, sex, race/

ethnicity, social vulnerability index (*7*) deciles, rural or urban location, immunocompromise status (Appendix Table 4), nonimmunocompromising underlying medical conditions (Appendix Table 5), previous season influenza vaccination (Appendix Table 6), and current season COVID-19 vaccination (Appendix Table 7). We stratified results by immunocompromise status (immunocompetent or immunocompromised), age group (65–74 and ≥75 years of age), time since vaccination (14–59, 60–119, or ≥120 days), and RSV vaccine product (Arexvy, GSK, https://www.gsk.com; and Abrysvo, Pfizer, https://www.pfizer.com).

Sensitivity analyses consisted of an extended follow-up period for thromboembolic events through October 6, 2024; a follow-up limited to periods of high RSV circulation (defined as the period between 2 consecutive weeks >3% and 2 consecutive weeks <3% RSV prevalence) based on data from the National Respiratory and Enteric Virus Surveillance System (*8*); all-cause thromboembolic events, regardless of prior RSV diagnosis; and, to reduce residual confounding, models that incorporated inverse probability of treatment weights (IPTW). This activity was reviewed by the Centers for Disease Control and Prevention and deemed not to be research; it was conducted consistent with applicable federal law and agency policy per 45 CFR §46. This study presented minimal risk to participants because no patient interaction or intervention occurred; therefore, a waiver of informed consent was granted. This study followed the Strengthening the Reporting of Observational Studies in Epidemiology reporting guidelines (https://www.strobe-statement.org).

The analytic population consisted of 15,558,386 beneficiaries (Appendix Table 8); 58% (n = 8,998,133) were women, 80% (n = 12,376,268) were in an urban location, and 13% had immunocompromising conditions (Appendix Table 9). RSV VE against RSV-associated thromboembolic events was 79% (95% CI 74%–83%) for all beneficiaries (Table). VE estimates did not differ substantially between immunocompromised beneficiaries (VE 69% [95% CI 56%–78%]) and immunocompetent beneficiaries (VE 82% [95% CI 77%–86%]). Estimated VE among beneficiaries 65–74 years of age was 75% (95% CI 63%–83%), and estimated VE among beneficiaries ≥75 years of age was 80% (95% CI 74%–84%). VE point estimates by time since vaccination were all within 4 percentage points (14–59 days, VE 80% [95% CI 72%–86%]; 60–119 days, VE 79% [95% CI 72%–84%]; ≥120 days, VE 75% [95%

Table. Adjusted VE of RSV vaccine against RSV-associated TEs among community-dwelling Medicare beneficiaries ≥65 years of age, United States, October 1, 2023–March 30, 2024*

Stratification or vaccination status	No. beneficiaries	No. RSV-associated TEs	Total no. TEs per 10,000 person-years	Median follow-up days contributed to category	Outcome rates per 10,000 person-years	Adjusted VE, % (95% CI)
Overall						
Unvaccinated	12,353,511	2,405	627	181	3.84	Referent
Vaccinated	3,204,875	96	109	132	0.88	79 (74–83)
Immunocompromised						
Unvaccinated	1,587,615	523	81	181	6.46	Referent
Vaccinated	509,928	36	17	131	2.07	69 (56–78)
Immunocompetent						
Unvaccinated	10,765,895	1,882	546	181	3.45	Referent
Vaccinated	2,694,947	60	92	132	0.65	82 (77–86)
Age 65–74 y						
Unvaccinated	6,711,712	630	341	181	1.85	Referent
Vaccinated	1,605,200	27	55	132	0.49	75 (63–83)
Age ≥75 y						
Unvaccinated	5,641,799	1,775	286	181	6.20	Referent
Vaccinated	1,599,675	69	54	131	1.27	80 (74–84)
Time since vaccination, d						
14–59	208,379	33	38	46	0.87	80 (72–86)
60–119	840,280	44	44	60	1.01	79 (72–84)
≥120†	2,156,216	19	28	46	0.68	75 (60–84)
Vaccine product						
Arexvy‡	2,193,463	74	74	130	1.00	76 (70–81)
Abrysvo§	1,011,412	22	35	137	0.63	85 (77–90)

*Adjusted VE estimates from multivariable Cox proportional hazards models after controlling for age group, sex, race/ethnicity, social vulnerability index deciles, rural or urban category (determined by location of a beneficiary's facility in a US Census Core Based Statistical Area or not), a count of the number of underlying medical conditions, immunocompromise status, influenza vaccination in the previous season, and COVID-19 vaccination during the current season. VE calculated by using the formula VE = (1 – hazard ratio) × 100 (Appendix, https://wwwnc.cdc.gov/EID/article/32/2/25-1520-App1.pdf). RSV, respiratory syncytial virus; TEs, thromboembolic events; VE, vaccine effectiveness.
†Maximum number of days a beneficiary in interim analysis is contributing is 127 days.
‡GlaxoSmithKline, https://www.gsk.com.
§Pfizer, https://www.pfizer.com.

CI 60%–84%]). Product-specific VE estimates did not differ substantially (Arexvy, VE 76% [95% CI 70%–81%]; Abrysvo, VE 85% [95% CI 77%–90%]).

Extending the follow-up period for thromboembolic events yielded VE estimates of 78% (95% CI 74%–82%), and limiting analyses to periods of high RSV circulation yielded VE estimates of 79% (95% CI 73%–83%) (Appendix Tables 10, 11). Estimates of RSV VE against all-cause thromboembolic events, regardless of prior RSV diagnosis, were lower (VE 21% [95% CI 19%–22%]) than for primary analyses (Appendix Table 12). VE against RSV-associated thromboembolic events based on models with IPTW was 71% (95% CI 62%–77%) (Appendix Table 13), which was not substantially different from the estimate obtained in models without IPTW (Table).

Conclusions

Among a retrospective cohort of >15 million community-dwelling Medicare beneficiaries ≥65 years of age, RSV vaccines provided protection against RSV-associated thromboembolic events in the same season as RSV vaccination. Across all immunocompetent subgroups, VE estimates ranged from 75% to 85%; VE was 69% among immunocompromised beneficiaries. As expected, RSV vaccines provided higher protection against RSV-associated thromboembolic events compared with all-cause thromboembolic events.

This study demonstrates the effectiveness of RSV vaccines against RSV-associated thromboembolic events, including myocardial infarction, ischemic stroke, and venous thromboembolism. Our findings are consistent with studies demonstrating that influenza and COVID-19 vaccines reduce the likelihood of thromboembolic events in adults (*9*,*10*). Estimates from these analyses are comparable to other surveillance platforms that have estimated RSV VE against RSV-associated hospitalization (*6*,*11*). Time since vaccination results suggest minimal to no waning over the first 4 months postvaccination. Other analyses of RSV-associated hospitalization demonstrated more noticeable waning over a shorter period (*6*).

One limitation of these estimates are that Medicare beneficiaries with parts A, B, and D coverage might not be representative of the US population of adults ≥65 years of age. In addition, misclassification of RSV vaccination and RSV-associated outcomes are possible because both rely on administrative claims data. Vaccinations and outcome events not recorded in the claims data were not captured. The extent to which potential misclassification and under capture might have affected VE estimates is not clear. Although models adjusted for multiple covariates, residual confounding attributable to differences between the vaccinated and unvaccinated groups might still exist, especially in unmeasured confounders (e.g., smoking history). Our results indicate that VE against all-cause thromboembolic events was lower than VE against RSV-associated thromboembolic events but not 0%, which might suggest misclassification of the outcome or residual confounding. We did not have sufficient power to evaluate VE against the components of our definition of thromboembolic events.

In summary, we found that RSV vaccinations provided protection against RSV-associated thromboembolic events in adults ≥65 years of age in the same season as vaccine receipt. Protection was high regardless of immunocompromise status, age group, or RSV vaccine product. As of June 2025, RSV vaccine recommendations for adults in the United States have expanded to a single dose of RSV vaccine for adults 50–64 years of age with certain high-risk conditions and all adults ≥75 years of age (*12*,*13*).

The data that support the findings of this investigation are available from Centers for Medicare and Medicaid Services. Restrictions apply to the availability of these data.

This investigation was funded through an intra-agency agreement that authorized an exchange of data and reports and funding between the Centers for Disease Control and Prevention and the Centers for Medicare & Medicaid Services (CMS) to create data files and reports. The Centers for Disease Control and Prevention contributed funding to a task order contract managed by CMS. Acumen LLC is a contractor for CMS.

Author contributions: R.E.W. prepared the manuscript. All authors contributed to the study design, discussed the results, read the manuscript and appendix, and provided critical feedback.

About the Author

Dr. Wiegand is a mathematical statistician in the Coronavirus and Other Respiratory Viruses Division, National Center for Immunization and Respiratory Diseases, Centers for Disease Control and Prevention. His primary research interests include vaccine effectiveness against respiratory viruses and evaluating the bias in statistical methods.

References

1. Meier CR, Jick SS, Derby LE, Vasilakis C, Jick H, Meier CR, et al. Acute respiratory-tract infections and risk of first-time acute myocardial infarction. Lancet. 1998;351:1467–71. https://doi.org/10.1016/S0140-6736(97)11084-4
2. Clarke M, Falcione S, Boghozian R, Todoran R, Zhang Y, C Real MG, et al. Viral infection and ischemic stroke:

emerging trends and mechanistic insights. J Am Heart Assoc. 2024;13:e035892. https://doi.org/10.1161/JAHA.124.035892
3. Smilowitz NR, Subashchandran V, Newman J, Barfield ME, Maldonado TS, Brosnahan SB, et al. Risk of thrombotic events after respiratory infection requiring hospitalization. Sci Rep. 2021;11:4053. https://doi.org/10.1038/s41598-021-83466-9
4. Woodruff RC, Melgar M, Pham H, Sperling LS, Loustalot F, Kirley PD, et al.; Respiratory Syncytial Virus Hospitalization Surveillance Network (RSV-NET). Acute cardiac events in hospitalized older adults with respiratory syncytial virus infection. JAMA Intern Med. 2024;184:602–11. https://doi.org/10.1001/jamainternmed.2024.0212
5. Melgar M, Britton A, Roper LE, Talbot HK, Long SS, Kotton CN, et al. Use of respiratory syncytial virus vaccines in older adults: recommendations of the Advisory Committee on Immunization Practices—United States, 2023. MMWR Morb Mortal Wkly Rep. 2023;72:793–801. https://doi.org/10.15585/mmwr.mm7229a4
6. Payne AB, Watts JA, Mitchell PK, Dascomb K, Irving SA, Klein NP, et al. Respiratory syncytial virus (RSV) vaccine effectiveness against RSV-associated hospitalisations and emergency department encounters among adults aged 60 years and older in the USA, October, 2023, to March, 2024: a test-negative design analysis. Lancet. 2024;404:1547–59. https://doi.org/10.1016/S0140-6736(24)01738-0
7. Flanagan BE, Gregory EW, Hallisey EJ, Heitgerd JL, Lewis B. A social vulnerability index for disaster management. J Homel Secur Emerg Manag. 2011;8:3. https://doi.org/10.2202/1547-7355.1792
8. Hamid S, Winn A, Parikh R, Jones JM, McMorrow M, Prill MM, et al. Seasonality of respiratory syncytial virus—United States, 2017–2023. MMWR Morb Mortal Wkly Rep. 2023;72:355–61. https://doi.org/10.15585/mmwr.mm7214a1
9. Holodinsky JK, Zerna C, Malo S, Svenson LW, Hill MD. Association between influenza vaccination and risk of stroke in Alberta, Canada: a population-based study. Lancet Public Health. 2022;7:e914–22. https://doi.org/10.1016/S2468-2667(22)00222-5
10. Payne AB, Novosad S, Wiegand RE, Najdowski M, Gomes DJ, Wallace M, et al. Effectiveness of bivalent mRNA COVID-19 vaccines in preventing COVID-19-related thromboembolic events among Medicare enrollees aged ≥65 years and those with end stage renal disease—United States, September 2022–March 2023. MMWR Morb Mortal Wkly Rep. 2024;73:16–23. https://doi.org/10.15585/mmwr.mm7301a4
11. Fry SE, Terebuh P, Kaelber DC, Xu R, Davis PB. Effectiveness and safety of respiratory syncytial virus vaccine for US adults aged 60 years or older. JAMA Network Open 2025; 8:e258322-e. https://doi.org/10.1001/jamanetworkopen.2025.8322
12. Britton A, Roper LE, Kotton CN, Hutton DW, Fleming-Dutra KE, Godfrey M, et al. Use of respiratory syncytial virus vaccines in adults aged ≥60 years: updated recommendations of the Advisory Committee on Immunization Practices—United States, 2024. MMWR Morb Mortal Wkly Rep. 2024;73:696–702. https://doi.org/10.15585/mmwr.mm7332e1
13. Centers for Disease Control and Prevention. Advisory Committee on Immunization Practices meeting, April 15, 2025 [cited 2025 Jun 26]. https://www.youtube.com/live/dNCVr9AvFB8

Address for correspondence: Ryan E. Wiegand, Centers for Disease Control and Prevention, 1600 Clifton Road NE, Mailstop H24-5, Atlanta, GA 30329, USA; email: rwiegand@cdc.gov

Multiplex PCR to Differentiate Monkeypox Virus Clades

Christopher T. Williams, Alessandra Romero-Ramirez, Adeleye Adesola Semiu, Samuel Oluwafunmbi Ifabumuyi, Caitlin Greenland-Bews, Susan Gould, Dominic Wooding, Collette Allen, Anushri Somasundaran, Nicodemus Nnabuike Mkpuma, Dorcas Gado, Jolly Amoche Adole, Abdulakeem Eniola Amoo, Abisola Ajoke Adeyemi, Laure Bosquillon de Jarcy, Christine Goffinet, Jake Dunning, Malcolm G. Semple, The International Severe Acute Respiratory and Emerging Infection Consortium Investigators,[1] Esto Bahizire, Afolabi Akinpelu, Thomas E. Fletcher, Ana I. Cubas-Atienzar, Cristina Leggio, Adeyinka Adedeji, Adesuyi A. Omoare,[2] Thomas Edwards[2]

We designed a multiplex quantitative PCR to differentiate monkeypox virus clades. For clinical samples collected in the United Kingdom and Nigeria, sensitivity was 78% (95% CI 67.67%–86.14%) and specificity 94% (95% CI 80.84%–99.30%); for samples with cycle thresholds <35, sensitivity was 98% (95% CI 91.72%–99.96%) and specificity 94% (95% CI 80.84%–99.30%).

Mpox is a zoonotic viral disease caused by monkeypox virus (MPXV). There are 2 MPXV clades; clade I is historically associated with a higher disease severity and case-fatality ratio compared with clade II (*1*). Clade II is subdivided into IIa and IIb. Lineage B.1 emerged from IIb as the dominant MPXV lineage in 2022 (*2*), with marked human-to-human transmission linked to sexual activity (*3*,*4*) but lower mortality rates (*5*). Clade I is subdivided into Ia and Ib; Ib emerged in the Democratic Republic of the Congo in 2023 (*6*). Similar to lineage B.1, the clade Ib outbreak resulted in decreased mortality with sustained human-to-human transmission (*6*,*7*). An ≈1 kb deletion occurs in the OPG032 gene in clade Ib (*6*). This segment is the target of the US Centers for Disease Control and Prevention (CDC) clade I PCR (*8*).

Diagnosis of mpox relies on PCR testing performed on lesion swab specimens (*9*). Because the clinical manifestations of mpox are similar between clades, clade identification typically requires sequencing, which is time-consuming, expensive, and difficult to implement in low- and middle-income countries. We designed a multiplex quantitative PCR to differentiate monkeypox virus clades.

The Study

We used DNA extracted from cultured lineage B.1 MPXV (European Virus Archive Global, https://www.european-virus-archive.com; strain no. Slovenia_MPXV-1_2022, clade hMPXV-1, lineage B.1), and 47 clinical samples from the International Severe Acute Respiratory and Emerging Infection Consortium clinical characterization protocol study (ethics approval no. REC 13/SC/0149). We propagated viral isolates in Vero E6 cells and extracted DNA by using the QIAamp 96 Virus QIAcube-HT Kit (QIAGEN, https://www.qiagen.com) on a QIAcube-HT (QIAGEN), following manufacturer instructions. Samples collected in 2018

Author affiliations: Liverpool School of Tropical Medicine, Liverpool, UK (C.T. Williams, A. Romero-Ramirez, C. Greenland-Bews, S. Gould, D. Wooding, A. Somasundaran, L. Bosquillon de Jarcy, C. Goffinet, T.E. Fletcher, A. Cubas-Atienzar, T. Edwards); Nigeria Centre for Disease Control and Prevention, Abuja, Nigeria (A.A. Semiu, S.O. Ifabumuyi, A. Akinpelu, A.A. Omoare); UK Health Security Agency, Porton Down–Salisbury, UK (C. Allen, C. Leggio); National Veterinary Research Institute, Vom, Nigeria (N.N. Mkpuma, D. Gado, J.A. Adole, A. Adedeji, T. Edwards); Nigeria Centre for Disease Control and Prevention Central Public Health Laboratory, Yaba, Nigeria (A.E. Amoo, A.A. Adeyemi); Charité–Universitätsmedizin Berlin, Berlin, Germany (L. Bosquillon de Jarcy); Berlin Institute of Health, Berlin (L. Bosquillon de Jarcy); University of Oxford, Oxford, UK (J. Dunning); Infectious Diseases Department, Royal Free London NHS Foundation Trust, London, UK (J. Dunning); University of Liverpool, Liverpool (M.G. Semple); Catholic University of Bukavu, Bugabo Campus, Kinshasa, Democratic Republic of the Congo (E. Bahizire)

DOI: https://doi.org/10.3201/eid3202.250686

[1]Members of the International Severe Acute Respiratory and Emerging Infection Consortium are listed at the end of this article.

[2]These authors contributed equally to this article.

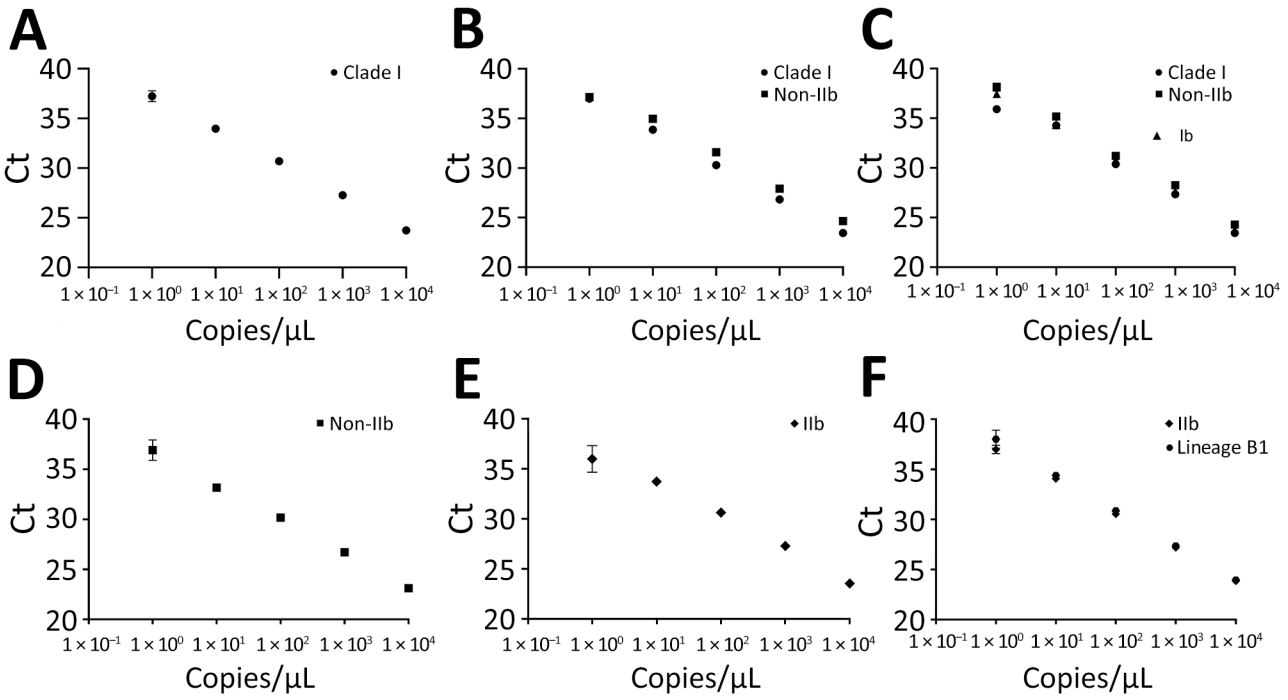

Figure. Standard curves of each monkeypox virus PCR target for multiplex PCR to differentiate monkeypox virus clades. A) Synthetic DNA containing clade I amplicon (R^2 0.997, efficiency 98.1%). B) DNA extracted from stock of clade Ia virus (clade I curve: R^2 0.998, efficiency 96.4%; non-IIb curve: R^2 0.992, efficiency 103.394%). C) DNA extracted from stock of clade Ib virus (clade I curve: R^2 0.986, efficiency 98.858%; non-IIb curve: R^2 0.996, efficiency 93.9%; Ib curve: R^2 0.996, efficiency 95.067%). D) Synthetic DNA containing non-IIb amplicon (R^2 0.994, efficiency 97%). E) Synthetic DNA containing IIb amplicon (R^2 0.98, efficiency 109.2%). F) DNA extracted from stock of lineage B.1 virus (IIb curve: R^2 0.999, efficiency 101.4%; lineage B.1 curve: R^2 0.996, efficiency 96.6%). Ct, cycle threshold, R^2, coefficient of determination.

(n = 11) were from persons with suspected West Africa travel–associated mpox, and samples from 2022 (n = 36) were from suspected United Kingdom mpox cases. According to the reference CDC mpox PCR (*10*), 32 samples were MPXV-positive. We made minor adjustments to the CDC PCR by reducing the reaction volume and not performing the RNase P assay. All confirmed UK cases from 2018 were clade IIb from West Africa, whereas the UK Health Security Agency sequencing data revealed that 99% of 2022 mpox cases were lineage B.1 (*11*).

We also tested 54 MPXV-positive lesion samples from routine mpox diagnostic surveillance at the National Reference Laboratory (Abuja, Nigeria) of the Nigerian Centre for Disease Control and Prevention (NCDC; approval granted by the Research Governance Unit). Samples were collected in 2017 (n = 7), 2018 (n = 11), 2019 (n = 10), 2021 (n = 10), 2023 (n = 12), and 2024 (n = 4). We used 20 varicella zoster virus PCR-positive samples (PCR-negative for mpox) as negatives. We extracted DNA by using QIAmp DNA mini kits (QIAGEN), following manufacturer instructions. We retrospectively analyzed serial dilutions of DNA from stocks of clade Ia (hMpxV/DRC-INRB/22MPX0422C/2023, 2023-WHO-LS-008) and Ib (hMpxV/DRC-INRB/24MPX0203V/2024, 2024-WHO-LS-003) MPXV to determine limits of detection.

We identified clade-specific mutations by using Nextstrain (genome NC_063383.1; https://nextstrain.org/mpox/all-clades). We downloaded

Table 1. Assay interpretation of multiplex PCR to differentiate monkeypox virus clades from the United Kingdom and Nigeria*

Result	Probe				
	Clade I (T46417C, G46421A, A46427C, C46435T)	Clade Ib (Δ19,128–20,270)	Non-IIb (G183695, C183696)	Clade IIb (G183695A, C183696T)	Lineage B.1 (C84587T)
Clade Ia	Positive	Negative	Positive	Negative	Negative
Clade Ib	Positive	Positive	Positive	Negative	Negative
Clade IIa	Negative	Negative	Positive	Negative	Negative
Clade IIb	Negative	Negative	Negative	Positive	Negative
Lineage B.1	Negative	Negative	Negative	Positive	Positive

*Values in parentheses are the sites of nucleotide mutations each probe was assigned to.

Table 2. Evaluation results of multiplex PCR to differentiate monkeypox virus clades from the United Kingdom and Nigeria*

Reference PCR and country	Result	True positive	True negative	False positive	False negative	Sensitivity, %	Specificity, %
CDC assay, United Kingdom	Total	31	13	2	1	97 (83.78–99.92)	87 (59.54–98.34)
	Total Ct ≤35	31	13	2	0	100 (88.78–100.00)	87 (59.54–98.34)
	Clade I	0	45	0	0	NA	100 (92.13–100.00)
	IIa	0	45	0	0	NA	100 (92.13–100.00)
	IIb	31	13	2	1	97 (83.78–99.92)	87 (59.54–98.34)
	Lineage B.1	20	22	0	5	80 (59.30–93.17)	100 (84.56–100.00)
CDC with Sansure, United Kingdom†	Total	33	13	0	1	97 (84.67–99.93)	100 (75.29–100.00)
CDC Assay, Nigeria	Total	36	20	0	18	67 (52.53–78.91)	100 (83.16–100.00)
	Total Ct ≤35	32	20	0	1	97 (84.24–99.92)	100 (83.16–100.00)
CDC assay; combined, United Kingdom and Nigeria	Total	67	33	2	19	78 (67.67–86.14)	94 (80.84–99.30)
	Total Ct ≤35	64	33	2	1	98 (91.72–99.96)	94 (80.84–99.30)

*Numbers in parentheses are 95% CIs. Ct, cycle threshold; NA, not applicable.
†Discrepant samples were tested by using the Sansure Monkeypox virus Kit (Sansure-Biotech, https://www.sansureglobal.com).

sequences for each clade and lineage from GenBank and aligned through ClustalW by using MEGA 11 (https://www.megasoftware.net). We manually designed the probes to contain mutations in the middle. We designed the primers by using PrimerQuest (Integrated DNA Technologies, https://eu.idtdna.com). The clade I probe targeted the F3L gene (mutation sites T46417C, G46421A, A46427C, C46435T), and the lineage B.1 probe targeted the OPG109 gene (mutation site C84587T). An assay on the OPG210 gene (mutation sites G183695A, C183696T) distinguishes clade IIb from non-IIb; clade IIb contains the F3L and OPG210 gene mutations, whereas clade IIa and clade I do not. The clade Ib assay targets the ≈1 kb deletion (Δ19,128–20,270) in the OPG032 gene (Table 1)

We used TaqPath-Fast mix (Thermo Fisher Scientific, https://www.thermofisher.com), primers and probes (Appendix, http://wwwnc.cdc.gov/EID/article/32/2/25-0686-App1.pdf), nuclease-free water, and 2.5 μl of DNA for quantitative PCR (qPCR) reactions. To improve specificity for lineage B.1, we designed a blocker oligo identical to the B.1 probe but without the mutation and with a 5′ end phosphate instead of a fluorophore. We conducted experiments on a Quantstudio 5 (Thermo Fisher Scientific) by using the thermal profile 95°C for 20 seconds, followed by 40 cycles of 95°C for 1 second and 60°C for 10 seconds. We used a positivity cutoff cycle threshold (Ct) of 38, with thresholds set at 10% of the maximum fluorescence of the positive control. We used synthetic double-stranded DNA containing target amplicons (Twist Bioscience, https://www.twistbioscience.com) or DNA from viral stocks as positive controls.

We created standard curves of clade I, IIb, and non-IIb DNA controls in triplicate from 1×10^4 to 1 copies/μL (Figure). We quantified DNA extracted from lineage B.1 and clade Ia and Ib viral stocks from the DNA controls to make standard curves. We conducted all analysis with the finalized multiplex. We conducted 20 replicates at 10 copies/μL and 1 copy/μL for each target; all replicates at 10 copies/μL successfully amplified.

In the UK evaluation, our assay had 97% (95% CI 83.78%–99.92%) sensitivity and 87% (95% CI 59.54%–98.34%) specificity compared with the CDC mpox PCR (Table 2). We tested discrepant samples by using the Sansure Monkeypox Virus Kit (Sansure-Biotech, https://www.sansureglobal.com). The 2 false positives and 1 false negative were positive according to Sansure, suggesting 2 false negative and 1 true positive result by using the CDC PCR. Our assay was 100% specific and 80% sensitive for detecting lineage B.1. The 5 false negatives had Cts ≥ 34.

In the NCDC evaluation, our assay showed sensitivity of 67% (95% CI 52.53%–78.91%) and specificity of 100% (95% CI 83.16%–100.00%) compared with the CDC assay (Table 2). Of the available samples, 20% (n = 11) had a Ct >35; typically, Ct values from lesion swab specimens in the acute phase are lower (*12*), and

samples with Ct >35 are predicted to have no or very little infectivity (*13*). In samples with Ct ≤35, we observed 97% sensitivity (95% CI 84.24%–99.92%) and 100% specificity (95% CI 83.16%–100.00%). All samples were confirmed to be clade IIb. One sample had a Ct of 25.59 for IIb and 36.77 for B.1; this difference discounted a true B.1 positive and was classified as a false positive, giving a 98% specificity for this target.

Conclusions

Sensitivity for our assay was high in samples with a reference qPCR Ct ≤35 but lower with higher Ct values, supporting assay use for reflex testing samples with a Ct ≤35. Clade I and IIa clinical samples were unavailable. Although the other assays compared were created on the basis of multiple single nucleotide polymorphisms, the lineage B.1 assay is based on a single mutation. If this single mutation were to naturally occur in nonlineage B.1 strains, it could compromise the assay. Mutations will be monitored on Nextstrain. We assigned clinical samples to clades on the basis of date and location of collection after failed attempts to generate full genome assemblies after sequencing. Although this process is suboptimal, 99% of MPXV sequenced in the United Kingdom in 2022 by UK Health Security Agency was lineage B.1; the 2018 samples were imported cases from Nigeria, and only clade IIb is known to have circulated in Nigeria during our collection dates (*4*). Other assays can distinguish between clades; a qPCR that detects clade I, clade II, clade IIb, and lineage B.1 was previously published (*14*) but requires 2 tubes per sample and does not include clade Ib. Another assay detects clade Ib by using singleplex assays (*15*).

Rapid identification of MPXV clades is vital with outbreaks occurring attributed to different clades. Clade and lineage identification is necessary because of differences in disease severity and epidemiologic tracking, particularly for new outbreaks. Although sequencing is the standard diagnostic practice, PCR remains necessary when access to sequencing is limited or extra throughput is required.

Members of the International Severe Acute Respiratory and Emerging Infection Consortium members: Mike Beadsworth, Ingeborg Welters, Lance Turtle, Jane Minton, Karl Ward, Elinor Moore, Elaine Hardy, Mark Nelson, David Brealey, Ashley Price, Brian Angus, Graham Cooke, and Oliver Koch.

Acknowledgments

We thank the World Health Organization BioHub for providing monkeypox virus clade Ia and Ib.

This research was funded by The Pandemic Institute, formed of 7 founding partners: The University of Liverpool, Liverpool School of Tropical Medicine, Liverpool John Moores University, Liverpool City Council, Liverpool City Region Combined Authority, Liverpool University Hospital Foundation Trust, and Knowledge Quarter Liverpool. The UK Public Health Rapid Support Team is funded by UK Aid from the Department of Health and Social Care and is jointly run by the UK Health Security Agency and the London School of Hygiene & Tropical Medicine. The International Severe Acute Respiratory and Emerging Infection Consortium is funded from the National Institute for Health Research (award no. CO-CIN-01), the Medical Research Council (grant no. MC_PC_19059), and by Liverpool Pandemic Institute and the National Institute for Health Research Health Protection Research Unit in Emerging and Zoonotic Infections at University of Liverpool in partnership with UK Health Security Agency, in collaboration with Liverpool School of Tropical Medicine and the University of Oxford (award no. 200907), Wellcome Trust and Department for International Development (grant no. 215091/Z/18/Z), and the Bill and Melinda Gates Foundation (grant no. OPP1209135), and Liverpool Experimental Cancer Medicine Centre (grant no. C18616/A25153). This work was partially funded as part of FIND's work as coconvener of the diagnostics pillar of the Pandemic Threats Programme, who received funds from the Germany (Federal Ministry of Economic Cooperation and Development) and Canada governments. L.B.J. is supported by the Berlin Institute of Health Clinician Scientist program.

About the Author

Mr. Williams is a senior research technician at the Liverpool School of Tropical Medicine. His main research interests involve designing and evaluating novel diagnostic methods for infectious diseases that affect low- and middle-income countries.

References

1. McCollum AM, Damon IK. Human monkeypox. Clin Infect Dis. 2014;58:260–7. https://doi.org/10.1093/cid/cit703
2. Isidro J, Borges V, Pinto M, Sobral D, Santos JD, Nunes A, et al. Phylogenomic characterization and signs of microevolution in the 2022 multi-country outbreak of monkeypox virus. Nat Med. 2022;28:1569–72. https://doi.org/10.1038/s41591-022-01907-y
3. Endo A, Murayama H, Abbott S, Ratnayake R, Pearson CAB, Edmunds WJ, et al. Heavy-tailed sexual contact networks and monkeypox epidemiology in the global outbreak, 2022. Science. 2022;378:90–4. https://doi.org/10.1126/science.add4507
4. Ndodo N, Ashcroft J, Lewandowski K, Yinka-Ogunleye A, Chukwu C, Ahmad A, et al. Distinct monkeypox

virus lineages co-circulating in humans before 2022. Nat Med. 2023;29:2317–24. https://doi.org/10.1038/s41591-023-02456-8
5. Fink DL, Callaby H, Luintel A, Beynon W, Bond H, Lim EY, et al.; Specialist and High Consequence Infectious Diseases Centres Network for Monkeypox. Clinical features and management of individuals admitted to hospital with monkeypox and associated complications across the UK: a retrospective cohort study. Lancet Infect Dis. 2023;23:589–97. https://doi.org/10.1016/S1473-3099(22)00806-4
6. Vakaniaki EH, Kacita C, Kinganda-Lusamaki E, O'Toole Á, Wawina-Bokalanga T, Mukadi-Bamuleka D, et al. Sustained human outbreak of a new MPXV clade I lineage in eastern Democratic Republic of the Congo. Nat Med. 2024;30:2791–5. https://doi.org/10.1038/s41591-024-03130-3
7. Kibungu EM, Vakaniaki EH, Kinganda-Lusamaki E, Kalonji-Mukendi T, Pukuta E, Hoff NA, et al.; International Mpox Research Consortium. Clade I–associated mpox cases associated with sexual contact, the Democratic Republic of the Congo. Emerg Infect Dis. 2024;30:172–6. https://doi.org/10.3201/eid3001.231164
8. Li Y, Zhao H, Wilkins K, Hughes C, Damon IK. Real-time PCR assays for the specific detection of monkeypox virus West African and Congo Basin strain DNA. J Virol Methods. 2010;169:223–7. https://doi.org/10.1016/j.jviromet.2010.07.012
9. World Health Organization. Diagnostic testing for the monkeypox virus (MPXV): interim guidance, 9 November 2023. 2023 [cited 2024 Nov 14]. https://www.who.int/publications/i/item/WHO-MPX-Laboratory-2023.1
10. Centers for Disease Control and Prevention. Test procedure: monkeypox virus generic real-time PCR test. 2022 [cited 2024 May 1]. https://stacks.cdc.gov/view/cdc/119661
11. UK Health Security Agency. Investigation into monkeypox outbreak in England: technical briefing 8. 2024 [cited 2024 Nov 14]. https://www.gov.uk/government/publications/monkeypox-outbreak-technical-briefings/investigation-into-monkeypox-outbreak-in-england-technical-briefing-8#part-6genomic-surveillance.
12. Edman-Wallér J, Jonsson O, Backlund G, Muradrasoli S, Sondén K. Results of PCR analysis of mpox clinical samples, Sweden, 2022. Emerg Infect Dis. 2023;29:1220–2. https://doi.org/10.3201/eid2906.230253
13. Paran N, Yahalom-Ronen Y, Shifman O, Lazar S, Ben-Ami R, Yakubovsky M, et al. Monkeypox DNA levels correlate with virus infectivity in clinical samples, Israel, 2022. Euro Surveill. 2022;27:2200636. https://doi.org/10.2807/1560-7917.ES.2022.27.35.2200636
14. Huo S, Chen Y, Lu R, Zhang Z, Zhang G, Zhao L, et al. Development of two multiplex real-time PCR assays for simultaneous detection and differentiation of monkeypox virus IIa, IIb, and I clades and the B.1 lineage. Biosaf Health. 2022;4:392–8. https://doi.org/10.1016/j.bsheal.2022.10.005
15. Schuele L, Masirika LM, Udahemuka JC, Siangoli FB, Mbiribindi JB, Ndishimye P, et al.; GREATLIFE MPOX group collaborators. Real-time PCR assay to detect the novel clade Ib monkeypox virus, September 2023 to May 2024. Euro Surveill. 2024;29:2400486. https://doi.org/10.2807/1560-7917.ES.2024.29.32.2400486

Address for correspondence: Thomas Edwards, Liverpool School of Tropical Medicine, CTID Building, Pembroke Place, Liverpool L3 5QA, UK; email: Thomas.Edwards@lstmed.ac.uk

Measles Outbreak Driven by Nosocomial Transmission, Armenia, February–July 2023

Karo Palayan, Ani Manukyan, Gayane Sahakyan, Svetlana Grigoryan, Lilit Karapetyan, Shushan Sargsyan, Artavazd Vanyan, Pawel Stefanoff

During March–July 2023, we investigated a measles outbreak in Armenia. Of 287 patients, 130 were <5 years of age and 215 (75%) were unvaccinated. Among 3 transmission chains involving 183 cases, 70% of patients were exposed in healthcare facilities. To minimize nosocomial transmission, measles vaccination should be encouraged among healthcare workers.

In 2002, Armenia adopted the World Health Organization (WHO)'s measles elimination plan and incorporated the trivalent live measles, mumps, and rubella (MMR) vaccine into its national immunization schedule. For children, the first dose (MMR1) was administered at 12 months of age, and the second dose (MMR2) at 6 years of age. In 2020, the recommended age for MMR2 was revised to 4–6 years. In 2007, after a large measles outbreak during 2004–2005 involving 4,064 cases, the Ministry of Health (MoH) implemented a supplementary immunization campaign targeting 1.2 million persons 6–27 years of age, offering 1 dose to each person (*1*,*2*).

During 2008–2022, Armenia reported primarily imported measles cases, and incidence rates remained <1 case/100,000 population. During 2009–2019, national 2-dose MMR vaccine coverage among target groups consistently exceeded the WHO's 95% target. However, after 2020, coverage declined below 95% at national and regional levels (*3*,*4*).

On March 3, 2023, the Armenian National Center for Disease Control and Prevention (NCDC) received a report of 13 persons with suspected measles cases hospitalized at a 105-bed multidisciplinary pediatric hospital in Yereven. In response, NCDC established an outbreak investigation team to assess the extent of the outbreak and trace transmission chains to inform the national measles elimination strategy. We report findings from that activity, which was conducted as part of an emergency response and, in accordance with guidance from the Armenia MoH, did not require ethics approval.

Author affiliations: National Centre for Disease Control and Prevention, Ministry of Health, Yerevan, Armenia (K. Palayan, A. Manukyan, G. Sahakyan, S. Grigoryan, L. Karapetyan, S. Sargsyan, A. Vanyan); European Centre for Disease Prevention and Control, Mediterranean and Black Sea Programme in Intervention Epidemiology Training, Stockholm, Sweden (K. Palayan, P. Stefanoff)

DOI: https://doi.org/10.3201/eid3202.250474

The Investigation

We defined a suspected case as illness in any person with clinical signs and symptoms, including fever and maculopapular rash, accompanied by cough, conjunctivitis, or both. We defined a confirmed case as a suspected case with laboratory confirmation of measles-specific IgM, an epidemiologic link to a laboratory-confirmed case, or both. During March–July 2023, local and regional outbreak investigation teams assessed each suspected case by using a standardized form that captured demographic information, clinical symptoms, and vaccination status. Local epidemiologists attempted to collect a serum specimen from each suspected case-patient, preferably 4–28 days after symptom onset. Upon laboratory confirmation, the investigation team contacted each confirmed case-patient to obtain a list of close contacts, defined as persons who shared a household, worked or were hospitalized in the same room, or frequently visited the same locations and for whom potential exposure occurred 6–18 days before rash onset.

Next, investigators interviewed each close contact for symptoms and vaccination status, informed contacts of their possible exposure, and offered MMR vaccination. Interviewers referred all close contacts who met the criteria for a suspected case to local epidemiologists for further investigation. Vaccination

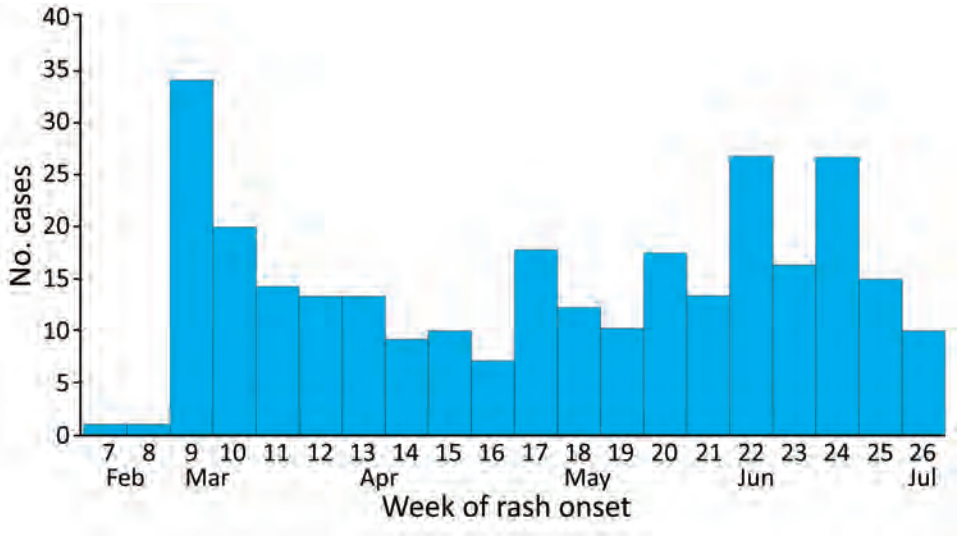

Figure. Number of confirmed cases by week of rash onset during measles outbreak driven by nosocomial transmission, Armenia, February–July 2023.

status was verified by using immunization records maintained at public health centers run by the MoH. We classified persons with unknown vaccination status as unvaccinated. The NCDC Reference Laboratory detected measles-specific IgM antibodies in serum specimens by using Measles IgM ELISA kits (EUROIMMUN, https://www.euroimmun.com), following WHO guidelines (*5*).

We defined a measles transmission chain as an uninterrupted series of epidemiologically linked confirmed cases, in which each link was supported by plausible close contact and rash onset dates separated by a 6–18-day incubation interval. We considered cases not linked if we could not identify an epidemiologic connection to other cases. We classified a confirmed case as imported if the person had traveled abroad during the incubation period and had no known close contact with a confirmed case.

During February 3–July 3, 2023, we interviewed ≈7,000 contacts, of whom 868 met the criteria for suspected measles cases. Among those, 284 were laboratory-confirmed and 3 were epidemiologically linked, resulting in a total of 287 confirmed cases. The epidemic curve indicated continuous measles transmission throughout the observation period (Figure). An additional 828 suspected cases were reported during August 2023–December 2024, an average of ≈49 cases per month, suggesting ongoing transmission.

Of the 287 confirmed cases, 130 (45%) were among children ≤5 years of age, 152 (53%) case-patients were female and 135 (47%) were male, and 172 (60%) resided in Yerevan, the capital city. The median age was 8 (interquartile range [IQR] 1–25; range 0–64) years; 38 cases were imported. Healthcare workers (HCWs) accounted for 15 cases, of whom only 1 had received a single dose of a measles-containing vaccine. Among all 287 case-patients, 215 (75%) were unvaccinated, 29 (10%) had received 1 dose, 22 (7.7%) had received 2 doses, and 20 (7%) had unknown vaccination status (Table 1).

Most (71%, n = 204) case-patients were hospitalized. The most common signs and symptoms were maculopapular rash (100%), fever (100%), cough (75%), coryza (65.5%), and conjunctivitis (40%). The median duration of rash was 4 days. The most frequently reported complications were pneumonia (5%) and diarrhea (1%).

The index case-patient was a 5-year-old boy who had received 1 dose of the MMR vaccine and started having symptoms on February 4, 2023, after traveling through several countries in Europe. He exposed a nurse working in a pediatric clinic, initiating a transmission chain that lasted 13 generations and involved 177 cases (Table 2). Of the 287 total cases, 183 were linked to transmission chains, but 104 could not be linked. Among the 183 cases with a known exposure location, 129 (70%) were exposed in healthcare settings and 54 (30%) in community settings. Of the 104 unlinked cases, 66 had an unknown source of infection, and 38 were classified as imported, having been infected abroad.

Table 1. Distribution of cases by age group and vaccination status during measles outbreak driven by nosocomial transmission, Armenia, February–July 2023.

Age range, y	Not vaccinated	1 dose	≥2 doses	Total
<1	52	0	0	52
1–5	63	14	1	78
6–9	17	2	3	22
10–14	18	6	9	33
15–19	9	3	6	18
≥20	77	4	3	84
Total	236	29	22	287

Table 2. Characteristics of cases and transmission chains during measles outbreak driven by nosocomial transmission, Armenia, February–July 2023

Characteristic	Transmission chain			Not linked*
	1	2	3	
No. cases	177	4	2	104
No. in healthcare facilities	125	2	2	–
No. in community settings	52	2	0	–
No. generations	13	2	1	–
No. cases among healthcare workers	9	1	0	5
Vaccination status				
Not vaccinated	142	4	2	87
1 dose	21	0	0	9
2 doses	14	0	0	8

*Includes cases with unknown infection source and imported cases.

Unvaccinated or undervaccinated HCWs and nosocomial transmission contributed to this prolonged measles outbreak in Armenia. In addition, the high percentage of unvaccinated children highlights gaps in the childhood immunization program. Although Armenia achieved measles control nearing elimination during 2007–2022, national immunization coverage surveillance failed to identify inadequately immunized groups, which enabled sustained measles transmission for >5 months during 2023.

The most affected group was unvaccinated children <4 years of age. High national vaccination coverage did not ensure transmission control because immunity gaps persisted at subregional and community levels. Infants <1 year of age who had not yet reached the recommended age for immunization (n = 53) were mostly infected in healthcare facilities. As part of the outbreak response, children 6–9 months of age who were identified as close contacts of measles cases were offered vaccination. Cases among infants who are not yet eligible for vaccination pose a substantial challenge to achieving measles eradication (*2*,*3*).

We implemented immediate control measures, including offering MMR vaccination to all inadequately immunized close contacts of confirmed cases (*6*). A total of 33,385 persons were immunized, including 6,693 HCWs. In addition, NCDC launched risk communication and awareness campaigns directed to the public and to persons traveling abroad. In addition, we recommended revising the national strategic plan for measles elimination to include mandatory immunization for front-line HCWs (*7*) and to strengthen monitoring of vaccination uptake within specific community subgroups.

Conclusions

Our investigation revealed gaps in measles surveillance and infection prevention and control in Armenia. Limited resources prevented routine PCR testing and genotyping, and many children were not referred for testing because of parental refusal. In addition, some HCWs failed to adhere to isolation and infection control protocols. Continued transmission after August 2023, primarily occurring outside healthcare settings, highlighted the lack of effective measles control, driven by persistence of underimmunized groups and emergence of displaced populations after the Armenia–Azerbaijan conflict in September 2023.

In summary, during this large measles outbreak, most case-patients were exposed in healthcare facilities, and unvaccinated HCWs played a key role in the spread of infection, especially in the first phase of the outbreak. To minimize the risk for nosocomial transmission, HCWs should be made aware of measles and the critical role of vaccination in measles prevention.

Acknowledgments

We thank Gohar Mheryan, Mariam Ghukasyan, Brijida Simonyan, Naira Khachatryan, Marine Kirakosyan, Gohar Hovhannisyan, and Aram Yeritsyan for aiding in the investigation and Shushan Makhsudyan for invaluable help.

K.P. is a fellow of the MediPIET program, supported financially by the European Centre for Disease Prevention and Control. The views and opinions expressed herein do not state or reflect those of ECDC. ECDC is not responsible for the data and information collation and analysis and cannot be held liable for conclusions or opinions drawn.

About the Author

Mr. Palayan is a biosafety engineer and former head of the Department of Physical Factors Impact on Human Health at the NCDC of Armenia. He currently serves as a lead specialist and lecturer at the National Scientific Research Center of Healthcare Programs at Yerevan State Medical University. His research interests include the analysis of medical and epidemiologic data to inform evidence-based decision-making in healthcare.

References

1. Sindoni A, Baccolini V, Adamo G, Massimi A, Migliara G, De Vito C, et al. Effect of the mandatory vaccination law on measles and rubella incidence and vaccination coverage in Italy (2013–2019). Hum Vaccin Immunother. 2022;18:1950505. https://doi.org/10.1080/21645515.2021.1950505
2. Hovhannisyan HS, Melkonyan NS. The immunoprophylaxis and prevalence of measles, rubella in Armenia [in Armenian]. Med Sci Armenia. 2017;57:83–91.
3. Melkonyan N, Badalyan A, Hovhannisyan H, Poghosyan K. Impact of the COVID-19 pandemic on routine immunization services in Yerevan and vaccinations against COVID-19 in Armenia. J Infect Dev Ctries. 2022;16:1687–95. https://doi.org/10.3855/jidc.17028
4. Kazaryan AM, Edwin B, Darzi A, Tamamyan GN, Sahakyan MA, Aghayan DL, et al.; Doctors Against The War collaborators. War in the time of COVID-19: humanitarian catastrophe in Nagorno-Karabakh and Armenia. Lancet Glob Health. 2021;9:e243–4. https://doi.org/10.1016/S2214-109X(20)30510-6
5. Hiebert J, Zubach V, Charlton CL, Fenton J, Tipples GA, Fonseca K, et al. Evaluation of diagnostic accuracy of eight commercial assays for the detection of measles virus–specific IgM antibodies. J Clin Microbiol. 2021;59:e03161-20. https://doi.org/10.1128/JCM.03161-20
6. Dimala CA, Kadia BM, Nji MAM, Bechem NN. Factors associated with measles resurgence in the United States in the post-elimination era. Sci Rep. 2021;11:51. https://doi.org/10.1038/s41598-020-80214-3
7. Sá Machado R, Perez Duque M, Almeida S, Cruz I, Sottomayor A, Almeida I, et al. Measles outbreak in a tertiary level hospital, Porto, Portugal, 2018: challenges in the post-elimination era. Euro Surveill. 2018;23:18–00224. https://doi.org/10.2807/1560-7917.ES.2018.23.20.18-00224

Address for correspondence: Karo Palayan, National Centre for Disease Control and Prevention, Ministry of Health, 12 Heratsi, Yerevan 0025, Armenia; email: palayankaro@mail.ru

etymologia

Mumps [muhmps]

Shaan Mohan, Ahmad Khan

Mumps virus (*Orthorubulavirus parotitidis*) is a paramyxovirus that causes the infective syndrome commonly known as mumps. Mumps often is characterized by a parotitic warping of facial morphology. In obsolete English, *mump* referred to an exaggerated facial expression or grimace.

A possible etymologic origin of mumps suggested by the Oxford English Dictionary is the Old French word *mommer*, which appears to date back to 1263. In the 1400s, that term was used to mean "play[ing] dice in a mask." Later kindred words include the Middle Dutch term *mommen* (to go about in a mask or disguise) and the regional Norwegian word *mompe* (to chew with a full mouth).

The Centers for Disease Control and Prevention noted that US mumps cases plummeted by >99% after the mumps vaccination program started in 1967, but mumps cases and outbreaks have increased since 2006. Vaccination coverage for kindergartners during the 2023–24 school year decreased to 92.7% for the measles, mumps, and rubella (MMR) vaccine; US kindergartner exemptions from ≥1 vaccines increased from 3.0% to 3.3%, an uptrend mainly modified by the increase in nonmedical exemptions.

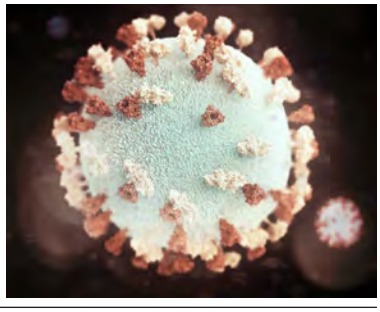

Figure. Three-dimensional graphic representation of a spherical-shaped mumps virus particle. Illustrated by Alissa Eckert. Source: Centers for Disease Control and Prevention Public Health Image Library (https://phil.cdc.gov).

Sources

1. Oxford English Dictionary. Mump; noun and adjective [cited 2025 Jan 12]. https://www.oed.com/dictionary/mump_n1?tab=meaning_and_use#35472983
2. Oxford English Dictionary. Mum [cited 2025 Jan 22]. https://www.oed.com/dictionary/mum_v?tab=etymology#35457321
3. Oxford English Dictionary. Mump; verb [cited 2025 Jan 22]. https://www.oed.com/dictionary/mump_v1?tab=etymology#35473046
4. Centers for Disease Control and Prevention. Mumps cases and outbreaks [cited 2025 Jan 22]. https://www.cdc.gov/mumps/outbreaks/index.html
5. Centers for Disease Control and Prevention. V accination coverage and exemptions among kindergartners. SchoolVaxView [cited 2025 Jan 22]. https://www.cdc.gov/schoolvaxview/data/index.html

Authors affiliation: University of Leicester Medical School, Leicester, UK

Address for correspondence: Shaan Mohan, University of Leicester Medical School, 15 Lancaster Rd, Leicester LE1 7HA, UK; email: drshaanmohan@gmail.com

DOI: https://doi.org/10.3201/eid3202.240153

Avian Influenza A(H9N2) Virus Transmission across Chicken Production and Distribution Networks, Vietnam

Mathew Hennessey, Thuy Hoang Thi, Jayna Raghwani, Younjung Kim, Hoa Thi Thanh Pham, Trang Huyen Nguyen, Hung Quoc Nguyen, Joshua G. Lynton-Jenkins, Ashley C. Banyard, Ian H. Brown, Joe James, Tom Lewis, Nicola S. Lewis, Dirk Pfeiffer, Fiona Tomley, Damer Blake, Ngoc Pham Thi, Anne Conan, Vuong Nghia Bui,[1] Guillaume Fournié[1]

In northern Vietnam, during March 2021–March 2022, prevalence of influenza A(H9N2) in chickens was higher in distribution facilities than on farms and varied between facility types. Phylogenetic analysis indicated extensive viral mixing along networks of chicken production and distribution, highlighting a need for risk mitigation across the entire network.

High-pathogenicity avian influenza A subtype H5N1 viruses of the Goose/Guangdong/1/96 lineage and low pathogenicity avian influenza A subtype H9N2 viruses are endemic in Southeast Asia, including Vietnam. Both subtypes affect poultry production and pose zoonotic risks (*1*) directly and through their involvement in the generation of novel virus reassortments (*2*). In Vietnam, the subtypes are frequently detected in live bird markets, and higher prevalence is associated with practices such as mixing poultry from multiple sources (*3*). However, that finding should be interpreted cautiously because farms and the markets they supply have limited prevalence data, and the focus on markets has diverted attention from larger slaughter facilities despite those facilities playing a key role in poultry distribution. Together, those gaps constrain understanding of avian influenza virus (AIV) transmission risk along the production and distribution network (PDN) through which poultry are raised, traded, and consumed. We conducted a cross-sectional study in northern Vietnam to assess avian influenza A(H5N1) and A(H9N2) prevalence in chickens, determine how AIV prevalence varied between farms and the different distribution facility types, and examine how viral genetic diversity was structured along the PDN.

The Study

We selected 50 farms and 52 distribution facilities, including retail and wholesale markets, small-scale slaughter points, and industrial slaughterhouses, across 4 provinces (Bac Giang, Ha Noi, Hai Duong, and Quang Ninh) (Figure 1). We identified distribution facilities trading or processing slow-growing colored broiler chickens (i.e., hybrids of indigenous roosters and fast-growing broiler hens that account for most chicken meat produced in Vietnam [*4*]) through consultation with provincial

Author affiliations: Royal Veterinary College, London, UK (M. Hennessy, J. Raghwani, N.S. Lewis, D. Pfeiffer, F. Tomley, D. Blake, G. Fournié); National Institute of Veterinary Research, Hanoi, Vietnam (T.H. Thi, T.H. Nguyen, H.Q. Nguyen, N.P. Thi, V.N. Bui); University of Oxford, Oxford, UK (Y. Kim); Université de Montpellier, Montpellier, France (H.T.T. Pham, A. Conan); World Organisation for Animal Health/Food and Agriculture Organization International Reference Laboratory for Avian Influenza Animal and Plant Health Agency, Addlestone, UK (J.G. Lynton-Jenkins, A.C. Banyard, J. James, T. Lewis); Pirbright Institute, Pirbright, UK (I.H. Brown); World Health Organization Collaborating Centre for Influenza Reference and Research, London (N.S. Lewis); City University, Hong Kong, China (A. Conan); French Agricultural Research Centre for International Development, Harare, Zimbabwe (A. Conan); Université de Lyon, Marcy l'Etoile, France (G. Fournié); Université Clermont Auvergne, Saint Genes Champanelle, France (G. Fournié)

DOI: https://doi.org/10.3201/eid3202.251416

[1]These authors contributed equally to this article.

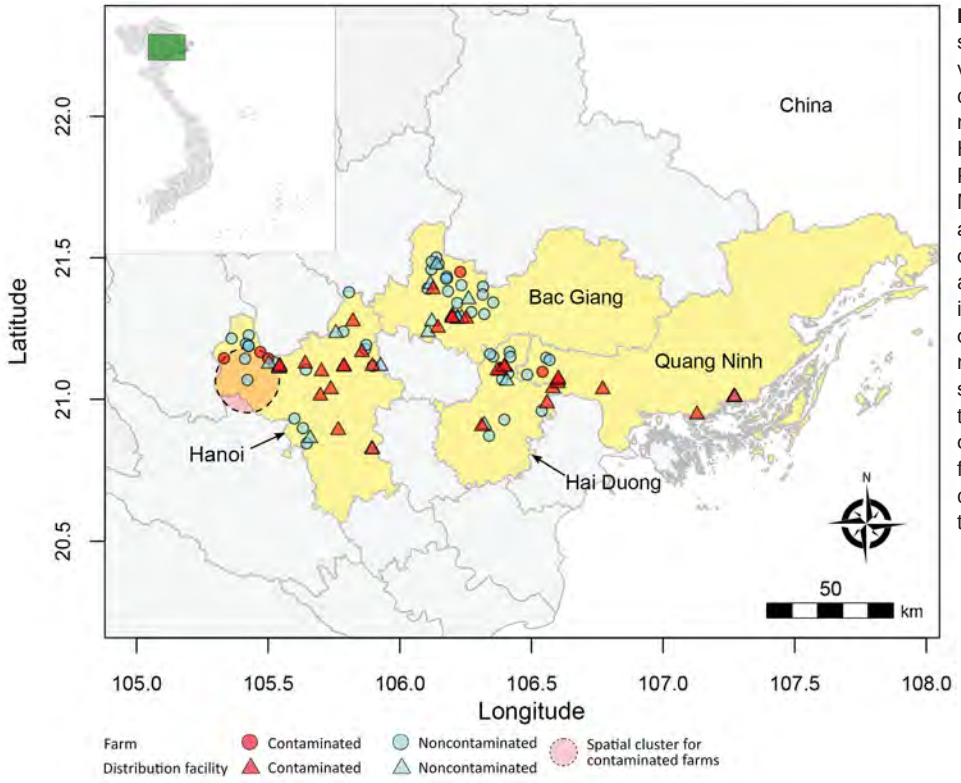

Figure 1. Geographic area and sites for study of avian influenza virus A(H9N2) prevalence across chicken production and distribution networks, Bac Giang, Hanoi, Hai Duong, and Quang Ninh Provinces, Vietnam, March 2021–March 2022. The 4 study provinces and the individual sites (farms and distribution facilities) are shown alongside the detection of avian influenza viruses (contaminated defined as ≥1 positive sample; noncontaminated defined as all samples testing negative) and the spatiotemporal cluster of contaminated farms. The 2 other farms that appear located in the cluster were not sampled during the temporal window.

authorities and traders. We randomly selected 4 retail markets and 4–5 slaughter points in the urban area of each province and recruited all wholesale markets and slaughterhouses in the study area. We traced farming areas supplying distribution facilities through interviews and snowball sampling. We randomly selected 1 farm per distribution facility from the list of farms of these supplying areas. During March 2021–March 2022, we collected oropharyngeal and cloacal swab specimens from 15 slow-growing broilers at each site and from fast-growing broilers when present. On farms, we sampled flocks near the end of production cycles. We administered structured questionnaires to capture husbandry, vaccination, and trade practices. Our study was approved by the National Institute of Veterinary Research (Vietnam) (approval no. 020-480433/DD-YTCC) and the Royal Veterinary College (UK) Ethics and Welfare Committee (approval no. URN: 20204811983-3). Participants were informed about the study and then asked to provide their verbal consent to take part.

We screened samples for the influenza A virus matrix gene by using real-time reverse transcription PCR (*5*) and then subtyped positive samples (i.e., those with cycle threshold values <40) for H5 and H9 (Appendix 1, https://wwwnc.cdc.gov/EID/article/32/2/25-1416-App1.pdf). We sequenced samples with cycle threshold values ≤30, compared them with genomes from Vietnam during 2018–2022 for which sequences were available through GISAID (https://www.gisaid.org), and submitted the genomes to

Table. Posterior estimates and posterior predictive values of avian influenza virus A(H9N2) prevalence across chicken production and distribution networks, Bac Giang, Ha Noi, Hai Duong, and Quang Ninh Provinces, Vietnam, March 2021–March 2022*

Site	No. sites	No. chickens	H9N2-positive chickens, no (%)	H9N2 prevalence, median % (95% HDI)		
				Site-level	Bird-level in contaminated sites	Overall† bird-level
Farms	50	750	31 (4.1)	0.111 (0.037–0.202)	0.414 (0.305–0.525)	0.045 (0.014–0.086)
Distribution facilities	52	932	168 (18.0)			
Retail market	16	240	38 (15.8)	0.778 (0.559–0.967)	0.212 (0.123–0.309)	0.161 (0.088–0.244)
Wholesale market	11	210	14 (6.7)	0.481 (0.163–0.850)	0.125 (0.033–0.238)	0.057 (0.014–0.117)
Slaughter point	19	363	106 (29.2)	0.725 (0.527–0.898)	0.413 (0.308–0.515)	0.295 (0.190–0.402)
Slaughterhouse	6	119	10 (8.4)	0.233 (0.014–0.542)	0.483 (0.158–0.795)	0.103 (0.002–0.286)

*HDI, high density interval.
†Estimated prevalence across both contaminated and uncontaminated sites.

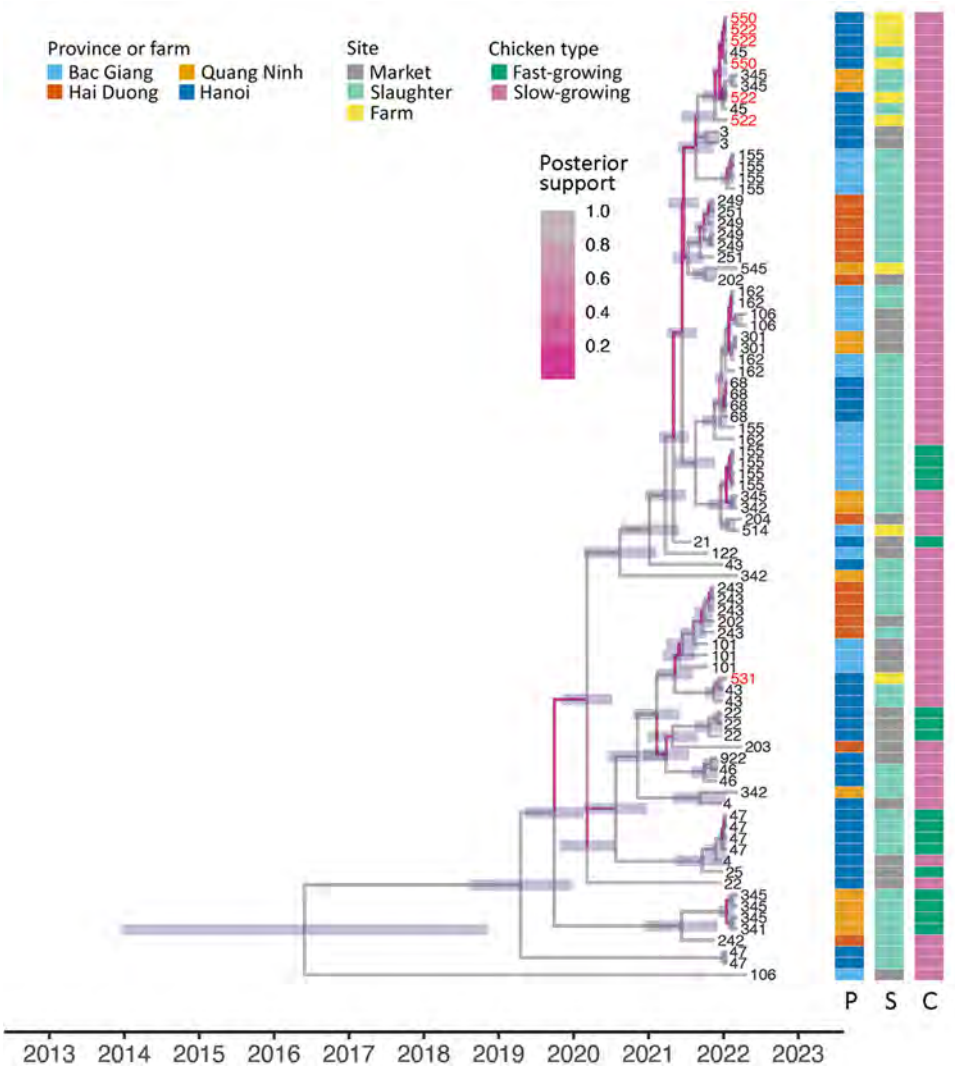

Figure 2. Time-scaled phylogenies of hemagglutinin sampled avian influenza virus A(H9N2) virus genomes in study of H9N2 virus prevalence across chicken production and distribution networks, Bac Giang, Hanoi, Hai Duong, and Quang Ninh Provinces, Vietnam, March 2021–March 2022. Tree tips are labeled by the unique sampled site identification; red text indicates sequences from 3 farms in the spatiotemporal cluster. Branches are colored by posterior support, and horizontal node bars represent 95% highest posterior density intervals of node ages. Heatmaps indicate province, site type, and chicken type of each sequence. C, chicken type; P, province; S, site type.

GISAID (Appendix 2, https://wwwnc.cdc.gov/EID/article/32/2/25-1416-App2.xlsx). We conducted phylogenetic analyses by using Bayesian methods to infer lineage structure and reassortment patterns (*6*). We performed separate analysis for distribution facilities and farms by using space-time cluster analysis by using a Bernoulli model (SaTScan, https://www.satscan.org) and Bayesian hierarchical logistic regression models (https://doi.org/10.32614/CRAN.package.R2jags) to estimate AIV prevalence at site and bird levels.

All farms were independently owned and held 100–15,000 (median 2,000) slow-growing broilers 70–240 days old (mean 116 days) at sampling. Sixty percent of farmers reported AIV vaccination for their flocks.

Among 1,682 sampled chickens (750 from farms and 932 from distribution facilities), a single chicken from a Quang Ninh slaughter point tested positive for H5, a finding consistent with farm-level H5N1 virus prevalences of 0%–0.1% reported in Egypt and Bangladesh (*7*,*8*). Depending on their pathogenicity, some H5N1 virus lineages can circulate in waterfowl without causing overt clinical disease. Spillover into chickens has frequently been associated with close proximity to free-grazing ducks and rice paddy ecosystems (*9*), and proximity of these species within markets probably facilitates cross-species transmission. In contrast, we detected H9N2 virus in 11.7% (197/1,682) of all sampled chickens. On farms, estimated bird-level prevalence of H9N2 virus was 4.5%, and detection was more frequent in unvaccinated (4/20) than vaccinated (1/30) flocks, although that difference was not significant ($p = 0.14$ by Fisher exact test). Such high prevalence in farmed chickens is similar to that for Egypt but higher than for previous reports from southern Vietnam and Bangladesh (*7*,*10*,*11*).

The best-fitting model differentiated distribution facilities by type and supplying area (Appendix 1 Table 4), whereas including chicken type or sampling period did not improve the model fit. Overall, bird-level prevalence in distribution facilities was ≈5-fold higher than on farms and was highest in informal slaughter points, followed by retail markets, slaughterhouses, and wholesale markets (Table). Influenza A(H9N2) virus prevalence was nearly as high on farms as in wholesale markets and was estimated to increase by 254% (95% highest density interval 4%–754%) from farms to retail markets and 545% (95% highest density interval 108%–1396%) from farms to slaughter points (Table).

On the basis of H9 sequences, we assigned all viruses to clade B4.71 (maximum identity >96%). Time-scaled phylogenies of H9N2 virus genomes showed limited genetic diversity (Figure 2, 3; Appendix 1 Figure 5, 6). The estimated time to most recent common ancestor for all sampled viruses spanned a broad range (95% highest posterior density interval 2008–2018 across all segments), although most sequences shared a more recent time to most recent common ancestor (95% highest posterior density interval ≈2017–2019). Our dataset included sequences from 3 farms forming a spatiotemporal cluster in Hanoi (23.5-fold higher risk than for farms outside; p = 0.045) (Figure 2, 3; Appendix 1 Figure 5, 6). Viruses from 2 farms had high genetic identity, consistent with epidemiologic linkage, whereas virus from a third farm (site 531) clustered separately in all 8 gene segments, suggesting that the spatiotemporal cluster involved ≥2 genetically distinct lineages. Alongside detection of genetically distinct viruses within and between distribution facilities, these findings demonstrate the presence of distinct H9N2 virus lineages at local scales and frequent reassortment in the region (Figure 2, 3).

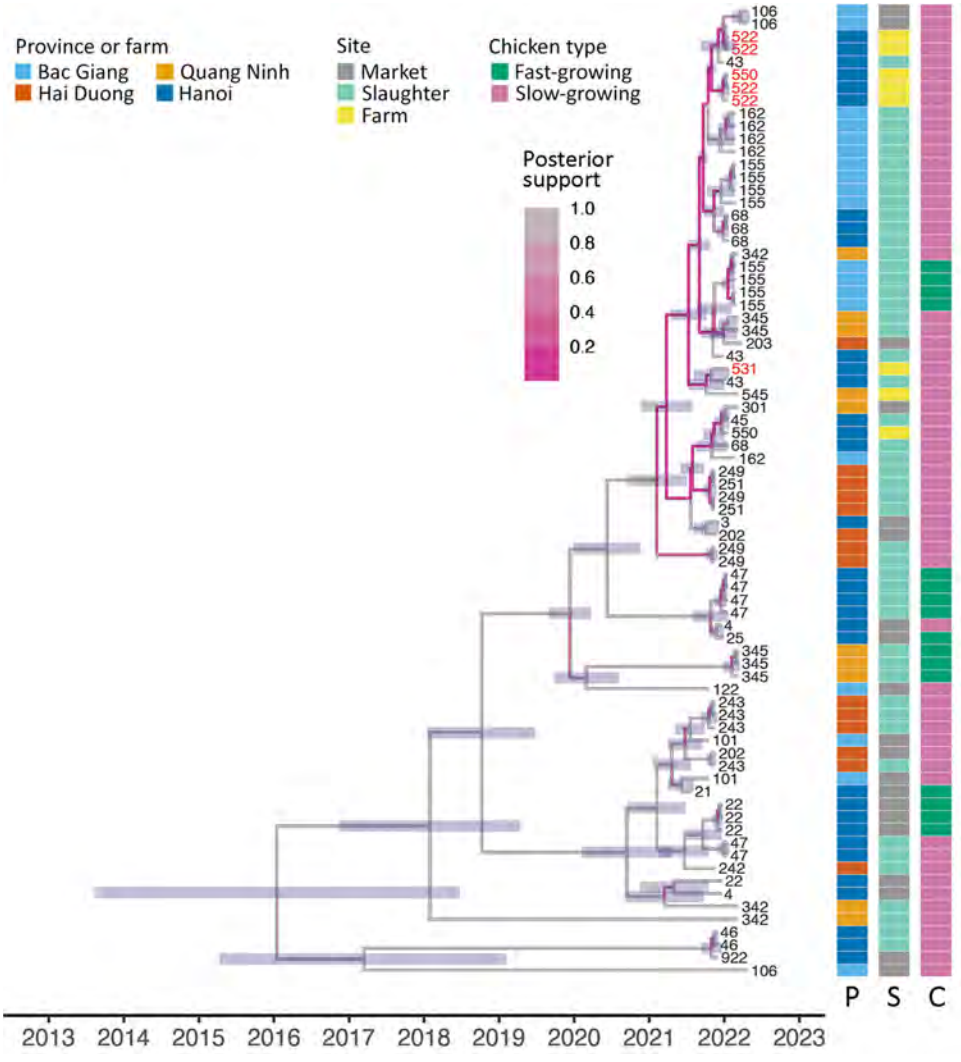

Figure 3. Time-scaled phylogenies of neuraminidase of sampled avian influenza virus A(H9N2) virus genomes in study of H9N2 virus prevalence across chicken production and distribution networks, Bac Giang, Hanoi, Hai Duong, and Quang Ninh Provinces, Vietnam, March 2021–March 2022. Tree tips are labeled by the unique sampled site identification; red text indicates sequences from 3 farms in the spatiotemporal cluster. Branches are colored by posterior support, and horizontal node bars represent 95% highest posterior density intervals of node ages. Heatmaps indicate province, site type, and chicken type of each sequence. C, chicken type; P, province; S site type.

Conclusions

Our results indicate that poultry production and distribution network configurations, including the origins of supplying farms, influence H9N2 virus prevalence and thus human exposure risk. The pattern of viral circulation amplification along the PDN is consistent with studies in southern Vietnam and Bangladesh (*7*,*11*) and probably reflects trading conditions. For example, birds are mixed from multiple sources and experience lengthy, stressful transportation (i.e., crowding and lack of sustenance), creating opportunities for virus exposure and transmission en route; that finding was supported by the improved model fit when we included supplying areas, suggesting that procurement and distribution practices influence viral prevalence at distribution facilities.

High viral prevalence in slaughter points and retail markets probably reflects sourcing involving multiple suppliers, including wholesale markets, indicating that chickens spent longer in the PDN before sampling. The lack of geographic structure in AIV genetic diversity further points to extensive viral mixing among poultry populations. Control and surveillance efforts should therefore address the entire poultry PDN.

The Vietnam Avian and Human Influenza Preparedness program has prioritized upgrading wholesale markets and industrial slaughterhouses and promoting their use (*12*). Although low prevalence in such facilities supports this focus, slaughterhouses remain underused, and informal slaughter points are still preferred (*13*). Surveillance and risk mitigation strategies must also target the numerous distribution facilities in Vietnam that are small and informal but widely used.

Acknowledgments

We thank Saira Butt for support in the initial development of the Bayesian model, the Food and Agricultural Organization and the Vietnamese Department for Animal Health for sharing information about the locations of markets and slaughter facilities, and the numerous participants for giving up their time to take part in this study.

Financial support for this study was obtained through the United Kingdom Research and Innovation Global Challenge Research Fund One Health Poultry Hub (grant no. BB/S011269/1) awarded to the Royal Veterinary College, 1 of 12 interdisciplinary research hubs funded under the UK government's Global Challenges Research Fund Interdisciplinary Research Hub initiative. G.F. is supported by the French National Research Agency and the French Ministry of Higher Education and Research. Animal and Plant Health Agency staff were funded by the UK Department for the Environment, Food and Rural Affairs and the devolved Scottish and Welsh governments (grant nos. SE2213, SE2227, and SV3006).

About the Author

Dr. Hennessey is a postdoctoral researcher at the Royal Veterinary College, London, UK. His primary research interests are the safety and sustainability of food systems and how human–animal–environmental relations influence disease transmission.

References

1. Nguyen LT, Stevenson MA, Firestone SM, Sims LD, Chu DH, Nguyen LV, et al. Spatiotemporal and risk analysis of H5 highly pathogenic avian influenza in Vietnam, 2014–2017. Prev Vet Med. 2020;178:104678. https://doi.org/10.1016/j.prevetmed.2019.04.007
2. Sims LD, Tripodi A, Swayne DE. Spotlight on avian pathology: can we reduce the pandemic threat of H9N2 avian influenza to human and avian health? Avian Pathol. 2020;49:529–31. https://doi.org/10.1080/03079457.2020.1796139
3. Sealy JE, Fournie G, Trang PH, Dang NH, Sadeyen JR, Thanh TL, et al. Poultry trading behaviours in Vietnamese live bird markets as risk factors for avian influenza infection in chickens. Transbound Emerg Dis. 2019;66:2507–16. https://doi.org/10.1111/tbed.13308
4. Thi Dien N, Thi Minh Khue N, Ebata A, Fournié G, Huyen LTT, Van Dai N, et al. Mapping chicken production and distribution networks in Vietnam: an analysis of socio-economic factors and their epidemiological significances. Prev Vet Med. 2023;214:105906. https://doi.org/10.1016/j.prevetmed.2023.105906
5. Centers for Disease Control and Prevention. CDC real-time RT-PCR (rRT-PCR) protocol for detection and characterization of swine influenza (version 2009). Reference no. I-007–05. 2009 [cited 2025 Jun 4]. https://www.hsdl.org/c/view?docid=778749
6. Suchard MA, Lemey P, Baele G, Ayres DL, Drummond AJ, Rambaut A. Bayesian phylogenetic and phylodynamic data integration using BEAST 1.10. Virus Evol. 2018;4:vey016. https://doi.org/10.1093/ve/vey016
7. Gupta SD, Hoque MA, Fournié G, Henning J. Patterns of Avian Influenza A (H5) and A (H9) virus infection in backyard, commercial broiler and layer chicken farms in Bangladesh. Transbound Emerg Dis. 2021;68:137–51. https://doi.org/10.1111/tbed.13657
8. El-Zoghby EF, Aly MM, Nasef SA, Hassan MK, Arafa AS, Selim AA, et al. Surveillance on A/H5N1 virus in domestic poultry and wild birds in Egypt. Virol J. 2013;10:203. https://doi.org/10.1186/1743-422X-10-203
9. Minh PQ, Morris RS, Schauer B, Stevenson M, Benschop J, Nam HV, et al. Spatio-temporal epidemiology of highly pathogenic avian influenza outbreaks in the two deltas of Vietnam during 2003-2007. Prev Vet Med. 2009;89:16–24 https://www.sciencedirect.com/science/article/pii/

S0167587709000178. https://doi.org/10.1016/j.prevetmed.2009.01.004
10. El-Sayed MM, Arafa AS, Abdelmagid M, Youssef AI. Epidemiological surveillance of H9N2 avian influenza virus infection among chickens in farms and backyards in Egypt 2015–2016. Vet World. 2021;14:949–55. https://doi.org/10.14202/vetworld.2021.949-955
11. Le KT, Stevenson MA, Isoda N, Nguyen LT, Chu DH, Nguyen TN, et al. A systematic approach to illuminate a new hot spot of avian influenza virus circulation in South Vietnam, 2016–2017. Transbound Emerg Dis. 2022;69:e831–44. https://doi.org/10.1111/tbed.14380
12. World Bank. Vietnam avian and human influenza control and preparedness. 2015 [cited 2023 Oct 17]. https://www.worldbank.org/en/results/2015/05/12/vietnam-avian-and-human-influenza-control-and-preparedness
13. Le Quyen. Surplus and shortage of centralized animal slaughter network. 2023 [cited 2025 Apr 16]. https://nhachannuoi.vn/thua-va-thieu-mang-luoi-giet-mo-dong-vat-tap-trung

Address for correspondence: Mathew Hennessey, Royal Veterinary College, Hawkshead Lane, Hatfield AL9 7TA, UK; email: mphennessey@rvc.ac.uk

Autochthonous Rat Lungworm *Angiostrongylus cantonensis* Infections in Accidental and Definitive Hosts, San Diego, California, USA

Shotaro Nakagun, Carlo G. Gonzalez Vera, Alexis Wohl, Deana L. Clifford, Garrett A. Fraess, Jordyn R. Nylander, Estefanía Montero, Javier Asin, Steven V. Kubiski, Rachel E. Burns

The rat lungworm, *Angiostrongylus cantonensis*, is an emerging veterinary and public health concern. We describe *A. cantonensis* infections in a zoo-housed parma wallaby and free-ranging Virginia opossums and roof rats in San Diego, California, USA. Angiostrongyliasis should be considered in central nervous system disease in humans and animals in this region.

Angiostrongylus cantonensis, the rat lungworm, is an invasive, zoonotic metastrongyle nematode that causes neurologic disease in humans and other vertebrate hosts (*1*). The usual life cycle of this parasite involves infection of the rodent definitive host by ingesting third-stage larvae (L3) found within gastropod intermediate hosts. Less commonly, paratenic hosts such as frogs, lizards, and crustaceans harbor the infective L3 and transfer *A. cantonensis* lungworm to rodents and accidental or aberrant hosts (*1*).

Since the original discovery of *A. cantonensis* lungworm in southern China in 1935 (*2*), the nematode has spread globally, including to Hawaii and more recently, the southeastern United States. In the continental United States, its range has gradually spread; infections in free-ranging rodents, gastropods, or both have been confirmed in Louisiana (*3*), Florida (*4*), Oklahoma (*5*), Georgia (*6*–*7*), and Texas (*8*). Hence, *A. cantonensis* lungworm is now considered endemic in those states. Cases in human and nonhuman accidental hosts have been reported in many more continental US states, with autochthonous infections suspected in Alabama (*9*), Mississippi (*10*), and Tennessee (*11*). In California, human cases have been sporadically reported in those who had traveled to endemic areas outside the continental United States and in those with unknown travel history (*12*). We describe *A. cantonensis* infections in a zoo-housed parma wallaby (*Notamacropus parma*) and free-ranging Virginia opossums (*Didelphis virginiana*) and roof rats (*Rattus rattus*) in San Diego, California, USA.

Author affiliations: San Diego Zoo Wildlife Alliance, San Diego, California, USA (S. Nakagun, C.G. Gonzalez Vera, G.A. Fraess, J.R. Nylander, S.V. Kubiski, R.E. Burns); San Diego Humane Society's Project Wildlife, San Diego (A. Wohl); California Department of Fish and Wildlife, Rancho Cordova, California, USA (D.L. Clifford); Universidad Cardenal Herrera-CEU, CEU Universities, Valencia, Spain (E. Montero); California Animal Health and Food Safety Laboratory, University of California, Davis, San Bernardino, California, USA (J. Asin)

DOI: https://doi.org/10.3201/eid3202.251081

The Study

In mid-December 2024, a 7-year-old male parma wallaby that was born and raised at the San Diego Zoo (San Diego, CA, USA) showed progressive neurologic signs, including head shaking, nystagmus, central blindness, ataxia, hindlimb paresis, and extensor rigidity in all limbs. The wallaby was euthanized after 11 days of hospitalization. Necropsy revealed multifocal hemorrhage in the cerebellum and half a dozen nematodes on the leptomeningeal surfaces of the cerebellum, brainstem, and cervical spinal cord (Figure 1). Histopathology revealed necrotizing and lymphoplasmacytic meningoencephalomyelitis with fibrinoid vascular necrosis, infarction, and hemorrhage, most severely affecting the cerebellum and right cerebrum. The lesions were occasionally associated with intralesional and

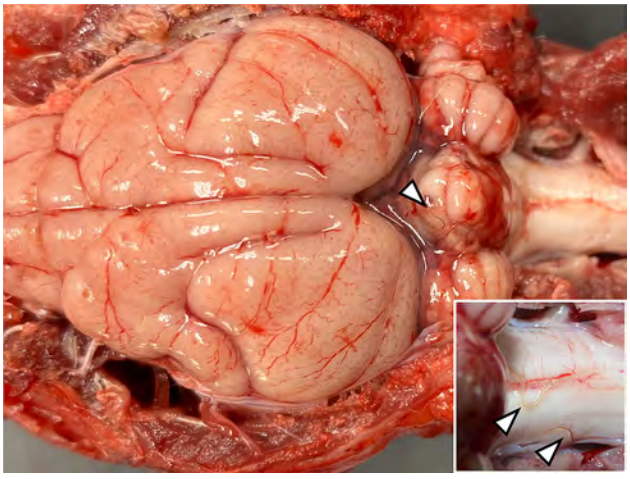

Figure 1. Brain and cervical spinal cord tissue from a parma wallaby (*Notamacropus parma*) with autochthonous rat lungworm *Angiostrongylus cantonensis* infection, San Diego, California, USA, 2024. The dorsal and caudal aspects of the cerebellum have coalescing foci of hemorrhage with nematodes (arrows) on the leptomeningeal surface. The inset depicts an enlarged view of the dorsal aspect of brainstem and C1 spinal cord with visible nematodes (arrows).

rarely intraparenchymal metastrongyle nematodes. A nematode collected in 70% ethanol was identified as *A. cantonensis* lungworm through PCR and sequencing (Appendix, https://wwwnc.cdc.gov/EID/article/32/2/25-1082-App1.pdf).

Because the diagnosis was unusual in this geographic area (*3*–*11*), we performed necropsies on free-ranging roof rats that were either euthanized as part of regular pest control or found dead on the San Diego Zoo grounds during January 14–February 14, 2025. We grossly examined 64 rats comprising both sexes and all life stages and evaluated lung and feces samples histologically and by the Baermann technique for all rats, regardless of gross findings. Two (3.1%) adult rats had lungworms and associated pneumonia. Histologically, the main findings were pulmonary arterial endothelial proliferation with thrombosis and adult metastrongyle nematodes (Figure 2) and granulomatous and fibrinosuppurative to fibrosing pneumonia with myriad intralesional adult and larval metastrongyle nematodes and eggs. Fecal examination of the 2 affected rats revealed numerous live, ≈300-μm–long larvae with coiled posterior ends. Molecular analyses of ethanol-fixed adult nematodes within the pulmonary artery and fresh feces revealed genetic sequences of *A. cantonensis* lungworm.

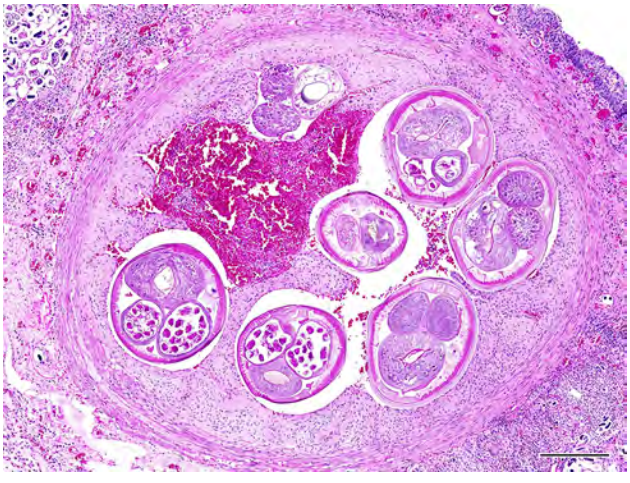

Figure 2. Lung tissue from a roof rat (*Rattus rattus*) with autochthonous rat lungworm *Angiostrongylus cantonensis* infection, San Diego, California, USA, 2025. Hematoxylin and eosin stain of pulmonary arteries with intravascular adult metastrongyle nematodes have severe endothelial proliferation. The surrounding lung parenchyma is replaced by granulomatous inflammation centered on numerous larvated and morulated eggs. Scale bar indicates 250 μm.

Concurrently, a local wildlife rehabilitation program had received multiple free-ranging juvenile Virginia opossums from throughout San Diego County (Figure 3) that exhibited ≥1 clinical signs, including dull mentation, circling, head tilt, ataxia, and respiratory distress. Most of the opossums were received during June–September in 2023–2025 and were euthanized after 0–3 days because of lack of clinical improvement. Ten opossums were submitted for postmortem examination. A consistent finding in 7 opossums was eosinophilic meningitis with intralesional metastrongyle nematodes (Appendix Figure), whereas 1 animal had eosinophilic meningitis without nematodes. The identity of the nematodes was confirmed as *A. cantonensis* lungworm in 6 of 7 animals through molecular analyses on formalin-fixed paraffin-embedded brain tissue (Appendix). We deposited generated nucleotide sequences from this study into GenBank (Table).

In addition, in an effort to investigate *A. cantonensis* lungworm in intermediate hosts, we opportunistically collected free-ranging slugs from the wallaby enclosure and adjacent areas at the San Diego Zoo (Appendix). One slug had nematode larvae encysted in various tissues, but we were unable to confirm the species identity.

Conclusions

We documented *A. cantonensis* infections in a zoo-housed parma wallaby (accidental host), free-ranging Virginia opossums (accidental host), and free-ranging roof rats (definitive host) in San Diego, California. Most cases were identified in 2025, but infection occurred as early as August 2023 in 1 opossum. Our findings indicate autochthonous infections, which

pose a substantial risk to humans and accidental vertebrate hosts. Whereas autochthonous infections had not previously been documented in the United States west of Texas, identifying angiostrongyliasis cases in wildlife in San Diego County provides support that *A. cantonensis* lungworm could now be considered endemic in this portion of southern California, with the potential to spread to other parts of the western continental United States.

Identifying the source of introduction of *A. cantonensis* lungworm into San Diego was beyond the scope of this study. In Louisiana, where the nematode was first identified in the continental United States in 1987, introduction was suspected to have been from infected rats on ships that docked in New Orleans (*3*). A similar situation is possible in this instance, given that San Diego is a major port city. However, the volume of traffic between regions on both national and international scales has dramatically expanded since the 1980s; thus, introduction of invasive species to new areas is a constant threat (*13*). A likely additional factor is the distributional spread of invasive gastropods (*4*,*8*) (Appendix).

Infections in the zoo-housed wallaby and free-ranging opossums were likely the result of ingestion of an infected intermediate host. The wallaby

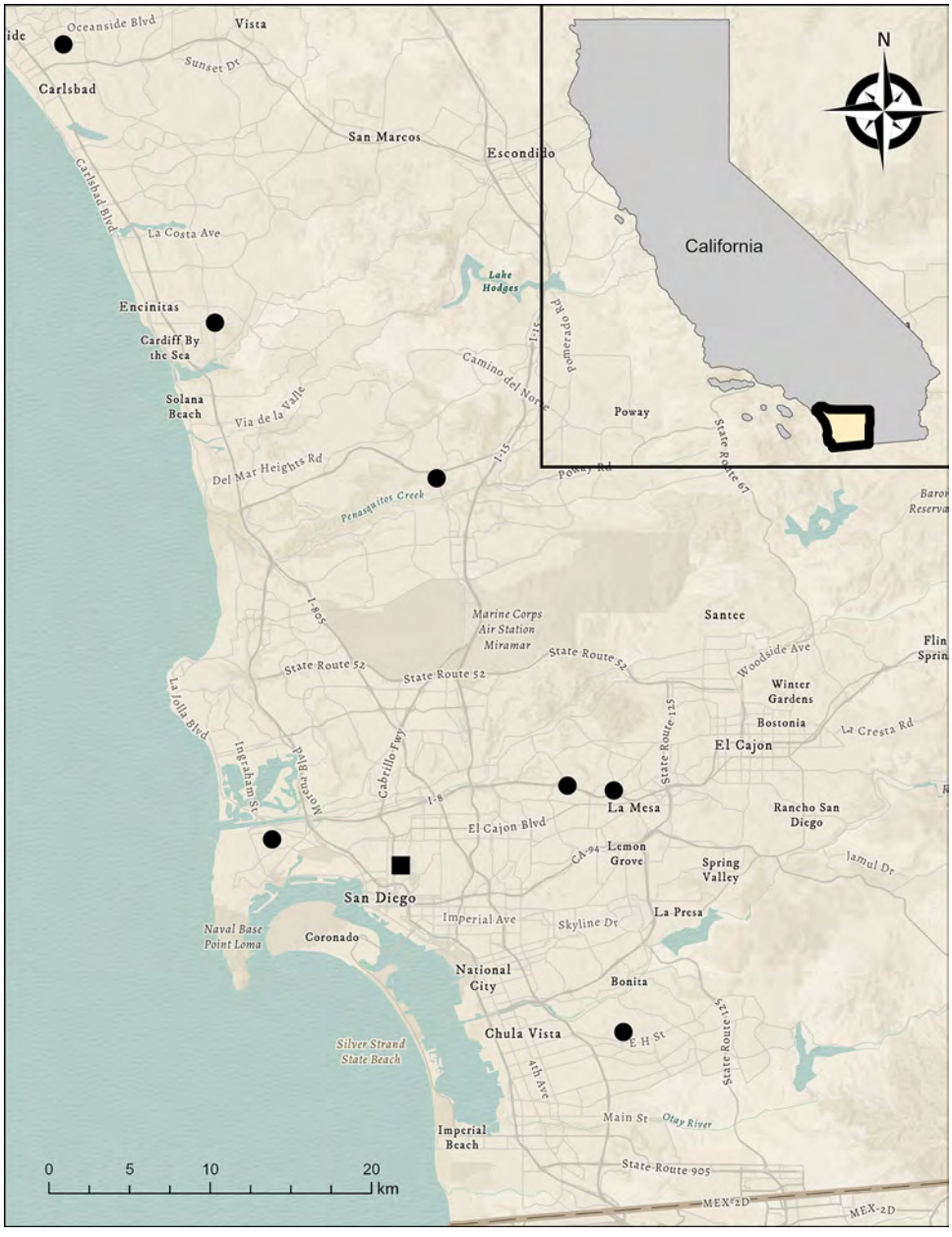

Figure 3. Distribution of Virginia opossums (*Didelphis virginiana*) identified with autochthonous rat lungworm *Angiostrongylus cantonensis* infections, San Diego, California, USA, 2023–2025. Black dots indicate opossum cases, which ranged over ≈68 km from north to south. The location of the San Diego Zoo, where cases of angiostrongyliasis were identified in a wallaby and rats, is included for reference (black square). Inset shows location of study area in California. Sources: Airbus Defence and Space, CGIAR, Danish Geodata Agency, Esri, Food and Agriculture Organization of the United Nations, Federal Emergency Management Agency, Garmin, General Services Admission, Geoland, Intermap, National Aeronautics and Space Administration, National Center for Ecological Analysis and Synthesis, National Geospatial-Intelligence Agency, National Land Service, National Mapping Agency, National Oceanic and Atmospheric Administration, ©OpenStreetMap contributors, Ordnance Survey, Rijkswaterstaat, Robinson Projection, TomTom, US Geological Society, Vantor, and the Geographic Information Systems user community.

Table. Clinical and molecular information for animals with autochthonous rat lungworm *Angiostrongylus cantonensis* infections, San Diego, California, USA, 2023–2025*

Case ID	Species	Sex	Age class	Death date	GenBank accession no.		
					COI	28S rRNA	18S rRNA
1	Parma wallaby	M	Adult	2024 Dec 17	PX623034	PX623182	PV933159
2	Roof rat	F	Adult	2025 Feb 3	PX623032	PX623180	PV933160
3	Roof rat	M	Adult	2025 Feb 5	PX623033	PX623181	PV933161
4	Virginia opossum	M	Juvenile	2023 Aug 27	PX623045	PX623179	NT
5	Virginia opossum	M	Juvenile	2025 Jun 27	PX623044	PX623178	NT
6	Virginia opossum	F	Juvenile	2025 Aug 15	NA†	PX663655	NT
7	Virginia opossum	F	Juvenile	2025 Sep 6	NA†	NA†	NT
8	Virginia opossum	M	Juvenile	2025 Sep 7	Partial‡	PX623200	NT
9	Virginia opossum	M	Juvenile	2025 Sep 7	Partial‡	PX663656	NT
10	Virginia opossum	M	Juvenile	2025 Sep 12	NA†	PX623201	NT

*ID, identification; COI, cytochrome C oxidase subunit I gene; NA, no amplification; NT, not tested.
†Lack of specific amplification after multiple PCR and sequencing attempts was attributed to the sample type (formalin-fixed paraffin embedded tissue).
‡Obtained partial sequences were too short to be deposited in GenBank.

was fed a commercially manufactured extruded diet with a mixture of grass hay and occasional browse material and fresh produce safe for human consumption; ingestion of an intermediate host was considered accidental environmental exposure. In contrast, opossums are naturally more vulnerable to infection, given that gastropods constitute a prominent part of their native diet, especially during the summer months (*14*). All the opossums identified with angiostrongyliasis in our study were juveniles found in the summer, suggesting the juvenile age group and summer season are risk factors for infection in this species.

A. cantonensis infection has previous been identified at the San Diego Zoo. In 2011, an African pygmy falcon (*Polihierax semitorquatus*) hatched and raised at the San Diego Zoo was diagnosed with meningoencephalitis caused by *A. cantonensis* infection (*15*). At that time, 20 free-ranging rats on the zoo grounds were opportunistically screened for nematode larvae in feces, but infection was not detected. With no detection in definitive hosts, the source of infection in that case and in 2 subsequent African pygmy falcons in 2014 and 2018 (San Diego Zoo, unpub. data) was suspected to be live feeder lizards (paratenic hosts) imported from Southeast Asia, where the parasite is endemic. However, given the prevalence (albeit low at 3.1%) of infected rats in our study, the parasite possibly has been present but undetected in San Diego County for some time.

In conclusion, we documented autochthonous *A. cantonensis* infections in southern California, highlighting a notable expansion of the range of this parasite in North America. Further studies are needed to analyze the effect of this geographic expansion and associated risks in California. Nevertheless, angiostrongyliasis should be part of the differential diagnosis for central nervous system disease in humans and animals in the wider southern United States.

Acknowledgments

We thank the Disease Investigations, Veterinary Services, and Clinical Laboratory teams as well as Trent Stanley and the animal care staff at the San Diego Zoo Wildlife Alliance for their assistance in this study. We additionally thank the San Diego Humane Society's Project Wildlife team for their support in sample collection and record maintenance, as well as John Randolph for producing the map used in this study and Molly Jarrells for assistance with case tracking. We also acknowledge Hernando Acevedo for assisting with postmortem examination of a Virginia opossum.

Testing of Virginia opossums was funded by the California Department of Fish and Wildlife through agreement no. P2480005 with the San Diego Zoo Wildlife Alliance.

About the Author

Dr. Nakagun is a veterinary pathologist at the San Diego Zoo Wildlife Alliance, San Diego, California, USA. His research interest focuses on infectious diseases in zoo and wildlife species.

References

1. Wang QP, Lai DH, Zhu XQ, Chen XG, Lun ZR. Human angiostrongyliasis. Lancet Infect Dis. 2008;8:621–30. https://doi.org/10.1016/S1473-3099(08)70229-9
2. Chen HT. A new pulmonary nematode, *Pulmonema cantonensis* n. g., n. sp., from rats in Canton [in French]. Ann Parasitol Hum Comp. 1935;13:312–7. https://doi.org/10.1051/parasite/1935134312
3. Campbell BG, Little MD. The finding of *Angiostrongylus cantonensis* in rats in New Orleans. Am J Trop Med Hyg. 1988;38:568–73. https://doi.org/10.4269/ajtmh.1988.38.568
4. Stockdale Walden HD, Slapcinsky JD, Roff S, Mendieta Calle J, Diaz Goodwin Z, Stern J, et al. Geographic distribution of *Angiostrongylus cantonensis* in wild rats (*Rattus rattus*) and terrestrial snails in Florida, USA. PLoS One. 2017; 12:e0177910. https://doi.org/10.1371/journal.pone.0177910
5. York EM, Creecy JP, Lord WD, Caire W. Geographic range expansion for rat lungworm in North America. Emerg Infect Dis. 2015;21:1234–6. https://doi.org/10.3201/eid2107.141980

6. Gottdenker NL, Nascimento Ramos RA, Hakimi H, McHale B, Rivera S, Miller BM, et al. *Angiostrongylus cantonensis* infection in brown rats (*Rattus norvegicus*), Atlanta, Georgia, USA, 2019–2022. Emerg Infect Dis. 2023;29:2167–70. https://doi.org/10.3201/eid2910.230706
7. Achatz TJ, Chun CH, Young MA, Page J, Rowe M, Cooper C, et al. Detection of rat lungworms in invasive mollusks, Georgia, USA, 2024. Emerg Infect Dis. 2025;31:1852–4. https://doi.org/10.3201/eid3109.250133
8. Sierra DA, Sanders TL, Edwards EE, Molter CM, Verocai GG. Zoonotic rat lungworm *Angiostrongylus cantonensis* in black rats, Houston, Texas, 2024. Emerg Infect Dis. 2025;31:1857–60. https://doi.org/10.3201/eid3109.251710
9. Kottwitz JJ, Perry KK, Rose HH, Hendrix CM. *Angiostrongylus cantonensis* infection in captive Geoffroy's tamarins (*Saguinus geoffroyi*). J Am Vet Med Assoc. 2014;245:821–7. https://doi.org/10.2460/javma.245.7.821
10. Costa LRR, McClure JJ, Snider TG III, Stewart TB. Verminous meningoencephalomyelitis by *Angiostrongylus* (=*Parastrongylus*) *cantonensis* in an American miniature horse. Equine Vet Educ. 2000;12:2–6. https://doi.org/10.1111/j.2042-3292.2000.tb01754.x
11. Flerlage T, Qvarnstrom Y, Noh J, Devincenzo JP, Madni A, Bagga B, et al. *Angiostrongylus cantonensis* eosinophilic meningitis in an infant, Tennessee, USA. Emerg Infect Dis. 2017;23:1756–8. https://doi.org/10.3201/eid2310.170978
12. Liu EW, Schwartz BS, Hysmith ND, DeVincenzo JP, Larson DT, Maves RC, et al. Rat lungworm infection associated with central nervous system disease—eight U.S. states, January 2011–January 2017. MMWR Morb Mortal Wkly Rep. 2018;67:825–8. https://doi.org/10.15585/mmwr.mm6730a4
13. Hulme PE. Trade, transport and trouble: managing invasive species pathways in an era of globalization. J Appl Ecol. 2009;46:10–8. https://doi.org/10.1111/j.1365-2664.2008.01600.x
14. Hopkins DD, Forbes RB. Dietary patterns of the Virginia opossum in an urban environment. Murrelet. 1980;61:20–30. https://doi.org/10.2307/3536187
15. Burns RE, Bicknese EJ, Qvarnstrom Y, DeLeon-Carnes M, Drew CP, Gardiner CH, et al. Cerebral *Angiostrongylus cantonensis* infection in a captive African pygmy falcon (*Polihierax semitorquatus*) in southern California. J Vet Diagn Invest. 2014;26:695–8. https://doi.org/10.1177/1040638714544499

Address for correspondence: Shotaro Nakagun, San Diego Zoo Wildlife Alliance, PO Box 120551, San Diego, CA 92112-0551, USA; email: snakagun@gmail.com

Temporal Clustering of *Mycoplasma pneumoniae*–Associated Encephalitis and Stroke, South Korea, 2024

Seung Ha Song, Dayun Kang, Ye Kyung Kim, Jaeso Cho, Hye Jin Kim, Woojoong Kim, Ki Wook Yun

Seventeen pediatric encephalitis (n = 12) or stroke (n = 5) cases clustered temporally during the 2023–2024 *Mycoplasma pneumoniae* epidemic in South Korea; similar patterns had not been noted in previous seasons. Those findings might reflect postpandemic changes in clinical manifestation and underscore the need for neurologic surveillance during *M. pneumoniae* epidemics.

Mycoplasma pneumoniae is a major cause of community-acquired pneumonia in children and can also lead to extrapulmonary complications affecting multiple organ systems, including the central nervous system (CNS) (*1*,*2*). Neurologic complications, including encephalitis and stroke, are clinically consequential because of their severity and sequelae.

During the COVID-19 pandemic, nonpharmaceutical interventions markedly reduced the circulation of common respiratory pathogens, including *M. pneumoniae* (*3*). However, since 2023, a resurgence of *M. pneumoniae* has been reported worldwide (*4*). Amid this resurgence, we observed increased numbers of pediatric encephalitis and ischemic stroke cases associated with *M. pneumoniae* in South Korea during the 2023–2024 season (*5*). To better characterize that phenomenon, we analyzed the clinical features and outcomes of affected children and evaluated institutional and national surveillance data to place those findings in broader temporal and epidemiologic contexts.

Author affiliations: SMG-SNU Boramae Medical Center, Seoul, South Korea (S.H. Song, H.J. Kim); Seoul National University College of Medicine, Seoul (S.H. Song, K.W. Yun); Seoul National University Children's Hospital, Seoul (D. Kang, W. Kim, K.W. Yun); Seoul National University Bundang Hospital, Seoul National University College of Medicine, Seongnam, South Korea (Y.K. Kim, J. Cho)

DOI: https://doi.org/10.3201/eid3202.251296

The Study

We conducted a retrospective study of children hospitalized with encephalitis or ischemic stroke at 2 tertiary hospitals (center A, Seoul; center B, Seongnam) and 1 secondary care hospital (center C, Seoul) during the October 2023–December 2024 *M. pneumoniae* epidemic in South Korea, as defined by the Korea Disease Control and Prevention Agency surveillance program (Appendix Figure 1, https://wwwnc.cdc.gov/EID/article/32/2/25-1296-App1.pdf). *M. pneumoniae* infection was confirmed by using PCR of respiratory samples or by using serology (particle agglutination titer ≥1:160 or IgM index ≥1.4 by using enzyme-linked immunosorbent assay) (*6*). We defined encephalitis as an altered mental status lasting ≥24 hours with supportive tests and stroke as focal deficits with radiographic infarctions.

We identified 17 cases of *M. pneumoniae*–associated encephalitis (n = 12) or ischemic stroke (n = 5). Of those cases, 13 occurred at center A, 4 at center B, and none at center C. Most cases were clustered during June–December 2024, which coincided with a marked increase in *M. pneumoniae* infections (Figure 1).

The median patient was 8.8 years of age; 52.9% of the patients were male and 47.1% female. Although 4 patients had no preceding respiratory symptoms, pneumonia was documented in 11 patients. The median interval from respiratory to neurologic symptom onset was 3 days (range 2–8 days). *M. pneumoniae* infection was confirmed in all 17 patients; 10 cases were confirmed by using both PCR (respiratory specimens) and serology, 6 cases by using serology, and 1 by using PCR (respiratory specimen). Cerebrospinal fluid PCR was performed on samples from 2 patients (1 positive case and 1 indeterminate case), and cerebrospinal fluid serology for *M. pneumoniae* was not performed. No other infectious or autoimmune etiologies were detected in the 17 patients. All 5 stroke patients

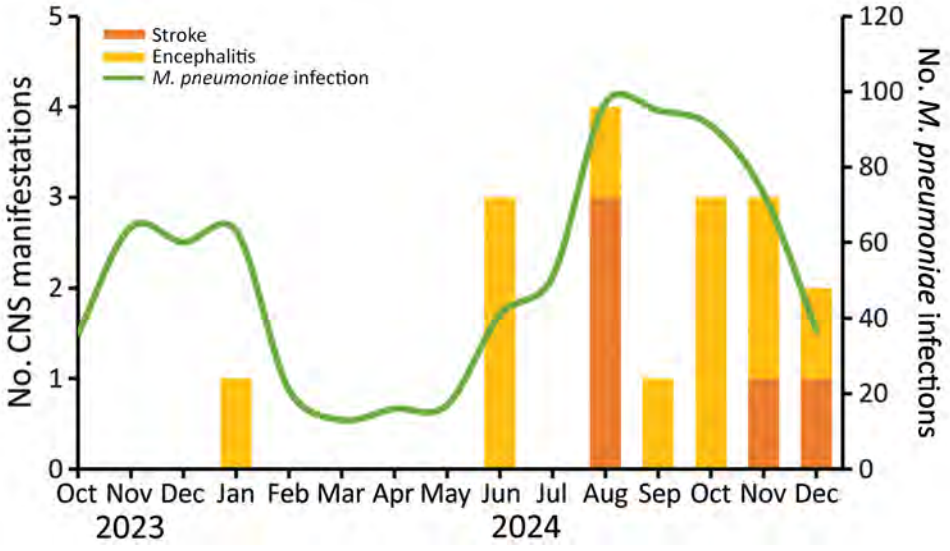

Figure 1. Monthly pediatric stroke and encephalitis cases (stacked bars) and *Mycoplasma pneumoniae* infections (green line) on the basis of aggregated data obtained from 3 hospitals in South Korea, October 2023–December 2024. Scales for the y-axes differ substantially to underscore patterns but do not permit direct comparisons.

had large-vessel infarctions in the middle cerebral artery or anterior cerebral artery territories; moreover, the clinical manifestations of 4 patients included multiterritorial involvement. Brain magnetic resonance imaging abnormalities (typically involving diffusion restriction or T2-weighted fluid-attenuated inversion recovery hyperintensities in the hippocampus, basal ganglia, or thalamus) were identified in 42% of the encephalitis patients.

Seven patients required intensive care unit admission. Twelve patients received intravenous antimicrobial drugs and 9 received corticosteroids; in addition, intravenous immunoglobulin was administered to 4 encephalitis patients. The outcomes were favorable; at the last follow-up, 83.3% of encephalitis and 60.0% of stroke patients demonstrated a modified Rankin scale score ≤2 (0–2 = no to mild disability), and no deaths were reported (Appendix Table 1).

During the same period (October 2023–December 2024), we identified 193 *M. pneumoniae*–associated hospitalizations without CNS involvement at the 3 hospitals for comparison. The median age and proportion of male patients were similar between the groups; however, the CNS complication group

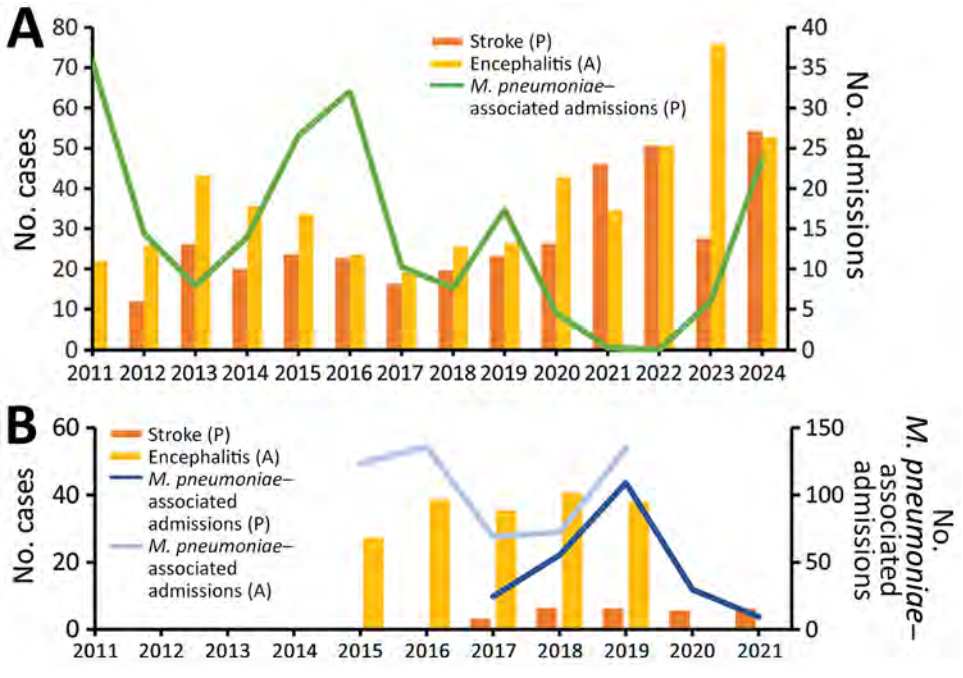

Figure 2. Annual trends in pediatric *Mycoplasma pneumoniae*–associated admissions and central nervous system complications in South Korea. A) Data obtained from 3 hospitals during 2011–2024. Bars represent ischemic stroke and encephalitis cases per 10,000 pediatric hospitalizations. Data line indicates annual *M. pneumoniae*–associated pediatric admissions per 1,000 hospitalizations. B) National data from 2015–2021. Bars show annual pediatric stroke and all-age encephalitis cases. Data lines represent *M. pneumoniae*–associated hospitalizations in pediatric and all-age populations reported to the Korea Disease Control and Prevention Agency sentinel surveillance system. All values in panel B are presented on a 1/100 scale. A, all age; P, pediatric. Scales for the y-axes differ substantially to underscore patterns but do not permit direct comparisons.

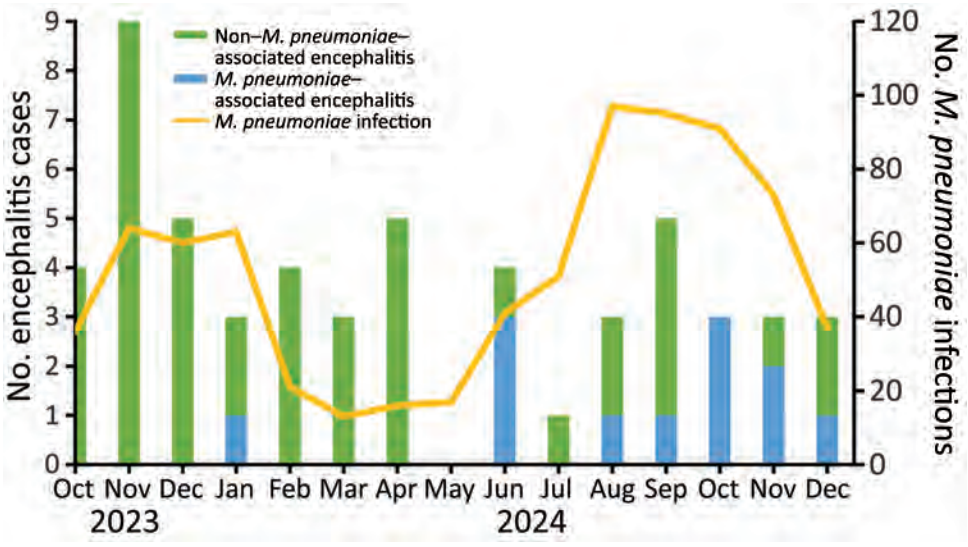

Figure 3. Monthly encephalitis cases by *Mycoplasma pneumoniae* association during the 2023–2024 epidemic, with concurrent *M. pneumoniae* infections (October 2023–December 2024). The bars show monthly encephalitis hospitalizations aggregated across 3 hospitals, which were divided into *M. pneumoniae*–associated and non–*M. pneumoniae*–associated cases. Data line denotes the number of *M. pneumoniae* infections identified at the 3 hospitals.

demonstrated substantially longer hospital stays (29 vs. 6 days; p<0.001) and a higher intensive care unit admission rate (41% vs. 3%; p<0.001) (Appendix Table 2).

We analyzed data from 2011–2024 to evaluate long-term trends in pediatric stroke, encephalitis, and *M. pneumoniae*–associated hospitalizations, which were identified by using administrative diagnostic codes from standardized clinical data warehouse records; in addition, we normalized annual case counts by total pediatric admissions for comparison. At the institutional level, the stroke and encephalitis rates did not consistently align with *M. pneumoniae* epidemic activity; however, both rates increased after 2020, possibly reflecting broader effects of the COVID-19 pandemic and its aftermath (Figure 2, panel A). In contrast, a distinct temporal overlap emerged in 2024; during June–December, *M. pneumoniae* infections accounted for 20%–100% of monthly encephalitis admissions across sites (Figure 3), suggesting a temporal association between *M. pneumoniae* circulation and neurologic complications during the epidemic.

We assessed nationwide trends in *M. pneumoniae*-associated admissions, encephalitis, and pediatric stroke from public datasets. We obtained *M. pneumoniae*–associated hospitalization data from the Korea Disease Control and Prevention Agency sentinel surveillance program (*5*), pediatric stroke data from the Korean Statistical Information Service (*7*), and nationwide encephalitis data from health insurance claims, excluding cases with confirmed pathogens (*8*). The incidence of encephalitis (all ages) remained stable from 2015–2019, with no apparent temporal association being detected with *M. pneumoniae* activity. In addition, the pediatric stroke data obtained from 2017–2021 did not demonstrate a temporal relationship with monthly *M. pneumoniae* activity (Figure 2, panel B).

The absence of temporal associations during previous epidemics contrasts with the clear increase in *M. pneumoniae*–associated CNS cases in 2024. That pattern might be partially explained by the immunity gap hypothesis (*9*), whereby prolonged suppression of respiratory pathogens during COVID-19 nonpharmaceutical interventions increased pediatric susceptibility, which is consistent with shifts in age distribution and disease severity reported in other studies (*10*,*11*). *M. pneumoniae* neurologic complications might result from direct CNS invasion, immune-mediated damage, and cerebrovascular occlusion *(12*). In this context, an increase in primary *M. pneumoniae* infections among seronegative children during 2023–2024 plausibly increased the risk for immune-mediated CNS complications; however, that relationship warrants further investigation. Moreover, strain features might contribute to increased severity; in 2023–2024, several studies reported P1 type 1 predominance and widespread A2063G macrolide resistance, accompanied by a high proportion of severe pulmonary manifestations (*13*,*14*). Strains exhibiting greater neurotropism might have been circulating during this period, although further validation is needed. Increased clinical awareness and the large scale of the epidemic might have increased the absolute number of rare complications.

The first limitation of this study is that the use of serologic testing to confirm *M. pneumoniae* infection reveals known constraints, including potential false positivity, delayed antibody responses, and interassay variability. Second, nationwide datasets lacked

monthly resolution and pediatric detail and originated from different sources (the Korean Statistical Information Service and insurance claims data), limiting comparability. Finally, the absence of pathogen characterization precluded the evaluation of strain-specific factors potentially associated with neurologic complications.

Conclusions

Despite those limitations, our study provides clinical data highlighting increased pediatric CNS manifestations of *M. pneumoniae* infection observed during the 2023–2024 epidemic. In contrast to prior years, we observed a distinct temporal clustering of *M. pneumoniae*–associated CNS manifestations in South Korea in 2024. It is unclear whether the observed pattern reflects diagnostic capacity, heightened clinical vigilance, or a true shift in disease dynamics potentially driven by host, pathogen, or environmental factors. Further large-scale and longitudinal studies are warranted to determine whether this clustering represents an isolated event or signals an emerging trend in pediatric infectious diseases. Our findings underscore the importance of sustained epidemiologic surveillance and molecular characterization of circulating strains to better elucidate the mechanisms underlying extrapulmonary complications of *M. pneumoniae* infection.

About the Author

Dr. Song is a clinical assistant professor in the Department of Pediatrics, Division of Infectious Diseases, SMG-SNU Boramae Medical Center, Seoul, South Korea. Her research interests include pediatric respiratory infections, including *M. pneumoniae* and respiratory syncytial virus.

References

1. Waites KB, Xiao L, Liu Y, Balish MF, Atkinson TP. *Mycoplasma pneumoniae* from the respiratory tract and beyond. Clin Microbiol Rev. 2017;30:747–809. https://doi.org/10.1128/CMR.00114-16
2. Narita M. Pathogenesis of extrapulmonary manifestations of *Mycoplasma pneumoniae* infection with special reference to pneumonia. J Infect Chemother. 2010;16:162–9. https://doi.org/10.1007/s10156-010-0044-X
3. Chow EJ, Uyeki TM, Chu HY. The effects of the COVID-19 pandemic on community respiratory virus activity. Nat Rev Microbiol. 2023;21:195–210.
4. Meyer Sauteur PM, Beeton ML, Pereyre S, Bébéar C, Gardette M, Hénin N, et al.; European Society of Clinical Microbiology and Infectious Diseases (ESCMID) Study Group for Mycoplasma and Chlamydia Infections (ESGMAC), and the ESGMAC Mycoplasma pneumoniae Surveillance (MAPS) study group. *Mycoplasma pneumoniae*: delayed re-emergence after COVID-19 pandemic restrictions. Lancet Microbe. 2024;5:e100–1. https://doi.org/10.1016/S2666-5247(23)00344-0
5. Korea Disease Control and Prevention Agency. Acute respiratory infections surveillance system. 2025 [cited 2025 Aug 22]. https://dportal.kdca.go.kr/pot/is/st/ari.do
6. Kim G, Yun KW, Kang D, Lee TJ, Eun BW, Lee H, et al. Diagnostic accuracy of serological tests for *Mycoplasma pneumoniae* infections in children with pneumonia, based on symptom onset. Ann Lab Med. 2025. https://doi.org/10.3343/alm.2025.0125
7. Korean Statistical Information Service. National stroke-related hospitalization statistics [cited 2025 Aug 22]. https://kosis.kr/index/index.do
8. Kim SH, Baek JY, Han M, Lee M, Lim SM, Lee JY, et al. A decrease in the incidence of encephalitis in South Korea during the COVID-19 pandemic: a nationwide study between 2010 and 2021. J Med Virol. 2023;95:e28490. https://doi.org/10.1002/jmv.28490
9. Cohen R, Ashman M, Taha M-K, Varon E, Angoulvant F, Levy C, et al. Pediatric Infectious Disease Group (GPIP) position paper on the immune debt of the COVID-19 pandemic in childhood, how can we fill the immunity gap? Infect Dis Now. 2021;51:418–23. https://doi.org/10.1016/j.idnow.2021.05.004
10. Dungu KHS, Holm M, Hartling U, Jensen LH, Nielsen AB, Schmidt LS, et al. *Mycoplasma pneumoniae* incidence, phenotype, and severity in children and adolescents in Denmark before, during, and after the COVID-19 pandemic: a nationwide multicentre population-based cohort study. Lancet Reg Health Eur. 2024;47:101103. https://doi.org/10.1016/j.lanepe.2024.101103
11. You J, Zhang L, Chen W, Wu Q, Zhang D, Luo Z, et al. Epidemiological characteristics of *Mycoplasma pneumoniae* in hospitalized children before, during, and after COVID-19 pandemic restrictions in Chongqing, China. Front Cell Infect Microbiol. 2024;14:1424554. https://doi.org/10.3389/fcimb.2024.1424554
12. Narita M. Pathogenesis of neurologic manifestations of *Mycoplasma pneumoniae* infection. Pediatr Neurol. 2009;41:159–66. https://doi.org/10.1016/j.pediatrneurol.2009.04.012
13. Chen Y, Li X, Fu Y, Yu Y, Zhou H. Whole-genome sequencing unveils the outbreak of *Mycoplasma pneumoniae* in mainland China. Lancet Microbe. 2024;5:100870. https://doi.org/10.1016/S2666-5247(24)00086-7
14. Xu L, Wang P, Wang Y, Liu B, Xu X, Yang Q, et al. Epidemiological, clinical, and genotypic characteristics of pediatric *Mycoplasma pneumoniae* infections: an 8-year survey in Suzhou, China in the pre- and post-COVID-19 eras. Front Microbiol. 2024;15:1483152. https://doi.org/10.3389/fmicb.2024.1483152

Address for correspondence: Ki Wook Yun, Department of Pediatrics, Seoul National University Children's Hospital, 101, Daehak-ro Jongno-gu, 03080, South Korea; email: pedwilly@snu.ac.kr

Case of *Legionella pneumophila* Serogroup 1 Infection Linked to Water Flosser, France

Céline Slekovec, Adrien Biguenet, Audrey Jeanvoine, Didier Hocquet, Xavier Bertrand

Legionnaires' disease is a severe respiratory infection that causes increased mortality in hospitalized and immunocompromised patients. We report a nosocomial case in France linked to a water flosser. Our findings underscore the need for vigilance regarding such devices and highlight strategies for their safe management within healthcare settings.

Legionnaires' disease is a respiratory infection caused by inhaling particles contaminated with *Legionella* spp. bacteria (*1*). Although most cases are community-acquired, mortality is nearly 3 times higher for hospital-acquired infections (8.6% vs. 28.6%) (*2*), especially among immunocompromised patients (*3*). This increase in mortality underscores the need for routine monitoring of water systems and the use of protective measures such as point-of-use filters. Environmental investigations are critical for identifying sources of contamination; however, whereas healthcare facilities have the infrastructure to conduct such investigations, implementation in private homes remains challenging. Of consequence, extra-hospital sources of exposure are likely underrecognized. In this article, we describe a case of nosocomial Legionnaires' disease traced to a water flosser from the patient's home.

The Study

A 48-year-old man with IgG Kappa myeloma was hospitalized in August 2024 for a peripheral autologous hematopoietic stem cell transplantation in the hematology unit of Besançon University Hospital (Besançon, France). On day 4, the patient underwent an autograft without complications. On day 10, a fever developed, and *Escherichia coli* was isolated from blood cultures. We began piperacillin/tazobactam (4 g every 6 hours) therapy adapted to the strain resistance profile, and the following blood cultures were negative. However, the fever persisted, and respiratory symptoms developed on day 16. His condition worsened on day 17, and we transferred the patient to the medical intensive care unit (MICU). At admission in MICU, results of a BinaxNOW Legionella urinary antigen test for *Legionella pneumophila* serogroup 1 (Lp1) (Abbott, https://www.abbott.com) were positive. The same day, we detected Lp1 by using PCR on bronchoalveolar samples and cultured endotracheal aspiration samples. No tests for *Legionella* spp. were conducted before day 17. The respiratory distress syndrome caused by pneumonia led to a stay in MICU with mechanical ventilation, dialysis, and cardiorespiratory arrest without sequelae. The patient experienced multiple organ failure with acute renal failure requiring extrarenal purification. Complications including necrosis of the extremities, sacral pressure ulcer, malnutrition, and amyotrophy developed. His condition gradually improved, enabling his discharge from MICU after 47 days.

Because the incubation period was consistent with acquisition in the hematology unit, we searched for environmental sources of *Legionella* spp. During his hospitalization in the unit, the patient stayed in a room intended for immunocompromised patients, and the sink and shower were equipped with the Filt'Ray 2G anti-*Legionella* filters (Aquatools, https://www.aqua-tools.com). We took water samples from the bathroom in the patient's room (sink and shower with and without filter and the toilet bowl).

We analyzed samples in accordance with the NF T 90-431 standard (Association Française de

Author affiliations: Centre Hospitalier Universitaire, Besançon, France (C. Slekovec, A. Biguenet, A. Jeanvoine, D. Hocquet, X. Bertrand); Université Marie et Louis Pasteur, Besançon (C. Slekovec, A. Biguenet, D. Hocquet, X. Bertrand).

DOI: https://doi.org/10.3201/eid3202.251386

Normalization, https://www.afnor.org) for counting *Legionella* spp. We sampled 500 mL of water in sterile vials containing 20 mg sodium thiosulfate. First, we inoculated 0.2 mL of water on glycine, vancomycin, polymyxin, cycloheximide plates (Thermo Fisher Scientific, https://www.thermofisher.com). Then, we filtered 10 mL and 100 mL of water through 0.2-µm pore polycarbonate membranes placed on glycine, vancomycin, polymyxin, cycloheximide media. We incubated the plates at 36°C (±2°C) for 8–11 days. We subcultured suspicious colonies to buffered charcoal yeast extract media with and without cystein and identified them by using matrix-assisted laser desorption/ionization time-of-flight mass spectrometry (Bruker, https://www.bruker.com).

We tested the mixed water from the sink and shower (with the filter and after removing the filter) and the toilet bowl water and did not find evidence of *Legionella* spp. In addition, the 10 routine tests conducted in 2024 on the water network supplying the ward were also all negative for *Legionella* spp. During the environmental investigation, a water flosser (Panasonic, https://www.panasonic.com) was found in the patient's bathroom. This device was not listed in the inventory performed at admission to the hematology department. The device belonged to the patient, which he used at home with tap water, and it was brought in without informing the healthcare team. Because the patient was unable to be interviewed, we were unable to gather information on the use of the device (i.e., frequency of use during hospitalization, type of water used, frequency of cleaning and disinfection). To sample the water flosser, we filled its tank with sterile water, ran the device, and collected 100 ml of water from the jet. We recovered Lp1 and *L. pneumophila* serogroup 2–14 at a concentration of 300 CFU/L (Figure).

We sequenced the genomes of the 2 Lp1 isolates (1 from the patient and 1 from the water flosser) by using Oxford Nanopore technology (Oxford Nanopore, https://nanoporetech.com). We assembled genomes by using Flye (*4*) and deduced sequence types from whole-genome sequencing data by using legsta (https://github.com/tseemann/legsta). The 2 strains had identical genomes and belonged to sequence type 42, which has been described in France and other countries but is not a major clone (*5*).

Our investigation indicates it is likely the clinical strain and the Lp1 strain identified from the water flosser have a common origin. After this incident, no new cases have been reported in our hospital. The patient was ultimately hospitalized for 62 days, including 47 days in MICU.

Conclusions

We report a case of Legionnaires' disease transmitted by a contaminated water flosser. This conclusion was supported by the genomic identity of Lp1 isolates recovered from the patient and water flosser. The other commonly suspected sources, such as shower or sink, or less common, such as toilet (*6*,*7*), were negative for *Legionella* spp. The *Legionella* spp. found in the device (including Lp1, responsible for infection, and *L. pneumophila* serogroup 2–14) likely originated from the patient's home water network. Unfortunately, no investigation could be conducted to confirm that suspicion. Moreover, the reservoir of the device showed signs of fouling, indicative of the use of nonsterile water and the lack of regular cleaning. Most

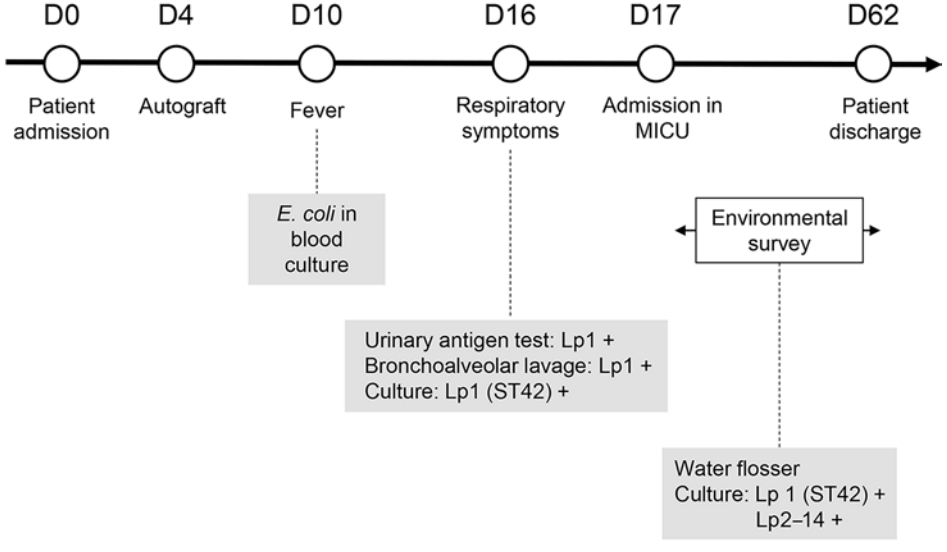

Figure. Timeline of patient hospitalization, symptoms, and tests performed in a case of *Legionella pneumophila* serogroup 1 infection linked to water flosser, France. D, day; Lp1, *Legionella pneumophila* serogroup 1; Lp2–14, *Legionella pneumophila* serogroups 2–14; MICU, medical intensive care unit; ST, sequence type; +, positive.

manufacturers do not advocate for the use of sterile or microbiologically controlled water; instead, they recommend regular cleaning and disinfection procedures. The global water flosser market is experiencing growth ($966.726 million in 2021, projected to reach $1,189 million by 2025), driven by increased awareness of oral hygiene, a growing preference for wireless and portable devices, and guidelines issued by oral health professionals (*8*). Because of the increasing use of such devices, a growing number of immunocompromised patients at risk of Legionnaires' disease could be exposed. We did not find other cases of contamination through water flossers reported in the literature, indicating a low risk; nevertheless, unrecognized cases cannot be excluded.

Water flossers might provide favorable conditions for bacterial growth, especially *Legionella* spp. The use of nonsterile water can lead to biofilm accumulation within the device tubing. In addition, the pressurized spray directed into the patient's mouth may generate aerosols that are readily inhaled. Several studies have demonstrated bacterial colonization of water flossers and the potential transmission of contaminated water jets; in particular, colonization by the major caries-associated pathogen *Streptococcus mutans* appears difficult to prevent (*9*,*10*). Therefore, it is necessary to raise awareness among manufacturers and users regarding the potential risk to immunocompromised patients. In healthcare settings, the use of such devices should be carefully controlled to prevent nosocomial Legionnaires' disease, and healthcare workers should be aware of the potential risk of devices being brought from the outside into healthcare settings by patients or family members. Our report demonstrates that despite all the measures implemented in hospitals to control the risk for *Legionella* spp. transmission to immunocompromised patients, attention should be paid to unconventional modes of *Legionella* spp. transmission.

Acknowledgment

We thank the healthcare teams and all those who contributed to the investigation of this case. We also acknowledge the patient for his cooperation.

The study was approved by the Institutional Review Board of Besançon University Hospital and conducted in accordance with the principles of the Declaration of Helsinki. Patients were informed about the use of their data during hospitalization and had the right to refuse participation in the study.

About the Author

Dr. Slekovec is a pharmacist specializing in infection prevention and control at the University Hospital of Besançon, France. His research focuses on improving the prevention of healthcare-associated infections, particularly those related to waterborne pathogens such as *Legionella pneumophila* and *Pseudomonas aeruginosa*.

References

1. Rello J, Allam C, Ruiz-Spinelli A, Jarraud S. Severe Legionnaires' disease. Ann Intensive Care. 2024;14:51. https://doi.org/10.1186/s13613-024-01252-y
2. Beauté J, Plachouras D, Sandin S, Giesecke J, Sparén P. Healthcare-associated Legionnaires' disease, Europe, 2008–2017. Emerg Infect Dis. 2020;26:2309–18.
3. Francois Watkins LK, Toews KE, Harris AM, Davidson S, Ayers-Millsap S, Lucas CE, et al. Lessons from an outbreak of Legionnaires' disease on a hematology-oncology unit. Infect Control Hosp Epidemiol. 2017;38:306–13. https://doi.org/10.1017/ice.2016.281
4. Kolmogorov M, Yuan J, Lin Y, Pevzner PA. Assembly of long, error-prone reads using repeat graphs. Nat Biotechnol. 2019;37:540–6. https://doi.org/10.1038/s41587-019-0072-8
5. Pijnacker R, Brandsema P, Euser S, Vahidnia A, Kuiter A, Limaheluw J, et al. An outbreak of Legionnaires' disease linked to a municipal and industrial wastewater treatment plant, The Netherlands, September–October 2022. Euro Surveill. 2024;29:2300506. https://doi.org/10.2807/1560-7917.ES.2024.29.20.2300506
6. Couturier J, Ginevra C, Nesa D, Adam M, Gouot C, Descours G, et al. Transmission of Legionnaires' disease through toilet flushing. Emerg Infect Dis. 2020;26:1526–8. https://doi.org/10.3201/eid2607.190941
7. Bechmann L, Bauer K, Zerban P, Esser T, Tersteegen A, Fuchs SA, et al. Prevention of *Legionella* infections from toilet flushing cisterns. J Hosp Infect. 2024;146:37–43. https://doi.org/10.1016/j.jhin.2023.12.016
8. Zarei Z, Yazdi M, Sadeghalbanaei L, Tahamtan S. The effectiveness of oral irrigators on periodontal health status and oral hygiene of orthodontic patients: a systematic review and meta-analysis. BMC Oral Health. 2024;24:1469. https://doi.org/10.1186/s12903-024-05255-w
9. Bertl K, Geissberger C, Zinndorf D, Johansson PE, Al-Shammari H, Eick S, et al. Bacterial colonisation during regular daily use of a power-driven water flosser and risk for cross-contamination. Can it be prevented? Clin Oral Investig. 2022;26:1903–13. https://doi.org/10.1007/s00784-021-04167-1
10. Bertl K, Edlund Johansson P, Bruckmann C, Leonhard M, Davies JR, Stavropoulos A. Bacterial colonization of a power-driven water flosser during regular use. A proof-of-principle study. Clin Exp Dent Res. 2021;7:656–63. https://doi.org/10.1002/cre2.393

Address for correspondence: Xavier Bertrand, Hygiène Hospitalière, Centre Hospitalier Universitaire, 3 boulevard Fleming, Besançon CEDEX 25030, France; email: xbertrand@chu-besancon.fr

Neospora caninum Infection in Marine Mammals Stranding in Northeastern Pacific Ocean Region

Stephen A. Raverty, Pádraig Duignan, Dyanna M. Lambourn, Paul Cottrell, Verena A. Gill,[1] Pamela Tuomi, Lorraine Barbosa, Brendan Cottrell, Spencer L. Magargal, Amanda K. Gibson, Elizabeth R. Zhang, Michael E. Grigg

We used immunohistochemistry and PCR to identify *Neospora caninum* in 6 infected marine mammal species, including 2 pups, that stranded in the northeastern Pacific Ocean. Our findings suggest the expansion of this parasite's host range to marine mammals, underscoring the effect of terrestrial pathogens that flow from land to sea.

Researchers using immunohistochemistry and PCR-DNA sequencing analyses have confirmed high infection rates of the protozoan parasites *Toxoplasma gondii* and *Sarcocystis neurona*, often as mixed infections, in a range of stranded pinniped, cetacean, and mustelid species (*1*,*2*). Parasite transmission is closely linked to land-to-sea pathogen flow (*3*,*4*). We identified *Neospora caninum*, a protozoan pathogen known to affect reproductive fitness in livestock, in 6 different species of marine mammals stranded in the northeastern Pacific Ocean region. The emergence of *N. caninum* illustrates a third terrestrially sourced parasite (also referred to as a pollutagen) flowing from land to sea to infect marine mammals in this region. This parasite is distinct from previously reported *N. caninum*–like parasites that circulate between pinnipeds in a marine cycle (*5*).

In cattle, *N. caninum* is considered among the most efficient pathogens to be transmitted transplacentally (*6*). This pathogen is a major contributor of reproductive loss in the dairy industry worldwide. Dogs and wild canids, including foxes, wolves, and coyotes, are among the recognized hosts, both definitive and intermediate, for this parasite. Unlike most coccidian parasites that have a limited host range, *N. caninum* is increasingly detected in a wide array of terrestrial and avian species (*7*). Although reports have identified antibodies to *N. caninum* in prior serosurveys of marine mammals in Australia, Japan, and the United States (*8*–*10*), those assays were not validated for wildlife. Cross-reactivity with related coccidian parasites that commonly circulate between marine mammals in a marine cycle may have confounded interpretation of the results (*11*). We report 8 confirmed cases of *N. caninum* infection in 6 marine mammal species, including 2 pups and a pregnant female.

The Study

Throughout the northeastern Pacific region, local and regional marine mammal stranding networks respond to live stranded and dead marine mammals. In this case series, wildlife officials delivered a California sea lion (*Zalophus californianus*) for rehabilitation. Despite supportive care, the animal declined and was euthanized. We identified a solitary *N. caninum* infection using PCR, observing no discernible parasites by histopathology. As a result of

Author affiliations: Animal Health Center, British Columbia Ministry of Agriculture, Abbotsford, British Columbia, Canada (S.A. Raverty); The Marine Mammal Center, Sausalito, California, USA (P. Duignan, L. Barbosa); University of Calgary, Veterinary Medicine, Calgary, Alberta, Canada (P. Duignan); Washington Department of Fish and Wildlife, Lakewood, Washington, USA (D.M. Lambourn); Department of Fisheries and Oceans, Vancouver, British Columbia, Canada (P. Cottrell); US Fish and Wildlife Service, Anchorage, Alaska, USA (V.A. Gill); Alaska SeaLife Center, Seward, Alaska, USA (P. Tuomi); McGill University, Montreal, Quebec, Canada (B. Cottrell); National Institutes of Health, Bethesda, Maryland, USA (S.L. Magargal, A.K. Gibson, E.R. Zhang, M.E. Grigg)

DOI: http://doi.org/10.3201/eid3202.251507

[1]Current affiliation: National Oceanic and Atmospheric Administration Fisheries, PRD/Alaska Region, US Department of Commerce, Anchorage, Alaska, USA.

that finding, we conducted a retrospective database analysis on 410 stranded marine mammals previously screened by PCR-DNA sequencing at the internal transcribed spacer (ITS) 1 marker. We identified 7 additional cases of *N. caninum* infection in another 5 species of marine mammals. The geographic range of the *N. caninum*–infected animals (Figure 1) suggested multiple points, rather than a single point source, of parasite exposure.

We documented the stranding location, recorded signalment, compiled morphometrics, and performed a necropsy for all 8 cases (Table). We also harvested representative tissues for histopathology and immunohistochemistry and froze samples for ancillary diagnostic studies. We conducted PCR-DNA sequencing using pan-Apicomplexan primers that amplify across the ITS1 region for speciation. We carried out immunohistochemistry for *N. caninum*, *T. gondii,* and *S. neurona* on available tissues from 4 PCR-positive animals, following previously reported protocols (*1*,*12*).

Phylogenetic analysis at the ITS1 locus established unequivocally that all 8 animals were infected with an identical sequence type that resolved as *N. caninum* (GenBank accession nos. PX529932–8) (Figure 2). For comparison, we included in the tree sequences recovered from other pinnipeds infected by *N. caninum*–like parasites that commonly circulate within a marine transmission cycle (*5*). We conducted PCR testing, determining 7 of the 8 *N. caninum*–infected animals had polyparasite infections with 1 or 2 other terrestrially sourced coccidian agents (*T. gondii*, *S. neurona*) in their tissues. Infected animals were 2 sea otters (*Enhydra lutris*), 2 harbor seals (*Phoca vitulina*), 1 northern elephant seal (*Mirounga angustirostris*), 1 Guadelupe fur seal (*Arctocephalus townsendi*), and 1 Steller sea lion (*Eumetopias jubatus*) (Table).

We diagnosed nonsuppurative and necrotizing encephalitis (n = 2), meningoencephalomyelitis (n = 1), and meningoencephalitis (n = 1) by histology of the brain for 4 of 6 cases, including the pup and subadult harbor seals, adult Steller sea lion, and yearling California sea lion. We conducted immunohistochemistry in 4 encephalitic cases, observing *N. caninum* antigen in brain samples from the harbor seal pup and *T. gondii* and *S. neurona* (one or both) antigens in the other 3 animals (Figure 3). We found no pathognomonic lesions in this case series directly attributed to *N. caninum* infection. The cause of death for all 8 animals was independent of *N. caninum* infection (Appendix Table, https://wwwnc.cdc.gov/EID/article/32/2/25-1507-App1.pdf).

Figure 1. Stranding locations and animal species in study of *Neospora caninum* infection in marine mammals stranding in the northeastern Pacific Ocean region. NES, northern elephant seal (*Mirounga angustirostris*); CSL, California sea lion (*Zalophus californianus*); HS, harbor seal (*Phoca vitulina*); GFS, Guadalupe fur seal (*Arctocephalus townsendi*); SSL, Steller sea lion (*Eumetopias jubatus*); SO, sea otter (*Enhydra lutris*).

Conclusion

We identified 8 animals from 6 marine mammal species unequivocally infected with *N. caninum*. Infection by this parasite alone was confirmed in 1 animal, a yearling California sea lion, and the infection represents another example of land-to-sea flow of a pollutagen of parasite origin. The contribution of this pathogen to marine mammal health is unknown. All infected animals we studied were from species with varying degrees of philopatry, with either short natal dispersal distances or extended oceanic to pelagic migrations. Seasonal haul out associated with pupping and breeding, coupled with accounts of wild canids scavenging at rookeries (*13*), provide insights into potential parasite introduction, persistence, and dissemination. For sea otters, bioaccumulation of parasites by invertebrate prey species may be inferred from observations of transmission dynamics with *T. gondii* (*4*). On the basis of gross and microscopic findings, we determined *N. caninum* infection to be unre-

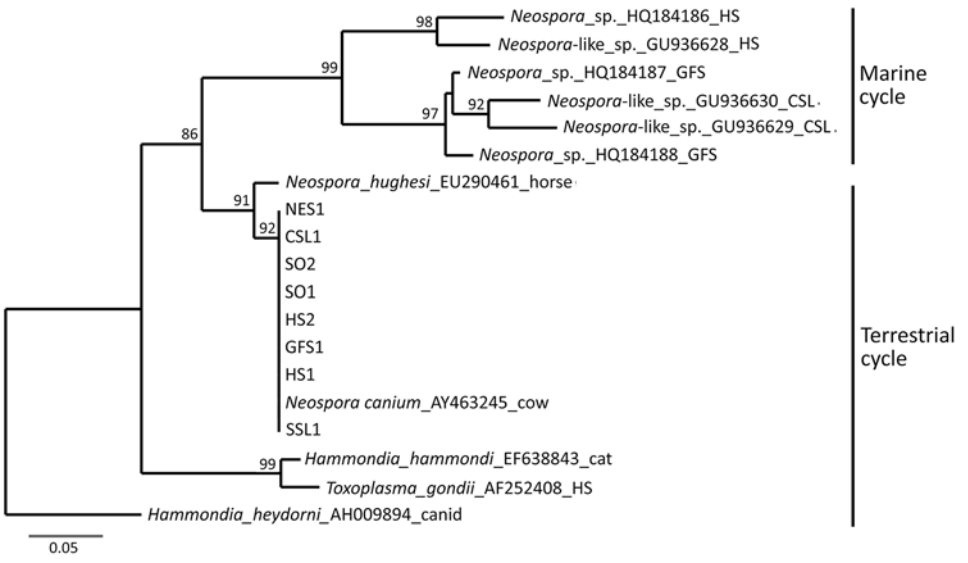

Figure 2. Phylogenetic relationships among *Neospora caninum*–like species that circulate in a marine cycle compared with terrestrial-sourced species from study of *N. caninum* infection in marine mammals stranding in the northeastern Pacific Ocean region. Neighbor-joining consensus tree shows marine strains that commonly infect pinnipeds and terrestrial strains (GenBank accession numbers PX529932–8) that transferred from land to sea to infect 5 species of pinnipeds. Evolutionary distances computed using the Tamura-Nei genetic distance model at the complete internal transcribed spacer 1 locus. Tree inferred using the outgroup sequence from *Hammondia heydorni* to root the tree; 1,000 bootstrap values listed at supported nodes. NES, northern elephant seal (*Mirounga angustirostris*); CSL, California sea lion (*Zalophus californianus*); HS, harbor seal (*Phoca vitulina*); GFS, Guadalupe fur seal (*Arctocephalus townsendi*); SSL, Steller sea lion (*Eumetopias jubatus*); SO, sea otter (*Enhydra lutris*).

lated to the proximate cause of death in the examined animals. Nevertheless, detection of *N. caninum* in a pregnant Steller sea lion, as well as in a harbor seal pup and northern elephant seal pup (weanling), is concerning. Recrudescence of latent infection during pregnancy contributes to parasite reactivation that results in vertical transmission in cattle and dogs (*6*), and we propose this phenomenon might be occurring sporadically in marine mammals.

Documented reports have confirmed land-to-sea transmission of protozoan parasites, and serosurveys for *N. caninum* have detected titers in marine mammal species. A recent review documents the global extent of land-to-sea pathogen flow (*14*). Seals and sea lions are monophyletic, members of the order Carnivora, and share a common ancestry with terrestrial canids. This evolutionary relationship may predispose these marine mammals to pollutagens defecated by canids. Cross reactivity with previously described nonpathogenic *N. caninum*–like parasites that circulate among pinnipeds in a marine transmission cycle, including coccidia types A and B (with California sea lions as definitive hosts) (*5*), may have contributed to false-positive results in prior serosurveys. The contribution of these *N. caninum*–like parasites to immune protection of hosts against *N. caninum* is unknown. In this limited series, we confirmed *N. caninum* infection in 2 sea otters, 2 harbor seals, 1 California sea lion, 1 northern elephant seal, 1 Steller sea lion, and 1 Guadelupe fur seal, none of which had been infected with previously described *N. caninum*–like parasites. Those findings extend the host range and ecologic niche for *N. caninum*. Infections were predominantly mixed with *T. gondii*, *S. neurona*, or both. Climate change, ecologic marine regime shifts, rural and urban development, weather events, and other environmental perturbations may lead to incursion of previously recognized land-based pathogens into the marine environment.

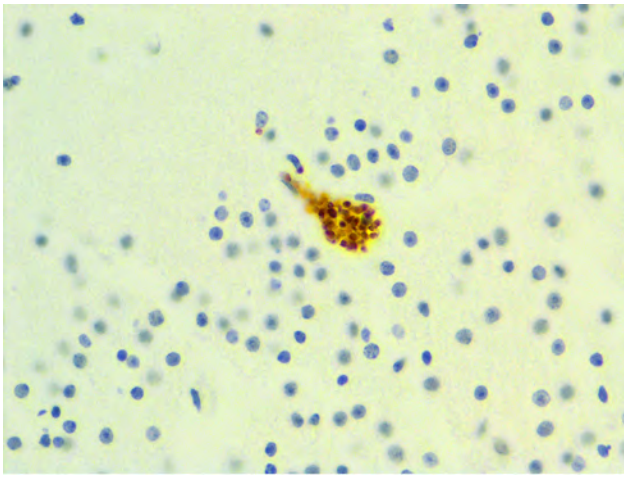

Figure 3. Immunohistochemistry of a harbor seal pup with *Neospora caninum* antigen localized within a neuron from study of *N. caninum* infection in marine mammals stranding in the northeastern Pacific Ocean region. Original magnification ×600.

In conclusion, our results indicate that further investigations to characterize the life history of *N. caninum* in the marine environment, the role of polyparasitism in disease manifestation, and the potential pathogenicity in susceptible host species are

warranted. Whereas we cannot definitively attribute *N. caninum* as the cause of illness or death for the animals described here, future investigations of similar unexpected deaths, particularly those involving abortion storms among coastal breeding marine mammals in the northeastern Pacific, should consider molecular screening for this pathogen.

Acknowledgments

We gratefully acknowledge the postmortem room and histology staff at the Animal Health Center.

We obtained Letters of Authorization from Regional Stranding Coordinators, Convention on International Trade in Endangered Species permits, National Oceanic and Atmospheric Administration (TMMC permit no. 26532), and United States Fish and Wildlife Service declarations for this investigation.

Prescott Awards to P.D. and D.M.L. funded this project. This research was supported in part by the Intramural Research Program of the National Institutes of Health (NIH). The contributions of the NIH author(s) were made as part of their official duties as NIH federal employees, are in compliance with agency policy requirements, and are considered Works of the United States Government. However, the findings and conclusions presented in this paper are those of the author(s) and do not necessarily reflect the views of the NIH, the US Department of Health and Human Services, or any other Agency of the US Government.

About the Author

Dr. Raverty is a veterinary pathologist at the Animal Health Center, British Columbia Ministry of Agriculture, Abbotsford, British Columbia, Canada. He has investigated infectious and noninfectious disease entities in live and dead stranded marine mammals throughout the northeastern Pacific.

References

1. Gibson AK, Raverty S, Lambourn DM, Huggins J, Magargal SL, Grigg ME. Polyparasitism is associated with increased disease severity in *Toxoplasma gondii*-infected marine sentinel species. PLoS Negl Trop Dis. 2011;5:e1142. https://doi.org/10.1371/journal.pntd.0001142
2. Miller MA, Shapiro K, Murray MJ, Haulena M, Raverty SA. Protozoan parasites of marine mammals. In: Gulland FMD, Dierauf LA, Whitman KL, editors. CRC handbook of marine mammal medicine, 3rd edition. Oxford: CRC Press; 2018;chap 20:p. 1-46.
3. Burgess TL, Tinker MT, Miller MA, Smith WA, Bodkin JL, Murray MJ, et al. Spatial epidemiological patterns suggest mechanisms of land-sea transmission for *Sarcocystis neurona* in a coastal marine mammal. Sci Rep. 2020;10:3683. https://doi.org/10.1038/s41598-020-60254-5
4. Conrad PA, Miller MA, Kreuder C, James ER, Mazet J, Dabritz H, et al. Transmission of Toxoplasma: clues from the study of sea otters as sentinels of *Toxoplasma gondii* flow into the marine environment. Int J Parasitol. 2005;35:1155–68. https://doi.org/10.1016/j.ijpara.2005.07.002
5. Carlson-Bremer D, Johnson CK, Miller RH, Gulland FM, Conrad PA, Wasmuth JD, et al. Identification of two novel coccidian species shed by California sea lions (*Zalophus californianus*). J Parasitol. 2012;98:347–54. https://doi.org/10.1645/GE-2752.1
6. Dubey JP, Schares G, Ortega-Mora LM. Epidemiology and control of neosporosis and *Neospora caninum*. Clin Microbiol Rev. 2007;20:323–67. https://doi.org/10.1128/CMR.00031-06
7. Almería S. *Neospora caninum* and wildlife. ISRN Parasitol. 2013;2013:947347. https://doi.org/10.5402/2013/947347
8. Dubey JP, Zarnke R, Thomas NJ, Wong SK, Van Bonn W, Briggs M, et al. *Toxoplasma gondii*, *Neospora caninum*, *Sarcocystis neurona*, and *Sarcocystis canis*-like infections in marine mammals. Vet Parasitol. 2003;116:275–96. https://doi.org/10.1016/S0304-4017(03)00263-2
9. Omata Y, Umeshita Y, Watarai M, Tachibana M, Sasaki M, Murata K, et al. Investigation for presence of *Neospora caninum*, *Toxoplasma gondii* and *Brucella*-species infection in killer whales (Orcinus orca) mass-stranded on the coast of Shiretoko, Hokkaido, Japan. J Vet Med Sci. 2006;68:523–6. https://doi.org/10.1292/jvms.68.523
10. Wong A, Lanyon JM, O'Handley R, Linedale R, Woolford L, Long T, et al. Serum antibodies against *Toxoplasma gondii* and *Neospora caninum* in southeast Queensland dugongs. Mar Mamm Sci. 2020;36:180–94. https://doi.org/10.1111/mms.12629
11. Donahoe SL, Lindsay SA, Krockenberger M, Phalen D, Šlapeta J. A review of neosporosis and pathologic findings of *Neospora caninum* infection in wildlife. Int J Parasitol Parasites Wildl. 2015;4:216–38. https://doi.org/10.1016/j.ijppaw.2015.04.002
12. Barbosa L, Johnson CK, Lambourn DM, Gibson AK, Haman KH, Huggins JL, et al. A novel *Sarcocystis neurona* genotype XIII is associated with severe encephalitis in an unexpectedly broad range of marine mammals from the northeastern Pacific Ocean. Int J Parasitol. 2015;45:595–603. https://doi.org/10.1016/j.ijpara.2015.02.013
13. Reid RE, Gifford-Gonzalez D, Koch PL. Coyote (*Canis latrans*) use of marine resources in coastal California: a new behavior relative to their recent ancestors. Holocene. 2018;28:1781–90. https://doi.org/10.1177/0959683618788714
14. Song L, Hu C, Zhang X, Liu Y, Song G, Wu J, et al. Effects of feeding on microbial community structure and pathogen abundance in marine aquaculture ponds. Mar Environ Res. 2025;210:107319. https://doi.org/10.1016/j.marenvres.2025.107319

Address for correspondence: Michael E. Grigg, Laboratory of Parasitic Diseases, NIAID National Institutes of Health, 4 Center Dr, Rm B1-06, Bethesda, MD 20892 USA; email: griggm@niaid.nih.gov

Donor-Derived West Nile Virus Infection in Kidney Transplant Recipients, France, 2025

Aurélie Truffot, Anne-Sophie Montcuquet, Gilda Grard, Laura Pezzi, Raphaelle Klitting, Gabriel Clavel, Sylvain Trincal, Paolo Malvezzi, Lionel Rostaing, Lara Meyer, Stéphanie Dieterle, Sophie Lucas Samuel, Vincent Foulongne, Laura Le Fleur, Patricia Pavese, Gaël Pradel, Florian Franke, Syria Laperche, Julien Lupo, Anne Signori-Schmuck, Raphaële Germi, Patrice Morand

We report 2 cases of donor-derived West Nile virus infection in kidney transplant recipients in France. Both recipients had mild disease develop and recovered without sequelae. A more proactive screening strategy in France, particularly during periods of highest risk for West Nile virus circulation, would help reduce risk for donor-derived infections.

The clinical manifestation of West Nile virus (WNV) infections is a wide spectrum, ranging from asymptomatic (≈80% of cases) to mild febrile illness (fever, rash) in ≈20% of cases; severe neuroinvasive disease develops in a small proportion of patients (*1*). Immunocompromised patients, such as solid organ transplant (SOT) recipients, are at higher risk for complicated neuroinvasive forms of WNV with unfavorable outcomes (*2*–*4*).

In France, the High Council for Public Health updated its recommendations in 2020 for transfusion and transplant safety in relation to WNV circulation (https://www.hcsp.fr/Explore.cgi/AvisRapports). According to those guidelines, individual screening of human-derived biologic products relies at minimum on WNV genome detection, combined with IgM testing for organ donors. Annually, in mainland France, screening measures are implemented at the department level after the first human autochthonous case, regardless of history of WNV circulation. Since 2024, during the period of enhanced surveillance of arboviruses (May–November), a decision-making support unit convenes weekly to discuss adapting screening strategies in light of reported detections (https://cartosan.fr/rs). In this article, we describe 2 cases of donor-derived West Nile virus (DD-WNV) infection in kidney transplant recipients from a donor in France and discuss the current strategy for WNV screening of human-derived biologic products.

The Study

In August 2025, a 38-year-old woman was admitted to Grenoble University Hospital (Grenoble, France) with acute kidney failure, fever, headaches, and diarrhea occurring 3 weeks after left kidney transplantation. Extensive microbiological investigations detected WNV genome in multiple specimens and WNV IgM in serum collected 14 days after symptom onset, whereas serum collected just before kidney transplantation was negative by quantitative reverse transcription PCR (RT-PCR) and serology (WNV IgM and IgG) (Appendix Figure, https://wwwnc.cdc.gov/

Author affiliations: Université Grenoble Alpes, CNRS, CEA, IRIG IBS, Laboratoire de virologie, Grenoble, France (A. Truffot, J. Lupo, A. Signori-Schmuck, R. Germi, P. Morand); Université Grenoble Alpes, CHU Grenoble Alpes, Service de néphrologie, Grenoble (A.-S. Montcuquet, G. Clavel, S. Trincal, P. Malvezzi, L. Rostaing); Centre National de Référence des Arbovirus, Inserm-IRBA, Marseille, France (G. Grard, L. Pezzi, R. Klitting); Unité des Virus Émergents, Aix-Marseille Université, Universita di Corsica, IRD, Inserm, Marseille (G. Grard, L. Pezzi, R. Klitting); Service de Néphrologie, Montpellier, France (L. Meyer); Direction Générale Médicale et Scientifique, Agence de la Biomédecine, Saint-Denis, France (S. Dieterle, S.L. Samuel); Centre Hospitalier Universitaire de Montpellier, Montpellier (V. Foulongne, L. Le Fleur); Grenoble-Alpes University Hospital, La Tronche, France (P. Pavese); Centre Hospitalier d'Avignon Henri Duffaut, Avignon, France (G. Pradel); Santé Publique France, Marseille (F. Franke); Etablissement Français du Sang, Saint-Denis (S. Laperche)

DOI: https://doi.org/10.3201/eid3202.251569

EID/article/32/2/25-1569-App1.pdf). A graft biopsy showed mild capillaritis affecting both glomeruli and tubules, along with granular tubular casts consistent with infection; WNV genome was also detected in the kidney biopsy specimen. Fever and headache resolved within a few days, and no neurologic signs were noted. Fifteen days later, kidney function remained impaired but stable, and she was discharged (Appendix Figure). WNV quantitative RT-PCR of urine still showed positive result 2.5 months after the graft. During the transplant, the recipient received twice-packed red blood cells that retrospectively tested negative for WNV by quantitative RT-PCR.

The right kidney recipient, a 61-year-old man, was admitted to Montpellier University Hospital (Montpellier, France) 20 days after transplantation, in August 2025, with isolated fever without neurologic symptoms. Virologic tests were negative except for WNV-positive quantitative RT-PCR results in whole blood, urine, saliva, and serology (WNV IgM and IgG) 24 days after transplant. Fever spontaneously resolved within 5 days, and the patient was discharged with favorable outcome (Appendix Figure).

Because DD-WNV infection was suspected, the cases were reported to the French Biomedicine Agency, the national authority responsible for regulating and supervising organ, tissue, and cell donation and transplantation. The organ donor was a man in his 50s who died mid-July 2025 from a cerebral hemorrhage caused by hypertensive crisis. On the day of death, he demonstrated no suggestive clinical signs except for lesions on his abdomen and lower limbs suggestive of eruptive pseudo-angiomatosis (Figure 1). Only the kidneys were retrieved and grafted. Donor specimens collected just before organ donation were retrospectively tested; WNV genome was identified in both serum and plasma, whereas IgM and IgG were negative, confirming ongoing WNV infection (Appendix Figure).

DD-WNV was confirmed by next-generation sequencing of complete WNV genomes identified in the donor's plasma and in left kidney recipient's urine (GenBank accession nos. OZ313260.1, OZ313201.1) (*5*). Unfortunately, the viral load identified in the right kidney recipient was too low to enable virus genome sequencing. Virus genomes obtained from the donor and the recipient were 100% identical, confirming a direct link between infections. Further phylogenetic inference using a maximum-likelihood approach showed that the virus strain responsible for the initial infection belonged to WNV lineage 2 and was related to strains sampled in the Provence-Alpes-Côte d'Azur region in 2024, aligning with the donor's region of residence rather than with that of the kidney recipient (Auvergne-Rhône-Alpes) (Figure 2).

For the left kidney recipient, WNV genome was detected by RT-PCR using the ELITe MBG kit (ELITech Group, https://www.elitechgroup.com), and WNV IgM and IgG were detected using the Vircell VIRCLIA monotest (https://www.vircell.com). For the right kidney recipient, WNV genome was detected by RT-PCR Altona Real Star kit (https://altona-diagnostics.com), and serologic testing was performed with the EUROIMMUN ELISA (https://www.euroimmun.com). The results were confirmed by the National Reference Center using an in-house WNV quantitative RT-PCR on the Panther Fusion system (Hologic, https://www.hologic.com) and the EUROIMMUN ELISA for WNV serology.

The first cases of DD-WNV were reported in the United States in 2002, involving 4 SOT recipients from a common donor (*4*). Through 2017, WNV was estimated to account for >6% of DD infections occurring in kidney recipients (*6*). Review of previous cases indicates that 85% of SOT recipients from WNV-infected donors acquire the infection; 70%

Figure 1. Diffuse skin lesions on donor's leg in case of donor-derived West Nile virus infection in kidney transplant recipients, France, 2025. Lesions were suggestive of eruptive pseudo-angiomatosis associated with West Nile virus infection.

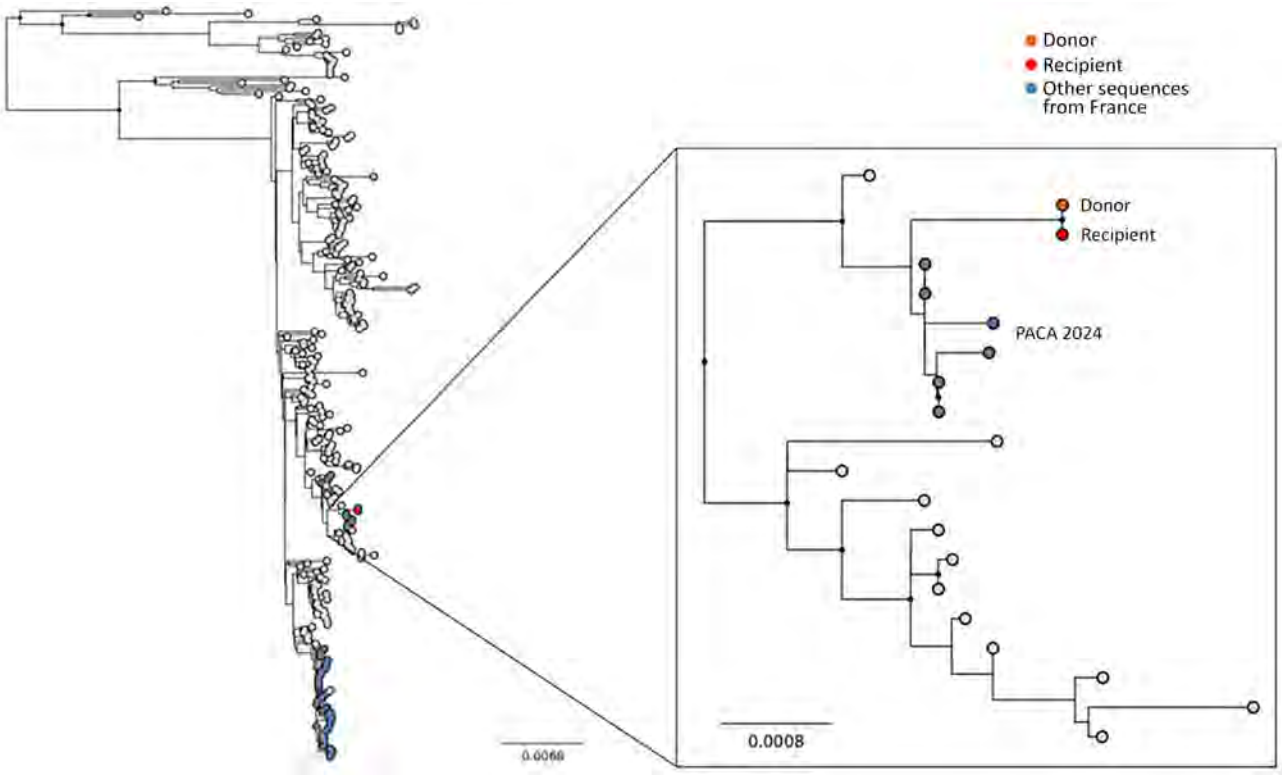

Figure 2. Phylogeny of West Nile virus lineage 2 highlighting sequences from the infected donor and recipient in case of donor-derived West Nile virus infection in kidney transplant recipients, France, 2025. Maximum-likelihood phylogeny was reconstructed with IQ-TREE version 1.6.12 (https://iqtree.github.io/release/v1.6.12). The best-fit nucleotide substitution model was selected using ModelFinder (https://iqtree.github.io/ModelFinder), and branch support was evaluated with ultrafast bootstrap approximation using 1,000 replicates. We used 226 sequences representative of the phylogenetic diversity within lineage 2 (subsampled from a comprehensive set of public sequences from GenBank accessed via Pathoplexus, https://doi.org/10.62599/PP_SS_67.1), including those from the donor and recipient produced in this study, as well as other sequences from France, including those from Provence-Alpes Côte d'Azur (PACA) region. The length of the branches is proportional to the degree of divergence.

develop neuroinvasive disease, and the mortality rate is 26% (*4*). In this instance, both kidney recipients developed a mild infection and had favorable outcomes and no sequelae.

Laboratory investigations confirmed WNV infection in both recipients, and genomic and phylogenetic analysis demonstrated DD-WNV. Of note, genome testing of whole blood was more sensitive than plasma testing, consistent with previous findings (*7*–*10*). The RT-PCR–positive result in saliva suggests this type of specimen can be useful for WNV genome detection, although the diagnostic value of saliva warrants further investigation (*11*).

The donor had not recently traveled to known WNV risk areas and resided in the Vaucluse department, where no WNV activity had been reported at the time of organ donation. The first department identified as at risk in 2025 was Var, which was added to the list of at-risk areas in July (after transplant) (*12*). This donor was retrospectively classified as the first autochthonous case of WNV infection in Vaucluse department, which was added to the list in August 2025 (*13*). He had not received recent blood transfusions, and the lesions observed at hospital admission have been described in association with various viral infections, including WNV (*14*). Vectorborne transmission is the most likely acquisition scenario. Equine cases of WNV were confirmed in July 2025 <30 km from the donor's residence, providing additional evidence of active WNV circulation at the time of death (https://www.plateforme-esa.fr/fr/bulletin-hebdomadaire-de-veille-sanitaire-internationale-du-05-08-2025).

Conclusions

This case underscores the limitations of WNV surveillance in France, particularly regarding the timing of screening and the criteria used to define areas requiring mandatory screening. The current reactive approach, in which screening of human-derived biologic products is mandatory only after the first human autochthonous case is identified, is limited by the

high proportion of asymptomatic WNV infections in humans (*1*). In areas with recurrent WNV circulation and favorable conditions, a proactive and systematic screening of human-derived biologic products during the vector activity season would likely be more appropriate, provided it is financially feasible and that laboratories have adequate diagnostic capacity. This approach was successfully implemented during the 2024 Summer Olympics, when the public transfusion service in France introduced WNV nucleic acid testing for blood donations in areas with documented previous viral circulation, and the first PCR-positive blood donation was identified 3 weeks before the first human symptomatic case (*15*). Conversely, in regions with no evidence of WNV circulation, a reactive approach seems sufficient to prevent transmission through transfusion and transplants. Both proactive and reactive screening strategies would greatly benefit from entomological and animal surveillance, which might detect WNV circulation before the onset of human cases (*5*). Integrating such early alerts into the decision-making process for initiating WNV donor screening would further help reduce the risk for WNV transmission.

About the Author

Dr. Truffot is a medical biologist specializing in viral reactivations in immunocompromised patients, particularly kidney transplant recipients. Her primary research interests are viral reactivations in immunocompromised patients.

References

1. Sejvar JJ. West Nile virus infection. Microbiol Spectr. 2016;4.
2. Abbas A, Qiu F, Sikyta A, Fey PD, Florescu DF. Neuroinvasive West Nile virus infections after solid organ transplantation: single center experience and systematic review. Transpl Infect Dis. 2022;24:e13929. https://doi.org/10.1111/tid.13929
3. Kumar D, Prasad GVR, Zaltzman J, Levy GA, Humar A. Community-acquired West Nile virus infection in solid-organ transplant recipients. Transplantation. 2004; 77:399–402. https://doi.org/10.1097/01.TP.0000101435.91619.31
4. Soto RA, McDonald E, Annambhotla P, Velez JO, Laven J, Panella AJ, et al. West Nile virus transmission by solid organ transplantation and considerations for organ donor screening practices, United States. Emerg Infect Dis. 2022;28:403–6. https://doi.org/10.3201/eid2802.211697
5. Bigeard C, Pezzi L, Klitting R, Ayhan N, L'Ambert G, Gomez N, et al. Molecular Xenomonitoring (MX) allows real-time surveillance of West Nile and Usutu virus in mosquito populations. PLoS Negl Trop Dis. 2024; 18:e0012754. https://doi.org/10.1371/journal.pntd.0012754
6. Shingde R, Habachou LI, Calisa V, Craig JC, Tong A, Chen SC, et al. Unexpected donor-derived infectious transmissions by kidney transplantation: a systematic review. Transpl Infect Dis. 2018;20:e12851. https://doi.org/10.1111/tid.12851
7. Barzon L, Pacenti M, Franchin E, Squarzon L, Sinigaglia A, Ulbert S, et al. Isolation of West Nile virus from urine samples of patients with acute infection. J Clin Microbiol. 2014;52:3411–3. https://doi.org/10.1128/JCM.01328-14
8. Lustig Y, Mannasse B, Koren R, Katz-Likvornik S, Hindiyeh M, Mandelboim M, et al. Superiority of West Nile virus RNA detection in whole blood for diagnosis of acute infection. J Clin Microbiol. 2016;54:2294–7. https://doi.org/10.1128/JCM.01283-16
9. Rios M, Daniel S, Chancey C, Hewlett IK, Stramer SL. West Nile virus adheres to human red blood cells in whole blood. Clin Infect Dis. 2007;45:181–6. https://doi.org/10.1086/518850
10. Lanteri MC, Lee TH, Wen L, Kaidarova Z, Bravo MD, Kiely NE, et al. West Nile virus nucleic acid persistence in whole blood months after clearance in plasma: implication for transfusion and transplantation safety. Transfusion. 2014;54:3232–41. https://doi.org/10.1111/trf.12764
11. Gorchakov R, Gulas-Wroblewski BE, Ronca SE, Ruff JC, Nolan MS, Berry R, et al. Optimizing PCR detection of West Nile virus from body fluid specimens to delineate natural history in an infected human cohort. Int J Mol Sci. 2019;20:1934. https://doi.org/10.3390/ijms20081934
12. Agence de la Biomédecine. Update to the list of countries and territories identified as being at risk of West Nile virus (WNV) transmission–2025 season–addition of the Var department [in French] [cited 2025 Aug 14]. https://www.santepubliquefrance.fr/maladies-et-traumatismes/maladies-a-transmission-vectorielle/chikungunya/documents/bulletin-national/chikungunya-dengue-zika-et-west-nile-en-france-hexagonale.-bulletin-de-la-surveillance-renforcee-du-27-aout-2025
13. Agence de la Biomédecine. Update to the list of countries and territories identified as being at risk of West Nile virus (WNV) transmission—2025 season—addition of the Vaucluse department [in French] [cited 2025 Aug 14]. https://www.hcsp.fr/explore.cgi/avisrapportsdomaine?clefr=1437
14. Pacenti M, Sinigaglia A, Franchin E, Pagni S, Lavezzo E, Montarsi F, et al. Human West Nile virus lineage 2 infection: epidemiological, clinical, and virological findings. Viruses. 2020;12:458. https://doi.org/10.3390/v12040458
15. Grard G, Franke F, Laperche S, Cochet A, Paty MC, Gonzalez G, et al. Blood donation screening and West Nile virus surveillance strategy in France. JAMA Netw Open. 2025;8:e2524494. https://doi.org/10.1001/jamanetworkopen.2025.24494

Address for correspondence: Aurélie Truffot, Institut de biologie et de pathologie, CHU Grenoble, laboratoire de virologie, 38400 La Tronche, France; email: atruffot@chu-grenoble.fr

Severe Respiratory Diphtheria-Like Illness Caused by Toxigenic *Corynebacterium ulcerans*

Rita Helleren, Hans Kristian Fløystad, Odd Alexander Tellefsen, Miroslav Boskovic, Terje Skraastad, Anne Torunn Mengshoel, Kristian Alfsnes, Vegard Skogen

Author affiliations: Sørlandet Hospital, Kristiansand, Norway (R. Helleren, H.K. Fløystad, O.A. Tellefsen, M. Boskovic, T. Skraastad); Norwegian Institute of Public Health, Oslo, Norway (A.T. Mengshoel, K. Alfsnes); Faculty of Health Sciences, UiT The Arctic University of Norway, Tromsø, Norway (V. Skogen); University Hospital of North Norway, Tromsø (V. Skogen)

DOI: https://doi.org/10.3201/eid3202.250908

We report a possible zoonotic case of severe diphtheria-like respiratory illness in Norway caused by a previously unreported toxigenic *Corynebacterium ulcerans* sequence type. This case highlights *C. ulcerans* as an emerging pathogen that can cause life-threatening disease. Clinicians should be aware of *C. ulcerans* infection, even in regions where diphtheria is rare.

Corynebacterium ulcerans bacteria can cause respiratory and nonrespiratory infections in humans, and respiratory diphtheria-like illness caused by toxigenic *C. ulcerans* is increasing (*1*). Globally, *C. ulcerans* bacteremia is rare, and limited clinical data are available. We describe a case of severe respiratory diphtheria-like illness caused by toxigenic *C. ulcerans* bacteremia in an immunocompromised patient in Norway without travel history.

On January 11, 2024, a 74-year-old immunocompromised man was referred to the emergency department for a 2-day history of breathlessness, productive cough, malaise, and cognitive impairment. He had a sore throat and cold-like symptoms 8–9 days earlier. He lived in an urban area with his wife and dog. Medical history included coronary disease, type 2 diabetes mellitus, chronic obstructive pulmonary disease with obstructive sleep apnea, and a hemicolectomy for cancer in 2019. He had been immunocompromised since 2021 from weekly methotrexate (20 mg) and etanercept (50 mg) for psoriatic arthritis.

At admission, he was afebrile but in respiratory distress with marked hoarseness and wheezing on auscultation; throat examination was unremarkable. He was hemodynamically stable; oxygen saturation was 88% on room air. Electrocardiograph showed sinus rhythm; echocardiography revealed preserved biventricular systolic function. Chest radiograph showed a retrocardiac infiltrate; laboratory findings indicated infection (Table).

He was treated with ampicillin (1 g 4×/d), prednisolone (40 mg), inhaled bronchodilators for suspected exacerbation of his pulmonary disease, and 2 L/min of oxygen via nasal cannula. Blood cultures taken at admission showed gram-positive rods after 27 hours using the BD Bactec FX system (Becton Dickinson, https://www.bd.com). MALDI BioTyper (Bruker Daltonik GmbH, https://www.bruker.com) identified *C. ulcerans*, prompting a diphtheria-like illness diagnosis. The Norwegian Institute of Public Health confirmed *C. ulcerans* using API Coryne version 4.0 system (bioMérieux, https://www.biomerieux.com) and by PCR. We also identified the *tox* gene by PCR and toxin production by a modified Elek test (*2*). We sequenced the isolate on a NextSeq platform (Illumina, https://www.illumina.com), and curators at BIGSdb-Pasteur MLST database (https://bigsdb.pasteur.fr) identified it as sequence type 1032.

Two days after admission, antibiotic therapy was changed to intravenous penicillin G (3 g 4×/d), and the patient received 100,000 units of diphtheria antitoxin. Respiratory distress worsened, and the patient was transferred to the intensive care unit. Four days after admission, ventricular tachycardia developed but was successfully cardioverted after intubation.

The patient required mechanical ventilation for 7 days. Bronchoscopy revealed pseudomembranes in the lower airways, which were removed (Figure). He completed 14 days of antibiotic therapy, mainly benzylpenicillin, and 7 days of cefotaxime for ventilator-associated *Staphylococcus aureus* pneumonia.

An initial throat swab sample from hospitalization day 2 was *C. ulcerans*–negative, but follow-up samples from days 5 and 8 were *C. ulcerans*–positive. Follow-up samples on days 18 and 19 were negative, and the patient's isolation was discontinued; he was discharged after 23 days. Comparison of antibody levels against diphtheria toxoid showed a protective level in 2020 (0.18 IU/mL) and >3.0 IU/mL on hospitalization day 7.

Table. Laboratory findings from blood collected at admission in a case of severe respiratory diphtheria-like illness caused by toxigenic *Corynebacterium ulcerans*, Norway*

Test	Value	Reference range
C-reactive protein, mg/L	329	0.00–5.0
Leukocytes, × 10^9 cells/L	24	3.5–10.0
Neutrophils, × 10^9 cells/L	22	1.5–7.1
Creatinine, μmol/L	183	60–105
GFR, mL/min	31	≥90

*GFR, glomerular filtration rate.

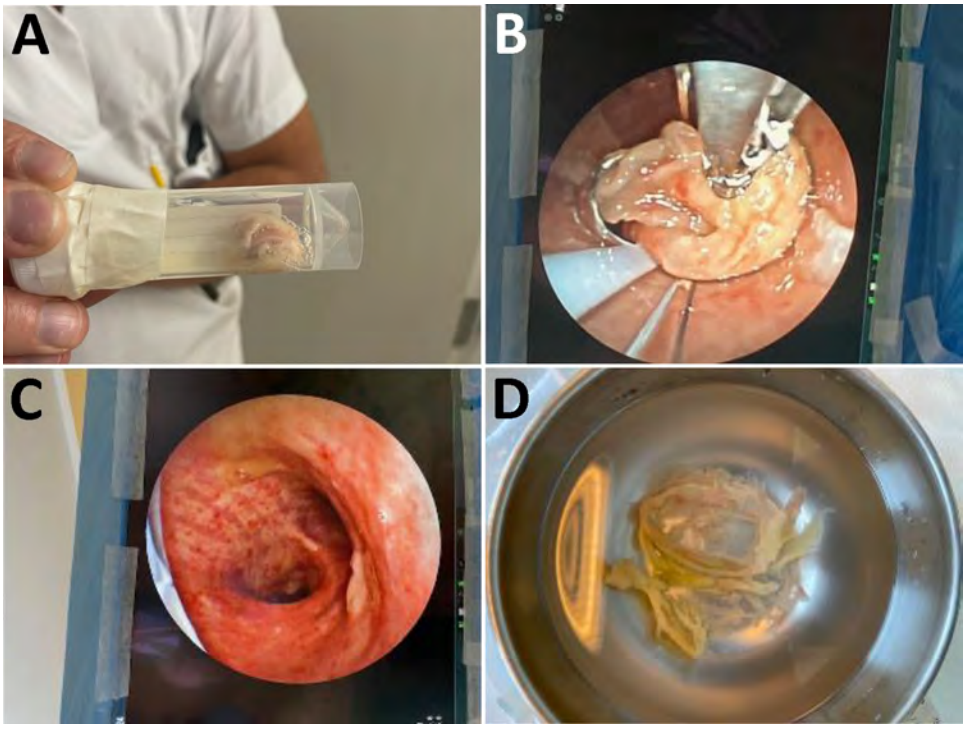

Figure. Clinical findings from a case of severe respiratory diphtheria-like illness caused by toxigenic *Corynebacterium ulcerans*, Norway. A) Pseudomembranes coughed up by the patient on day 1 of hospitalization. B) Pseudomembranes removed by bronchoscopy on day 4 of hospitalization. C) Trachea and carina after bronchoscopy on day 4 of hospitalization. D) Pseudomembranes removed from lower airways via bronchoscopy on day 4 of hospitalization.

At 2-month follow-up, the patient had bilateral thigh numbness. Electroneurography confirmed sensorimotor polyneuropathy.

Although severe *C. ulcerans* infections have been described (*3*,*4*), detailed clinical data on patients with positive blood cultures remain rare. Bacteremia appears linked to severe immunosuppression (*3*,*5*). This patient had protective diphtheria antibody titers but fulminant illness developed, requiring ventilation, antibiotics, and diphtheria antitoxin. A similar pattern was observed during a diphtheria epidemic in Russia in the 1990s (*6*). Although nontoxigenic *C. diphtheriae* can cause severe disease, diphtheria toxin remains the main virulence factor, inhibiting protein synthesis and causing cell death, especially in myocardium and peripheral nerves (*7*). This patient's ventricular arrhythmia and subsequent polyneuropathy were consistent with diphtheria toxin–mediated toxicity (*7*).

Toxigenic *C. ulcerans* transmission remains uncertain. Although primarily zoonotic, with dairy cattle as a classic reservoir (*1*), infections from domestic and wild animals have been reported (*3*,*4*). We suspected but could not confirm transmission from this patient's dog because no microbial samples were collected. The dog showed no signs of respiratory or skin disease before the patient's hospitalization and remained in good health.

Because *C. ulcerans* among animals is not notifiable in Norway, no official data or surveillance results are available. The sequence type 1032 variant had not been previously reported in humans and has since been identified in 1 other sample from another patient in Norway 6 months later; however, the 2 patients had no known epidemiologic link (V. Skogen, unpub. data). Whole-genome sequence analysis revealed substantial genomic differences between the 2 patients' isolates, supporting separate infection sources. Because potential human-to-human transmission has been suggested (*8*–*10*), we applied isolation precautions, but no secondary cases were detected among close contacts or healthcare workers.

In summary, diagnosing diphtheria-like illness in low-prevalence settings is difficult because selective media are rarely used, and standard respiratory culture media might not detect *Corynebacterium* spp. bacteria. In this case, positive blood culture aided in early recognition, an uncommon but critical finding because classic diphtheria symptoms developed. This case underscores that *C. ulcerans* is an emerging zoonotic pathogen capable of causing life-threatening disease and highlights that early microbiological diagnosis is crucial, even in regions where diphtheria is rare.

About the Author

Dr. Helleren is a specialist in internal medicine and infectious diseases and is the head of the infectious diseases section at Sørlandet Hospital Kristiansand, Norway. Her current research interest is outpatient parenteral antimicrobial therapy.

References

1. Hacker E, Antunes CA, Mattos-Guaraldi AL, Burkovski A, Tauch A. *Corynebacterium ulcerans*, an emerging human pathogen. Future Microbiol. 2016;11:1191–208. https://doi.org/10.2217/fmb-2016-0085
2. World Health Organization. WHO laboratory manual for the diagnosis of diphtheria and other related infections. Geneva: The Organization; 2021.
3. Yamamoto A, Hifumi T, Ato M, Iwaki M, Senoh M, Hatanaka A, et al. Clinical characteristics of *Corynebacterium ulcerans* infection, Japan. Emerg Infect Dis. 2023;29:1505–15. https://doi.org/10.3201/eid2908.220058
4. Lartigue MF, Monnet X, Le Flèche A, Grimont PA, Benet JJ, Durrbach A, et al. *Corynebacterium ulcerans* in an immunocompromised patient with diphtheria and her dog. J Clin Microbiol. 2005;43:999–1001. https://doi.org/10.1128/JCM.43.2.999-1001.2005
5. Bonmarin I, Guiso N, Le Flèche-Matéos A, Patey O, Grimont Patrick AD, Levy-Bruhl D. Diphtheria: a zoonotic disease in France? Vaccine. 2009;27:4196–200. https://doi.org/10.1016/j.vaccine.2009.04.048
6. Danilova E, Jenum PA, Skogen V, Pilnikov VF, Sjursen H. Antidiphtheria antibody responses in patients and carriers of *Corynebacterium diphtheriae* in the Arkhangelsk region of Russia. Clin Vaccine Immunol. 2006;13:627–32. https://doi.org/10.1128/CVI.00026-06
7. Sharma NC, Efstratiou A, Mokrousov I, Mutreja A, Das B, Ramamurthy T. Diphtheria. Nat Rev Dis Primers. 2019;5:81. https://doi.org/10.1038/s41572-019-0131-y
8. Wagner KS, White JM, Crowcroft NS, De Martin S, Mann G, Efstratiou A. Diphtheria in the United Kingdom, 1986–2008: the increasing role of *Corynebacterium ulcerans*. Epidemiol Infect. 2010;138:1519–30. https://doi.org/10.1017/S0950268810001895
9. Othieno R, Mark K, Etherson M, Foster G, Murray S, Kalima P, et al. A case of cutaneous toxigenic *Corynebacterium ulcerans* likely acquired from a domestic dog. Access Microbiol. 2019;1:e000025. https://doi.org/10.1099/acmi.0.000025
10. Metz AR, White A, Ripplinger J, Spence Davizon E, Barnes M, Bauer M, et al. Notes from the field: toxigenic *Corynebacterium ulcerans* in humans and household pets—Utah and Colorado, 2022–2023. MMWR Morb Mortal Wkly Rep. 2024;73:534–5. https://doi.org/10.15585/mmwr.mm7323a3

Address for correspondence: Vegard Skogen, Faculty of Health Sciences, University of Tromsø, The Arctic University of Norway, PO Box 6050 Langnes, N-9037 Tromsø, Norway; email: vegard.skogen@unn.no

Acute Severe Hepatitis B Virus Infection in Previously Vaccinated Patient during Acalabrutinib Treatment

Lukasz Rojek, Tomasz Wnuk-Lipinski, Iwona Marek, Hubert Grabowski, Krystian Adrych

Author affiliation: Medical University of Gdansk, Gdansk, Poland

DOI: https://doi.org/10.3201/eid3202.251111

We describe acute severe hepatitis B virus (HBV) infection with liver failure requiring transplantation in a patient in Poland treated with acalabrutinib. The patient was fully vaccinated against HBV and had adequate HBV antibody titers and no HBV exposure documented before therapy. Differential diagnoses for jaundice should consider HBV in patients receiving acalabrutunib.

Hepatitis B virus (HBV) infection is the most prevalent long-term viral disease globally (*1*). The World Health Organization estimates that ≈254 million persons worldwide are chronic carriers of the hepatitis B surface antigen (HBsAg) (*2*). HBV is one of the most common causes of liver cirrhosis and hepatocellular carcinoma (*3*). Widespread hepatitis B (HepB) vaccination has been available since 1981 and remains the most effective strategy for preventing HBV infection (*1*,*4*). Immunocompetent adults and children with vaccine-induced HBsAg antibody levels ≥10 mIU/mL after a full ≥3-dose HepB series are generally considered seroprotected and classified as vaccine responders (*5*). Some reports suggest a loss of immunity against HBV, manifested by a decline in HBs antibody titers (*6*). That phenomenon is particularly observed in patients receiving B cell–depleting therapies, such as anti-CD20 monoclonal antibodies (*7*).

Bruton tyrosine kinase (BTK) is a vital protein involved in B cell proliferation, maturation, and differentiation (*8*). Its central role in the B-cell antigen signaling pathway has made BTK a key target for developing therapies to treat B-cell malignancies (*8*). Acalabrutinib, a second-generation BTK inhibitor, is approved for treating chronic lymphocytic leukemia (*8*). Patients with hematologic malignancies undergoing BTK inhibitor therapy can have an intermediate risk for HBV reactivation (*9*). We report possible primary acute hepatitis B with liver failure, despite successful prior vaccination against HBV, in a patient in Poland who was receiving acalabrutinib.

Table 1. Blood test results from a case of severe HBV infection in previously vaccinated patient during acalabrutinib treatment, Poland*

Biochemical parameter	Before HBV infection	Day of hospitalization						
		−13	−3	0	1	2	3	4
Total bilirubin, mg/dL	0.84	2.19	23.04	43.02	32.17	33.76	33.89	35.66
Alanine aminotransferase, U/L	27	NA	2,688	3,780	2,603	2,024	1,340	875
Aspartate aminotransferase, U/L	29	945	3,877	4,400	3,146	2,384	1,058	NA
Alkaline phosphatase, U/L	NA	NA	212	211	164	NA	147	NA
Gamma-glutamyltransferase, U/L	NA	NA	421	233	171	NA	107	NA
Ammonia, µmol/L	NA	NA	NA	221	NA	NA	92	NA
International normalized ratio	NA	NA	2.89	>6.12	>6.12	>6.12	>8.6	>8.6
Creatinine, mg/dL	0.79	0.66	0.69	1.63	2.33	3.13	3.94	4.43
Sodium, mmol/L	141	136	136	129	126	121	118	117
Potassium, mmol/L	4.3	4.5	4.5	6.4	5.9	5.1	4.6	4.6
Hemoglobin, g/dL	13.7	13.9	NA	14.3	11.8	11.1	9.9	9.5
Erythrocytes, × 10^{12} cells/L	4.02	4.13	NA	4.4	3.55	3.38	3.0	2.9
Platelets, × 10^{9}/L	207	150	NA	245	159	135	89	80
Total leukocytes, × 10^{9} cells/L	8.01	6.1	NA	8.33	7.43	6.24	5.27	5.04
C-reactive protein, mg/L	1.12	NA	21.17	14.85	9.38	NA	4.08	NA
Procalcitonin, ng/mL	NA	NA	NA	NA	0.84	0.81	NA	0.61

*HBV, hepatitis B virus; NA, not available.

A 58-year-old female patient was referred to the hospital because her general condition had deteriorated, and she had jaundice, abdominal pain, nausea, and anorexia. She had symptoms of an upper respiratory infection 6–7 weeks earlier, which had resolved. The patient had been treated with oral acalabrutinib (100 mg 2×/d) for chronic lymphocytic leukemia since April 2023. Normalization of peripheral leukocytes and partial remission of nodal changes were achieved with treatment. However, in early February 2024, hematologist observed an increase in liver enzyme levels (Table 1) and discontinued acalabrutinib treatment.

The patient's medical history included type 2 diabetes mellitus, hypothyroidism, and obesity (body mass index 36). Her surgical history included hysterectomy, bariatric surgery via adjustable gastric band, and cholecystectomy.

The patient was previously vaccinated against HBV with 3 HepB doses before 2019. In January 2023, her HBs antibody level before acalabrutinib initiation was 120.25 mIU/mL. Total hepatitis B core (HBc) antibodies were not detected.

At admission, the patient had severe jaundice (total bilirubin 43 mg/dL [reference range 0.1–1.2 mg/dL]), hepatomegaly, grade 1 ascites without peripheral edema, anuria, and mean arterial pressure 65 mm Hg (reference ≥60 mm Hg). She was afebrile, and her mental status was at baseline without evidence of encephalopathy.

Ultrasound examination showed the liver without cholestasis or focal changes and flow in the hepatic veins, portal veins, and hepatic artery within reference ranges. Ultrasound also revealed lymphadenopathy in the liver hilum and fluid in the peritoneal cavity.

Virology results were positive for HBsAg, hepatitis B envelope (HBe) antigen, HBc total antibodies, and HBc IgM. PCR on HBV DNA confirmed high viremia at 1.67 × 10^{7} IU/mL (Tables 1, 2). Hepatitis C virus, Epstein-Barr virus, and cytomegalovirus infections were excluded.

Eventually, acute viral hepatitis B with multiorgan failure involving the liver, kidneys, circulation, and coagulation was diagnosed. Entecavir was initiated (0.5 mg orally 1×/d), and empirical antibiotic therapy (750 mg intravenous cefuroxime 2×/d) was introduced. Because of high ammonia in blood serum (221 µmol/L [reference range 18–72 µmol/L]), we also administered oral rifaximin (400 mg 3×/d),

Table 2. Virologic test results from a case of severe HBV infection in previously vaccinated patient during acalabrutinib treatment, Poland*

Test	Before starting acalabrutinib		Acute hepatitis B†	After liver transplant‡
	2022	2023		
HBsAg	Undetectable	NA	Detectable	Undetectable
HBeAg	NA	NA	Detectable	NA
Anti-HBs, mIU/mL	104	120.25	0	41.8
Anti-HBc total antibodies	Undetectable	Undetectable	Detectable	Detectable
Anti-HBc IgM	NA	NA	Detectable	NA
HBV DNA, IU/mL	NA	NA	1.67 ×10^{7}	Undetectable

*Anti-HBS, antibody to HBsAG; anti-HBc, antibody to HBcAG; HBcAg, hepatitis B core antigen; HBeAg, hepatitis B envelope antigen; HBsAg, hepatitis B surface antigen; HBV, hepatitis B virus; NA, not available.
†February 2024.

intravenous L-ornithine L-aspartate (50 g total dose), and oral lactulose (20 mL 3×/d). Because hepatorenal syndrome was causing acute kidney injury, we administered 20% albumin (100 mL intravenously 2×/d) and continuous intravenous infusion of terlipressin (2 mg/d). Because renal function worsened and fluid overload increased, we implemented hemodialysis and supported circulation by a noradrenaline infusion. Despite treatment, the patient's condition deteriorated, and she was transferred to the transplant department, where successful liver transplantation was performed 19 days after onset of jaundice.

Current guidelines emphasize the need for comprehensive HBV serologic screening before initiating immunosuppressive therapy, including testing for HBsAg and HBc and HBs antibodies (*10*). However, those guidelines do not provide clear recommendations regarding monitoring HBs antibody levels during treatment. Routine HBs antibody monitoring might have prevented complete loss of vaccine-induced immunity and subsequent severe clinical course in this patient.

This report highlights that screening for HBV hepatitis is vital for patients treated with acalabrutunib, even those appropriately vaccinated against hepatitis B. HBV reactivation has been reported in patients who had previous HBV contact and initial HBc antibodies (*9*). Our patient's history of BTK inhibitor treatment shows that differential diagnosis of jaundice or infection should also consider diseases for which patients have been vaccinated.

About the Author

Dr. Rojek is an associate professor in the Department of Gastroenterology and Hepatology at the Medical University of Gdansk, Poland. His research interests involve chronic liver inflammation and complications associated with liver cirrhosis.

References:

1. Trépo C, Chan HLY, Lok A. Hepatitis B virus infection. Lancet. 2014;384:2053–63. https://doi.org/10.1016/S0140-6736(14)60220-8
2. World Health Organization. Guidelines for the prevention, diagnosis, care and treatment for people with chronic hepatitis B infection [cited 2025 Dec 6]. https://iris.who.int/server/api/core/bitstreams/34470cc8-af90-4d7b-a949-ef27e5d0726f/content
3. Ginès P, Krag A, Abraldes JG, Solà E, Fabrellas N, Kamath PS. Liver cirrhosis. Lancet. 2021;398:1359–76. https://doi.org/10.1016/S0140-6736(21)01374-X
4. Broeckhoven E, Dallmeier K. Mission 2030: toward universal hepatitis B immunization. Hum Vaccin Immunother. 2025; 21:2473222. https://doi.org/10.1080/21645515.2025.2473222
5. Schillie S, Murphy TV, Sawyer M, Ly K, Hughes E, Jiles R, et al.; Centers for Disease Control and Prevention (CDC). CDC guidance for evaluating health-care personnel for hepatitis B virus protection and for administering postexposure management. MMWR Recomm Rep. 2013;62(RR-10):1–19.
6. Araujo-Neto JM, Guimarães GS, Fernandes FF, Soares MA. Hepatitis B surface antibody (anti-HBs) kinetics during rituximab chemotherapy and performance of hepatitis B vaccine before immunosuppression: two prospective studies. Viruses. 2022;14:1780. https://doi.org/10.3390/v14081780
7. Yeo W, Chan TC, Leung NWY, Lam WY, Mo FKF, Chu MT, et al. Hepatitis B virus reactivation in lymphoma patients with prior resolved hepatitis B undergoing anticancer therapy with or without rituximab. J Clin Oncol. 2009;27:605–11. https://doi.org/10.1200/JCO.2008.18.0182
8. Lu J, Do B, Primeaux B. Evaluation of second-generation Bruton's tyrosine kinase inhibitors for the treatment of mantle cell lymphoma. J Oncol Pharm Pract. 2025;31:230–5. https://doi.org/10.1177/10781552241232331
9. Chiu CY, Ahmed S, Thomas SK, Wang LS, Mustafayev K, Fayad LE, et al. Hepatitis B virus reactivation in patients receiving Bruton tyrosine kinase inhibitors. Clin Lymphoma Myeloma Leuk. 2023;23:610–5. https://doi.org/10.1016/j.clml.2023.04.006
10. Ali FS, Nguyen MH, Hernaez R, Huang DQ, Wilder J, Piscoya A, et al. AGA clinical practice guideline on the prevention and treatment of hepatitis B virus reactivation in at-risk individuals. Gastroenterology. 2025;168:267–84. https://doi.org/10.1053/j.gastro.2024.11.008

Address for correspondence: Lukasz Rojek, Department of Gastroenterology and Hepatology, Medical University of Gdansk, ul. Smoluchowskiego 17, 80-214 Gdansk, Poland; email: lrojek@gumed.edu.pl

Invasive Pneumococcal Disease among Childbearing-Age Women, United States, 2007–2023

Namrata Prasad, Sopio Chochua, Bridget J. Anderson, Kathy M. Angeles, Meghan Barnes, Lee H. Harrison, Corinne Holtzman, Jessica R. Howard-Anderson, Shannon O'Brien, Susan Petit, Arthur Reingold, William Schaffner, Lesley McGee, Adam L. Cohen, Miwako Kobayashi

Author affiliations: Centers for Disease Control and Prevention, Atlanta, Georgia, USA (N. Prasad, S. Chochua, L. McGee, A.L. Cohen, M. Kobayashi); New York State Department of Health, Albany, New York, USA (B.J. Anderson); New Mexico Department of Health, Santa Fe, New Mexico, USA (K.M. Angeles); Colorado Department of Public Health and the Environment, Denver, Colorado, USA (M. Barnes); Johns Hopkins Bloomberg School of Public Health, Baltimore, Maryland, USA (L.H. Harrison); Minnesota Department of Health, St. Paul, Minnesota, USA (C. Holtzman); Emory University School of Medicine, Atlanta (J.R. Howard-Anderson); Oregon Health Authority, Portland, Oregon, USA (S. O'Brien); Connecticut Department of Public Health, Hartford, Connecticut, USA (S. Petit); California Emerging Infections Program, Oakland, California, USA (A. Reingold); University of California, Berkeley, California (A. Reingold); Vanderbilt University School of Medicine, Nashville, Tennessee, USA (W. Schaffner)

DOI: https://doi.org/10.3201/eid3202.251279

US data on invasive pneumococcal disease incidence among pregnant and postpartum women are limited. We estimated incidence in those groups using population-based surveillance. Compared with nonpregnant women of childbearing age, incidence was similar for pregnant women but 3.5 times higher for postpartum women. Our findings could inform pneumococcal vaccine recommendations.

Streptococcus pneumoniae is a leading cause of serious bacterial infections, including invasive pneumococcal disease (IPD), defined as *S. pneumoniae* infection in a normally sterile site (e.g., blood, cerebrospinal fluid). IPD most commonly affects young children, older adults, and people with certain underlying conditions (*1*). For adolescents and adults <50 years of age with specific conditions, the Advisory Committee on Immunization Practices (ACIP) recommends use of 15-valent, 20-valent, or 21-valent pneumococcal conjugate vaccines (PCV) (*2*). However, ACIP has not reviewed data on PCV use in pregnant or postpartum women and does not offer recommendations for those groups (*3*). The American College of Obstetricians and Gynecologists, by contrast, recommends PCV for pregnant women at increased risk for severe disease (*4*). To help address this gap in recommendations, we analyzed IPD epidemiology among US women of childbearing age. We conducted research in accordance with applicable federal law and Centers for Disease Control and Prevention policy.

We included all IPD cases among pregnant, postpartum, and nonpregnant childbearing-age women (15–44 years of age) reported by Active Bacterial Core surveillance (ABCs) during 2007–2023. ABCs is an active laboratory- and population-based, multistate surveillance system. We defined IPD as isolation of *S. pneumoniae* bacteria from a sterile site in a surveillance-area resident (*5*). We defined the postpartum period as ≤30 days after delivery.

We reported IPD incidence as cases per 1,000 person-years. We estimated denominators for incidence rates using published methods (*6*). In brief, we estimated the number of pregnant women by multiplying annual live births, induced abortions, and early and late fetal losses by the mean proportion of the year a woman is pregnant for each outcome (live birth = 0.75, abortion = 0.12, early loss = 0.14, late loss = 0.52). We estimated the number of postpartum women by multiplying live births by one twelfth. We estimated the number of nonpregnant women by subtracting pregnant and postpartum women from the total number of childbearing-age women in ABCs areas. We used a mixed-effects Poisson model, including ABCs site as a random effect, to estimate incidence rates, incidence rate ratios (IRRs), and 95% CIs.

We compared demographic and clinical characteristics and PCV20 and PCV21 serotype groups by pregnancy status across cases. We assessed differences using *t* test, Pearson χ^2 test, or Fisher exact test and considered $p<0.05$ statistically significant. We conducted analyses using R version 4.0.4 (The R Project for Statistical Computing, https://www.r-project.org) across the entire surveillance period and during the more recent period of 2019–2023 to account for changes in PCV recommendations and serotype distribution over time.

During 2007–2023, we identified 3,651 IPD cases among childbearing-age women, including 146 (4.0%) pregnant, 61 (1.7%) postpartum, and 3,444 (94.4%) nonpregnant women (Figure 1). Gestational week data were available for 77 (52.7%) cases; of those, 12 (15.6%) were in the first trimester, 31 (40.3%) the second trimester, and 34 (44.2%) the third trimester at the time of illness. During 2019–2023, IPD incidence in pregnant women (0.017 [95% CI 0.011–0.028] per 1,000 person-

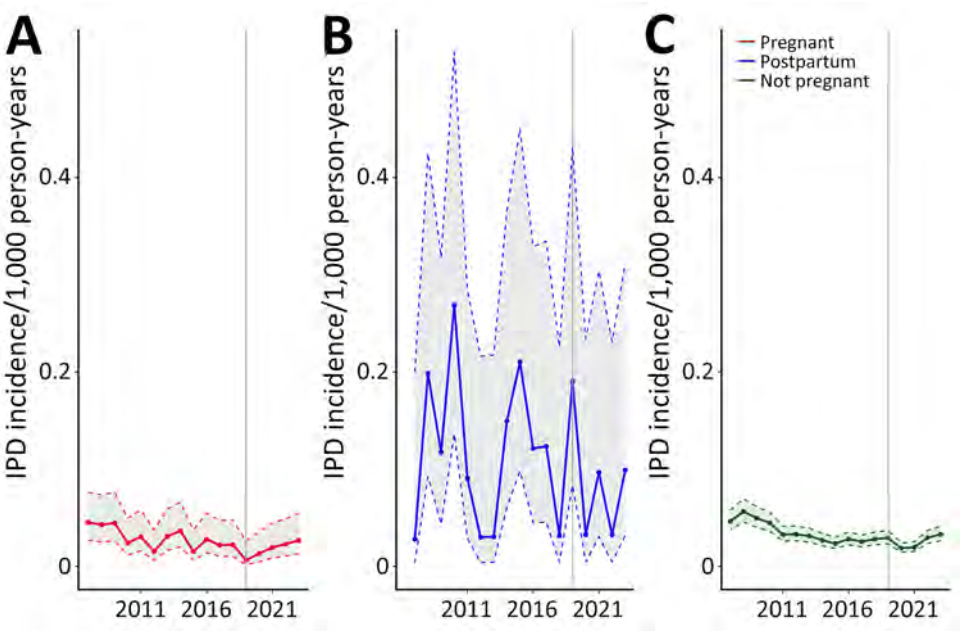

Figure. Incidence of IPD among pregnant (A), postpartum (B), and nonpregnant (C) women of childbearing age, United States, 2007–2023. Data were obtained from Active Bacterial Core surveillance. Shaded areas represent 95% CIs. IPD, invasive pneumococcal disease.

years) was not significantly different from that in nonpregnant women (0.025 [95% CI 0.019–0.034] per 1,000 person-years) (IRR 0.68 [95% CI 0.47–1.00]). In contrast, postpartum women (0.088 [95% CI 0.048–0.161] per 1,000 person-years) had higher IPD risk than did nonpregnant women (IRR 3.49 [95% CI 2.06–5.90]).

Table. Characteristics of invasive pneumococcal disease cases among pregnant, postpartum, and nonpregnant childbearing-age women, United States, 2007–2023*

Characteristic	Pregnant, n = 146		Postpartum, n = 61		Nonpregnant, n = 3,444
	Value	p value	Value	p value	
Mean age, y (IQR)	29 (25–34)	<0.001	30 (25–34)	<0.001	35 (30–41)
Clinical manifestations, no. (%)†					
Bacteremia	33 (22.6)	0.012	10 (16.4)	0.850	506 (14.7)
Meningitis	7 (4.8)	0.135	5 (8.2)	1.000	299 (8.7)
Pneumonia	93 (63.7)	0.142	38 (62.3)	0.263	2,403 (69.8)
Other	25 (17.1)	0.008	19 (31.1)	0.626	947 (27.5)
Patient outcome					
Admitted to ICU	28/89 (31.4)	0.056	15/47 (31.9)	0.205	1,000/2,369 (42.2)
Death	3/146 (2.1)	0.014	0/61 (0.0)	NA	273/3,443 (7.9)
Fetal outcome in cases with available data					
Survived, no apparent illness or still pregnant	98/118 (83.1)		42/55 (76.4)		NA
Survived, clinical infection	1/118 (0.8)		3/55 (5.5)		NA
Miscarriage/stillbirth	18/118 (15.3)		8/55 (14.5)		NA
Underlying conditions, no. (%)‡	66 (45.2)	<0.001	25 (41.0)	<0.001	2,407 (69.9)
Chronic conditions	53 (36.3)	0.463	20 (32.8)	0.336	1,367 (39.7)
Immunocompromising conditions, cerebrospinal fluid leak, or cochlear implant	13 (8.9)	<0.001	5 (8.2)	<0.001	1,040 (30.2)
Healthy	80 (54.8)	<0.001	36 (59.0)	<0.001	1,037 (30.1)
Serotyped IPD cases during 2019–2023					
PCV20-covered serotypes§	16/23 (69.6)	0.598	8/12 (66.7)	1.000	460/743 (61.9)
PCV21-covered serotypes¶	15/23 (65.2)	0.346	8/12 (66.7)	0.497	564/743 (76.0)
Covered by neither	1/23 (4.3)	1.000	2/12 (16.7)	0.265	61/743 (8.9)

*Values are no. positive/total no. (%) except as indicated. ICU, intensive care unit; IPD, invasive pneumococcal disease; IQR, interquartile range; NA, not applicable; PCV20, 20-valent pneumococcal conjugate vaccine; PCV21, 21-valent pneumococcal conjugate vaccine.
†Sum of proportions could be >100% because case-patients could have had >1 clinical manifestation identified.
‡Conditions included chronic conditions (alcoholism; chronic heart, liver, or lung disease; chronic renal failure; cigarette smoking; diabetes mellitus) and immunocompromising conditions (congenital or acquired asplenia; generalized malignancy; HIV; Hodgkin disease; immunodeficiency; iatrogenic immunosuppression; leukemia, lymphoma, or multiple myeloma; nephrotic syndrome; solid organ transplant; or sickle cell disease or other hemoglobinopathies). Cerebrospinal fluid leak and cochlear implant were grouped together with immunocompromising conditions to align with 2023 vaccine recommendations (*3*).
§PCV20 serotypes: 1, 3, 4, 5, 6A, 6B, 7F, 8, 9V, 10A, 11A, 12F, 14, 15B, 18C, 19A, 19F, 22F, 23F, and 33F.
¶PCV21 serotypes: 3, 6A, 7F, 8, 9N, 10A, 11A, 12F, 15A, 15B, 15C, 16F, 17F, 19A, 20A, 22F, 23A, 23B, 24F, 31, 33F, and 35B. PCV21 is approved for the prevention of invasive pneumococcal disease caused by serotype 15B based upon prespecified criteria for the proportion of participants with 4-fold or more rise in opsonophagocytic activity responses. Source: US Food and Drug Administration (https://www.fda.gov/media/179426/download?attachment).

Compared with IPD cases among nonpregnant women (mean age 35 years), pregnant (mean age 29 years; p<0.001) and postpartum case-patients (mean age 30 years; p<0.001) were younger and less likely to have underlying conditions (pregnant women = 45.2%; postpartum women = 41.0%; nonpregnant women = 69.9%; p<0.001) (Table). That difference was particularly noticeable for women with immunocompromising conditions. Pregnant women had a lower IPD case-fatality ratio (2.1%) than did nonpregnant women (7.9%; p = 0.014). Among IPD cases in pregnant and postpartum women, most (>75%) experienced favorable fetal outcomes (no pregnancy loss or clinical infection). During 2019–2023, the proportion of IPD cases caused by PCV20, PCV21, or nonvaccine serotypes did not vary significantly by pregnancy status; 484/778 (62.2%) of cases were caused by serotypes covered by PCV20 and 587/778 (75.4%) by serotypes covered by PCV21 (Table).

Our findings align with previous studies showing no increased IPD risk during pregnancy but elevated risk postpartum (*7*,*8*). One study also found IPD risk was slightly increased in third-trimester pregnant women compared with nonpregnant women (*7*). Similar stratifications were not possible in our study because we lacked complete gestational week data. In our study, pregnant and postpartum women were younger and healthier than nonpregnant women, which likely reflected the underlying population that becomes pregnant. Those differences might have influenced observed IPD risk and outcomes; we could not account for them in incidence and IRR estimations because we lacked denominator data stratified by age and underlying conditions. Further studies are needed to determine factors associated with increased risk for IPD in the postpartum period.

In conclusion, we found that IPD incidence was similar among pregnant and nonpregnant women but higher among postpartum women. Our findings could inform pneumococcal vaccine recommendations for women of childbearing age.

Acknowledgments

For their invaluable contributions to Active Bacterial Core surveillance, we thank Maria Rosales, Joelle Nadle (California Emerging Infections Program); Amanda Hickey, Carmen Marquez, Htet Htet Wrigley, Daniel Wurm (Connecticut Department of Public Health); Stepy Thomas, Amy Tunali, Samantha Sefton (Georgia Emerging Infections Program, Emory University School of Medicine); Shannon Seopaul, Terresa Carter, Vijitha Lahanda Wadu, and Laura Jeffrey (Maryland Emerging Infections Program); Brenda Jewell, Lori Triden, Theresa Weber, Richard Danila, Catherine Lexau, Jean Rainbow, Kathy Como-Sabetti, Ruth Lynfield, Craig Morin, Paula Snippes, Kerry MacInnes, Melanie Carroll, Annah Schneider, and Alexys Ruckdaschel (Minnesota Department of Health); Jessica Houston, Salina Torres, Mayvilynne Poblete, Zachary Landis, Sarah A. Khanlian (New Mexico Emerging Infections Program); Suzanne McGuire, Kari Burzlaff, Cassandra Sherman, Lauren Ryan, Kerianne Engesser, and Rachel Wester (New York Emerging Infections Program); H. Keipp Talbot, Tiffanie Markus, Anise Swain, Danielle Ndi, Gail Hughett and Melinda Eady (Vanderbilt University Medical Center); Melissa Arvay, Yunmi Chung, Jasmine Varghese, Sylvia Tangney (Centers for Disease Control and Prevention)

L.H.H. reported serving as a consultant to Sanofi Pasteur, Merck, GSK, Pfizer, and CSL Seqirus. J.R.H.-A. reported grant funding from National Institutes of Health unrelated to this work and travel support from the Society for Healthcare Epidemiology of America, the American Society for Microbiology, the Infectious Diseases Society of America, and National Institutes of Health.

About the Author

Dr. Prasad is an epidemiologist within the Pneumonia *Streptococcus* Epidemiology Branch, Division of Bacterial Diseases, National Center for Immunization and Respiratory Diseases, Centers for Disease Control and Prevention. Her research interests include the epidemiology of infectious diseases among pregnant women and infants and the use of maternal vaccines as a preventative strategy.

References

1. Centers for Disease Control and Prevention. Pneumococcal disease: causes and how it spreads. [cited 2025 May 21]. https://www.cdc.gov/pneumococcal/causes
2. Centers for Disease Control and Prevention. Pneumococcal vaccine recommendations. 2024 [cited 2025 May 21]. https://www.cdc.gov/pneumococcal/hcp/vaccine-recommendations
3. Kobayashi M, Pilishvili T, Farrar JL, Leidner AJ, Gierke R, Prasad N, et al. Pneumococcal vaccine for adults aged ≥19 years: recommendations of the Advisory Committee on Immunization Practices, United States, 2023. MMWR Recomm Rep. 2023;72:1–39. https://doi.org/10.15585/mmwr.rr7203a1
4. American College of Obstetricians and Gynecologists. Maternal immunization. 2022 [cited 2025 Jun 9]. https://www.acog.org/clinical/clinical-guidance/practice-advisory/articles/2022/10/maternal-immunization
5. Centers for Disease Control and Prevention. Active Bacterial Core surveillance (ABCs). [cited 2025 Jun 9]. https://www.cdc.gov/abcs
6. Centers for Disease Control and Prevention. Estimating the number of pregnant women in a geographic area—a reproductive health tool. 2024 [cited 2024 May 12].

https://www.cdc.gov/reproductive-health/media/pdfs/emergency/Pregnant-Population-Size-Estimator-508.pdf
7. Amin-Chowdhury Z, Bertran M, Abdullahi F, Sheppard CL, Eletu SD, Litt DJ, et al. Risk of invasive pneumococcal disease during pregnancy and postpartum and association with adverse maternal and foetal outcomes: a prospective cohort study, England, 2014–19. J Infect. 2025;90:106363. https://doi.org/10.1016/j.jinf.2024.106363
8. Deutscher M, Lewis M, Zell ER, Taylor TH Jr, Van Beneden C, Schrag S; Active Bacterial Core Surveillance Team. Incidence and severity of invasive *Streptococcus pneumoniae*, group A *Streptococcus*, and group B *Streptococcus* infections among pregnant and postpartum women. Clin Infect Dis. 2011;53:114–23. https://doi.org/10.1093/cid/cir325

Address for correspondence: Namrata Prasad, Centers for Disease Control and Prevention, 1600 Clifton Rd NE, Mailstop H24-8, Atlanta, GA 30329-4018, USA; email: riz9@cdc.gov

Multicenter Serologic Investigation of Influenza D Virus in Cats and Dogs, Europe, 2015–2024

Claudia Maria Trombetta, Aurora Fiori,[1] Alessandro Falsini,[1] Francesco Pellegrini, Sophie Le Poder, Amit Eichenbaum, Venetia Cardona, Justine Oliva, Gilles Meyer, Nataliia Muzyka, Denys Muzyka, Emanuele Montomoli, Barbara di Martino, Mariette F. Ducatez, Gianvito Lanave, Vito Martella, Michele Camero

Authors affiliations: University of Siena, Siena, Italy (C.M. Trombetta, A. Fiori, A. Falsini, E. Montomoli); University of Bari Aldo Moro, Valenzano, Italy (F. Pellegrini, G. Lanave, V. Martella, M. Camero); Ecole Nationale Vétérinaire d'Alfort, Maisons-Alfort, France (S. Le Poder, A. Eichenbaum, V. Cardona); Université de Toulouse, Toulouse, France (J. Oliva, G. Meyer, M.F. Ducatez); National Scientific Center Institute of Experimental and Clinical Veterinary Medicine, Kharkiv, Ukraine (N. Muzyka; D. Muzyka); Linnaeus University, Kalmar, Sweden (D. Muzyka); VisMederi srl, Siena (E. Montomoli); University of Teramo, Teramo, Italy (B. di Martino); University of Veterinary Medicine, Budapest, Hungary (V. Martella)

DOI: https://doi.org/10.3201/eid3202.251164

[1]These authors contributed equally to this article.

We conducted a multicenter study in Europe (France, Italy, and Ukraine) to assess the seroprevalence of influenza D virus (IDV) in domestic cats and dogs. Serum samples from France (2015–2018) and Italy (2023–2024) showed no IDV positivity. In Ukraine, 2.46% of dogs and 0.85% of cats tested IDV-positive in 2024.

Influenza D virus (IDV) has cattle as its primary reservoir but can occasionally spill over into other species (*1*,*2*). Recent serologic findings in dogs (Italy) and cats (China) suggest a broader host range than previously recognized (*3*,*4*). We investigated IDV seroprevalence in feline and canine samples in a multicenter study in Italy, France, and Ukraine.

In the Apulia region of Italy, we obtained serum samples from 76 domestic cats in 2023 and 56 domestic cats in 2024 collected by veterinary offices either for presurgical evaluation or routine analysis. In France, we obtained serum samples from 114 dogs and 47 cats collected during animal hospitalizations in 2015–2018 at the companion animal clinic at École Vétérinaire de Maisons-Alfort in the Ile-de-France region. Dog nasal swab (n = 41) and lung tissue (n = 24) samples originated from either a shelter or from clinics from animals with respiratory clinical signs. In Ukraine, we collected serum samples from 118 domestic cats and 122 dogs in 2020, 2023, and 2024 from veterinary clinics from the oblasts (i.e., administrative divisions) of Donetsk, Zaporizhzhia, Khmelnytska, Odesa, Kyiv, Lviv, Kharkiv, and Dnipropetrovsk (Table 1; Appendix, https://wwwnc.cdc.gov/EID/article/32/2/25-1164-App1.pdf).

We tested all samples in duplicate by hemagglutination inhibition (HI) assay by using IDV strains from 2 viral lineages: strain D/bovine/Oklahoma/660/2013, D/660 lineage, and either strain D/swine/Italy/199724–3/2015 or strain D/bovine/France/5920/2014, D/OK lineage. Samples from France and Ukraine underwent further testing (Table 1).

Samples from 3/122 dogs (2.46% [95% CI 0.51%–7.02%]) and 1/118 cat (0.85% [95% CI 0.02%–4.63%]) collected in Ukraine in 2024 tested positive for D/660; the samples originated primarily from Odesa Oblast, except for 1 dog sample from Zaporizhzhia Oblast (Table 2). All samples were negative for influenza A virus by ELISA. All swab and tissue samples from France were IDV-negative by real-time reverse transcription PCR.

Our findings provide evidence of IDV exposure in clinical healthy domestic cats (0.85%) and dogs (2.46%) from the Odesa and Zaporizhzhia oblasts in Ukraine, although the dogs and cats from those regions had relatively low IDV seropositivity rates and titers. Those results align with 2 recent studies on IDV circulation in dogs and cats, indicating seroprevalences of 1.2% in

Table 1. Overview of samples, including country, year of collection, testing assays, IDV strains, and other information, analyzed for multicenter serologic investigation of IDV in cats and dogs, Europe, 2015–2024*

Animal species	Country	No. samples (type)	Year of collection	Assay	IDV strain	Other tests or assays
Cat	France	47 (serum)	2015–2018	HI	D/OK	ICV HI, IAV NP ELISA
	Italy	132 (serum)	2023–2024	HI	D/OK, D/660	None
	Ukraine	118 (serum)	2020–2023–2024	HI	D/OK, D/660	None
Dog	France	114 (serum), 41 (nasal swab), 24 (lung fragment)	2015–2018	HI, qRT-PCR	D/OK	ICV HI, IAV NP ELISA
	Ukraine	122 (serum)	2020–2023–2024	HI	D/OK, D/660	IAV NP ELISA

*HI, hemagglutination inhibition; IAV NP ELISA, influenza A virus antibodies by nucleoprotein ELISA; ICV, influenza C virus; IDV, influenza D virus, qRT-PCR, real-time reverse transcription PCR.

2016 and 4.7% in 2023 for D/660 in dogs in southern Italy and of 2.22% in cats in northern China (*3*,*4*). In the study in China, household cats showed substantially higher exposure rates than stray cats, probably because of increased human contact, whereas the independent lifestyles of stray cats might limit exposure.

In our study, the source of IDV infection in cats remains unclear. Although serologic testing cannot confirm active transmission or whether infection with IDV can cause disease or clinical signs, the seroprevalence in domestic cats and dogs suggests that close human–animal interactions might increase exposure risks. All the positive samples from 2024 belonged to the D/660 lineage, which was first detected in Europe in 2018 (*5*). None of these samples reacted against the D/OK lineage, which was likely replaced by D/660 lineage in Europe since 2019 (*5*).

The samples from pets in Italy and France tested negative for IDV. Because the samples in France were only tested against D/OK, results suggest that the D/OK lineage possibly was no longer circulating in France or, at least, not in the surveyed area. Factors such as urbanization and the limited presence of cattle and other susceptible species might be involved.

We also tested samples in France for influenza C virus (ICV); 2.63% of dogs tested positive, and HI titers ranged from 20 to 80, supporting previous evidence of dog susceptibility to ICV infection. An older study conducted in France during 1988–1989 found HI reactivity in dogs as high as 32% and titers ranging from 1:20 to 1:320 (*6*).

One limitation of our study is that we used a convenience collection of samples. In addition, in Italy and France we collected samples from a single geographic area. Moreover, information on age and sex of the collected animals was not available. Furthermore, we used different assays and different IDV strains and lineages for screening at the various locations. For example, for the IDV screening, we tested the samples in France only for D/OK, but we tested the samples in Italy and Ukraine for D/OK and D/660. Only the France samples were tested for ICV.

Overall, our findings suggest that household dogs and cats might be exposed to IDV and could serve as a potential source of human infection. Proactive surveillance in pets is critical to understand the changing epidemiology of IDV and to mitigate potential public health concerns. In a One Health perspective, cats and dogs are uniquely positioned to act as reservoirs for influenza virus infections in both household and rural environments.

Table 2. HI titers of IDV-positive samples collected in 2024 in Ukraine, as part of multicenter serologic investigation of IDV in cats and dogs, Europe, 2015–2024*

	HI assay titers	
Sample no.	D/660 lineage	D/OK lineage
Dog	20–20	<10
180	20–20	<10
182	20–20	<10
184	10–10	<10
Cat		
181	20–20	<10

*Titers below the detectable threshold of 10 were expressed as <10 and considered negative. HI, hemagglutination inhibition; IDV, influenza D

This article was preprinted at https://doi.org/10.64898/2026.01.03.697426.

Acknowledgments

We thank Feng Li for kindly providing the strain D/bovine/Oklahoma/660/2013. The strain D/swine/Italy/199724-3/2015 was obtained from the European Virus Archive.

Ethics approval for this research was waived by the Ethics Committee for Animal Experimentation, University of Bari (Valenzano, Italy) (protocol no. 5040-II/13). The animal study was reviewed and approved by the Institutional Animal Care and Use Committee of the National Scientific Center Institute of Experimental and Clinical Veterinary Medicine, Ukraine (protocol no. 1-23, 19.04.2023). Ethical review and approval were waived for the samples in France because they were collected and analyzed for diagnostic purposes.

The original data contributions presented in the study are included in the article; further inquiries can be directed to the corresponding author.

This publication was supported by the European Virus Archive GLOBAL project that received funding from the

European Union's Horizon 2020 research and innovation program (grant no. 871029). The research was supported by a grant from the National Research Foundation of Ukraine (grant no. 2021.01/0006) and by France's Agence Nationale de la Recherche (grant no. ANR-15-CE35-0005).

V.M. was supported by the University of Veterinary Medicine Budapest's National Laboratory for Infectious Animal Diseases, Antimicrobial Resistance, Veterinary Public Health, and Food Chain Safety (grant no. RRF-2.3.1-21-2022-00001).

E.M. discloses he is founder and Chief Scientific Officer of VisMederi srl.

Author contributions: conceptualization, C.M.T.; formal analysis, C.M.T.; investigation, A.F., A.F., A.E., J.O.; resources, C.M.T., F.P., M.C., S.L.P., G.M., M.F.D., N.M., D.M., E.M.; data curation, C.M.T., J.O., M.F.D., S.L.P.; original draft preparation, C.M.T.; review and editing, M.F.D., V.M., C.M., F.P., G.L.; visualization, A.F.; supervision, C.M.T., S.L.P., G.M., M.F.D.; project administration, C.M.T., S.L.P., G.M., M.F.D. All authors have read and agreed to the published version of the manuscript.

About the Author

Dr. Trombetta is an associate professor of hygiene and public health at the University of Siena. Her primary research interests include zoonotic viruses, infectious disease, and vaccine-preventable diseases.

References

1. Manuguerra JC, Hannoun C. Natural infection of dogs by influenza C virus. Res Virol. 1992;143:199–204. https://doi.org/10.1016/S0923-2516(06)80104-4
2. Hause BM, Ducatez M, Collin EA, Ran Z, Liu R, Sheng Z, et al. Isolation of a novel swine influenza virus from Oklahoma in 2011 which is distantly related to human influenza C viruses. PLoS Pathog. 2013;9:e1003176. https://doi.org/10.1371/journal.ppat.1003176
3. Gaudino M, Moreno A, Snoeck CJ, Zohari S, Saegerman C, O'Donovan T, et al. Emerging influenza D virus infection in European livestock as determined in serology studies: are we underestimating its spread over the continent? Transbound Emerg Dis. 2021;68:1125–35. https://doi.org/10.1111/tbed.13812
4. Shen M, Zhao X, Zhang J, Liu C, Qi C, Wang R, et al. Influenza D virus in domestic and stray cats, northern China, 2024. Emerg Infect Dis. 2025;31:1668–70. https://doi.org/10.3201/eid3108.250042
5. Trombetta CM, Marchi S, Marotta MG, Moreno A, Chiapponi C, Montomoli E, et al. Detection of influenza D antibodies in dogs, Apulia region, Italy, 2016 and 2023. Emerg Infect Dis. 2024;30:1045–7. https://doi.org/10.3201/eid3005.231401
6. Gaudino M, Chiapponi C, Moreno A, Zohari S, O'Donovan T, Quinless E, et al. Evolutionary and temporal dynamics of emerging influenza D virus in Europe (2009–22). Virus Evol. 2022;8:veac081. https://doi.org/10.1093/ve/veac081

Address for correspondence: Claudia Maria Trombetta, Department of Molecular and Developmental Medicine, University of Siena, Aldo Moro 2, 53100, Siena, Italy; email: trombetta@unisi.it

Vesicular Disease Caused by Seneca Valley Virus in Pigs, England, 2022

Bryony Armson, Valérie Mioulet, Britta A. Wood, Antonello Di Nardo, Nick J. Knowles, Jemma Wadsworth, David J. Paton, Jozhel Baguisi, Harry Bull, Amy McCarron, Clare Browning, Ashley Gray, Tomasz Zaleski, Andrew E. Shaw, Anna B. Ludi, Mark Henstock, Hayley M. Hicks, Ginette Wilsden, Krupali Parekh, Julie Maryan, Sarah Belgrave, Noemi Polo, Simon Gubbins, Claire Colenutt, Melanie Nicholls, Emma Brown, Efthymia Nasou, Anca Drelciuc, Livio Pittalis, David Jorge, Caroline Wilson, Susana Taylor, Jose Bis, Charles Nfon, Susanna Williamson, Donald P. King

Author affiliations: The Pirbright Institute, Woking, UK (B. Armson, V. Mioulet, B.A. Wood, A. Di Nardo, N.J. Knowles, J. Wadsworth, D.J. Paton, J. Baguisi, H. Bull, A. McCarron, C. Browning, A. Gray, T. Zaleski, A.E. Shaw, A.B. Ludi, M. Henstock, H.M. Hicks, G. Wilsden, K. Parekh, J. Maryan, S. Belgrave, N. Polo, S. Gubbins, C. Colenutt, M. Nicholls, E. Brown, D.P. King); University of Cambridge, Cambridge, UK (T. Zaleski); Animal and Plant Health Agency, Bury St Edmunds, UK (T. Zaleski, E. Nasou, A. Drelciuc, L. Pittalis, D. Jorge, C. Wilson, S. Taylor, J. Bis, S. Williamson); National Centre for Foreign Animal Disease, Canadian Food Inspection Agency, Winnipeg, Manitoba, Canada (C. Nfon)

DOI: http://doi.org/10.3201/eid3202.251194

Vesicular disease caused by Seneca Valley virus infection occurred in pigs from 5 outdoor pig farms in England during June–September 2022. Clinical signs resembled notifiable vesicular diseases, such as foot-and-mouth disease. Full genome sequences shared a common ancestor with a virus circulating in the United States.

Researchers reported vesicular disease associated with Seneca Valley virus (SVV; *Senecavirus valles*, family Picornaviridae) in pigs imported into the United States from Canada in 2007 (*1*). Similar reports subsequently emerged from other countries, including Brazil, China, Thailand, Chile, India, Vietnam, Columbia, and Mexico (*2*–*4*). We describe cases of SVV infection in pigs from 5 pig breeding farms in eastern England during June–September 2022.

Farm staff initially observed signs of vesicular disease in recently inseminated sows at an outdoor breeding unit (SVV2022-01): lameness, reluctance to move, and lesions on the nose and feet, varying from discrete vesicles on the coronary band and interdigital space to deep erosions and heel horn separation. We collected blood and vesicular tissue samples as part of an official vesicular disease investigation; all samples tested negative by real-time reverse transcription PCR (rRT-PCR) for notifiable diseases (foot-and-mouth disease virus, swine vesicular disease virus, and vesicular stomatitis virus) (*5*). However, we observed cytopathic effect during virus isolation, and parallel rRT-PCR testing (*6*) generated positive results for SVV.

We subsequently identified vesicular disease in recently inseminated sows on 3 additional farms (SVV2022-02 [Figure 1], SVV2022-03 and SVV2022-05). Again, official veterinary investigations yielded negative results for notifiable diseases and confirmed the presence of SVV by rRT-PCR. Gilts, young boars, and weaners appeared clinically unaffected, despite evidence of SVV in rectal and nasal swab specimens. Retrospective tracing identified another farm (SVV2022-04) with confirmed SVV in a group of recently lame sows.

We collected samples including vesicular epithelium, vesicular fluid, rectal and nasal swabs, blood, and tonsils from dead pigs. We also collected samples from weaners derived from 4 of the 5 affected farms and from sows and postmortem pigs at farm SVV2022-03 for up to 4 months after the initial disease reports. In total, 461 (35.0%) of 1,319 samples tested positive for SVV by rRT-PCR from the 5 farms (Appendix Table). On farms SVV2022-01 and SVV2022-02, we initially collected blood samples, with 17 of 34 positive by rRT-PCR; however, because viremia is short-lived, that sampling matrix was not ideal for surveillance. Analysis revealed the highest viral loads

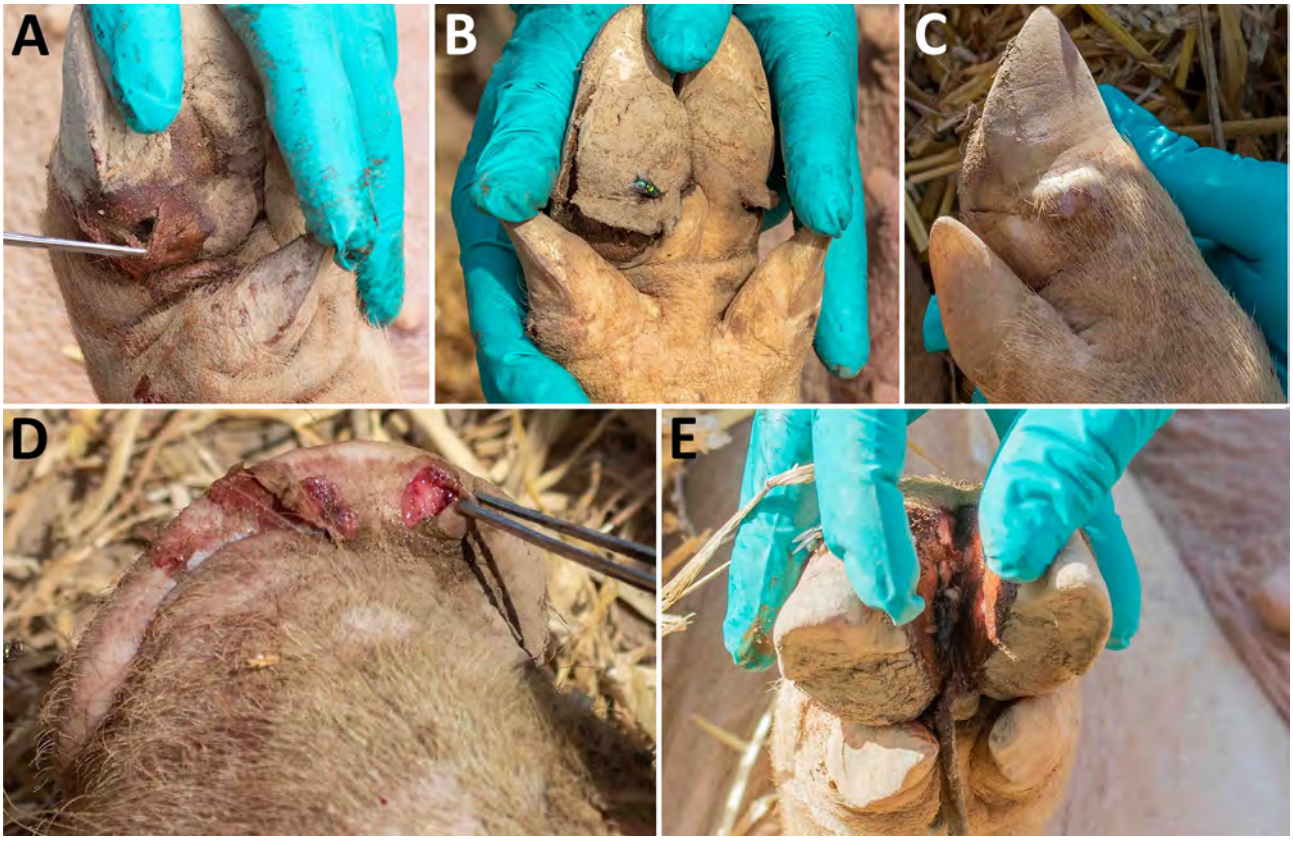

Figure 1. Affected pigs on farm SVV2022-02, from study of vesicular disease caused by Seneca Valley virus in pigs, England, 2022. Vesicular lesions can be seen on the coronary bands (A-C), snout (D), and interdigital cleft (E). Hoof horn separation also occurred in some infected pigs (B). Some lesions resembled those of foot-and-mouth disease (D), but others were more deep-seated (A).

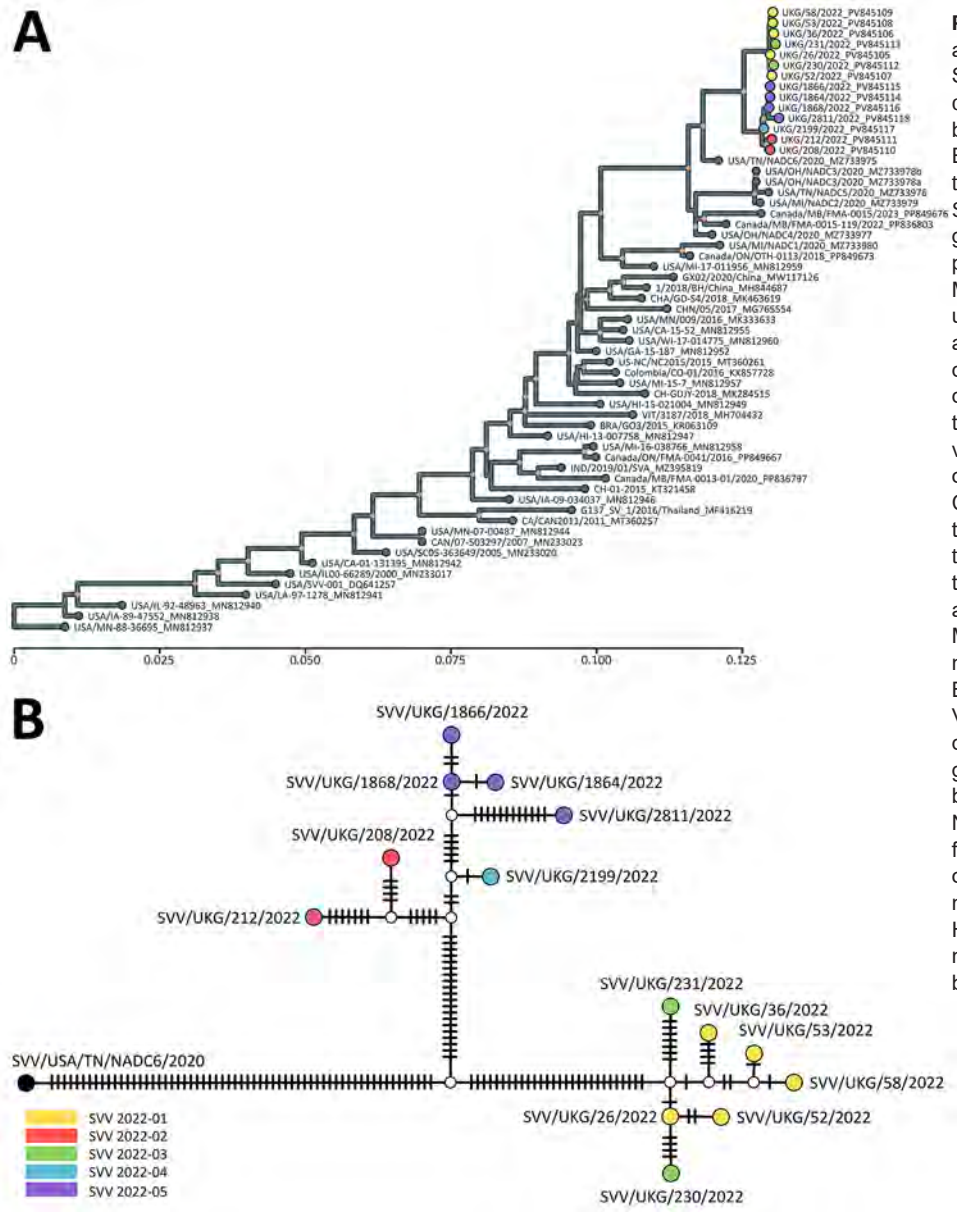

Figure 2. Evolutionary history and genetic relationships of Seneca Valley viruses from study of vesicular disease caused by Seneca Valley virus in pigs, England, 2022. A) Tree represents the evolutionary history of Seneca Valley viruses isolated globally and reconstructed using polyprotein-coding sequences. Maximum-likelihood tree inferred using the Tamura-Nei model (*9*) and setting a discrete gamma distribution for evolutionary rate differences among sites. Colored tips represent Seneca Valley virus–infected farms during the outbreak in England in 2022. Colored internal nodes represent the percentage of trees in which the associated taxa clustered together on >50%. Evolutionary analyses were conducted in MEGA11 (*10*). Scale bar indicates nucleotide substitutions per site. B) Genetic relationship of Seneca Valley viruses isolated in England during 2022 based on the full-genome length, as reconstructed by statistical parsimony analysis. Nodes are colored according to farm on which clinical cases were observed; white nodes denote missing unsampled haplotypes. Hatch marks represent single-nucleotide substitutions estimated between the connected nodes.

in vesicular lesion and tonsil samples (strongest cycle threshold value 10.8). Rectal swabs were the most frequently collected sample type (n = 914) owing to ease of collection. Nasal swab specimens were useful in revealing acute stages of disease, but rectal swab specimens proved more useful in detecting SVV in recovering pigs, despite weaker rRT-PCR responses. That observation supports the use of rectal swab sampling in pigs of unknown SVV status, where resources or logistics limit sampling options. Our data also highlight the value of testing tonsils, illustrated by detection of SVV RNA in a tonsil from a dead piglet >35 days after the episode of clinical signs (farm SVV2022-02).

We conducted serologic investigations 5 weeks after the disease episode at farm SVV2022-04 and during the acute stage of disease at farm SVV2022-01. A total of 55 of 63 serum samples from farm SVV2022-01 and 10 of 10 samples from farm SVV2022-04 were positive for SVV-specific antibodies as determined by the virus neutralization test using SK6 cells.

Paired rectal and semen samples collected from boars supplying semen and historic batches of feed and soya bean meal samples supplied to affected farms all tested negative for SVV by rRT-PCR. We detected SVV RNA in 76 (56.7%) of 134 environmental samples (*7*) collected 3.5 weeks

after the disease occurrence from farm SVV2022-01, where pigs no longer remained on the premises. Sample sites included walls, doors, feeders, drinkers, floors, gates, and a trailer. We also detected SVV RNA in 6 (10.2%) of 59 samples collected 6 weeks after the disease occurrence from farm SVV2022-04, where pigs remained (sites included loading area, drinker, ark, and trailer) (Appendix Figure). Our data highlight the importance of cleaning, disinfection, and stringent biosecurity to limit the spread of SVV.

We characterized SVV isolates using next-generation sequencing (*8*) and found they share a common ancestor with a virus isolated in the United States during 2020 (SVV/USA/TN/NADC6/2020; GenBank accession no. MZ733975) (Figure 2), predicted to have circulated around November 2020 (95% highest posterior density June 2020–March 2021). The SVV sequences were assigned into 2 sister clades differing at >50 nt sites, consistent with 2 possible epidemiologic scenarios: a single virus introduction, with the resulting diversity accruing from within-country transmissions and evolution; or independent introductions into England of viruses characterized by a slightly different genetic signature. Further epidemiologic investigation could determine the most important risk pathways for introduction, transmission routes between farms, and geographic spread of SVV infection in the United Kingdom.

In conclusion, the clinical similarity of the SVV disease outbreaks we describe to notifiable vesicular diseases highlights the value of passive surveillance and the legal requirement for pig keepers and veterinarians to report vesicular lesions promptly. Cases of SVV infection were transient, and pigs recovered quickly, with minimal productivity losses. We alerted regional veterinarians and farmers of the need to remain vigilant for vesicular disease, and there have been no further clinical cases of SVV in England since September 2022.

We submitted the 14 full genome sequences associated with this study to GenBank and received the corresponding accession numbers: PV845105 (UKG/26/2022), PV845106 (UKG/36/2022), PV845107 (UKG/52/2022), PV845108 (UKG/53/2022), PV845109 (UKG/58/2022), PV845110 (UKG/208/2022), PV845111 (UKG/212/2022), PV845112 (UKG/230/2022), PV845113 (UKG/231/2022), PV845114 (UKG/1864/2022), PV845115 (UKG/1866/2022), PV845116 (UKG/1868/2022), PV845117 (UKG/2199/2022), and PV845118 (UKG/2811/2022).

Acknowledgments

The authors are grateful to the pig farmers, their staff, and veterinary surgeons for their cooperation with official veterinary investigations. We also recognize the contribution of a wide number of staff from the Animal and Plant Health Agency and The Pirbright Institute as part of their routine work.

This study was funded by a combination of UK Department for Environment, Food and Rural Affairs–funded projects at the Animal and Plant Health Agency: Scanning surveillance for Diseases in Pigs (ED1200) and The Pirbright Institute (SE2722, SE2945, SE2947, SE0573, SE0579 and SE1131). The Pirbright Institute also receives grant-aided support from the Biotechnology and Biological Sciences Research Council of the United Kingdom (projects BBS/E/I/00007037, BBS/E/PI/230001A, BBS/E/PI/230002C, and BBS/E/PI/23NB0004).

About the Author

Dr Armson is a postdoctoral scientist at The Pirbright Institute. Her research interests include the epidemiology, diagnostics, and control of viral diseases of livestock.

References

1. Pasma T, Davidson S, Shaw SL. Idiopathic vesicular disease in swine in Manitoba. Can Vet J. 2008;49:84–5.
2. Bennett B, Urzúa-Encina C, Pardo-Roa C, Ariyama N, Lecocq C, Rivera C, et al. First report and genetic characterization of Seneca Valley virus (SVV) in Chile. Transbound Emerg Dis. 2022;69:e3462–8. https://doi.org/10.1111/tbed.14747
3. Maan S, Batra K, Chaudhary D, Punia M, Kadian V, Joshi VG, et al. Detection and genomic characterization of Senecavirus from Indian pigs. Indian J Anim Res. 2023;57:1344–50.
4. Navarro-López R, Perez-De la Rosa JD, Rocha-Martínez MK, Hernández GG, Villarreal-Silva M, Solís-Hernández M, et al. First detection and genetic characterization of Senecavirus A in pigs from Mexico. J Swine Health Prod. 2023;31:289–94. https://doi.org/10.54846/jshap/1358
5. Reid SM, Grierson SS, Ferris NP, Hutchings GH, Alexandersen S. Evaluation of automated RT-PCR to accelerate the laboratory diagnosis of foot-and-mouth disease virus. J Virol Methods. 2003;107:129–39. https://doi.org/10.1016/S0166-0934(02)00210-0
6. Fowler VL, Ransburgh RH, Poulsen EG, Wadsworth J, King DP, Mioulet V, et al. Development of a novel real-time RT-PCR assay to detect Seneca Valley virus-1 associated with emerging cases of vesicular disease in pigs. J Virol Methods. 2017;239:34–7. https://doi.org/10.1016/j.jviromet.2016.10.012
7. Colenutt C, Brown E, Nelson N, Wadsworth J, Maud J, Adhikari B, et al. Environmental sampling as a low-technology method for surveillance of foot-and-mouth disease virus in an area of endemicity. Appl Environ Microbiol. 2018;84:e00686–18. https://doi.org/10.1128/AEM.00686-18

8. Logan G, Freimanis GL, King DJ, Valdazo-González B, Bachanek-Bankowska K, Sanderson ND, et al. A universal protocol to generate consensus level genome sequences for foot-and-mouth disease virus and other positive-sense polyadenylated RNA viruses using the Illumina MiSeq. BMC Genomics. 2014;15:828. https://doi.org/10.1186/1471-2164-15-828
9. Tamura K, Nei M. Estimation of the number of nucleotide substitutions in the control region of mitochondrial DNA in humans and chimpanzees. Mol Biol Evol. 1993;10:512–26.
10. Tamura K, Stecher G, Kumar S. MEGA11: Molecular evolutionary genetics analysis version 11. Mol Biol Evol. 2021;38:3022–7. https://doi.org/10.1093/molbev/msab120

Address for correspondence: Bryony Armson, The Pirbright Institute, Ash Road, Woking, Surrey GU24 0NF, UK; email: bryony.armson@pirbright.ac.uk

Vaccine-Like African Swine Fever Virus Strain in Domestic Pigs, Thailand, 2024

Trong Tung Nguyen, Dhithya Venkateswaran, Anwesha Prakash, Quynh Anh Nguyen, Roypim Suntisukwattana, Anan Jongkaewwattana, Theeradej Thaweerattanasinp, Janya Saenboonrueng, Van Phan Le, Dachrit Nilubol

Author affiliations: Swine Viral Evolution and Vaccine Development Research Unit, Chulalongkorn University, Bangkok, Thailand (T.T. Nguyen, D. Venkateswaran, A. Prakash, Q.A. Nguyen, R. Suntisukwattana, D. Nilubol); National Center for Genetic Engineering and Biotechnology, Pathum Thani, Thailand (A. Jongkaewwattana, T. Thaweerattanasinp, J. Saenboonrueng); College of Veterinary Medicine, Vietnam National University of Agriculture, Hanoi, Vietnam (V.P. Le)

DOI: http://doi.org/10.3201/eid3202.251245

African swine fever virus genotype II is endemic in Thailand, typically causing acute disease. We investigated a vaccine-like strain, characterized by 6 multigene family gene deletions, from nonvaccinated herds. We found this strain was associated with chronic disease in pigs.

African swine fever (ASF) is a fatal hemorrhagic disease of pigs, caused by African swine fever virus (ASFV), a complex DNA virus in the Asfarviridae family (*1*). Researchers first identified ASF in Kenya in 1921, and subsequent reports identified 24 genotypes in Africa on the basis of nucleotide variations within the partial B646L gen (*2*,*3*). Reports in the medical literature confirm incidence of only ASFV genotype I and genotype II outside Africa.

In 2018, researchers identified ASFV genotype II in China (*4*), and it rapidly spread across Asia within a few months. Since then, the situation in Asia has shifted from an epidemic to an endemic stage, with the highly virulent genotype II strain causing peracute, acute, and subacute disease. Recent research suggests the emergence of more genetically diverse ASFV variants, including chronic disease–associated genotype I, highly virulent recombinants of genotypes I and II, and naturally and artificially attenuated strains in domestic pigs in China and Vietnam (*5*–*7*).

Thailand health authorities officially reported ASFV in Thailand in 2022 (*8*), and the strain was genetically identical to the strain first reported in China and Vietnam. Currently, ASF cases in Thailand involve patients with chronic symptoms and low mortality rates, suggesting the emergence of low-virulent strains. We conducted a survey of ASFV from recent outbreaks in Thailand, employing whole-genome sequencing to investigate the underlying causes.

Veterinary clinicians reported suspected disease in pigs from 2 herds located in the western region of Thailand, ≈500 miles apart, all displaying clinical signs related to chronic forms of ASF: chronic respiratory disease, joint swelling, slow weight gain, and sporadic deaths. Both herds housed only finishing pigs, operating on an all-in/all-out basis, and pigs were not vaccinated with any types of ASF vaccines.

We submitted 25 blood and organ samples from ASF-suspected pigs to a Biosafety Level 3 laboratory at the National Center for Genetic Engineering and Biotechnology (Thailand Science Park, Pathum Thani, Thailand). We extracted viral DNA from samples following the protocol of the DNeasy blood and tissue kit (QIAGEN, https://www.qiagen.com). We detected ASFV by real-time PCR targeting the B646L gene, according to the World Health Organisation for Animal Health's International Office of Epizootics manual (*9*). We performed whole-genome sequencing on the Illumina NovaSeq X platform (Illumina, https://www.illumina.com), generating 151 bp paired-end reads. We analyzed raw sequences according to methods described in a previous study (*8*). We used FastQC v0.74 to assess the raw data

quality and removed adapters using BBDuk version 38.84. We aligned high-quality reads with Sscrofa11.1 (GCA_000003025.6) by Bowtie2 (https://bowtie-bio.sourceforge.net/bowtie2/index.shtml), eliminating >95% of host-derived contamination. We assembled cleaned reads de novo using SPAdes version 4.2.0 (https://github.com/ablab/spades/releases/tag/v4.2.0). We then mapped reads back to the assembled genome using Burrow-Wheeler Aligner-MEM (https://janis.readthedocs.io/en/latest/tools/bioinformatics/bwa/bwamem.html) and calculated coverage depth with Samtools version 1.21 (https://sourceforge.net/projects/samtools) to confirm average coverage. We analyzed the assembled genomes by BLASTn (https://blast.ncbi.nlm.nih.gov), choosing the closest match as the reference genome. We aligned 32 ASFV genomes from GenBank with the newly determined sequences using MAFFT version 7.526 (https://mafft.cbrc.jp/alignment/software). Finally, we constructed a phylogenetic tree in MEGA11 (https://www.megasoftware.net) with the neighbor-joining method and 1,000 bootstrap replicates.

We detected ASFV in 18 of 25 samples; cycle threshold (Ct) values ranged from 19.82 to 33.83. We performed whole-genome sequencing on samples with the lowest Ct from each herd,(Ct 19.82 for sample TH1_24/RB and Ct 21.25 for sample TH2_24/RB). We analyzed 2 completely sequenced ASFV genomes, which exhibited 38.5% guanine-cytosine content and average coverages of ≈163× and >96% breadth of 10× coverage. We deposited raw sequencing reads in the National Center for Biotechnology Information Sequence Read Archive (https://www.ncbi.nlm.nih.gov/sra; BioProject PRJNA1344271). We submitted the genomes to GenBank (accession nos. PX119974 and PX11995) and analyzed them in comparison with the Georgia 2007/1 strain (accession no. FR682468). Both genomes revealed the deletion of 6 genes in the multigene family (MGF) region (MGF 505-1R, MGF 360-12L, MGF 360-13L, MGF 360-14L, MGF 505-2R, and MGF 505-3R) and 2,348 bp of an *Escherichia coli* GusA gene (GUS) inserted at the deletion site (Figure 1). This deletion pattern was like a live-attenuated vaccine strain (ASFV-G-ΔMGF) and a field-attenuated isolate (ASFV-GUS-Vietnam) described in previous studies (*6*,*10*). Phylogenetic analysis based on full-length genome indicated that the 2 isolates belonged to genotype II; however, the isolates were genetically distinct from the genotype II variant responsible for the first outbreak in Thailand (Figure 2). The 2 variants contained a total of 15 mutations throughout the genome, mostly silent and in noncoding regions, when compared with the Georgia 2007/1 strain. In addition, a 3-nucleotide insertion resulted in 1 additional amino acid in the MGF 110-10-L-MGF110-14L fusion protein.

In conclusion, we characterized a vaccine-like genotype II strain, similar to ASFV-G-ΔMGF, detected in finishing pigs unvaccinated against ASFV in Thailand. The spread of such vaccine-like strains with MGF deletions in this region is of concern, and the origin of the strains remains unknown. Further genomic surveillance and epidemiologic tracing would assist in clarifying the route of introduction. Possible explanations include the unauthorized use of live attenuated vaccines or cross-border movement of pigs and pork products.

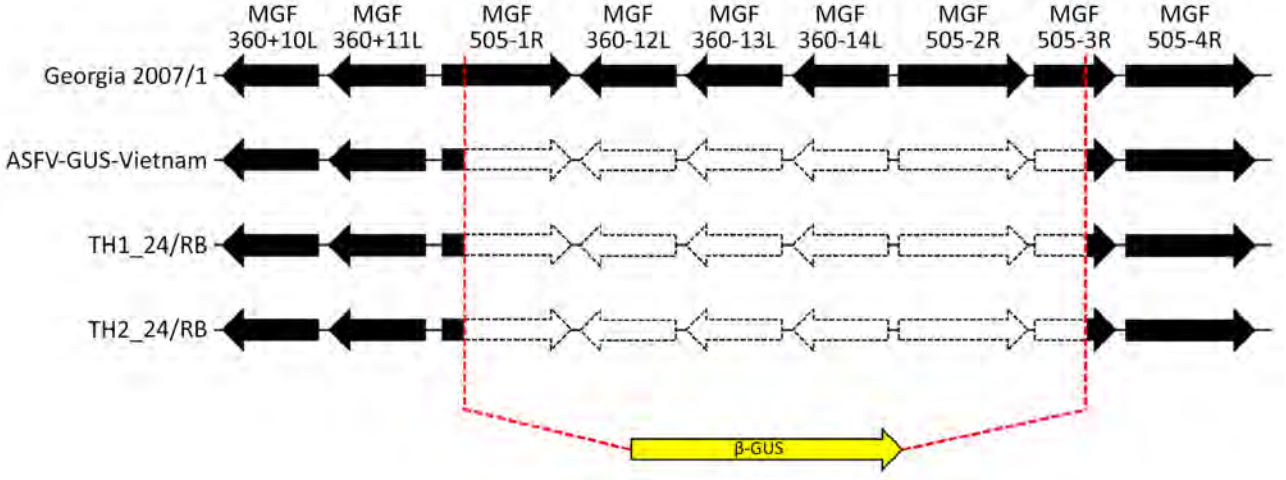

Figure 1. Schematic diagram from study of vaccine-like African swine fever virus strain in domestic pigs, Thailand, 2024, showing the deletion of the MGF gene region replaced by the β-GUS marker gene in the following strains: Georgia 2007/1, ASFV-GUS-Vietnam, and the 2 isolates from this study, TH1_24/RB and TH2_24/RB . Reference sequences obtained from GenBank. Deleted regions represented by dashed white arrows, intact genes by solid black arrows, and the inserted β-GUS gene by a yellow arrow. GUS, GusA gene; MGF, multigene family.

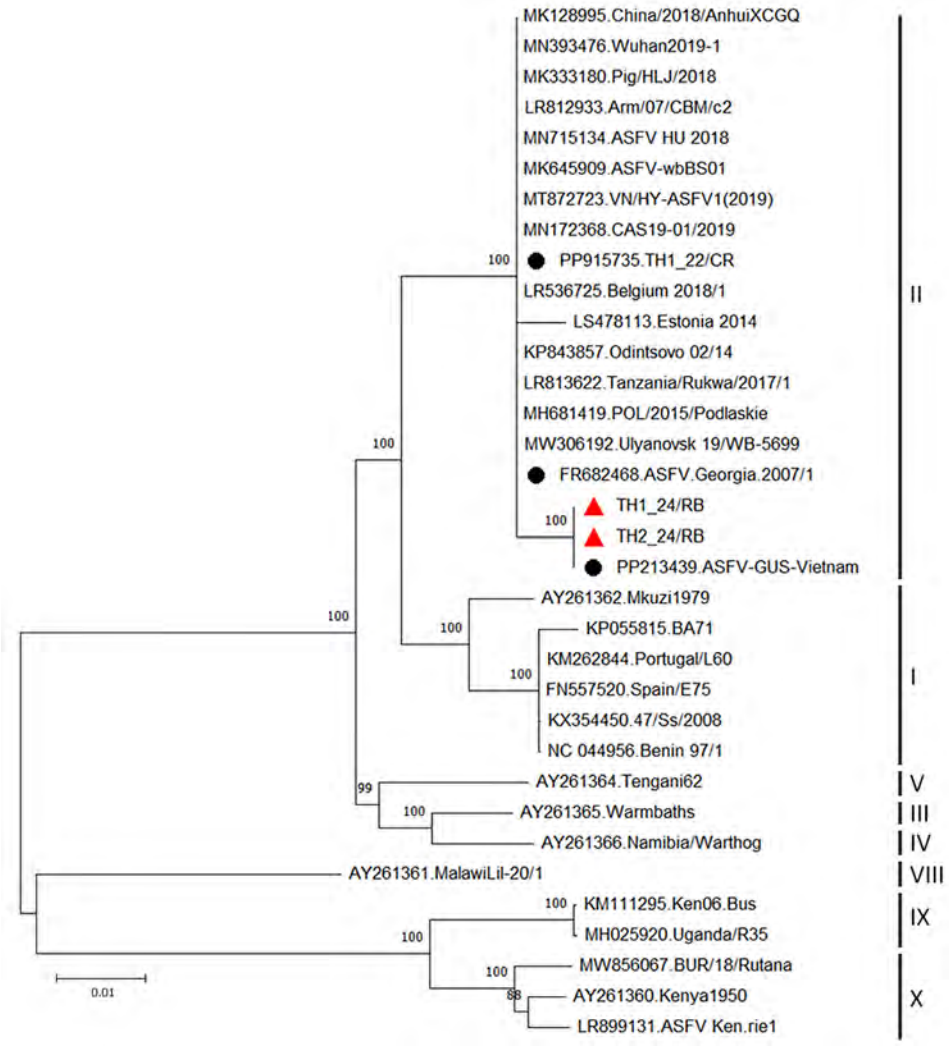

Figure 2. Phylogenetic tree based on whole-genome sequences of ASFV from a study of vaccine-like ASFV strain in domestic pigs, Thailand, 2024. Maximum-likelihood method and general time reversible model used in analyzing phylogenetic trees in MEGA 11 software (https://www.megasoftware.net). Red triangles indicate samples from this study; black circles indicate first ASFV strain in Thailand (TH1_22/CR), Georgia.2007/1, and ASFV-GUS-Vietnam. Genotypes are shown at right. Bootstrap analysis performed with 1,000 replicates; only bootstrap values >80 are shown. GenBank accessio numbers are provided for reference isolates. ASFV, African swine fever virus; GUS, GusA gene.

Acknowledgments

This research was supported by the National Center for Genetic Engineering and Biotechnology, Thailand Science Park, Pathum Thani, Thailand.

This study analyzed only diagnostic samples submitted to the laboratory. No live animals were used and IACUC approval was not required (IACUC: 237/2025).

T.T.N received ASEAN (Association of Southeast Asian Nations) and non-ASEAN countries scholarships to the graduate school at Chulalongkorn University. D.N. received financial support from Thailand Science Research and Innovation Fund at Chulalongkorn University (Bangkok, Thailand), Agricultural Research Development Agency (Bangkok, Thailand), and Chulalongkorn University for the Research Unit: Swine Viral Evolution and Vaccine Development Research Unit (GRU 6502731003-1)

About the Author

Mr. Nguyen is a veterinarian and a graduate student at the Department of Veterinary Microbiology, Chulalongkorn University, Thailand. His research interests focus on molecular characterization and virology.

References

1. Chapman DA, Darby AC, Da Silva M, Upton C, Radford AD, Dixon LK. Genomic analysis of highly virulent Georgia 2007/1 isolate of African swine fever virus. Emerg Infect Dis. 2011;17:599–605. https://doi.org/10.3201/eid1704.101283
2. Bastos AD, Penrith ML, Crucière C, Edrich JL, Hutchings G, Roger F, et al. Genotyping field strains of African swine fever virus by partial p72 gene characterisation. Arch Virol. 2003;148:693–706. https://doi.org/10.1007/s00705-002-0946-8
3. Quembo CJ, Jori F, Vosloo W, Heath L. Genetic characterization of African swine fever virus isolates from soft ticks at the wildlife/domestic interface in Mozambique and identification of a novel genotype. Transbound Emerg Dis. 2018;65:420–31. https://doi.org/10.1111/tbed.12700

4. Zhou X, Li N, Luo Y, Liu Y, Miao F, Chen T, et al. Emergence of African swine fever in China, 2018. Transbound Emerg Dis. 2018;65:1482–4. https://doi.org/10.1111/tbed.12989
5. Sun E, Zhang Z, Wang Z, He X, Zhang X, Wang L, et al. Emergence and prevalence of naturally occurring lower virulent African swine fever viruses in domestic pigs in China in 2020. Sci China Life Sci. 2021;64:752–65. https://doi.org/10.1007/s11427-021-1904-4
6. Ambagala A, Goonewardene K, Kanoa IE, Than TT, Nguyen VT, Lai TNH, et al. Characterization of an African swine fever virus field isolate from Vietnam with deletions in the left variable multigene family region. Viruses. 2024;16:571. https://doi.org/10.3390/v16040571
7. Le VP, Nguyen VT, Le TB, Mai NTA, Nguyen VD, Than TT, et al. Detection of recombinant African swine fever virus strains of p72 genotypes I and II in domestic pigs, Vietnam, 2023. Emerg Infect Dis. 2024;30:991–4. https://doi.org/10.3201/eid3005.231775
8. Salman M, Venkateswaran D, Prakash A, Nguyen QA, Suntisukwattana R, Atthaapa W, et al. The comparative full-length genome characterization of African swine fever virus detected in Thailand. Animals (Basel). 2024;14:2602. https://doi.org/10.3390/ani14172602
9. World Health Organisation for Animal Health. Chapter 3.9.1. African swine fever (infection with African swine fever virus). Manual of diagnostic tests and vaccines for terrestrial animals. 2025 [cited 2025 Feb 20]. https://www.woah.org/en/what-we-do/standards/codes-and-manuals
10. O'Donnell V, Holinka LG, Gladue DP, Sanford B, Krug PW, Lu X, et al. African Swine Fever virus Georgia isolate harboring deletions of MGF360 and MGF505 genes is attenuated in swine and confers protection against challenge with virulent parental virus. J Virol. 2015;89:6048–56. https://doi.org/10.1128/JVI.00554-15

Address for correspondence: Dachrit Nilubol, Department of Veterinary Microbiology, Faculty of Veterinary Science, Chulalongkorn University, Henri-Dunant Road, Pathumwan, Bangkok 10330, Thailand; email: dachrit@gmail.com

Monkeypox Virus Antibodies in Healthy Persons after Vaccination with MVA-BN, United Kingdom

Victoria H. Sheridan, Craig W. Duffy, Jake Dunning, Lance Turtle, Julian A. Hiscox, Krishanthi S. Subramaniam, on behalf of the ISARIC4C Investigators[1]

Author affiliations: University of Liverpool, Liverpool, UK (V.H. Sheridan, C.W. Duffy, L. Turtle, J.A. Hiscox, K.S. Subramaniam); University of Oxford, Oxford, UK (J. Dunning); Royal Liverpool University Hospital, Liverpool (L. Turtle)

DOI: https://doi.org/10.3201/eid3202.251553

A 2-dose regimen of the vaccine modified vaccinia Ankara–Bavarian Nordic (MVA-BN) can generate neutralizing antibodies for monkeypox virus clades Ib and IIb. We observed higher response to clade IIb; that result provides evidence that MVA-BN vaccination can induce cross-neutralizing antibodies for monkeypox virus clade Ib as well as for clade IIb.

Mpox is a zoonotic viral disease caused by monkeypox virus (MPXV), which is divided into clades I and II; clade II is subdivided into subclades IIa and IIb (*1*,*2*). In 2023 a new subclade of clade I, termed clade Ib, emerged in the Democratic Republic of the Congo (DRC). Since the first human case identified in August 1970 in DRC, mpox has been reported in 11 countries in Africa; in 2022 a global outbreak occurred in nonendemic areas caused by the clade IIb strain (*1*). More recently, the emergence of clade Ib, designated a public health emergency of international concern in August 2024 and associated with increased disease severity and mortality rate, particularly among children, posed a substantial public health threat (*3*). The World Health Organization recommends that persons at high risk of contracting mpox, especially during an outbreak, be vaccinated (*2*) with the modified vaccinia Ankara-Bavarian Nordic (MVA-BN) smallpox vaccine, a live attenuated vaccine (*1*).

Evidence demonstrates that vaccination with MVA-BN can generate low levels of neutralizing antibodies for clade IIb and clade Ia (*4*,*5*). In the United Kingdom, 1 dose of MVA-BN gives short-term protection of 78% against mpox, predominantly in men who have sex with men (*6*). Whether vaccination

[1]More information about the group is at the end of this article.

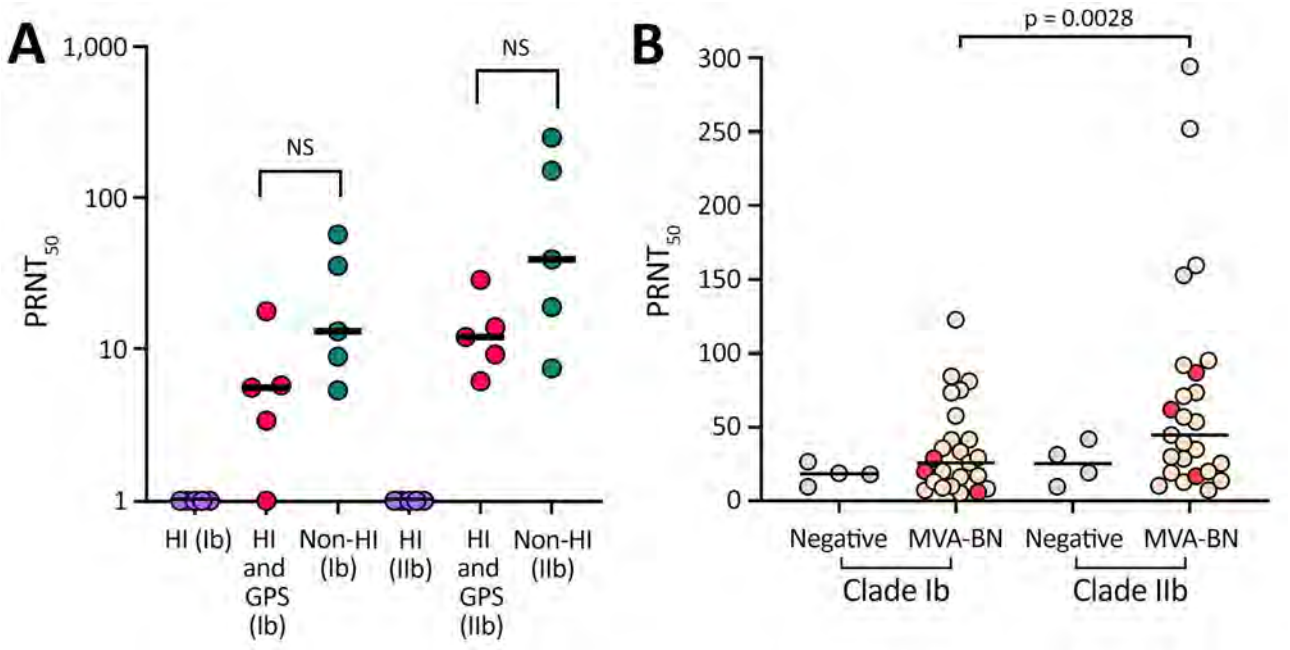

Figure. Titer results in study of monkeypox virus antibodies in healthy persons after MVA-BN vaccination, United Kingdom. $PRNT_{50}$ titers for participants vaccinated with 2 doses of MVA-BN vaccine demonstrated neutralizing antibody responses to monkeypox virus clade Ib and clade IIb. A) Assessment of the contribution of complement on neutralization illustrating the different conditions tested: purple, HI; red, HI and GPS; blue, non-HI. Mann Whitney U test used to determine p values. B) $PRNT_{50}$ values for clades Ib and IIb. Wilcoxon matched pairs signed rank test used to determine p values. Blue indicates negative controls; yellow, vaccine recipients; red, participants with underlying conditions. Each data point represents the geometric mean titer of 2 experimental replicates; horizontal black lines indicate medians. $PRNT_{50}$ values were determined using Probit regression. GPS, guinea pig serum; HI, heat-inactivation; MVA-BN, modified vaccinia Ankara–Bavarian Nordic vaccine; NS, not significant; $PRNT_{50}$, log of 50% endpoint plaque reduction neutralization test.

can also induce neutralizing antibodies for clade Ib has not been addressed. We recruited a convenience sample of healthcare workers (n = 25) vaccinated with MVA-BN for occupational exposure to mpox to measure neutralizing antibodies for clades Ib and IIb using a plaque reduction neutralization test (PRNT).

The importance of complement in relation to neutralization levels has been reported for MPXV (*7*) and other viruses (*8*). To assess the contribution of complement in our cohort, we exposed serum samples to different conditions: heat inactivation (HI), HI supplemented with guinea pig serum as a complement source, and non-HI. We found, as previously reported (*7*), that complement is required for neutralization of MPXV in vitro (Figure, panel A). We detected no significant difference in MPXV neutralization between HI serum in the presence of a complement source and non-HI (p = 0.0625 by Wilcoxon signed-rank test). On the basis of those data, we used non-HI serum for the remainder of the experiments.

We measured neutralization of MPXV clade Ib and IIb in non-HI serum samples from 25 vaccine recipients. We included 4 persons who did not receive the MVA-BN vaccine but were immunized with another live attenuated vaccine, IMOJEV (Substipharm, https://www.substipharm.com), as controls. In the MVA-BN vaccine group, 3 participants had underlying conditions of multiple sclerosis, psoriasis, or asthma (Table). The median $PRNT_{50}$, which is defined as the reciprocal of the serum dilution that results in 50% reduction in virus plaques, was 25.9

Table. Demographics of the participant cohort in study of monkeypox virus antibodies in healthy persons after MVA-BN vaccination, United Kingdom*

Characteristic	MVA-BN vaccine recipients, N = 25
Median age, y (IQR)	39 (30–45)
Sex, no. (%)	
M	9 (36)
F	16 (64)
Ethnicity, no. (%)	
White	20 (80)
Asian	3 (12)
Latin	2 (8)
Underlying conditions, no.	
Multiple sclerosis	1
Psoriasis	1
Asthma	1

*IQR, interquartile range; MVA-BN, modified vaccinia Ankara–Bavarian Nordic.

(interquartile range [IQR] 10.05–49.7) for clade Ib and 44.8 (IQR 19.55–89.4) for clade IIb. Comparisons across these samples demonstrated that 2 doses of MVA-BN generated greater neutralization of MPXV clade IIb than of clade Ib, a difference we found to be statistically significant (p = 0.0028 by Wilcoxon signed-rank test) (Figure, panel B). The difference in neutralizing antibody titers is small, and the relevance for clinical protection is uncertain. The protective threshold for MPXV neutralizing antibodies is not defined; case–control studies could define antibody-specific correlates of protection. The negative controls did exhibit low levels of nonspecific neutralization ($PRNT_{50}$ 18.5 for clade Ib and 25 for clade IIb), which were lower than those observed in the MVA-BN vaccine group.

Our results showed low levels of MPXV neutralization from MVA-BN vaccination, consistent with previous studies (*4*,*5*,*9*). We found that neutralization of clade Ib was lower than for clade IIb. Although our study is limited by relatively small sample size, we demonstrated neutralization of MPXV clade Ib in vaccine recipients without a history of mpox and compare those results with clade IIb neutralization. Moreover, given that the study cohort included healthcare workers at highest risk for exposure, evidence of vaccine-associated neutralization is relevant to determine policies regarding future vaccine rollouts.

MPXV neutralization is known to require complement (*7*). We observed low levels of neutralization when guinea pig serum was added to virus and when pooled human plasma was added to virus (data not shown), highlighting the nonspecific effect that foreign complement sources can have on MPXV neutralization; guinea pig serum alone exhibits neutralization activity against mumps virus compared with purified antibodies alone (*10*). Therefore, our approach was to use non–heat-inactivated serum to measure MPXV neutralization as described previously (*9*).

The low levels of neutralization we observed, particularly against MPXV clade Ib, suggest that vaccination with MVA-BN can confer moderate protection against disease caused by that clade. The durability of those responses, and whether a third dose is required to enhance protection against mpox clade Ib infections (*4*,*5*,*9*), were beyond the scope of our study.

This article was preprinted at https://www.medrxiv.org/content/10.1101/2025.09.17.25335983v1.

The International Severe Acute Respiratory and Emerging Infection Consortium (ISARIC) World Health Organization Clinical Characterisation Protocol (CCP-UK) United Kingdom is co-led and maintained by J. Kenneth Baillie (Baillie Gifford Pandemic Science Hub, University of Edinburgh) and Malcolm G. Semple (Liverpool) on behalf of the ISARIC4C investigators (isaric4c.net).

Acknowledgments

We thank Neil Blake for his work amplifying the monkeypox virus clade Ib strain.

This study was funded by the DECIPHER Consortium, consisting of the University of Liverpool, National Health Laboratory Services, Makerere University, Uganda National Health Research Organisation, McMaster University, Institut National De Recherche Biomedicale Du Zaire, and Universite Catholique de Bukavu. V.S., C.D., and J.H. are based at the University of Liverpool. The study was also funded by the Pandemic Institute, which is formed of 7 founding partners: the University of Liverpool, Liverpool School of Tropical Medicine, Liverpool John Moores University, Liverpool City Council, Liverpool City Region Combined Authority, Liverpool University Hospital Foundation Trust, and Knowledge Quarter Liverpool. K.S. and L.T. are based at the University of Liverpool. L.T. is supported by the National Institute for Health Research Health Protection Research Unit in Emerging and Zoonotic Infections (grant no. NIHR207393) at University of Liverpool in partnership with the UK Health Security Agency, in collaboration with Liverpool School of Tropical Medicine and the University of Oxford. L.T. is based at University of Liverpool.

L.T. has received consulting fees from MHRA and Bavarian Nordic and speakers' fees from Eisai Ltd, Medscape, the Primary Care Cardiovascular Society, and Bavarian Nordic. He has received consulting fees from AstraZeneca, Synairgen, and GeoVax paid to the University of Liverpool and support for conference attendance from AstraZeneca.

About the Author

Dr. Sheridan is a postdoctoral researcher in the laboratory of Julian Hiscox, University of Liverpool. Her research focuses on virus host interactions and the use of medical countermeasures.

References

1. Sun Y, Nie W, Tian D, Ye Q. Human monkeypox virus: epidemiologic review and research progress in diagnosis and treatment. J Clin Virol. 2024;171:105662. https://doi.org/10.1016/j.jcv.2024.105662
2. World Health Organization. Mpox. 2025 [cited 2025 Jul 27]. https://www.who.int/health-topics/mpox

3. Srivastava S, Laxmi, Sharma K, Sridhar SB, Talath S, Shareef J, et al. Clade Ib: a new emerging threat in the Mpox outbreak. Front Pharmacol. 2024;15:1504154. https://doi.org/10.3389/fphar.2024.1504154
4. Zaeck LM, Lamers MM, Verstrepen BE, Bestebroer TM, van Royen ME, Götz H, et al. Low levels of monkeypox virus-neutralizing antibodies after MVA-BN vaccination in healthy individuals. Nat Med. 2023;29:270–8. https://doi.org/10.1038/s41591-022-02090-w
5. Collier AY, McMahan K, Jacob-Dolan C, Liu J, Borducchi EN, Moss B, et al. Decline of mpox antibody responses after modified vaccinia Ankara-Bavarian Nordic vaccination. JAMA. 2024;332:1669–72. https://doi.org/10.1001/jama.2024.20951
6. Bertran M, Andrews N, Davison C, Dugbazah B, Boateng J, Lunt R, et al. Effectiveness of one dose of MVA-BN smallpox vaccine against mpox in England using the case-coverage method: an observational study. Lancet Infect Dis. 2023;23:828–35. https://doi.org/10.1016/S1473-3099(23)00057-9
7. Hubert M, Guivel-Benhassine F, Bruel T, Porrot F, Planas D, Vanhomwegen J, et al. Complement-dependent mpox-virus-neutralizing antibodies in infected and vaccinated individuals. Cell Host Microbe. 2023;31:937–948.e4. https://doi.org/10.1016/j.chom.2023.05.001
8. Mellors J, Dhaliwal R, Longet S, Tipton T, Barnes E, Dunachie SJ, et al.; OPTIC Consortium. Complement-mediated enhancement of SARS-CoV-2 antibody neutralisation potency in vaccinated individuals. Nat Commun. 2025;16:2666. https://doi.org/10.1038/s41467-025-57947-8
9. Phipps K, Yates J, Pettit J, Bialosuknia S, Hunt D, DuPuis AP II, et al. Short-lived neutralizing antibody responses to monkeypox virus in smallpox vaccine–naive persons after JYNNEOS vaccination. Emerg Infect Dis. 2025;31:237–45. https://doi.org/10.3201/eid3102.241300
10. Brgles M, Kurtović T, Lang Balija M, Hećimović A, Mušlin T, Halassy B. Impact of complement and difference of cell-based assay and ELISA in determination of neutralization capacity against mumps and measles virus. J Immunol Methods. 2021;490:112957. https://doi.org/10.1016/j.jim.2021.112957

Address for correspondence: Krishanthi Subramaniam, Department of Clinical Infection, Microbiology and Immunology, Institute of Infection, Veterinary and Ecological Sciences, University of Liverpool, Liverpool L69 7BE, UK; email: ksubrama@liverpool.ac.uk

Airport Malaria Cluster in Certified Malaria-Free Country, Libya, 2024

Ahmed M. Alarbi, Ahmed B. Elhaddad, Nafesa M. Almehdawi, Walid K. Saadawi, Hanan Aqeehal, Mohamed Elalem

Author affiliations: Mediterranean and Black Sea Programme in Intervention Epidemiology Training, European Centre for Disease Prevention and Control, Stockholm, Sweden (A.M Alarbi); National Center for Disease Control, Tripoli, Libya (A.M. Alarbi, W.K. Saadawi, H. Aqeehal, M. Elalem); University of Benghazi, Benghazi, Libya (A.B. Elhaddad); Benghazi Medical Center, Benghazi, (A.B. Elhaddad, N.M. Almehdawi)

DOI: https://doi.org/10.3201/eid3202.251508

In November 2024, an autochthonous cluster of 4 *Plasmodium falciparum* cases (1 fatal) was identified near Benina International Airport, Benghazi, Libya. Epidemiologic and entomologic investigation ruled out local transmission, pointing to airport malaria as the cause and highlighting the vulnerability of malaria-free regions to imported vectors.

Libya, which was certified malaria-free by the World Health Organization in 1973, faces continuous risk for malaria reintroduction from population movements in malaria-endemic regions (*1*). Although imported cases are occasionally reported, local transmission has not been documented in eastern Libya for >50 years.

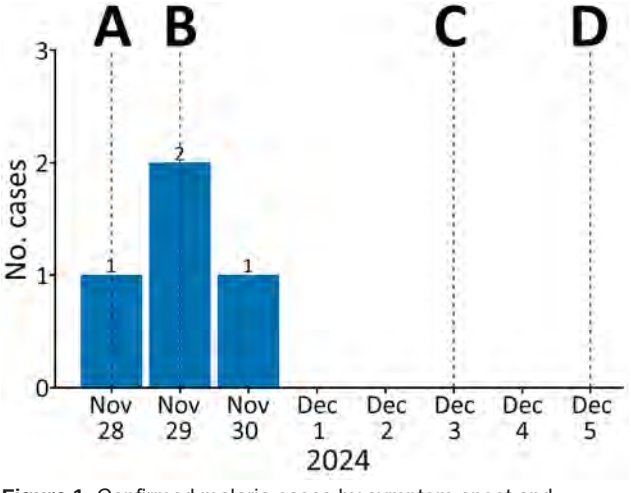

Figure 1. Confirmed malaria cases by symptom onset and public health response timeline in study of airport malaria cluster in certified malaria-free country, Benghazi, Libya, November–December 2024. A) Index case death notified; B) investigation and case finding initiated; C) no *Anopheles* mosquito vectors confirmed in traps; D) public health recommendations issued.

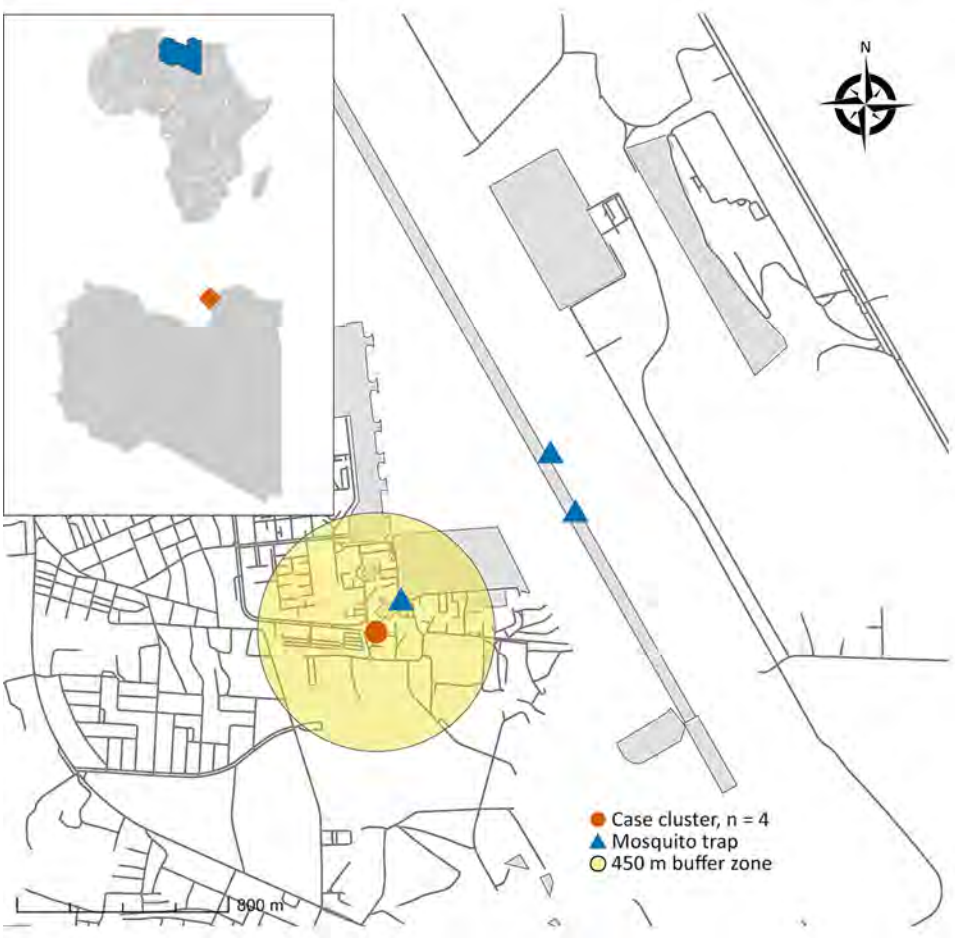

Figure 2. Location of airport malaria cluster in certified malaria-free country, Benghazi, Libya, November 2024. The map displays the location of the case cluster (n = 4) and mosquito traps relative to the Benina International Airport runway. The yellow shaded area indicates a 450-meter buffer zone from the cluster center. Inset maps show the location of Libya in Africa and Benghazi within Libya.

On November 28, 2024, the Libya National Centre for Disease Control was notified of a fatal case of *Plasmodium falciparum* malaria in a 63-year-old resident of Benghazi, Libya, who had no history of travel. Within 48 hours, infection was confirmed in 3 of his children (ages 12, 16, and 23). This familial cluster was located ≈450 meters from Benina International Airport, prompting an investigation to determine the outbreak's source. This investigation was considered a public health response to an urgent event by the Libya National Center for Disease Control and, as such, was not subject to institutional review board approval. Oral informed consent was obtained from the family members for interviews and testing.

Our investigation defined a case as malaria-like symptoms in a resident near the airport during from mid-November through mid-December 2024 (Figure 1). Active case finding through local healthcare and community outreach identified 20 other suspected patients; all tested negative. All 4 confirmed case-patients, belonging to a single family of 8, were laboratory-confirmed as positive for *P. falciparum*. None had traveled internationally or received blood transfusions. We formulated 2 primary hypotheses: local transmission from indigenous *Anopheles* mosquitoes infected by human carrier or airport malaria from an infected *Anopheles* mosquito imported by aircraft.

To evaluate those hypotheses, we conducted entomological surveillance during November 29–December 2, 2024, deploying National Centre for Disease Control light traps around the family's residence and within the airport perimeter (Figure 2). We collected 8 mosquitoes, all of which were identified as *Culex pipiens*. We found no *Anopheles* mosquitoes, a finding consistent with recent national surveillance data, which documented certain *Anopheles* species in specific ecologic niches but confirmed their general absence in coastal urban areas such as Benghazi (H. Aqeehal, unpub. data). The absence of competent local vectors enabled us to eliminate local transmission, making airport malaria the most plausible explanation (2).

This investigation concluded that an infected anopheline mosquito was likely imported by aircraft, probably within cargo given the absence of recent passenger flights from malaria-endemic areas, and

subsequently infected members of a family living nearby. Although importation of vectors overland through migrant routes is a theoretical possibility (*3*,*4*), the acute, geographically tight cluster in a non-migrant family points strongly toward a point-source introduction at the airport.

This event is a critical reminder that malaria-free status does not eliminate risk, because points of entry are permeable frontiers for vectorborne diseases (*5*,*6*). Our findings prompted immediate recommendations to Libya health authorities to strengthen entomologic surveillance at points of entry and rigorously enforce aircraft and cargo disinsection protocols in accordance with the World Health Organization's International Health Regulations (2005) (*7*). We also emphasize the need for clinicians near airports to consider malaria in patients with fever, regardless of travel history. The vulnerability of nonendemic regions requires constant vigilance to prevent the reestablishment of malaria.

Acknowledgments

The authors collectively thank the staff at the Benghazi Medical Center and the field and laboratory teams at the National Center for Disease Control for their timely response and unwavering dedication during this investigation. We are also grateful to our colleagues in the European Centre for Disease Prevention and Control (ECDC) Project Review Module for their invaluable feedback, which significantly improved this manuscript. A.A. wishes to extend his personal gratitude to his frontline coordinator, Pawel Stefanoff, for his continuous guidance, and to his supervisor, Zeinab Saleh, for her expert mentorship and steadfast support throughout this project.

ChatGPT-4 (OpenAI, November 2023 version) was used to assist with language editing, formatting, and refining the manuscript for clarity and adherence to journal guidelines.

A.A. is a fellow of the MediPIET program, supported financially by the ECDC. The views and opinions expressed herein do not state or reflect those of ECDC. ECDC is not responsible for the data and information collation and analysis and cannot be held liable for conclusions or opinions drawn.

About the Author

Dr. Alarbi is a fellow of the Mediterranean and Black Sea Programme in Intervention Epidemiology Training at the National Center for Disease Control, Tripoli, Libya. His primary research interest is the epidemiology of emerging and vectorborne diseases in North Africa.

References

1. Gebreel AO, Gilles HM, Prescott JE. Studies on the sero-epidemiology of endemic diseases in Libya, IV. Malaria. Ann Trop Med Parasitol. 1985;79:341–7. https://doi.org/10.1080/00034983.1985.11811930
2. Kessel J, Rosanas-Urgell A, Dingwerth T, Goetsch U, Haller J, Huits R, et al. Investigation of an airport-associated cluster of falciparum malaria in Frankfurt, Germany, 2022. Euro Surveill. 2024;29:2300298. https://doi.org/10.2807/1560-7917.ES.2024.29.5.2300298
3. Tabbabi A, Alkishe AA, Samy AM, Rhim A, Peterson AT. Malaria in North Africa: a review of the status of vectors and parasites. J Entomol Sci. 2020;55:25–37. https://doi.org/10.18474/0749-8004-55.1.25
4. Nebbak A, Almeras L, Parola P, Bitam I. Mosquito vectors (Diptera: Culicidae) and mosquito-borne diseases in North Africa. Insects. 2022;13:962. https://doi.org/10.3390/insects13100962
5. Schlagenhauf P, D'Acremont V, Buhler S, Hatz C. Airport malaria and odyssean malaria. In: Keystone A, Kozarsky P, Connor B, Nothdurft H, Mendelson M, Cartwright K, editors. Travel medicine. 4th ed. Philadelphia: Elsevier; 2019. p. 64–7.
6. Ibáñez-Justicia A, Smitz N, den Hartog W, van de Vossenberg B, De Wolf K, Deblauwe I, et al. Detection of exotic mosquito species (Diptera: Culicidae) at international airports in Europe. Int J Environ Res Public Health. 2020;17:3450. https://doi.org/10.3390/ijerph17103450
7. World Health Organization. International Health Regulations (2005). 3rd ed. Geneva: The Organization; 2016.

Address for correspondence: Ahmed Alarbi, National Center for Disease Control, Zawiat Aldahmani, Bldg 6, Apt 16, Tripoli 1040, Libya; email: a.alarbi@ncdc.gov.ly

Candida auris Testing by the Antimicrobial Resistance Laboratory Network, United States, 2022–2023

Jessica E. Laury, Kaitlin Forsberg, Elizabeth L. Berkow, Sophie Jones, D. Joseph Sexton, Dawn M. Sievert, Shawn R. Lockhart, Jeremy A.W. Gold,[1] Meghan Lyman[1]

Author affiliation: Centers for Disease Control and Prevention, Atlanta, Georgia, USA

DOI: https://doi.org/10.3201/eid3202.251043

During 2022–2023, the Antimicrobial Resistance Laboratory Network tested 8,033 *Candida auris* clinical isolates in the United States. Overall, 95% of isolates were fluconazole resistant, 15% amphotericin B resistant, and 1% echinocandin resistant. Laboratory capacity for *C. auris* identification and antifungal susceptibility testing is essential to address this emerging public health threat.

Candida auris is an urgent public health threat because of frequent multidrug resistance, high transmissibility in healthcare settings, and association with high-mortality invasive infections (*1*–*5*). The Centers for Disease Control and Prevention Antimicrobial Resistance Laboratory Network (AR Lab Network) adopted *C. auris* testing, including antifungal susceptibility testing, in 2016 to meet clinical and public health needs (https://www.cdc.gov/antimicrobial-resistance-laboratory-networks/php/about/testing-services.html). National annual *C. auris* clinical case counts have increased from <100 in 2016 to >4,500 in 2023 (*5*,*6*). To inform prevention, clinical practice, and surveillance efforts, we describe 2022–2023 AR Lab Network *C. auris* clinical isolate testing.

Clinical *C. auris* isolates are obtained from patient specimens collected during clinical care, not for colonization detection, and can be from any body site (*5*). Isolates were identified by matrix-assisted laser desorption/ionization time-of-flight mass spectrometry. MICs for fluconazole and echinocandins (anidulafungin, micafungin) were determined by using frozen custom broth microdilution panels and, for amphotericin B, by using gradient diffusion strip. According to tentative breakpoints (https://www.cdc.gov/candida-auris/hcp/laboratories/antifungal-susceptibility-testing.html), isolates were considered echinocandin-resistant if resistant to either echinocandin and panresistant if resistant to all 3 antifungal classes.

We examined the number of clinical isolates tested and antifungal susceptibility testing results by year, AR Lab Network region of specimen collection (https://www.cdc.gov/antimicrobial-resistance-laboratory-networks/php/about/domestic.html), and body site. We analyzed clinical specimens only to avoid biases from local screening intensity and protocol differences. We excluded specimens for which it was unclear whether they originated from colonization screening versus clinical isolates (≈14%).

During 2022–2023, a total of 8,033 clinical isolates were tested (Table). Most were from the West (24%), Southeast (21%), or Northeast (19%) regions; <1% were from the Central region. The number of clinical isolates increased from 3,064 in 2022 to 4,969 in 2023, increasing in all regions except the Mountain region (288 to 238). The most common body sites were blood (36%) and urine (32%). The distribution of body sites was similar across regions and years (data not shown).

Overall, 95% (7,244/7,594) of tested isolates were fluconazole-resistant; that percentage exceeded 90% in all regions except the Midwest (83%, 666/801) (Appendix, https://wwwnc.cdc.gov/EID/article/32/2/25-1043-App1.pdf). In total, 15% (1,128/7,458) of isolates were amphotericin B–resistant; that percentage was <5% in all regions except the Central (22%, 4/18), Northeast (44%, 629/1,420), and Mid-Atlantic (62%, 290/469). Fewer isolates were echinocandin-resistant (1%, 97/7,574); the highest percentages were in the Midwest (2%, 13/799), Northeast (2%, 31/1,420), and Mountain (3%, 14/463) regions. Overall, 16/7,438 (<1%) isolates were panresistant, mostly from the Northeast (n = 10).

Fluconazole resistance was higher in 2023 (96%, 4,441/4,616) than in 2022 (94%, 2,803/2,978); the largest differences were in the Midwest (90% [433/481] vs. 73% [233/320]) and Southeast (95% [906/957] vs. 90% [582/646]). Amphotericin B resistance was higher in 2023 (19%, 838/4,497) than in 2022 (10%, 290/2,961); the largest difference was in the Northeast (64% [508/794] vs. 19% [121/626]). Echinocandin resistance was 1% in both years, but in the Mountain region, it was higher in 2023 (7%, 13/187) than in 2022 (<1%, 1/276). Antifungal resistance was similar across body sites for fluconazole. More echinocandin-resistant isolates were from urine (3% [72/2,470] vs. ≤1% for each other site), and fewer amphotericin

[1]These senior authors contributed equally to this article.

Table. Clinical isolates of *Candida auris*, by region and body site, Antimicrobial Resistance Laboratory Network, United States, 2022–2023

Characteristic	No. (%) isolates		
	All, n = 8,033	2022, n = 3,064	2023, n = 4,969
Region where specimen was collected			
Central	37 (0)	2 (0)	35 (1)
Mid-Atlantic	513 (6)	156 (5)	357 (7)
Midwest	904 (11)	329 (11)	575 (12)
Mountain	526 (7)	288 (9)	238 (5)
Northeast	1,512 (19)	665 (22)	847 (17)
Southeast	1,672 (21)	647 (21)	1,025 (21)
West	1,967 (24)	775 (25)	1,192 (24)
Not reported	902 (11)	202 (7)	700 (14)
Body site			
Blood	2,856 (36)	1,185 (39)	1,671 (34)
Respiratory	715 (9)	277 (9)	438 (9)
Urine	2,598 (32)	933 (30)	1,665 (34)
Wound	1,026 (13)	393 (13)	633 (13)
Other	838 (10)	276 (9)	562 (11)

B–resistant isolates were from wounds or respiratory sites (10% [89/861] for wounds, 13% [99/761] for respiratory, vs. ≥15% each other site).

This analysis of AR Lab Network *C. auris* testing revealed a 1.5-fold increase in clinical isolate testing volume from 2022 to 2023, mirroring increases in national *C. auris* case prevalence. The proportion of clinical isolates tested by region generally mirrored regional proportions of national case counts (*6*). Fluconazole resistance rates were slightly higher in 2023 (96%) versus 2022 (94%) and were higher than in 2020 (86%), potentially because of increased circulation of fluconazole-resistant strains, primarily driven by isolates from the Midwest, where the fluconazole resistance rate was 90% in 2023 versus 11% during 2018–2020 (*5*). Amphotericin B resistance rates were higher in 2023 (19%) than in 2022 (10%) but were lower overall during 2022–2023 (15%) compared with 2020 (26%) (*5*). That finding might reflect lack of amphotericin B drug selection pressure, because maintaining resistance likely incurs fitness costs, or changes in circulating strains (*7*).

The frequency of echinocandin resistance (1%) and panresistance (<1%) among *C. auris* isolates remains low, including among blood isolates, supporting use of echinocandins as first-line therapy against *C. auris* infections. However, the number of resistant isolates has increased, and possible spread among patients has been documented (*8*,*9*). Echinocandin resistance was found more often in urine than in blood isolates (3% vs. 1%), which might relate to the limited urinary excretion of echinocandins (*10*).

AR Lab Network *C. auris* testing primarily supports local detection and outbreak response, rather than serving as nationally representative surveillance. Testing performed outside the network, an increasing proportion in recent years, is not captured. Data could not be analyzed at the patient level (including repeat isolates) and lacked information on antifungal exposure, clade, and facility type. Nonetheless, our findings highlight the persistence of *C. auris* as a multidrug-resistant threat requiring sustained investment in laboratory capacity for early detection and response.

Acknowledgments

The authors thank Malavika Rajeev; the Antimicrobial Resistance Coordination and Strategy Unit Science Team; and the many federal, state, jurisdictional, and local partners who have contributed to the success of the AR Lab Network and who performed the extensive *C. auris* testing described in this report.

This activity was reviewed by the Centers for Disease Control and Prevention (CDC) and was conducted consistent with applicable federal law and CDC policy (e.g., 45 C.F.R. part 46, 21 C.F.R. part 56; 42 USC. §241(d); 5 USC. §552a; 44 USC. §3501 et seq). The findings and conclusions in this report are those of the authors and do not necessarily represent the official position of the CDC.

ChatGPT (OpenAI, https://chatgpt.com) was used for language editing of this manuscript; all intellectual content is the sole responsibility of the authors.

About the Author

Ms. Laury is a health scientist in the Mycotic Diseases Branch, Division of Foodborne, Waterborne, and Environmental Diseases, National Center for Emerging and Zoonotic Infectious Diseases, Centers for Disease Control and Prevention, Atlanta, Georgia, USA. Her research interests include the epidemiology and prevention of fungal infections.

References

1. Lockhart SR, Etienne KA, Vallabhaneni S, Farooqi J, Chowdhary A, Govender NP, et al. Simultaneous emergence of multidrug-resistant *Candida auris* on 3 continents confirmed by whole-genome sequencing and epidemiological analyses. Clin Infect Dis. 2017;64:134–40. https://doi.org/10.1093/cid/ciw691
2. Benedict K, Forsberg K, Gold JAW, Baggs J, Lyman M. *Candida auris*–associated hospitalizations, United States, 2017–2022. Emerg Infect Dis. 2023;29:1485–7. https://doi.org/10.3201/eid2907.230540
3. Morales-López SE, Parra-Giraldo CM, Ceballos-Garzón A, Martínez HP, Rodríguez GJ, Álvarez-Moreno CA, et al. Invasive infections with multidrug-resistant yeast *Candida auris*, Colombia. Emerg Infect Dis. 2017;23:162–4. https://doi.org/10.3201/eid2301.161497
4. Chakrabarti A, Sood P, Rudramurthy SM, Chen S, Kaur H, Capoor M, et al. Incidence, characteristics and outcome of ICU-acquired candidemia in India. Intensive Care Med. 2015;41:285–95. https://doi.org/10.1007/s00134-014-3603-2
5. Lyman M, Forsberg K, Sexton DJ, Chow NA, Lockhart SR, Jackson BR, et al. Worsening spread of *Candida auris* in the United States, 2019 to 2021. Ann Intern Med. 2023;176:489–95. https://doi.org/10.7326/M22-3469
6. Centers for Disease Control and Prevention. Tracking *C. auris* [cited 2025 Apr 4]. https://www.cdc.gov/candida-auris/tracking-c-auris/index.html
7. Carolus H, Sofras D, Boccarella G, Sephton-Clark P, Biriukov V, Cauldron NC, et al. Acquired amphotericin B resistance leads to fitness trade-offs that can be mitigated by compensatory evolution in *Candida auris*. Nat Microbiol. 2024;9:3304–20. https://doi.org/10.1038/s41564-024-01854-z
8. Centers for Disease Control and Prevention. Clinical treatment of *C. auris* infections [cited 2025 May 24]. https://www.cdc.gov/candida-auris/hcp/clinical-care/index.html
9. Lyman M, Forsberg K, Reuben J, Dang T, Free R, Seagle EE, et al. Notes from the field: transmission of pan-resistant and echinocandin-resistant *Candida auris* in health care facilities—Texas and the District of Columbia, January–April 2021. MMWR Morb Mortal Wkly Rep. 2021;70:1022–3. https://doi.org/10.15585/mmwr.mm7029a2
10. Felton T, Troke PF, Hope WW. Tissue penetration of antifungal agents. Clin Microbiol Rev. 2014;27:68–88. https://doi.org/10.1128/CMR.00046-13

Address for correspondence: Jeremy A.W. Gold, Centers for Disease Control and Prevention, 1600 Clifton Rd NE, Mailstop H24-11, Atlanta, GA 30329-4018, USA; email: jgold@cdc.gov

Correction: Vol. 32, No. 1

Essential taxonomic information was inadvertently omitted from Detection of Novel Thermotolerant *Tepidimonas* sp. Bacteria in Human Respiratory Specimens, Hong Kong, China, 2024 (K.H.-Y. Chiu et al.). The article has been corrected online (https://wwwnc.cdc.gov/eid/article/32/1/25-0818_article).

Juan Manuel Blanes, *An Episode of Yellow Fever in Buenos Aires*, 1871 (detail). Oil on canvas. 230 cm × 180 cm. Museo Nacional de Artes Visuales, Montevideo, Uruguay. Source: Wikimedia Commons.

Yellow Fever in Buenos Aires

Terence Chorba

A vectorborne disease is an illness caused by viruses, bacteria, parasites, or fungi transmitted by arthropod vectors such as mosquitoes, ticks, or fleas. Annually, vectorborne diseases account for >700,000 deaths globally, including deaths from malaria, dengue, schistosomiasis, Chagas disease, yellow fever, human African trypanosomiasis, leishmaniasis, Japanese encephalitis, and onchocerciasis (*1*). Yellow fever is a viral disorder caused by an *Orthoflavivirus* that is a genus in the Flaviviridae family and is so named after the jaundice

Author affiliation: Centers for Disease Control and Prevention, Atlanta, Georgia, USA

DOI: https://doi.org/10.3201/eid3202.AC3202

(yellowing of the eyes and skin) that is associated with yellow fever virus infection; flavus means yellow in Latin. All orthoflaviviruses are small, spherical, enveloped viruses, ≈50 nm in diameter, sharing a similar architecture consisting of an ≈11,000-base single-stranded RNA virus genome, a nucleocapsid of a protein shell containing the viral RNA, and a host-derived lipid envelope that surrounds the nucleocapsid (*2*,*3*).

Yellow fever virus is transmitted to humans primarily through the bite of infected mosquitoes. The virus replicates in the liver and other organs, causing overwhelming inflammation and damage. Infection with this virus is believed to have first appeared in the Americas through the transatlantic slave trade from Africa, causing repeated epidemics in the 18th and 19th Centuries, primarily in the port cities of both North and South America. The disease often caused widespread terror and economic disruption, and notable outbreaks occurred in Philadelphia (1793), New Orleans (1853), and Buenos Aires (1871); lesser outbreaks had been reported in Buenos Aires in 1852, 1858, and 1870. It is now known that most orthoflaviviruses, including yellow fever virus, cause subclinical infections that go undetected in existing clinical-based disease surveillance programs (*4*); >85% of yellow fever virus infection cases are either asymptomatic or result in only mild illness (*5*). To this day, yellow fever remains endemic and is widely distributed in the tropical areas of Africa and Latin America, reportedly accounting for 67,000–173,000 severe infections and 31,000–82,000 deaths annually (*6*,*7*).

The scene featured on this month's cover, *An Episode of Yellow Fever in Buenos Aires* (*Un Episodio de la Fiebre Amarilla en Buenos Aires*), painted by Uruguayan artist Juan Manuel Blanes in 1871, is a depiction of the tragic events of death in a family from the yellow fever epidemic that devastated Buenos Aires in that same year. It is a somewhat chiaroscuro composition—that is, there is great contrast between light and darkness, although it is predominantly dark with ochres and grays. In his work, Blanes depicts the images of a man, lying dead on a bed and obscured in darkness, and of a young woman sprawled on a stone floor, also dead from the disease. Their orphaned child is seated beside the mother in stunned desperation, struggling to access her breast. Behind them are 2 members from the city's People's Commission (Comisión Popular) who have come upon the scene, lawyer José Roque Pérez (center) and Dr. Manuel Argerich (to his right), both of whom later also died in the epidemic as the result of their dedicated work, supporting the sick (*8*). The same epidemic lay claim to a reported 14,000 lives in an estimated population of 180,000; among them was another great artist and colleague of Blanes, the Argentine American Franklin Rawson (1791–1871),

Figure 1. Franklin Rawson, *Murder of Manuel Vicente Maza*, 1860. Oil on canvas. 175 cm × 219.5 cm. Complejo Museográfico Provincial "Enrique Udaondo," Ciudad de Luján, Buenos Aires, Argentina. Source: Wikimedia Commons.

Figure 2. Juan Manuel Blanes, *The Dressage*, ca. 1875. Oil on canvas. 80 cm × 100 cm. Museo Nacional de Artes Visuales, Montevideo, Uruguay. Source: Wikimedia Commons. Photograph by Eduardo Baldizan.

who was renowned for genre scenes and historical paintings and portraits with elements of romantic realism very similar to those in the work of Blanes (Figure 1) (*9*).

Juan Manuel Blanes was born in Montevideo, Uruguay, a newly independent country, in 1830, and from an early age demonstrated great talent serving as a self-taught illustrator and portrait painter in a politically destabilized environment—Uruguay endured a civil war from 1843 to 1851. In 1860, Blanes obtained a scholarship from the Uruguay government, and for several years, he studied under Antonio Ciseri, a widely recognized Italian portrait and neoclassicist realism painter of religious works (*10*). The influence of Ciseri can be seen in the photographic depiction of the family lost to disease in the Buenos Aires epidemic, Blanes' earliest renowned work. Blanes subsequently had a very successful and prolific career in Uruguay, Chile, Argentina, and Italy, making historical paintings, portraits, and depictions of gauchos (nomadic horsemen and cowhands of the grasslands in Uruguay and Argentina, renowned in the mid-18th to mid-19th Century) (Figure 2), and died in Pisa, Italy, in 1901, at the age of 70 (*11*). In recognition of his talent and contribution to his nation, the city of Montevideo named its Juan Manuel Blanes Municipal Museum of Fine Arts in his honor in 1930.

The first experiments that demonstrated that mosquitoes accounted for yellow fever transmission were conducted by Walter Reed and his colleagues at the turn into the 20th Century, building on findings of Carlos Finlay, a Cuban physician, who first theorized the transmission problem in 1881 (*12*). The history of yellow fever took another favorable turn in the 20th Century with the development of a yellow fever vaccine, for which Max Theiler was recognized with a Nobel Prize in 1951 (*13*). Fortunately, the vaccine has saved many lives, and investment in its development has resulted in a marked diminution in the frequency of scenarios like that depicted in the Blanes' yellow fever painting, by preventing or interrupting the outbreaks that repeatedly would devastate so many communities (*12*).

References

1. World Health Organization. Vector-borne diseases. September 2024 [cited 2026 Jan 12]. https://www.who.int/news-room/fact-sheets/detail/vector-borne-diseases
2. Pierson TC, Diamond MS. Degrees of maturity: the complex structure and biology of flaviviruses. Curr Opin Virol. 2012;2:168–75. https://doi.org/10.1016/j.coviro.2012.02.011
3. International Committee on Taxonomy of Viruses. Official taxonomic resources [cited 2026 Jan 12]. https://ictv.global
4. Liang Y, Dai X. The global incidence and trends of three common flavivirus infections (dengue, yellow fever, and Zika) from 2011 to 2021. Front Microbiol. 2024;15:1458166. https://doi.org/10.3389/fmicb.2024.1458166
5. Johansson MA, Vasconcelos PF, Staples JE. The whole iceberg: estimating the incidence of yellow fever virus infection from the number of severe cases. Trans R Soc Trop Med Hyg. 2014;108:482–7. https://doi.org/10.1093/trstmh/tru092
6. Garske T, Van Kerkhove MD, Yactayo S, Ronveaux O, Lewis RF, Staples JE, et al.; Yellow Fever Expert Committee. Yellow fever in Africa: estimating the burden of disease and impact of mass vaccination from outbreak and serological data. PLoS Med. 2014;11:e1001638. https://doi.org/10.1371/journal.pmed.1001638
7. World Health Organization. Yellow fever [cited 2026 Jan 12]. https://www.who.int/news-room/fact-sheets/detail/yellow-fever
8. Howlin D. Vómito negro [cited 2026 Jan 12]. https://www.revistapersona.com.ar/Persona34/34DHowlin.htm
9. Pagano JL, Vehils J. El arte de los argentinos. Buenos Aires: Editorial y Librería Goncourt; 1981.
10. Assuncao OC, Haber A, Manthorne KE, Sullivan EJ. The art of Juan Manuel Blanes. Buenos Aires: Fundacion Bunge y Born; 1994.
11. Ades D, editor. Art in Latin America: the modern era, 1820–1980. New Haven (CT): Yale University Press; 1993.
12. Gianchecchi E, Cianchi V, Torelli A, Montomoli E. Yellow fever: origin, epidemiology, preventive strategies and future prospects. Vaccines (Basel). 2022;10:372. https://doi.org/10.3390/vaccines10030372
13. Norrby E. Yellow fever and Max Theiler: the only Nobel Prize for a virus vaccine. J Exp Med. 2007;204:2779–84. https://doi.org/10.1084/jem.20072290

Address for correspondence: Terence Chorba, Centers for Disease Control and Prevention, 1600 Clifton Rd NE, Mailstop H24-4, Atlanta, GA 30329-4018, USA; email: tlc2@cdc.gov

EMERGING INFECTIOUS DISEASES®

Upcoming Issue • Vaccine-Preventable Diseases

- *Stenotrophomonas maltophilia* Bloodstream Infection Outbreak in Acute Care Hospital, California, United States, 2022–2023
- Lymphocytic Choriomeningitis Virus Seroprevalence among Urban Pregnant Women and Newborn Infants, Philadelphia, USA, 2021
- Projected Effects of Global Tuberculosis Epidemiology on *Mycobacterium tuberculosis* Prevalence and Immunoreactivity, 2024–2050
- *Blastomyces* Antigen Testing in Urine for Active Case Identification during Blastomycosis Outbreak, Michigan, USA, 2023
- Seroincidence Rate of Typhoidal Salmonella in Children, Kenya
- Insights into Strongyloides Genetic Diversity and its Sharing among Humans, Dogs, and Nonhuman Primates in the Central African Republic, 2016–2022
- Environmental and Phylogenetic Investigations of *Aspergillus flavus* Outbreak Linked to Contaminated Building Materials, Denmark, 2025
- Accelerated Increase in *Candidozyma* (*Candida*) *auris* Bloodstream Infections during COVID-19 Pandemic, South Africa
- Genetically Similar High-Risk Strains of Carbapenemase-Producing Enterobacterales Circulating in both Humans and Companion Animals, United States
- Rethinking Leptospirosis Prevention, the Philippines
- Optimal Specimens and Lesions for Mpox Diagnosis Using Real-Time PCR, South Korea
- Life-Threatening Extraintestinal Infection Caused by *Entamoeba moshkovskii* in Eastern India
- Natural Hendra Virus Infections in a Captive Cohort of Australian Black Flying Foxes (*Pteropus alecto*)
- Tuberculosis among Persons Initiating HIV Antiretroviral Therapy after TB Preventive Therapy, Mozambique, 2021–2024
- Rapid Interventions to Limit Outbreak of Invasive *Streptococcus pneumoniae* in Correctional Facility, North Carolina, USA, 2024
- Emerging Endemic Area for Blastomycosis, New York, USA, 2000–2024
- Crimean-Congo Hemorrhagic Fever Virus Seroprevalence among Hunter-Gatherers, Northeastern DRC,
- Costs of Extrapulmonary Nontuberculous Mycobacterial Disease, Denmark
- Occupational Transmission of Extensively Drug-Resistant Tuberculosis to Healthcare Worker Receiving TNF-α Inhibitor Therapy
- *Mycobacterium nanjing* sp. nov., a Novel Slowly Growing *Mycobacterium* Isolated from Cutaneous Infection in China
- Cutaneous *Paraconiothyrium cyclothyrioides* Infection in a Lung Transplant Recipient
- High Proportion of Indeterminate Results for Interferon-Gamma Release Assay among Refugee Children with Enlarged Spleens, Uganda
- Two Cases of Posttraumatic *Kosakonia oryzae* Infection
- *Mycobacterium riyadhense* Pulmonary Disease after Relocation from Saudi Arabia to Japan
- Repeated Acquisitions of *lsaC* and Tandem *lsaE-lnuB* Resistance Genes by Invasive Group A *Streptococci*us
- *Oestrus ovis* Nasal Myiasis with Pupation in Human
- Severe Acute Respiratory Infection Surveillance for Detecting Influenza A(H5N1) Viruses in Cambodia
- New 90-90-90 by 2030 Global Target for Histoplasmosis—International Society for Human and Animal Mycology 2025 Histoplasmosis Working Group Meeting

Complete list of articles in the March issue at https://wwwnc.cdc.gov/eid/#issue-330